Analysis and Design of Diversity Techniques for Terrestrial and Underwater Acoustic Communications

by

Homa Eghbali

M.A.Sc., Simon Fraser University, 2010

B.A.Sc., American University of Sharjah (U.A.E), 2009

A THESIS SUBMITTED IN PARTIAL FULFILLMENT
OF THE REQUIREMENTS FOR THE DEGREE OF

Doctor of Philosophy

in the
School of Engineering Science
Faculty of Applied Sciences

SIMON FRASER UNIVERSITY
Fall 2013

APPROVAL

Name: **Homa Eghbali**

Degree: **Doctor of Philosophy**

Title of Thesis: ***Analysis and Design of Diversity Techniques for Terrestrial and Underwater Acoustic Communications***

Examining Committee:

Chair: Shahram Payandeh
Professor, P. Eng.

Jie Liang
Senior Supervisor
Associate Professor, P. Eng.

Sami Muhaidat
Co-Senior Supervisor
Assistant Professor, P. Eng.

Rodney Vaughan
Supervisor
Professor, P. Eng.

Shawn Stapleton
Internal Examiner
Professor, P. Eng.
Department of Engineering Science

Serguei Primak
External Examiner
Associate Professor, Department of Electrical and Computer Engineering
University of Western Ontario

Date Defended: December 20th, 2013

Partial Copyright Licence

Abstract

Since the early 1880's, wireless broadband communications have been growing at explosive rates. While the personal communication systems have almost exhausted the spectrum, higher and higher data rates are required to support the ever demanding wireless services. Recently, to improve the spectral efficiency, diversity gains, and interference and power management for wireless multimedia and internet services, by combining the signals at both ends and effectively creating multiple parallel spatial data pipes, the multiple-input multiple-output (MIMO) technology has become a convenient framework.

Motivated by these practical concerns, this thesis addresses the analysis and design of diversity techniques for terrestrial and underwater acoustic communication channels, in two parts. Part I studies novel relay selection strategies and diversity techniques for single carrier frequency domain equalization (SC-FDE) multi-relay cooperative networks, considering maximum-likelihood (ML) and minimum mean-square error (MMSE) receivers. We further extend our analysis to two-way relaying (TWR) networks, while incorporating different power control techniques. Building on our results on the diversity and error performance of the single relay and TWR cooperative systems, we extend our analysis to design of MMSE-based optimum beamforming matrices at user and relay terminals in a multi-user, multi-antenna TWR cooperative system. We further present a joint user-relay antenna selection algorithm by applying the estimation of distribution algorithm (EDA). The final contribution of the first part of this thesis is to extend our analysis to large relay networks and address the prohibitive computational and implementation complexity cost of the exhaustive search algorithms for joint transceiver/relay beamforming matrix design in large amplify-and-forward (AF) MIMO TWR networks, while incorporating the orthogonal matching pursuit (OMP) algorithm.

The second part of this thesis focuses on the performance of differentially encoded space-time and space-frequency block coding techniques for terrestrial and underwater communication channels.

Dedication

I dedicate this thesis to my dearest parents and my lovely brother, Sadra,

for their constant support and unconditional love.

I love you all dearly.

Acknowledgements

Thank you God for all the blessings, your presence, and for giving me so much more than I deserve. Thank you God for the rain of life, that comes so often in Vancouver.

I would like to thank my family for all their love and encouragement. For my loving, supportive, and encouraging parents, Narges and Hassan, who raised me with a love of science, believed in me, and supported me in all my pursuits. For the presence of my brother Sadra, whose encouraging support is so appreciated.

I am sincerely thankful to my co-senior supervisor, Professor Sami Muhaidat. It has been an honor to be his first graduate student. His encouragement and support enabled me to develop an understanding of the subject, while giving me the freedom to explore and perform research in different areas in wireless communication that could grab my attention. I owe my heartfelt thanks to Professor Rodney G. Vaughan, who encouraged me throughout the course of my graduate studies at SFU. It has been a great privilege to know you these past years. Your continuous support has been valuable to my study and research. I would like to heartily thank Professor Shawn P. Stapleton for his consistent encouragement and beneficial advice to develop my academic interests and smoothly proceed with my research progress. I would like to thank Professor Jie Liang for his consistent support and accommodating me in the multimedia lab for the second half of my studies as a PhD student. I would like to gratefully thank Professor Paul Ho and Professor Ash Parameswaran for their consistent guidance and encouragement to equip myself with skills and experience it takes to be an SFU ENSC instructor. I would like to thank Professor Naofal Al-Dhahir from university of Texas at Dallas and Professor Militsa Stojanovic from Northeastern University for their helpful cooperation. I would like to thank my reading committee, Professor Rodney G. Vaughan and Professor Jie Liang for their time and interest, and Professor Shawn Stapleton for accepting to serve as the internal examiner in my committee. It is also my honor to thank the defense chair, Professor Shahram Payandeh, for his time and efforts, and Professor Serguei Primak from University of Western Ontario, for accepting to role as the external examiner.

Lastly, I offer my regards and blessings to my students from Engineering Science Department, SFU, for being my inspiration to stay enthusiastic, dedicated, and passionate for teaching, and to all of those who supported me in any respect during the course of my graduate studies at SFU.

Homa

Contents

List of Tables

List of Figures

List of Symbols

$\mathbf{a}$	A boldface lowercase letter denotes a vector.
$\mathbf{A}$	A boldface uppercase letter denotes a matrix.
$\bar{(.)}$	Conjugate operation.
$(.)^{\mathrm{T}}$	Transpose operation.
$(.)^{\mathrm{H}}$	Hermitian transpose operation.
$(.)^{-1}$	Inverse operation.
$[.]_{k,l}$	$(k,l)^{th}$ entry of a matrix.
$[.]_k$	k^{th} entry of a vector.
$\mathbf{I}_N$	identity matrix of size N.
$\mathbf{0}_{M\times M}$	all-zero matrix of size $M \times M$.
P_N	$N \times N$ permutation matrix.
$[\mathrm{P}_N^q \mathbf{a}]_s$	$\mathbf{a}\,((N-s+q) \bmod N)$, for $\mathbf{a} = [\ a_0 \ \cdots \ a_{N-1}]^{\mathrm{T}}$.
$\mathbf{Q}$	$N \times N$ FFT matrix with $\mathbf{Q}(l,k) = 1/\sqrt{N}\exp(-j2\pi lk/N)$.
$\|.\|_{\mathbf{F}}$	Frobenius norm.
$\|\cdot\|$	Euclidean norm of a vector.

Table 1: List of notations.

List of Acronyms

2G	second-generation
3G	third-generation
3GPP	Third Generation Partnership Project
4G	fourth-generation
AF	amplify-and-forward
AWGN	additive white Gaussian noise
BC	broadcast channel
BER	bit error rate
BRS	best relay selection
BS	base station
CBRS	instantaneous mutual information-based relay selection
CIR	channel impulse response
C-OFDM	coded OFDM
CP	cyclic prefix
CSI	channel state information
CSIT	channel state information at the transmitter
DAB/DVB	digital audio/video broadcasting
DF	decode-and-forward
DFT	discrete Fourier transform
DSL	digital subscriber lines
DST	differential space-tim
D-STBC	distributed space-time block coded
EA	Evolutionary Algorithm
EDA	estimation of distribution algorithm
EGC	equal gain combining
EQRS	equalizer quality-based relay selection
ESA	Exhaustive Search Algorithm
FD	frequency domain
FDE	frequency domain equalization
FFT	fast Fourier transform
FIR	finite impulse response

GSVD	generalzied singular value decomposition
HL2	HIPERLAN/2
IBI	inter-block interference
IFFT	inverse fast Fourier transform
ISI	intersymbol interference
KAM	2011 Kauaii Acoustic Comunications
LAN	local area networks
LCP	linear constellation precoding
LCP-OFDM	linear constellation precoded OFDM
LDC	linear dispersion codes
LOS	line-of-sight
LTEA	Long Term Evolution-Advanced
MAC	multiple access channel
MADO	maximum achievable diversity order
MCN	multihop cellular network
MFB	matched filter bound
MIMO	multiple-input-multiple-output
MISO	multiple-input-single-output
ML	maximum likelihood
MLD	maximum likelihood detector
MLSD	maximum likelihood sequence detection
MMSE	minimum mean square error
MRC	maximal ratio combining
MS	mobile station
MSE	mean-square-error
NAF	non-orthogonal amplify-and-forward
NBRS	norm-based relay selection
NLOS	non-line-of-sight
OFDM	orthogonal frequency division multiplexing
OFDMA	orthogonal frequency-division multiple access
OMP	orthogonal matching pursuit
pdf	probability density function
PAR	peak-to-average ratio
PEP	pairwise error probability

PSK	phase-shift keying
QAM	quadrature amplitude modulation
QPSK	quadrature phase shift keyin
RF	radio frequency
RS	relay station
SC	selection combining
SC	single carrier
SER	symbol error rate
SFBC	space frequency block cod
SFRS	selective-to-flat fading relay selection
SIMO	single-input-multiple-output
SINR	signal-to-interference noise ratio
SISO	single-input single-output
SNR	signal-to-noise ratio
SC-FDE	Single-Carrier Frequency-Domain Equalization
SO-STTC	super-orthogonal space-time trellis coding
SR	selection relaying
SSA	signal space alignment
ST	space-time
STBC	space-time block codes
STTCs	space-time trellis codes
SVD	singular value decomposition
TCM	trellis-coded modulation
TD	time domain
TDR	time domain relaying
TDMA	time-division multiple access
TWR	two-way relay
UWA	underwater acoustic
WPANs	wireless personal area network
WSN	wireless sensor networks
ZP	zero padding

Chapter 1

Introduction

1.1 Diversity Techniques for Fading Channels

Fading is a process of random fluctuations in the signal level, which results from the time-varying channel environment between the transmitter and receiver terminals. Fading imposes performance limitations on the wireless communication system and can be modeled through the time-varying channel impulse response into two classes, i.e. large-scale (long-term) fading and small-scale (short-term) fading.

Large-scale impairment includes propagation path loss and shadowing. Large scale fading effects are noticeable over relatively long distances between the transmitter and the receiver terminal. The path loss randomness mainly is due to the random position of mobile terminals. Shadowing incurs due to the presence of obstacles in the signal path and the random relative position of the mobile terminal with respect to the base station. Large-scale fading is used to predict the transmission coverage area and the average signal power at the receiver side.

Small-scale impairment involves rapid fluctuations of the amplitude of a signal over a travel distance in the order of the signal wavelength, caused by constructive and destructive interferences between two or more propagation paths between transmitter and receiver. Small-scale impairment is commonly referred to as fading and can negatively affect the signal-to-noise ratio (SNR). To give an example of the degrading performance effects of small-scale fading, one can consider the typical mobile wireless channel in urban areas where there is no line-of-sight (LOS) propagation and the number of scatterers is large. From the central limit theorem, the corresponding complex fading channel coefficient has

two quadrature components which are zero-mean Gaussian random processes. The corresponding amplitude of the fading envelope follows a Rayleigh distribution. This converts the exponential dependency of the bit-error probability on the SNR for the additive white Gaussian noise (AWGN) channel into an approximately inverse linear one, resulting in a large SNR penalty, i.e. transmitter should transmit with more power to achieve a low error probability.

Diversity techniques are commonly used to mitigate the degrading performance effects of fading. In this proposal, by diversity technique, we refer to a method that makes use of more than one independently faded version of the transmitted signal, such that the probability that all the independently faded signal components will undergo deep fading simultaneously, is reduced significantly. If we have supplied L independently faded replicas of transmitted signal to the receiver, and p is the probability that any one replica will undergo deep fading, p^L is the probability that all the L replicas will undergo deep fading simultaneously. There are various approaches to extract diversity from the wireless channel. The most common methods are briefly summarized as follows [1–3]:

1.1.1 Time Diversity

In this form of diversity, also known as temporal diversity, the channel coherence time equals or exceeds several symbol transmission periods. This implies that the same signal transmitted in different time slots separated by an interval longer than the coherence time of the channel, will experience channel realizations that are highly uncorrelated and can be used to obtain diversity. The simplest way to achieve time diversity is to form the symbols by using a repetition coding scheme. Interleaving is also an efficient technique to provide time diversity. In fast fading environments where the mobility is high, time diversity becomes very efficient. However, for slow-fading channels (e.g., low mobility environments or fixed-wireless applications), it offers little protection unless significant interleaving delays can be tolerated.

1.1.2 Frequency Diversity

In wideband systems where the available bandwidth exceeds the channel coherence bandwidth, it is possible to realize diversity by using channels that are a partition of the available bandwidth and are separated by more than the channel coherence bandwidth. This approach is applicable in multicarrier systems, where transmission is implemented by dividing the wideband channel into non-overlapping narrowband sub-channels. The symbol used for

transmission in each sub-channel has a long transmission period, such that the sub-channel appears as a flat fading channel. In this form of diversity, the same signal is sent over different frequency carriers, whose separation exceeds the channel coherence bandwidth to ensure independence among diversity sub-channels.

A natural way of frequency diversity, which is sometimes referred to as multipath diversity, arises for frequency-selective channels. Recall that the spectral components of the signal may undergo destructive or constructive interference of different magnitude depending on the delay, amplitude, and phase of the frequency response of the multipath channel. When the multipath delay spread is a significant fraction of the symbol period, the received signal can be interpreted as a linear combination of the transmitted signal, weighted by independent fading coefficients. Therefore, path diversity is obtained by resolving the multipath components at different paths using a RAKE correlator [1], which is the optimum receiver in the minimum mean square error (MMSE) sense, designed for this type of channels.

1.1.3 Space Diversity

In this form of diversity, also referred to as antenna diversity, the receiver and/or transmitter uses multiple antennas. This technique is especially attractive since it does not require extra bandwidth. To extract full diversity advantages, the spacing between antenna elements should be wide enough with respect to the carrier wavelength. The required antenna separation depends on the local scattering environment, as well as on the carrier frequency. For a mobile station which is near the ground with many scatters around, the channel decorrelates over shorter distances, and typical antenna separation of half to one carrier wavelength is sufficient. For base stations on high towers, a larger antenna separation of several to tens of wavelengths may be required.

1.1.4 Diversity Combining Techniques

Diversity combining techniques refer to the processing performed at the receiver, where the signal copies arriving through the multiple paths are constructively combined, so as to obtain a resulting signal of better quality or with better probability of successful reception. There exist different combining techniques, each of which can be used in conjunction with any of the aforementioned diversity forms. The most common diversity combining techniques are selection, equal gain, and maximal ratio combining [1]. Selection combining (SC) is conceptually the simplest; it consists of selecting at each time, among the available diversity branches (channels), the one with the largest value of SNR. Since it requires only a measure

of the powers received from each branch and a switch to choose among the branches, it is relatively easy to implement. However, the fact that it disregards the information obtained from all branches except the selected one, indicates its non-optimality. In equal gain combining (EGC), the signals at the output of diversity branches are combined linearly, and the phase of the linear combination are selected to maximize the SNR, disregarding the amplitude differences. Since each branch is combined linearly, compared to SC, EGC performs better. In maximal-ratio-combining (MRC), the signals at the output of diversity branches are again combined linearly, and the coefficients of the linear combination are selected to maximize the SNR using both the phase and the amplitude information. Hence, the MRC technique outperforms the other two, since it makes use of both fading amplitude and phase information. However, the difference between EGC and MRC is not considerably large in terms of power efficiency. Therefore, EGC can be preferred where implementation costs are crucial. The reader can refer to [1–3] and references therein for a broad overview of diversity combining systems.

1.2 Transmit Diversity and MIMO Systems for Wireless Communications

The goal of future wireless communications systems is to provide a wide variety of high-quality, high-rate services with minimum requirements on spectrum, power consumption, and hardware complexity. Toward this end, proper system structures as well as robust system designs are required to meet the challenges in wireless transmissions. Recent research results have unveiled the MIMO antenna diversity techniques, commonly deployed by using multiple transmit and receive antennas, as a promising transmission structure to achieve improved system performance and throughput in future wireless systems [4, 5].

Early work on multi-antenna systems involves the use of antenna arrays at the receiver side to exploit the underlying receive antenna diversity [1, 6–8]. By placing the receive antennas sufficiently apart, one can receive multiple independently fading copies of the transmitted signal, which can be further processed through different combining techniques [1]. Transmit antenna diversity techniques were proposed [9, 10] to alleviate the implementation constraints of receive diversity techniques for portable receivers, i.e. physical size constraints. In addition to the simpler receiver design, the proposed schemes yield spatial diversity with no additional power or bandwidth requirements.

A MIMO system can be designed to fully exploit the underlying transmit and receive

spatial diversity of the channel to combat channel fading. By sending signals that carry the same information through different paths, multiple independently fading replicas of the transmitted signal can be received at the receiver side, which enhances the reception reliability. For example, in a slow Rayleigh-fading environment with one transmit and n_R receive antennas, the transmitted signal is passed through n_R different paths. It is well known that if the fading is independent across antenna pairs, a maximal diversity gain of n_R can be achieved, i.e. the average error probability can be made to decay like SNR^{-n_R} at high SNR, in contrast to the SNR^{-1} for the single-antenna fading channel. There is a recent rich literature on employing multiple antennas at the transmitter side and achieving diversity through space-time coding, when there is no channel state information at the transmitter (CSIT) [9–13], or through transmit beamforming when there is perfect CSIT [14]. However, the underlying idea is still averaging over multiple path gains to increase the communication reliability. In a system with n_T transmit antennas and n_R receive antennas, assuming the path gains between individual antenna pairs are independent and identically distributed (i.i.d.) Rayleigh faded, the maximal diversity gain is $n_T n_R$, which is the total number of fading gains that one can average over. The use of multiple transmit and receive antennas also opens up the spatial domain for boosting data rate. While a flat-fading single-input single-output (SISO) Gaussian channel provides only a single narrow data pipe, a coherent MIMO channel can be represented as a set of parallel Gaussian channels and thus, creates multiple data pipes for data transmission without additional power or spectrum [15–17], an appealing feature to cope with the scarcity of wireless spectrum and the stringent power constraint on terminals. By transmitting independent information streams in parallel through the spatial channels, the data rate can be increased. The gain in terms of ergodic capacity achieved by a coherent MIMO channel over that of a SISO channel is termed the spatial multiplexing gain [18], and is particularly important in the high-SNR regime, where the system is degree-of-freedom limited (as opposed to power limited). In particular, in the high-SNR regime, the ergodic capacity of a coherent MIMO channel with n_T transmit and n_R receive antennas and i.i.d. Rayleigh-faded gains between each antenna pair, scales linearly with the minimum of (n_T, n_R) [17, 19]. The number of degrees of freedom is thus the minimum of n_T and n_R. In summary, a MIMO system can provide two types of gains, i.e. diversity gain and spatial multiplexing gain. Although both spatial multiplexing and diversity gains can be simultaneously achieved by a MIMO system, there is a basic tradeoff between them, i.e. maximizing one type of gain may not necessarily maximize the other type. In [18] it was shown that given a MIMO channel, both gains

can be simultaneously obtained, but there is a fundamental tradeoff between how much of each type of gain any coding scheme can extract, i.e. higher diversity gain may come at the price of sacrificing spatial multiplexing gain. More specifically, assuming a family of codes with a spatial multiplexing gain r (rate scales like $r \log SNR$) and a diversity gain d (average error probability decays like SNR^{-d}), an optimal tradeoff curve is characterized which bridges between the two extremes for r and d, which are $\min(n_T, n_R)$ and $n_T n_R$, respectively. The optimal trade-off between the diversity gain and spatial multiplexing gain in slow i.i.d Rayleigh fading environments was presented in [18], i.e. the optimal diversity gain achievable by a coding scheme of block length l and multiplexing gain r is precisely $(n_T - r)(n_R - r)$, as long as $l \geqslant n_T + n_R - 1$. This trade off can be interpreted as allocating r transmit and r receive antennas to multiplexing and using the remaining $n_T - r$ transmit and $n_R - r$ receive antennas to provide diversity gain.

For applications such as wireless local area networks (LAN), as well as cellular communications, MIMO systems are set up in a multiuser environment, where a multi-antenna base station (BS) simultaneously communicates information with several multi-antenna mobile stations (MSs). There are two classes of multiuser channels in typical multiuser environments, i.e. the multiple-access channel (MAC), also known as the uplink or the many-to-one channel [20, 21], and the broadcast channel (BC), also referred to as the downlink or the one-to-many channel [20]. Recent results from information-theoretic studies have completely characterized the capacity regions of the coherent Gaussian MIMO MAC [22, 23] and BC [24, 25]. It has been found that in a multiuser environment, the use of multiple antennas introduces more flexibility to deal with the multiuser interference and enables high-rate, multiuser communications, as well as spatial multiplexing and diversity gains [3].

1.3 Space-Time Coding

Space-time (ST) coding and its various combinations are becoming well understood in the research community. A detailed treatment of space-time coding can be found in recently published text-books, e.g., [4, 11]. ST coding technique is a class of linear processing of the transmitted signal at transmitting antennas in MIMO systems, designed to achieve both spatial diversity and temporal diversity gains. The main advantage of ST coding is that CSI is not required at transmitter side. There are two classes of ST codes, i.e. Space-Time Trellis Codes (STTCs) and Space-Time Block Code (STBCs).

STTCs were invented by Vahid Tarokh in 1998. This coding scheme transmits multiple

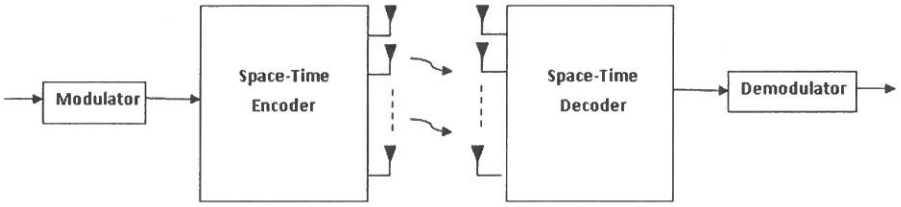

Figure 1.1: Block diagram of a space-time coded system.

redundant copies of trellis code which are distributed in time and space. The data symbols are cleverly coded across space and time to extract diversity advantages [9]. Figure 1.1 illustrates a space-time coded system. Let space-time code be represented as a $W \times M_S$ matrix, where M_S is the number of transmit antennas, and W is the codeword length. Each entry of X represents the modulated symbol transmitted from the m_S^{th} $(m_S = 1, 2, ...M_S)$ antenna during the w^{th} $(w = 1, 2, ...W)$ symbol period, as expressed below,

$$\mathbf{X} = \begin{bmatrix} x_1^1 & x_2^1 & ... & x_{M_S}^1 \\ x_1^2 & ... & ... & x_{M_S}^2 \\ : & ... & ... & : \\ x_1^W & x_2^W & ... & x_{M_S}^W \end{bmatrix}. \tag{1.1}$$

The signal at each receive antenna results from the superposition of the M_S transmitted signals corrupted by fading. The received signal at the n^{th} antenna within the w^{th} symbol period is given by

$$r_n^w = \sum_{m_S=1}^{M_S} h_{m_S}^n x_{m_S}^w + n_n^w, \tag{1.2}$$

where $h_{m_S}^n$ denotes the frequency flat fading coefficient from the ${m_S}^{th}$ transmit antenna to the n^{th} receive antenna. $h_{m_S}^n$ is modeled as a complex Gaussian random variable with variance 0.5 per dimension leading to the Rayleigh fading channel model, and is further considered to be quasi static constant over the codeword length W. In (1.2), n_n^w models the additive noise term and is zero-mean complex Gaussian random variable with variance $N_0/2$ per dimension. In matrix notation, the received signal can be written as follows,

$$\mathbf{R} = \mathbf{XH} + \mathbf{N}, \tag{1.3}$$

where $\mathbf{R}$ is the received signal matrix of size $W \times N$, N is the number of receive antennas, $\mathbf{H}$ is the channel matrix of size $M_S \times N$, and $\mathbf{N}$ is the additive noise matrix of size $W \times N$.

With coherent detection and perfect CSI at the receiver side, the maximum likelihood (ML) receiver depends on the minimization of the metric $\hat{\mathbf{X}}$, where

$$\hat{\mathbf{X}} = \arg\min_{\mathbf{X}} \|\mathbf{R} - \mathbf{X}\mathbf{H}\|^2. \tag{1.4}$$

Let $P\left(\mathbf{X}, \hat{\mathbf{X}}\right)$ denote the pairwise error probability (PEP), which represents the probability of choosing the codeword $\hat{\mathbf{X}}$ when indeed codeword $\mathbf{X}$ was transmitted. PEP is the building block for the derivation of union bounds to the error probability. It is widely used in the literature to predict the attainable diversity order where the closed-form error probability expressions are unavailable. In [9], Tarokh et al. derived a Chernoff bound on the PEP for space-time coded systems given by

$$P(\mathbf{X}, \hat{\mathbf{X}}) \leq \left(\prod_{j=0}^{r} \lambda_j\right) \left(\frac{E_S}{4N_0}\right)^{-rN}, \tag{1.5}$$

where E_S is the average symbol energy, r is the rank of the codeword difference matrix defined by $\mathbf{E} = \left(\mathbf{X} - \hat{\mathbf{X}}\right)\left(\mathbf{X} - \hat{\mathbf{X}}\right)^{\mathrm{H}}$, and λ_j denotes the non-zero eigenvalues of $\mathbf{E}$. In (1.5), rN represents the diversity advantage, (i.e., the slope of the performance curve), while the product of the non-zero eigen values of $\mathbf{E}$ denotes the coding advantage, (i.e., the horizontal shift of the performance curve). The design criteria for space-time codes are further discussed in [9]:

Rank criterion: The code difference matrix, taken over all possible combinations of code matrices, should be full rank. This criterion maximizes the diversity gain obtained from the space-time code. The maximum diversity order that can be achieved is $r = \min(W, M_S)$. Therefore, in order to achieve the maximum diversity of $M_S \times N$, $\mathbf{E}$ must be full rank.

Determinant criterion: The minimum determinant of E, taken over all possible combinations of code matrices, should be maximized. This maximizes the coding gain. From (1.5), it can be seen that at high SNR regimes, the diversity gain term dominates the error probability. Therefore, in the design of a space-time code, the diversity gain should be maximized before the coding gain.

Based on the above criteria, Tarokh et al. [9] proposed some handcrafted codes which perform very well, within the 2-3 dB of the outage capacity derived in [16] for multiple antenna systems. Since Tarokh's pioneering work, there has been an extensive research effort in this area for the design of optimized space-time trellis codes, a few to name are [26–28] among many others. Since every STTC has a well-defined trellis structure, standard soft decision techniques, such as a Viterbi decoder, can be used at the receiver. For a

fixed number of transmit antennas, the decoding complexity of STTCs (measured by the number of trellis states at the decoder) increases exponentially with the transmission rate. Overall, design of STTC is very difficult, and they require very high complexity encoders and decoders.

Space-time block codes (STBCs) [9, 10, 12] were proposed as an attractive alternative to STTCs with the provision of full diversity and a very simple decoding scheme. These codes are defined by a mapping operation of a block of input symbols into the space and time domains, transmitting the resulting sequences from different antennas simultaneously. Tarokh et al.'s work in [9] was inspired by Alamouti's early work [10], where a simple two-branch transmit diversity scheme was presented and shown to provide the same diversity order as MRC with two receive antennas. Alamouti's scheme is appealing in terms of its performance and simplicity. It requires a very simple decoding algorithm based only on linear processing at the receiver. STBCs based on orthogonal designs [9] generalizes Alamouti's scheme to an arbitrary number of transmit and receive antennas, while preserving the decoding simplicity, and are able to achieve full diversity gains at full transmission rate for real signal constellations, and at half rate for complex signal constellations such as QAM or PSK. Over the last few years, several contributions have been made to further improve the data rate of STBCs, e.g., [29] and the references therein.

1.4 Cooperative Diversity

1.4.1 Importance of Cooperative Diversity

One way to combat fading effects in the system is through communication diversity; i.e., transmitting several independent replicas of the signal in orthogonal channels so that the probability that all of them go into deep fade decreases. The conventional antenna diversity schemes [12] have some limitations. The spacing between antenna elements needs to be larger than half a wavelength to avoid fading correlation and antenna coupling. In many practical wireless applications, wireless devices are so miniaturized that such spacing between multiple antenna cannot be employed. One of the methods to achieve spatial diversity is through the use of relay terminals, where each relay re-transmits the signal received from a remote source to the destination [30]. Cooperative diversity, also known as user cooperation, was proposed to emulate transmit antenna diversity while overcoming the size, cost, and hardware limitations associated with transmit antenna diversity techniques [31–34]. In cooperative diversity, the signal transmitted by the source node is overheard by the other

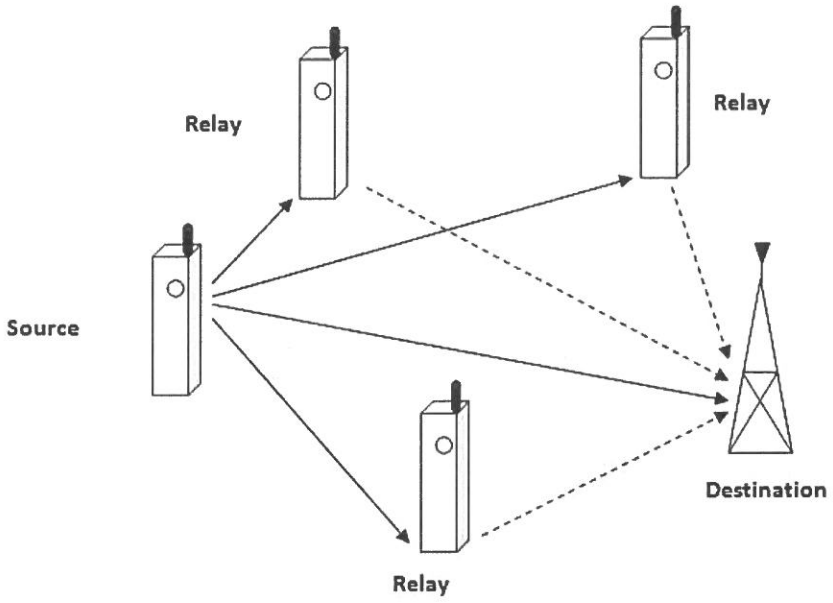

Figure 1.2: Relay assisted transmission.

participating nodes, also known as "partners" or "relays". The source node and its partners jointly process and transmit their information, creating an antenna array, even though each of them is equipped with a single antenna only. Note that similar to physical antenna arrays applying transmit diversity techniques, in cooperative communication, receiver is provided with redundant copies of the transmitted signal over independent channels that can be combined to average individual channel effects and combat the underlying multipath fading in wireless channels. Fig. 1.2 illustrates a schematic of the relay assisted transmission.

Cooperation and relaying have re-emerged as important research areas in wireless communication over the past half-decade. Although multihop relaying for coverage extension in wireless networks is an old concept, it became practical only recently. The basic idea of cooperative communications can be traced back to the 1970s. In 1970S, van der Meulen [35, 36] introduced and studied a basic three-terminal communication model in the context of mutual information. Since it was first introduced, cooperative communication has been extensively studied in most of the communication related aspects, including information theory [34, 37–40], the channel effect [41–43], relay selection mechanisms [44–47], and differential modulation in cooperative systems [48–50], for applications such as wireless sensor networks, ad-hoc networks, and cellular networks.

In the beginning, end users were supposed to be immobile and to have a LOS to the

base station (BS). With the 802.16e-2005 amendment [51] to the 802.16-2004 standard [52], the standard has moved into the mobile non-line-of-sight (NLOS) domain. Regardless of the advanced signal processing techniques employed in WiMAX (e.g., orthogonal frequency division multiple access (OFDMA) and MIMO), the projected data rates require a SNR at the receiver that may be difficult to obtain at the cell edge. Moreover, increasing data rates reduces reliability, and increasing the minimum reliability service reduces the coverage area.

The most widely used strategy to address these challenges is to shrink the cell size, while effectively increasing the number of BSs over a given area. This strategy will likely increase capacity by shortening the distance between users and their serving BSs, given that the increased interference won't outweigh the increased signal power. Nevertheless, benefits to this strategy is limited due to the increasing cost of BSs. For each BS, the provider must pay for antenna space, the wired backhaul to the network, as well as the digital and radio frequency (RF) equipments.

An alternative, yet increasingly attractive strategy is to employ fixed relays into the cell to aid communication from BS to MS and vice versa. Such networks are called multihop cellular networks (MCNs) which are the focus of recent research [53]. Although there are many unsolved problems in relaying, IEEE 802.16 has formed a task group to extend the IEEE 802.16e-2005 standard to include multihop communication, indicating that the field has reached a significant level of maturity. The IEEE 802.16j task group [54] is the first commercial wireless network to incorporate multi-hop communication networks [55]. The purpose of IEEE 802.16j is not to standardize a new cellular network that includes multihop capability, but instead to expand previous single-hop 802.16 standards to include multihop capability. In IEEE 802.16j, relays are created for different usage purposes. Relays may be placed by the service provider near newly developed areas to extend coverage, or may be purchased as commercial products to extend coverage into the subscribers' residences. The IEEE 902.16j task group has created the following relay usage scenarios:

- **Fixed Infrastructure**: Fixed-infrastructure relays, like BSs, are to be deployed by the service provider in stationary areas to cover general traffic. Fixed-infrastructure relays are likely to be placed above roof tops to allow an LOS with the BS, and hence can serve to increase both throughput and coverage. This category also includes commercial relays bought by subscribers, which may leave and enter the network at any time.

- **In-Building Coverage**: The in-building coverage relays are mostly placed inside or near the shell of the building to fill the coverage hole and improve the mobile phones'

performance inside buildings. They can also be deployed near tunnels or subways to improve coverage. These low-complexity relays can be nomadic, operate on battery, and operate with NLOS channels.

- **Temporary Coverage**: Temporary relays can be placed to enable the traffic generated by large group of people packed into small areas, to be routed to BSs in adjacent cells. This infrastructure can be deployed near stadiums as a permanent solution. In emergency situations where some BSs may have been damaged, temporary relays can be deployed as temporary solutions. For this reason, temporary coverage relays may be required to run on batteries and will range from small and simple to large and complex.

- **Coverage on a Mobile Vehicle**: To provide reliable coverage to the users located closely in mobile vehicles such as train or bus, moving sometimes very fast, a complex relay may be deployed on the vehicle and obviously, will be highly mobile.

The IEEE 802.16j amendment is fully compatible with 802.16e-2005 mobile and subscriber stations, but a BS specific to 802.16j is required for relays to operate. Also, the IEEE 802.16j's architecture constrains the relays to be served by a single base station and allows them to communicate in one direction at a time only (i.e., either uplink or downlink).

Compared to IEEE 802.16 j and its design-related limitations, Long Term Evolution-Advanced (LTE-A) standards may consider more sophisticated relay strategies and thus, may expect larger performance gains from the inclusion of relaying. The Third Generation Partnership Project (3GPP)'s LTEA considers an option for relay networks to provide cost-effective coverage extension and throughput enhancement. The goal for both LTEA [56] and IEEE802.16m [57] standards is to further enhance system spectral efficiency and data rates while supporting backward compatibility with their respective earlier releases. One of the main challenges faced by the developing LTEA standard is providing high throughput at the cell edge. Technologies like MIMO, OFDMA, and advanced error control codes enhance per-link throughput but do not inherently mitigate the effects of interference. Cell edge performance is becoming more important as cellular systems employ higher bandwidths with the same amount of transmission power. One solution to improve coverage is to combine LTEA with cooperative communication systems, i.e. forwarding messages between the BS and MSs through multi-hop communication [53, 58–64].

Many different relay transmission techniques have been developed over the past ten

years. The simplest strategy (already deployed in commercial systems) is the analog repeater, which uses a combination of directional antennas and a power amplifier to repeat the transmission signal [65]. More advanced strategies use signal processing of the received signal at the relay terminal. Depending on the type of processing that relay uses to handle the received signal, we can have different types of relaying techniques. The two main relaying techniques are studied in [33]: amplify-and-forward (AF) and Decode-and-Forward (DF):

- **Amplify and forward:** In this relaying technique, also known as "non-regenerative relaying", the relay terminal down-converts the received analogue signal, amplifies it, and up-converts it to another frequency band prior to re-transmitting it. The retransmitted relay signal includes the amplified version of the relay's received signal, as well as the amplified version of the additive noise at the relay terminal. As a result, at low SNRs, this protocol suffers from severe performance losses.

  In time division relaying (TDR), the incoming and outgoing information streams at a relay are allocated to different time slots and are separated in time. This leaves enough time for packet processing and results in packet processing delay. There will generally be a time gap between the received frame and the relayed frame that accounts for the time needed for the relay circuitry to switch from reception to transmission and the packet processing delay. In a relay transceiver with purely analog hardware radio components, the analog signal is received, frequency translated and retransmitted. As a point of a purely analog hardware architecture, the analogue received signal cannot be stored and hence requires immediate frequency translation. This implies two oscillators, two frequency bands and two fairly good filters [66]. As a result, the TDR protocols can not be used in the context of analog architectures. Alternatively, one has to use a digital architecture which is more complex and expensive compared to its purely analog counterpart [67].

- **Decode and forward:** In decode-and-forward relaying, which is also known as "regenerative relaying", the received signal is decoded, re-encoded, and retransmitted, which corresponds to a non-linear transformation of the relay terminal's received signal. This relaying scheme even though reduces the impact of the additive noise, yet suffers from the error propagation that may occur if the relay incorrectly detects a message and retransmits the erroneous information to the destination terminal.

In [68] Nabar et al. proposes three different cooperation configurations for single relay

wireless networks which effectively implements transmit diversity in a distributed manner. More specifically, they consider three (time-division multiple access) TDMA-based protocols named Protocol I, Protocol II, and Protocol III which correspond to traditional MIMO (multi-input-multi-output), SIMO (single-input-multi-output) and MISO (multi-input -single-output) schemes, respectively (Table I).

Table 1.1: Cooperation protocols for single-relay networks.

Terminal / Protocol	Protocol I		Protocol II		Protocol III	
	Time 1	Time 2	Time 1	Time 2	Time 1	Time 2
Source	•	•	•	–	•	•
Relay	○	•	○	•	○	•
Destination	○	○	○	○	–	○

•: Transmitting, ○: Receiving, –: Idle

As was explained previously, relay terminals, whether fixed or mobile, can be deployed in cellular networks to extend coverage, enhance the capacity of a specific regions with high traffic demands, and improve signal reception. By combining the signals from the relays and possibly the source signal from the BS, the MS is able to exploit the underlying diversity of the relay channel. Due to the opportunistic nature of mobile relays and the highly dynamic and unstable nature of the network topology, mobile relays are less reliable than fixed relays. Another major disadvantage of the mobile relays is that MS batteries can be used up by relay transmissions even if the user does not use them. Mobile user relays also complicate the billing problem, i.e., one can not tell who shall pay the bill when a user helps other users as a relay. On the other hand, fixed relays suffer from the additional delay associated with the relaying process, and the potentially increased levels of interference due to frequency reuse at the relay terminals. In this thesis, we adopt fixed relay scenario due to its practicality. The presented results, however, are not dependent on whether the relays are fixed or mobile

1.5 Frequency Domain Equalization

The growing demand for high data rate services for wireless multimedia and internet services has lead to intensive research efforts on high speed data transmission. A key challenge for high-speed broadband applications is the dispersive nature of frequency-selective fading channels, which causes the so-called intersymbol interference (ISI) leading to inevitable performance degradation. An efficient approach to mitigate ISI is the use of orthogonal frequency division multiplexing (OFDM) which converts the ISI channel with AWGN into

parallel ISI-free subchannels, by implementing IFFT at the transmitter and FFT at the receiver side [69]. It has been shown that OFDM is an attractive equalization scheme for digital audio/video broadcasting (DAB/DVB) [70], and it has successfully been applied to high-speed modems over digital subscriber lines (DSL) [71]. Recently, it has also been proposed for broadband television systems and mobile wireless local area networks such as IEEE802.11a and HIPERLAN/2 (HL2) standards [72].

The IFFT precoding at the transmitter side and insertion of cyclic prefix (CP) enable OFDM with very simple equalization of frequency-selective finite impulse response (FIR) channels. To avoid inter block interference (IBI) between successive FFT processed blocks, the CP is discarded, and the truncated blocks are FFT processed so that the frequency-selective channels are converted into parallel flat-fading independent subchannels. In this way, the linear channel convolution is converted into circular convolution, and the receiver complexity both in equalization and the symbol decoding stages is reduced [73]. However, since each symbol is transmitted over a single flat subchannel, the multipath diversity is lost along with the fact that there is no guarantee for symbol detectability when channel nulls occur in the subchannels. Due to the transmission of modulation symbols at those frequency bands with deep amplitude depression, the uncoded error-rate performance of OFDM transmission over frequency selective channels is relatively poor.

A single carrier (SC) system transmits a modulated single carrier at a high symbol rate and is basically the frequency domain (FD) analog of what is done by conventional linear time domain (TD) equalizers. Note that FDE is performed on a block of data at a time, where the operations on this block involve an efficient FFT operation and a simple channel inversion operation, which makes it computationally more efficient than the corresponding TD equalization, specifically for channels with severe delay spreads. Therefore, the single-carrier frequency-domain equalization (SC-FDE) has essentially the same performance and low complexity as OFDM, when combined with FFT processing and the use of cyclic prefixing [74]. Fig. 1.3 illustrates the system block diagram for the OFDM and SC-FDE wireless systems.

1.6 Contributions and Organization

Objectives of this research are to propose/extend and analyze diversity techniques for terrestrial and underwater communication channels. The following is a summary of the main topics and contributions in this thesis:

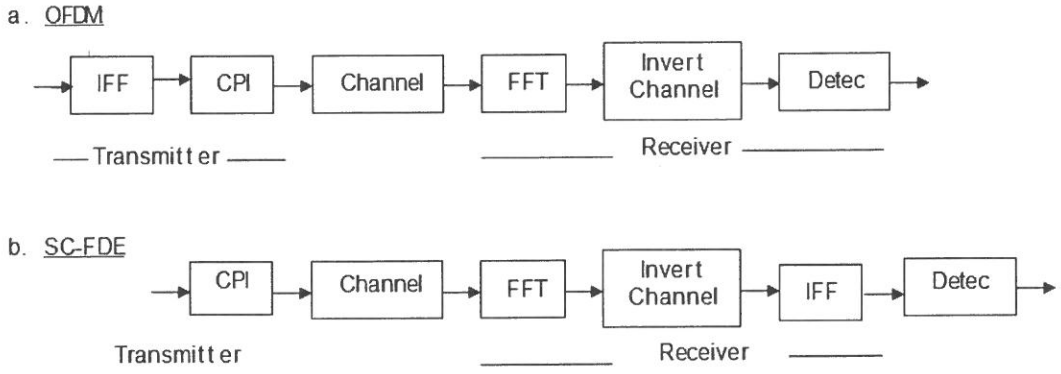

Figure 1.3: Block diagram of wireless systems: (a) OFDM, (b) SC-FDE [75]

1.6.1 Relay Selection Strategies for Single-Carrier Frequency-Domain Equalization in Multi-Relay Cooperative Networks

Chapter 2 discusses several relay selection strategies for cooperative SC-FDE with the AF protocol. Both ML-SC-FDE and MMSE-SC-FDE receivers are studied. Novel PEP-based selection criterion for frequency selective channels, referred to as SHARM, is proposed. Several selection strategies for cooperative (C) MMSE-SC-FDE receivers, which are motivated by minimizing the instantaneous error rate, are investigated. These are, norm-based relay selection (NBRS), instantaneous mutual information-based relay selection (CBRS), singular value based relay selection (SVRS), and equalizer output signal quality-based relay selection (EQRS) strategies. A novel relay selection strategy is proposed, in which from the effective frequency selective source-relay-destination channel link associated with the selected relay, only the channel tab with highest power is passed to the destination terminal. Additionally, to tackle the multiple relay selection problem considering generic mobile scenarios with moderately fast fading channels, in order to select the near best relay subset within the minimum processing time, the estimation of distribution algorithm (EDA) is applied, and a modified EDA for the relay selection problem is formulated. Simulation results show promising performance of EDA with comparable computational complexity.

1.6.2 Single-Carrier Frequency-Domain Equalization for Two-Way Multiple Relay Networks with Selection: Diversity order Analysis and Power Allocation

Chapter 3 discusses cooperative SC-FDE for two-way multiple relay networks with selection. Both ML-SC-FDE and MMSE-SC-FDE receivers are studied. We derive closed-form expressions for the conditional and average symbol error rate (SER) at the two end source terminals. We perform detailed diversity analysis for both MMSE and ML SC-FDE two-way relay (TWR) receivers. The maximum achievable diversity gain by the single relay ML SC-FDE TWR system is investigated and the existence of the performance bottleneck is verified. We extend our analysis to multiple relay cooperative ML SC-FDE TWR systems with best relay selection. Furthermore, asymptotic diversity analysis on the average SER reveals that the diversity gain is determined by both the number of participating relay nodes and the minimum of the multipath diversity orders experienced in the source to relay, and relay to destination links, which acts like a performance bottleneck for the relaying paths. We complete our analysis by introducing the bottleneck integral factor H that dictates the performance bottleneck existing in cooperative communication systems.

1.6.3 Multiuser Two-Way Relaying with Power Control for SC-FDE Systems

Chapter 4 investigates cooperative SC-FDE for two-way relay networks, where multiple users each equipped with multiple antennas exchange their information through a multi-antenna relay node in a bi-directional manner. Under network total power constraint, the optimal relay beamforming for the multiuser two-way relay system, where the relay transceiver processor is designed based on the MMSE criterion, is studied. Closed-form expression for the SINR at the end user terminals is derived, and further, a joint user-relay antenna selection algorithm which applies the EDA is presented. The proposed EDA has a low computational complexity, and its effectiveness is verified through simulation results.

1.6.4 Exploiting Sparsity for Beamforming with Power Control in Large AF Two-Way Relay Networks

Chapter 5 investigates a novel iterative user and relay beamforming matrix design algorithm joint with an effective user and relay power allocation technique for large cooperative multi-pair TWR networks, where multiple users are equipped with multiple antennas and exchange

their information through a multi-antenna AF relay node in a bi-directional manner. The two key ingredients in the proposed iterative technique are joint user and relay beamforming design based on mean-square-error (MSE) while applying the orthogonal matching pursuit (OMP) algorithm to explore the underlying sparsity of the user and relay beamforming matrices. This problem is primarily non-linear and non-convex and hence is difficult to solve. Aiming to find an efficient way to solve for the sparse beamforming matrices, the primal problem is decoupled into three convex sub-problems, and then an iterative algorithm is proposed, which solves for the sparse sub-optimal beamforming matrices, one at a time. The solution to each subproblem aims to minimize MSE, which also minimizes the total MSE, and hence the convergence of the iterative algorithm is guaranteed. Comprehensive simulation is conducted to evaluate the effectiveness of the beamforming design algorithm in terms of the error performance and convergence.

1.6.5 Differential Space-Time Block Coding with Linear constellation Precoding for OFDM Cooperative Networks

Chapter 6 studies the performance of differential space-time codes with linear constellation precoding (LCP) for OFDM cooperative networks over frequency selective channels. Through exploitation of the unitary structure of the orthogonal STBCs, a low complexity differential STBC-LCP-OFDM receiver for cooperative networks is designed. Both single relay and multi-relay scenarios for AF cooperative networks are investigated.

1.6.6 Differential Decoding for SFBC OFDM systems in Underwater MIMO Channels

Chapter 7 investigates the performance of differential space frequency block codes (SFBCs) for OFDM signals over underwater acoustic channels. By applying the unitary structure of the orthogonal SFBCs over the carriers of an OFDM system, the underlying transmit diversity in an underwater acoustic channel is exploited. Differential detection is further applied to eliminate the need for expensive signal processing required for channel tracking. It is assumed that there is sufficient spatial diversity between the channels of the transmitters, and that each channel changes slowly over the carriers, thus satisfying the basic Alamouti coherence requirement. System performance is demonstrated using real data transmitted in the 20−32 kHz acoustic band from a vehicle moving at 0.5−2 m/s and received over a shallow water channel, using 4-QAM and a varying number of carriers ranging from 128 to 2048. Performance results demonstrate the advantage of the differential coherent SFBC

detector over the conventional coherent SFBC detector which suffers from imperfect channel estimation.

Chapter 2

Relay Selection Strategies in Broadband Cooperative Networks

2.1 Introduction

There have been considerable research efforts on the area of cooperative diversity built upon the assumption of frequency flat fading channels (see for example [76–78]). Results have also been reported on relaying schemes for cooperative networks with underlying frequency selective channels [79–87] using OFDM technology. This chapter discusses several relay selection strategies for cooperative SC-FDE with the AF protocol. Both ML-SC-FDE and MMSE-SC-FDE receivers are studied. Novel PEP-based selection criterion for frequency selective channels, referred to as SHARM, is proposed. Several selection strategies for CMMSE-SC-FDE receivers, which are motivated by minimizing the instantaneous error rate, are investigated. These are NBRS, CBRS, SVRS, and EQRS strategies. A novel relay selection strategy is proposed, in which from the effective frequency selective source-relay-destination channel link associated with the selected relay, only the channel tab with highest power is passed to the destination terminal. Additionally, to tackle the multiple relay selection problem considering generic mobile scenarios with moderately fast fading channels, in order to select the near best relay subset within the minimum processing time, the EDA is applied, and a modified EDA for the relay selection problem is formulated. Simulation results show promising performance of EDA with comparable computational complexity.

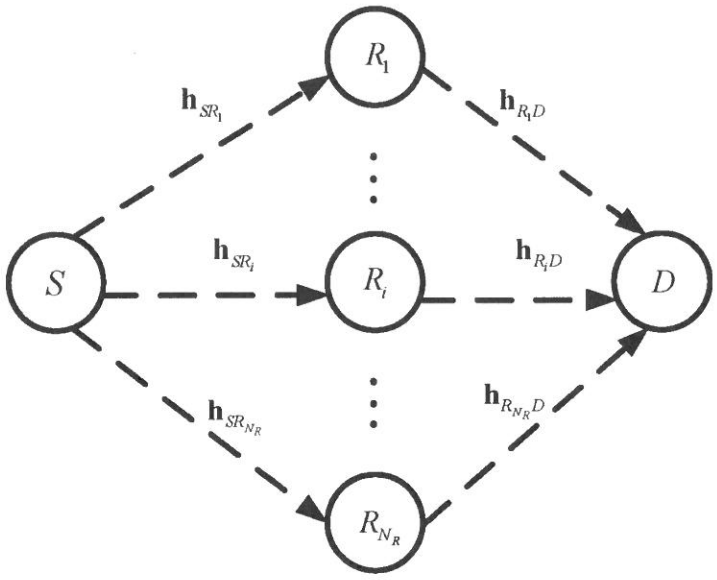

Figure 2.1: Wireless Relay Network.

2.2 System Model

The multiple-relay assisted cooperative wireless communication system under consideration comes with a single source (S), N_R half-duplex relay terminals (R_i), $i = 1, 2, ..., N_R$, and a single destination (D), as depicted in Fig. 2.1. The source, destination, and all relays are equipped with a single antenna which transmits and receives. System performs AF relaying, and adopts the user cooperation protocol proposed by Nabar *et al.* [68]. Specifically, in the broadcasting phase, the source node transmits to the relay nodes and the destination node. In the relaying phase, the relay nodes forward a scaled, noisy version of the received signal to the destination node. The channel impulse responses (CIRs) for $S \rightarrow R_i$, $S \rightarrow D$, and $R_i \rightarrow D$ links for the i^{th} relay terminal in the j^{th} transmission block are given by $\mathbf{h}^j_{SR_i} = \left[h^j_{SR_i}[0], ..., h^j_{SR}[L_{SR_i}]\right]^{\mathrm{T}}$, $\mathbf{h}^j_{SD} = \left[h^j_{SD}[0], ..., h^j_{SD}[L_{SD}]\right]^{\mathrm{T}}$ and $\mathbf{h}^j_{R_iD} = \left[h^j_{R_iD}[0], ..., h^j_{R_iD}[L_{R_iD}]\right]^{\mathrm{T}}$, respectively, where L_{SR_i}, L_{SD}, and L_{R_iD} denote the corresponding channel memory lengths. All channels are assumed to experience frequency selective Rayleigh fading. The random vectors $\mathbf{h}^j_{SR_i}$, $\mathbf{h}^j_{SD}$, and $\mathbf{h}^j_{R_iD}$ are assumed to be

independent zero-mean complex Gaussian with uniform power delay profile vectors.

During broadcasting phase I, the information symbols are parsed to streams of $M \times 1$ blocks $\mathbf{x}$. To remove inter-block interference and make the channel matrix circulant, a CP with length $L_{CP} = L_{SR_i} + L_{R_iD} + 1$ is added between adjacent information blocks. Without loss of generality, the index j in the system model derivations is dropped for brevity. After removing the cyclic prefix, the received block symbol at the i^{th} relay terminal during the broadcasting phase will be given by

$$\mathbf{r}_{R_i} = \sqrt{E_{SR_i}}\mathbf{H}_{SR_i}\mathbf{x} + \mathbf{n}_{R_i}, \tag{2.1}$$

where $\mathbf{n}_{R_i}$ is the additive white Gaussian noise vector with each entry having zero-mean and variance of $N_0/2$ per dimension, E_{SR_i} is the average energy available at the relay terminal R_i which takes into account possibly different path loss and shadowing effects between the $S \rightarrow R_i$ link, and $\mathbf{H}_{SR_i}$ is $N \times N$ circulant matrix with entries $[\mathbf{H}_{SR_i}]_{k,l} = \mathbf{h}_{SR_i}((k-l) \bmod N)$. The relay terminals normalize each entry of the received signal $[\mathbf{r}_{R_i}]_n$, $n = 1, 2, ..., N$ by a factor of $\mathrm{E}\left(|[\mathbf{r}_{R_i}]_n|^2\right) = E_{SR_i} + N_0$ to ensure unit average energy and re-transmit the signal during the relaying phase one at a time. After some mathematical manipulations, the i^{th} relay's received signal at the destination terminal during the second signaling phase is given by

$$\mathbf{r}_i = \sqrt{\frac{E_{R_iD}E_{SR_i}}{E_{SR_i} + N_0}}\mathbf{H}_{R_iD}\mathbf{H}_{SR_i}\mathbf{x} + \tilde{\mathbf{n}}_i, \tag{2.2}$$

where E_{R_iD} is the average energy available at the destination terminal which takes into account possibly different path loss and shadowing effects between the $R_i \rightarrow D$ link, $\mathbf{H}_{R_iD}$ is $N \times N$ circulant matrix with entries $[\mathbf{H}_{R_iD}]_{k,l} = \mathbf{h}_{R_iD}((k-l) \bmod N)$, and each entry of the *effective* noise term $\tilde{\mathbf{n}}_i$ (conditioned on $\mathbf{h}_{R_iD}$) has zero mean and a variance of $\rho_i N_0$ where ρ_i is defined by

$$\rho_i = 1 + \frac{E_{R_iD}}{E_{SR_i} + N_0}\sum_{m=0}^{L_{R_iD}} |\mathbf{h}_{R_iD}(m)|^2. \tag{2.3}$$

The destination terminal normalizes the received signal $\mathbf{r}_{R_i}$ by a factor of $\sqrt{\rho_i}$. This does not affect the SNR, but simplifies the mathematical presentation [68]. After normalization, it follows

$$\mathbf{r}_{D_i} = \sqrt{\gamma_i}\mathbf{H}_{R_iD}\mathbf{H}_{SR_i}\mathbf{x} + \mathbf{n}_i, \tag{2.4}$$

where $\mathbf{n}_i$ is complex Gaussian with zero mean and variance of $N_0/2$ per dimension, and the

scaling coefficient γ_i is defined as

$$\gamma_i = \frac{(E_{SR_i}/N_0)E_{R_iD}}{1 + E_{SR_i}/N_0 \sum_{l_{SR_i}=0}^{L_{SR_i}} |\mathbf{h}_{SR_i}(l_{SR_i})|^2 + E_{R_iD}/N_0 \sum_{l_{R_iD}=0}^{L_{R_iD}} |\mathbf{h}_{R_iD}(l_{R_iD})|^2}. \tag{2.5}$$

Next, by applying the Discrete Fourier Transform (DFT), i.e. multiplying by the $\mathbf{Q}$ matrix, the received signal $\mathbf{r}_{D_i}$ is transformed to the frequency domain, as follows

$$\mathbf{Q}\mathbf{r}_{D_i} = \sqrt{\gamma_i}\mathbf{Q}\mathbf{H}_{R_iD}\mathbf{H}_{SR_i}\mathbf{x} + \mathbf{Q}\mathbf{n}_i. \tag{2.6}$$

Exploiting the circulant structure of the channel matrices $\mathbf{H}_{SR_i}$ and $\mathbf{H}_{R_iD}$, it follows

$$\begin{aligned} \mathbf{H}_{SR_i} &= \mathbf{Q}^{\mathrm{H}}\Lambda_{SR_i}\mathbf{Q}, \\ \mathbf{H}_{R_iD} &= \mathbf{Q}^{\mathrm{H}}\Lambda_{R_iD}\mathbf{Q}, \end{aligned} \tag{2.7}$$

where $\mathbf{\Lambda}_{SR_i}$ and $\mathbf{\Lambda}_{R_iD}$ are diagonal matrices whose (n,n) elements are equal to the n^{th} DFT coefficient of $\mathbf{h}_{SR_i}$ and $\mathbf{h}_{R_iD}$, respectively. Thus, (2.6) can be rewritten as follows

$$\mathbf{Q}\mathbf{r}_{D_i} = \sqrt{\gamma_i}\mathbf{\Lambda_{R_iD}}\mathbf{\Lambda_{SR_i}}\mathbf{Q}\mathbf{x} + \mathbf{Q}\mathbf{n_i}. \tag{2.8}$$

Thus, the input signals to the ML detector are given by

$$\mathbf{r} = \left[\sqrt{\gamma_1}\mathbf{\Lambda_{R_1D}}\mathbf{\Lambda_{SR_1}}, \ldots, \sqrt{\gamma_{N_R}}\mathbf{\Lambda_{R_{N_R}D}}\mathbf{\Lambda_{SR_{N_R}}}\right]^T \mathbf{Q}\mathbf{x} + \mathbf{n}', \tag{2.9}$$

where $\mathbf{n}'$ is zero mean white Gaussian with variance of $N_0/2$ per dimension. Note that the effective SNR of the received signal is

$$\begin{aligned} SNR_{eff} &= \frac{E_{R_iD}E_{SR_i}\sum_{l_{SR_i}=0}^{L_{SR_i}}|\mathbf{h}_{SR_i}(l_{SR_i})|^2 \sum_{l_{R_iD}=0}^{L_{R_iD}}|\mathbf{h}_{R_iD}(l_{R_iD})|^2}{N_0\left(N_0 + E_{SR_i}\sum_{l_{SR_i}=0}^{L_{SR_i}}|\mathbf{h}_{SR_i}(l_{SR_i})|^2 + E_{R_iD}\sum_{l_{R_iD}=0}^{L_{R_iD}}|\mathbf{h}_{R_iD}(l_{R_iD})|^2\right)} \\ &= \frac{\left(SNR_{SR_i}\sum_{l_{SR_i}=0}^{L_{SR_i}}|\mathbf{h}_{SR_i}(l_{SR_i})|^2\right)\left(SNR_{R_iD}\sum_{l_{R_iD}=0}^{L_{R_iD}}|\mathbf{h}_{R_iD}(l_{R_iD})|^2\right)}{1 + SNR_{SR_i}\sum_{l_{SR_i}=0}^{L_{SR_i}}|\mathbf{h}_{SR_i}(l_{SR_i})|^2 + SNR_{R_iD}\sum_{l_{R_iD}=0}^{L_{R_iD}}|\mathbf{h}_{R_iD}(l_{R_iD})|^2} \\ &= \frac{XY}{1+X+Y}, \end{aligned} \tag{2.10}$$

where $SNR_{SR_i} = \frac{E_{SR_i}}{N_0}$, $SNR_{R_iD} = \frac{E_{R_iD}}{N_0}$, $X = SNR_{SR_i}\sum_{l_{SR_i}=0}^{L_{SR_i}}|\mathbf{h}_{SR_i}(l_{SR_i})|^2$ and $Y = SNR_{R_iD}\sum_{l_{R_iD}=0}^{L_{R_iD}}|\mathbf{h}_{R_iD}(l_{R_iD})|^2$. To recover the transmitted symbol $\mathbf{x}$, a receiver is required

to remove the linear transformation caused by $\mathbf{\Lambda}_{R_i D}\mathbf{\Lambda}_{SR_i}$ in (2.8). For this purpose, both ML and MMSE receivers can be applied. Note that the decoding complexity of the ML decoder increases exponentially with the number of relays. On the other hand, the linear receivers, such as MMSE, offer a significant reduction in complexity and thus, they are the practical choice for systems with large numbers of relaying nodes. The following section discusses different selection criteria for ML and MMSE receivers, accordingly.

2.3 Relay Selection Strategies

All strategies mentioned in this section perform calculations assuming full and perfect channel knowledge at the receiver. In the following, the distributed system's overall $NN_R \times N$ channel matrix $\mathbf{\Lambda}$ is defined as follows

$$\mathbf{\Lambda} = \begin{pmatrix} \sqrt{\gamma_1}\mathbf{\Lambda}_{R_1 D}\mathbf{\Lambda}_{SR_1} \\ \vdots \\ \sqrt{\gamma_{N_R}}\mathbf{\Lambda}_{R_{N_R} D}\mathbf{\Lambda}_{SR_{N_R}} \end{pmatrix} \tag{2.11}$$

whereas the $NK \times N$ $\mathbf{\Lambda}^{(K)}$ indicates the sub-channel matrix after applying the relay selection strategy, with K representing the number of the selected index rows from $\mathbf{\Lambda}$, i.e. from the selected relays.

2.3.1 Selection Criteria for ML-SC-FDE receivers

For the optimal ML receiver, the selection criteria should be designed to minimize the symbol error rate union bound. To find the effective selection criteria, one should first find the PEP for the case where all the relays are participating. Considering the ML-SC-FDE receiver, one should use the PEP that determines the probability of erroneously decoding $\mathbf{x}$ when $\hat{\mathbf{x}}$ is transmitted with $\mathbf{x} \neq \hat{\mathbf{x}}$. The distance is given as follows

$$d^2(\mathbf{x}, \hat{\mathbf{x}}) = \sum_{i=1}^{N_R} \gamma_i \sum_{l_{i,\max=0}}^{L_{i,\max}} |\mathbf{h}_{i,\max}(l_{i,\max})|^2 \|(\chi_i - \widehat{\chi_i})\, \mathbf{h}_{i,\min}\|^2, \tag{2.12}$$

where

$$\chi_\mathbf{i} = \begin{bmatrix} [\mathbf{x}]_0 & [\mathbf{x}]_{N-1} & \cdots & [\mathbf{x}]_{N-L_{i,\min}} \\ [\mathbf{x}]_{N-L_{i,\min}} & [\mathbf{x}]_0 & \cdots & [\mathbf{x}]_{N-L_{i,\min}+1} \\ \vdots & \vdots & \cdots & \vdots \\ [\mathbf{x}]_{N-1} & [\mathbf{x}]_{N-2} & \cdots & [\mathbf{x}]_{N-L_{i,\min}-1} \end{bmatrix}, \tag{2.13}$$

$L_{i,max} = \max(L_{SR_i}, L_{R_iD})$, $\mathbf{h}_{i,max}$ is the channel associated with $L_{i,max}$, and accordingly, $L_{i,min} = \min(L_{SR_i}, L_{R_iD})$, and $\mathbf{h}_{i,\min}$ is the channel associated with $L_{i,min}$, $i = 1, \ldots, N_R$. As an example, if $L_{1,\max} = \max(L_{SR_1}, L_{R_1D}) = L_{SR_1}$, then $\mathbf{h}_{1,\max} = \mathbf{h}_{SR_1}$, and similarly, if $L_{1,\min} = \min(L_{SR_1}, L_{R_1D}) = L_{R_1D}$, then $\mathbf{h}_{1,\min} = \mathbf{h}_{R_1D}$. Note that $\mathbf{Q}^H|\mathbf{\Lambda}_i|^2\mathbf{Q} = \mathbf{H}_i\mathbf{H}_i^H$. Using the Chernoff bound and applying it to (2.12), yields

$$P\left(\mathbf{x} \to \hat{\mathbf{x}}|\mathbf{h}_{SR_1}, \ldots, \mathbf{h}_{SR_{N_R}}, \mathbf{h}_{R_1D}, \ldots, \mathbf{h}_{R_{N_R}D}\right) \leq \prod_{i=1}^{N_R} \exp\left(-\frac{\alpha_i}{4N_0}\right), \tag{2.14}$$

where $\alpha_i = \gamma_i \sum_{l_{i,\max}=0}^{L_{i,\max}} |\mathbf{h}_{i,\max}(l_{i,\max})|^2 \|(\chi_i - \widehat{\chi_i})\,\mathbf{h}_{i,\min}\|^2$, $i = 1, \ldots, N_R$. Thus, the unconditional PEP can be expressed as follows

$$P(\mathbf{x} \to \hat{\mathbf{x}}) \leq \prod_{i=1}^{N_R} \iint \exp\left(-\frac{\alpha_i}{4N_0}\right) d\mathbf{h}_{SR_i}\, d\mathbf{h}_{R_iD}. \tag{2.15}$$

Note that $\alpha_i = \gamma_i \sum_{l_{i,\max}=0}^{L_{i,\max}} |\mathbf{h}_{i,\max}(l_{i,\max})|^2 \mathbf{h}_{i,\min}^H \underbrace{(\chi_i - \hat{\chi}_i)^H (\chi_i - \hat{\chi}_i)}_{\chi_i} \mathbf{h}_{i,\min}$, where χ is Hermitian and thus can be decomposed to $\chi_\mathbf{i} = \mathbf{U_i}^H \mathbf{\Delta_i} \mathbf{U_i}$, where $\mathbf{\Delta_i}$ has the Eigen values $\lambda_{l_{i,\min}}$, $l_{i,\min} = 0, \ldots, L_{i,\min}$ on its diagonal. Following that, α_i can be expressed as

$$\alpha_i = \frac{(E_{i,\max}E_{i,\min}/N_0) \underbrace{\sum_{l_{i,\max}}^{L_{i,\max}} |\mathbf{h}_{i,\max}(l_{i,\max})|^2}_{a_i} \sum_{l_{i,\min}}^{L_{i,\min}} \lambda_{l_{i,\min}} \left|\hat{\mathbf{h}}_{i,\min}(l_{i,\min})\right|^2}{1 + (E_{i,\max}/N_0) \underbrace{\sum_{l_{i,\max}=0}^{L_{i,amx}} |\mathbf{h}_{i,\max}(l_{i,\max})|^2}_{a_i} + E_{i,\min}/N_0 \underbrace{\sum_{l_{i,\min}=0}^{L_{i,\min}} |\mathbf{h}_{i,\min}(l_{i,\min})|^2}_{b_i}}, \tag{2.16}$$

where $a_i \sim \Gamma(L_{i,\max} + 1, 1)$, $b_i \sim \Gamma(L_{i,\min} + 1, 1)$, $E_{i,\min}$ and $E_{i,\max}$ are the average energies associated with $\mathbf{h}_{i,\min}$ and $\mathbf{h}_{i,\max}$ correspondingly, and $\hat{\mathbf{h}}_{i,\min} = \mathbf{U}_i\mathbf{h}_{i,\min}$ with same first and second order statistical information as $\mathbf{h}_{i,\min}$ with $\mathbf{U_i}$ being a unitary matrix. Define the ratio $r_i = \frac{a_i}{(E_{i,\max}/N_0)a_i + (E_{i,\min}/N_0)b_i}$ in terms of the two gamma variates a_i and b_i, with density [88]

$$f_{R_i}(r_i) = \frac{(SNR_{i,\min})^{-(L_{i,\min}+1)}}{B(L_{i,\max}+1, L_{i,\min}+1)} r_i^{(L_{i,\max})} (1 - SNR_{i,\max} r_i)^{L_{i,\min}} \left(\frac{1 + (SNR_{i,\min} - SNR_{i,\max})r_i}{SNR_{i,\min}}\right)^{-(L_{i,\max}+L_{i,\min}+2)}, \tag{2.17}$$

where $SNR_{i,\min} = {}^{E_{i,\min}}/_{N_0}$, $SNR_{i,\max} = {}^{E_{i,\max}}/_{N_0}$, and $B(a,b) = \frac{\Gamma(a)\Gamma(b)}{\Gamma(a+b)}$ is the beta function. Accordingly, the unconditional PEP in (2.15) can be rewritten as

$$P(\mathbf{x}\to\hat{\mathbf{x}}) \leqslant \prod_{i=1}^{N_R} \int_0^{\infty} \int_0^{\frac{1}{SNR_{i,\max}}} \exp\left(-\underbrace{\left(\frac{SNR_{i,\max} SNR_{i,\min}}{4} \overbrace{\sum_{l_{i,\min}}^{L_{i,\min}} \lambda_{l_{i,\min}} \mathbf{h}_{i,\min}(l_{i,\min})^2}^{f_i} \right) r_i}_{\Pi_i} \right) p_{r_i} dr_i p_{f_i} df_i,$$

$$\leqslant \prod_{i=1}^{N_R} \frac{(SNR_{i,\min})^{-(L_{i,\min}+1)}}{B(L_{i,\max}+1, L_{i,\min}+1)} \int_0^{\infty} \int_0^{\frac{1}{SNR_{i,\max}}} \exp(-\Pi_i r_i) r_i^{(L_{i,\max})} (1 - SNR_{i,\max} r_i)^{L_{i,\min}} \times \left(\frac{1+(SNR_{i,\min}-SNR_{i,\max})r_i}{SNR_{i,\min}} \right)^{-(L_{i,\max}+L_{i,\min}+2)} dr_i p_{f_i} df_i. \tag{2.18}$$

Table 2.1: List of Notations used in PEP derivations in (2.20)

I:	$1 - SNR_{i,\min} r_i = \frac{SNR_{i,\min} b_i}{SNR_{i,\max} a_i + SNR_{i,\min} b_i} \approx SNR_{i,\min} g_i \frac{a_i}{SNR_{i,\max} a_i + SNR_{i,\min} b_i} \approx SNR_{i,\min} g_i r_i,$
II:	$\frac{1+(SNR_{i,\min}-SNR_{SR_i})r_i}{SNR_{R_iD}} = \frac{a_i+b_i}{SNR_{i,\max} a_i + SNR_{i,\min} b_i} \approx d_i r_i.$

Following notations in Table. 2.1, (2.18) can be expressed as follows

$$\begin{aligned}
P(\mathbf{x}\to\hat{\mathbf{x}}) &\leq \prod_{i=1}^{N_R} \frac{(SNR_{i,\min})^{-(L_{i,\min}+1)} (SNR_{i,\min} g_i)^{L_{i,\min}}}{B(L_{i,\max}+1, L_{i,\min}+1) d_i^{(L_{i,\max}+L_{i,\min}+2)}} \int_0^{\infty} \int_0^{\frac{1}{SNR_{i,\max}}} \exp(-\Pi_i r_i)\, r_i^{-2} dr_i p_{f_i} df \\
&\leq \prod_{i=1}^{N_R} \frac{SNR_{i,\min}^{-1} g_i^{L_{i,\min}}}{B(L_{i,\max}+1, L_{i,\min}+1) d_i^{(L_{i,\max}+L_{i,\min}+2)}} \int_0^{\infty} \Gamma\left(-1, \tfrac{1}{SNR_{i,\max}} \Pi_i\right) \Pi_i p_{f_i} df, \text{ [10, eq.3.381.8]} \\
&\leq \prod_{i=1}^{N_R} \frac{g_i^{L_{i,\min}}}{B(L_{i,\max}+1, L_{i,\min}+1) d_i^{(L_{i,\max}+L_{i,\min}+2)}} \prod_{l_{R_iD}=0}^{L_{R_iD}} \frac{1}{\lambda_{l_{R_iD}}} \int_0^{\infty} f_{l_{R_iD}} \Gamma\left(-1, \tfrac{SNR_{i,\min}}{4} f_{l_{R_iD}}\right) \\
&\times \exp\left(-\lambda_{l_{R_iD}} f_{l_{R_iD}}\right) df_{l_{R_iD}}, \\
&\leq \prod_{i=1}^{N_R} \frac{(SNR_{i,\min})^{-(L_{i,\min}+1)} g_i^{L_{i,\min}}}{B(L_{i,\max}+1, L_{i,\min}+1) d_i^{(L_{i,\max}+L_{i,\min}+2)}} \prod_{l_{R_iD}=0}^{L_{R_iD}} \frac{1}{\lambda_{l_{R_iD}}} {}_2F_1\left(1, 1; 3; \frac{1}{\frac{SNR_{i,\min}\lambda_{l_{R_iD}}}{4}+1}\right), \text{ [10, eq.6.455.1]}
\end{aligned} \tag{2.19}$$

where $g_i = {}^{b_i}/_{a_i}$, $d_i = {}^{(a_i+b_i)}/_{a_i}$, f_i is distributed as $\Gamma\left(L_{R_iD}+1, \sum_{l_{R_iD}=0}^{L_{R_iD}} \kappa_{i,l_{R_iD}}\right)$, and ${}_2F_1(\cdot,\cdot;\cdot;.)$ is the hyper-geometric function [89].

Next, the best multiple relay selection criterion that minimizes the PEP expression can be formulated as in (2.19). Considering (2.19), the upper bound mainly depends on the relaying links' minimum SNRs, i.e. $SNR_{i,\min}$, $i = 1, \ldots, N_R$, as well as the channel powers, which are reflected in the terms $g_i = \frac{\|\mathbf{h}_{i,\min}\|^2}{\|\mathbf{h}_{i,\max}\|^2}$, and $d_i = 1 + \frac{\|\mathbf{h}_{i,\min}\|^2}{\|\mathbf{h}_{i,\max}\|^2}$. Therefore, assuming

average $SNR_{i,\min}$, $i = 1, \ldots, N_R$, the PEP-based best multiple relay selection criterion can be expressed as,

$$r_{SELECTION} = \arg \min_{k=1,\ldots,N_R} \prod_{i=1}^{k} \frac{g_i^{L_{i,\min}}}{B\left(L_{i,\max}+1, L_{i,\min}+1\right) d_i^{L_{i,\max}+L_{i,\min}+2}}. \tag{2.20}$$

Novel PEP-based SHARM Selection Criterion

Assuming similar received average SNR for all relay links, as well as similar channel lengths $L_{i,\min}$ and $L_{i,\max}$ for the underlying relaying links, a novel version of the harmonic mean selection criteria for frequency selective underlying channels (SHARM) can be realized from (20), namely,

$$\begin{aligned} r_{SHARM} &= \arg \min_{k=1,\ldots,N_R} \frac{g_i^{L_{i,\min}}}{d_i^{L_{i,\max}+L_{i,\min}+2}} = \\ &= \arg \min_{k=1,\ldots,N_R} \frac{\left(\frac{\left\|\mathbf{h}_{i,\min}\right\|^2}{\left\|\mathbf{h}_{i,\max}\right\|^2}\right)^{L_{i,\min}}}{\left(1+\frac{\left\|\mathbf{h}_{i,\min}\right\|^2}{\left\|\mathbf{h}_{i,\max}\right\|^2}\right)^{L_{i,\max}+L_{i,\min}+2}}. \end{aligned} \tag{2.21}$$

PEP upper bound for the best K relay selection

This sub-section, derives an upperbound on the PEP when selecting best K relays from the available N_R relays. This method is based on the property that the summation of the largest K out of N_R available numbers is greater than or equal to the average value of the N_R numbers multiplied by K. Refer to Appendix A for the proof. Similarly, having the channel powers ordered as

$$\begin{aligned} \frac{SNR_{SR_1}SNR_{R_1D}\left\|\mathbf{h}_{SR_1}\right\|^2\left\|\mathbf{h}_{R_1D}\right\|^2}{SNR_{SR_1}\left\|\mathbf{h}_{SR_1}\right\|^2+SNR_{R_1D}\left\|\mathbf{h}_{R_1D}\right\|^2} \geqslant \ldots \geqslant \frac{SNR_{SR_K}SNR_{R_KD}\left\|\mathbf{h}_{SR_K}\right\|^2\left\|\mathbf{h}_{R_KD}\right\|^2}{SNR_{SR_K}\left\|\mathbf{h}_{SR_K}\right\|^2+SNR_{R_KD}\left\|\mathbf{h}_{R_KD}\right\|^2} \geqslant \ldots \\ \geqslant \frac{SNR_{SR_{N_R}}SNR_{R_{N_R}D}\left\|\mathbf{h}_{SR_{N_R}}\right\|^2\left\|\mathbf{h}_{R_{N_R}D}\right\|^2}{SNR_{SR_{N_R}}\left\|\mathbf{h}_{SR_{N_R}}\right\|^2+SNR_{R_{N_R}D}\left\|\mathbf{h}_{R_{N_R}D}\right\|^2}, \end{aligned} \tag{2.22}$$

which yields

$$\sum_{i=1}^{K} \frac{SNR_{SR_i}SNR_{R_iD}\|\mathbf{h}_{SR_i}\|^2\|\mathbf{h}_{R_iD}\|^2}{SNR_{SR_i}\|\mathbf{h}_{SR_i}\|^2+SNR_{R_iD}\|\mathbf{h}_{R_iD}\|^2} \geqslant \frac{K}{N_R}\sum_{i=1}^{N_R} \frac{SNR_{SR_i}SNR_{R_iD}\|\mathbf{h}_{SR_i}\|^2\|\mathbf{h}_{R_iD}\|^2}{SNR_{SR_i}\|\mathbf{h}_{SR_i}\|^2+SNR_{R_iD}\|\mathbf{h}_{R_iD}\|^2}, \tag{2.23}$$

leading to

$$\underbrace{\sum_{i=1}^{K} \frac{SNR_{SR_i} SNR_{R_iD} \|\mathbf{h}_{SR_i}\|^2 \|(\chi - \hat{\chi})\, \mathbf{h}_{R_iD}\|^2}{SNR_{SR_i} \|\mathbf{h}_{SR_i}\|^2 + SNR_{R_iD} \|\mathbf{h}_{R_iD}\|^2}}_{d_K^2} \geqslant \frac{K}{N_R} \underbrace{\sum_{i=1}^{N_R} \frac{SNR_{SR_i} SNR_{R_iD} \|\mathbf{h}_{SR_i}\|^2 \|(\chi - \hat{\chi})\, \mathbf{h}_{R_iD}\|^2}{SNR_{SR_i} \|\mathbf{h}_{SR_i}\|^2 + SNR_{R_iD} \|\mathbf{h}_{R_iD}\|^2}}_{d_{N_R}^2}. \tag{2.24}$$

As a result,

$$\exp\left(-\frac{d_K^2}{4}\right) \leq \exp\left(-\frac{K}{N_R}\frac{d_{N_R}^2}{4}\right). \tag{2.25}$$

Applying (2.25) to the bound in (2.14) results in the PEP upper bound, when selecting the best K out of the N_R available relays, as follows,

$$P_K(\mathbf{x} \to \hat{\mathbf{x}}) \leq \left(\frac{K}{N_R}\right)^{-\sum_{i=1}^{N_R}(L_{i,\min}+1)} P_{N_R}(\mathbf{x} \to \hat{\mathbf{x}}). \tag{2.26}$$

2.3.2 Selection Criteria for SC-MMSE receivers

Unlike ML-SC-FDE, it's not easy to find a simple expression for the average error probability. Thus, one can develop different selection criteria based on the instantaneous error probability as follows:

Norm based Relay Selection (NBRS)

This method is inspired by the fact that selection based on maximum norm, maximizes the signal-to-noise ratio and minimizes the instantaneous probability of error [90]. NBRS method can be used because of its low computational complexity, yet, its general drawback is that its effective only for frequency flat or moderately frequency selective channels. NBRS calculates the Frobenius norm of all rows of the channel matrix $\mathbf{\Lambda}$ and selects the subset that maximizes the Frobenius norm. The resulting sub-channel matrix $\mathbf{\Lambda}^{(K)}$ contains K out of N_R rows of the channel matrix $\mathbf{\Lambda}$ such that

$$r_{NBRS} = \arg\max_{\in R} \sum_{r_k=1}^{K} \left\| \sqrt{\lambda_{r_k}} \mathbf{\Lambda}_{r_k D} \mathbf{\Lambda}_{S r_k} \right\|_F. \tag{2.27}$$

As an example, to select a single relay out of four available relays, r_k would be one element from $R = \{1, 2, 3, 4\}$, where if two relays were selected, r_k would be an element of the set $R = \{[1,2], [1,3], [1,4], [2,3], [2,4], [3,4]\}$.

Ergodic Capacity Based Relay Selection (CBRS)

In this strategy, the subset of relays that maximizes the instantaneous mutual information among all possible subsets is selected. Note that the source terminal doesn't have access to the CSI, thus, it distributes the power equally among all subcarriers. Considering frequency selective fading channels, the optimum relay selection is not feasible through CBRS, mainly because for different frequencies, different relay subsets are optimal, as reported in similar studies on antenna subset selection on MIMO channels [91,92]. Since the source node doesn't have access to CSI and only the destination terminal has the perfect channel knowledge, the channel mutual information is formulated as follows,

$$C^{(K)} = \log_2\left(\det\left(\mathbf{I}_{NK} + \frac{1}{KN_o}\mathbf{\Lambda}^{(K)}\left(\mathbf{\Lambda}^{(K)}\right)^H\right)\right), \tag{2.28}$$

and $r_{CBRS} = \arg\max_{\in R} C^{(K)}$, through which the subset of the relays that has maximum mutual information of all the subsets $\mathbf{\Lambda}^{(K)}$ is selected.

Singular Value based Relay Selection (SVRS)

Considering (2.4), the expression for the post-processing SNR of the k^{th} relaying path applying the MMSE equalizer $\mathbf{G}_k = \mathbf{H}_k^H\left[\mathbf{H}_k\mathbf{H}_k^H + N_0\mathbf{I}_N\right]^{-1}$ with $\mathbf{H}_k = \sqrt{\gamma_k}\mathbf{H}_{R_kD}\mathbf{H}_{SR_k}$ is given by

$$SNR_k = \frac{\left\|\mathbf{G}_k\mathbf{H}_k\mathbf{H}_k^H\mathbf{G}_k^H\right\|_F}{\left\|\mathbf{G}_kN_0\mathbf{I}_N\mathbf{G}_k^H\right\|_F}. \tag{2.29}$$

Assuming without loss of generality that the symbols have variance 1, the received SNR can be simplified as follows

$$SNR_k = \frac{\left\|\mathbf{G}_k\mathbf{H}_k\mathbf{H}_k^H\mathbf{G}_k^H\right\|_F}{\left\|\mathbf{G}_kN_0\mathbf{I}_N\mathbf{G}_k^H\right\|_F} \leq \left\|\frac{\mathbf{G}_k\mathbf{H}_k\mathbf{H}_k^H\mathbf{G}_k^H}{\mathbf{G}_kN_0\mathbf{I}_N\mathbf{G}_k^H}\right\|_F = \left\|\frac{\mathbf{G}_k\left[\mathbf{G}_k^{-1}\mathbf{H}_k^H - N_0\mathbf{I}_N\right]\mathbf{G}_k^H}{N_0\mathbf{G}_k\mathbf{G}_k^H}\right\|_F = \left\|\frac{\left[\mathbf{H}_k^H - N_0\mathbf{G}_k\right]\mathbf{G}_k^H}{N_0\mathbf{G}_k\mathbf{G}_k^H}\right\|_F = \left\|\frac{\mathbf{H}_k^H\mathbf{G}_k^H}{N_0\mathbf{G}_k\mathbf{G}_k^H} - \mathbf{I}\right\|_F. \tag{2.30}$$

Note that the minimum post-processing SNR is directly related to the error rate performance and dominates the receiver performance. Having this, to improve the error rate, it is desirable to improve the minimum SNR. Approximating (2.30), yields

$$\begin{aligned} SNR_{\min} &\geq \frac{1}{N_0\lambda_{\max}\left(\left(\mathbf{H}_k\mathbf{H}_k^H + N_0\mathbf{I}_N\right)^{-1}\right)} \\ &\geq \tfrac{1}{N_0}\lambda_{\min}\left(\left(\mathbf{H}_k\mathbf{H}_k^H + N_0\mathbf{I}_N\right)^{-1}\right) \\ &\geq \tfrac{1}{N_0}\lambda_{\min^2}\left(\mathbf{H}_k\right), \end{aligned} \tag{2.31}$$

where $\lambda_{\min}$ denotes the minimum singular value, and $\lambda_{\max}$ denotes the maximum singular value. Note that (2.30) follows from the fact that the highest eigenvalue maximizes the highest diagonal term of a square matrix. (2.31) shows that the performance of linear receiver, as with MMSE, improves as the smallest singular value of the channel $\mathbf{H}_k$ increases.Using this, the smallest eigenvalue of the $\mathbf{\Lambda}^{(K)}\left(\mathbf{\Lambda}^{(K)}\right)^H$, has the highest impact on the performance of linear receivers for the frequency selective channels. Following this method, the subset channel with the maximum minimum eigenvalue is selected as follows,

$$r_{SVRS} = \arg\max_{\in R} \min_{n=1,\ldots,N,\ k=1,\ldots,N_R} \lambda^{(k,n)} \tag{2.32}$$

where $\lambda^{(k,n)}$ is the eigenvalue of the matrix $\mathbf{\Lambda}^{(K)}\left(\mathbf{\Lambda}^{(K)}\right)^H$ for the n^{th} subcarrier.

Note that similar methods based on maximum ratio between the minimum and the maximum singular value were proposed in [93]. This ratio indicates the degree of spread of all the eigen values where lower spread means higher ratio and therefore a better conditioned channel and vice versa. Following this method, the selection metric is as follows,

$$r_{SVRS} = \arg\max_{\in R} \frac{\min\limits_{n=1,\ldots,N,\ k=1,\ldots,N_R} \lambda^{(k,n)}}{\max\limits_{n=1,\ldots,N,\ k=1,\ldots,N_R} \lambda^{(k,n)}}, \tag{2.33}$$

where N stands for the number of the carriers. Note that the computational complexity of this method is slightly higher than the first SVRS method, as it requires the calculation of two singular value and their ratios per frequency tone and subset combination. Note that both the SVRS methods are based solely on the acquired channel knowledge and can be deployed independently from the equalizer, yet, they are both very much sensitive to the channel estimation errors. This sensitivity is even higher for the second SVRS method which is based on the ratio of singular values.

Equalization Quality based Relay Selection (EQRS)

This selection technique is motivated by the fact that the post equalizer signal quality affects the succeeding detector's decisions. note that the major advantage of using the post equalizer signal quality as a metric is that all the possible effects such as synchronization or spatial correlation that can degrade the quality of the equalizer output signal are inherently handled in such way. The typical signal quality metric is the Euclidean distance between the equalizer output symbols $\hat{\mathbf{x}}$ and the known transmit symbols $\mathbf{x}$ which is used as the selection criterion. Note that $|\mathbf{x} - \hat{\mathbf{x}}|^2$ shows the equalizer's abilities, as well as the detector's quality

which in turn affects the selection [94]. Defining the distortion power to be

$$P_{distortion} = E\left\{|\mathbf{x} - \hat{\mathbf{x}}|^2\right\}, \tag{2.34}$$

The selection method can be based on the distortion power (DP) $P_{distortion}$, or the signal to distortion ratio (SDR) defined as follows

$$SDR = \frac{E\left\{|\hat{\mathbf{x}}|^2\right\}}{P_{distortion}}. \tag{2.35}$$

Selection scheme should select the relay that minimizes the distortion power $P_{distortion}$, or maximizes the output SDR.

Note that through this method, the receiver can directly recognize the loss of signal quality and take appropriate actions, i.e. switching to another relay. It should be taken into account that using such a metric requires channel training sequences or pilot symbols to be passed through the equalizer.

Selective to Flat Fading Relay Selection (SFRS)

This sub section proposes a novel relay selection method through which only the relay with the frequency selective source to destination link that acquires the highest norm flat fading channel tab is selected. The selected relay then pre-multiplies and normalizes the received signal from the source node, such that only the highest norm flat fading portion of the transmitted signal is received at the destination terminal.

Consider the circulant channel matrix $\mathbf{H}_k = \mathbf{H}_{R_kD}\mathbf{H}_{SR_k}$ for the k^{th} relaying channel in (2.4). Introducing the circulant flat fading matrices

$$[\mathbf{H}_{SR_kD,l}]_{p,q}, \quad l = 1, ..., L_{SR_k} + L_{R_kD} + 1 \quad = \begin{cases} [\mathbf{H}_{R_kD}\mathbf{H}_{SR_k}]_{p,q} & p - q \bmod N = l \\ 0 & p - q \bmod N \neq l \end{cases} \tag{2.36}$$

only the relay with $\arg \max_{k=1,...,N_R} \max_{l=1,...,L_{SR_k}+L_{R_kD}+1} \|\mathbf{H}_{SR_kD,l}\|_F$ is selected. Assuming that the m^{th} path from the k^{th} relaying channel is selected, the multiplier matrix can be formulated as follows,

$$\mathbf{P} = \mathbf{H}_{R_kD}^{-1}\mathbf{H}_{SR_kD,m}\mathbf{H}_{SR_k}^{-1}. \tag{2.37}$$

In order to have a fair comparison with the other proposed schemes, one can obtain the performance of the proposed receiver assuming an amplifier factor for the relay terminal

that results in the similar SNR as that of (2.4). The SNR associated to (2.4) is as follows

$$SNR_k = \frac{SNR_{SR_k} SNR_{R_k D} \left(\sum_{m=0}^{L_{R_k D}} |\mathbf{h}_{R_k D}(m)|^2 \right)}{1 + SNR_{SR_k} + \left(\sum_{m=0}^{L_{R_k D}} |\mathbf{h}_{R_k D}(m)|^2 \right) SNR_{R_k D}}, \tag{2.38}$$

where $SNR_{SR_k} = E_{SR_k}/N_0$, and $SNR_{R_k D} = E_{R_k D}/N_0$. Assuming that the relay R_k from the k^{th} path applies the amplifier factor A_k, the received signal at the destination node and its corresponding post processing SNR for the proposed method will be as follows

$$\mathbf{r}_{D_k,SFRS} = \sqrt{E_{SR_k} E_{R_k D} A_k} \mathbf{H}_{SR_k D,m} \mathbf{x} + \sqrt{E_{R_k D} A_k} \mathbf{n}_{R_k} + \mathbf{n}_D, \tag{2.39}$$

$$SNR_{K,SFRS} = \frac{E_{SR_K} SNR_{R_K D} A_k \left(\sum_{m=0}^{N} |\mathbf{h}_{SR_K D,l}(m)|^2 \right)}{1 + A_k E_{R_k D} \left(\sum_{m=0}^{L_P} |\mathbf{h}_P(m)|^2 \right)}, \tag{2.40}$$

where $\mathbf{h}_P$ is the vector containing the non-zero elements of the first row or column of the circulant matrix P, L_P is the number of nonzero elements in each row or column of P, and similarly, $\mathbf{h}_{SR_K D,l}$ is the first row or column of the circulant matrix $\mathbf{H}_{SR_k D,m}$ that is associated to the maximum norm flat fading tab. Thus, in order to maintain the post processing $SNR_{K,SFRS}$ in (2.38) similar to SNR_K in (2.36), A_k should be as follows

$$A_k = \frac{SNR_K}{SNR_{R_K D} E_{SR_K} \left(\sum_{m=0}^{N} |\mathbf{h}_{SR_K D,l}(m)|^2 \right) - SNR_K E_{R_k D} \left(\sum_{m=0}^{L_P} |\mathbf{h}_P(m)|^2 \right)}. \tag{2.41}$$

Note that as can be seen from (2.37), the frequency selective fading underlying channel $\mathbf{H}_{R_i D} \mathbf{H}_{SR_i}$ in (2.4), is converted to a flat fading channel $\mathbf{H}_{SR_k D,m}$ using the new selection method. Thus, selection is done from all the underlying flat fading subchannels of their corresponding frequency selective channels of all relaying paths, as follows

$$r_{SFRS} = \arg \max_{k=1,\ldots,N_R} \max_{m=1,\ldots,L_{SR_k}+L_{R_k D}+1} \left\| \mathbf{H}_{SR_k D,m} \right\|_F. \tag{2.42}$$

Note that all the five antenna selection schemes, i.e. NBRS, CBRS, and SVRS, the last two schemes, i.e. EQRS, and proposed SFRS methods use a low rate feedback information from the transmitter to the receiver, and from receiver to the relay node correspondingly, that as will be discussed in the following section, can significantly improve the performance of the open loop selection strategies.

2.4 Multiple relay selection scheme based on EDA

Considering the fast fading nature of the underlying links in the vehicular systems, as the number of the participating relays in the network increases, to satisfy the high data rate requirements, it is necessary to reach the optimal solution within the least processing time. In conventional methods, the best relay subset is selected after evaluating the selection criteria for each possible relay subset. This makes the relay selection problem NP-hard for the cooperative networks with large number of participating relays.

One can obtain the optimal solution using exhaustive search. However, for large number of relays N_R, it is very inefficient. Performance of the heuristic evolutionary algorithms for the multiple relay selection problem in the cooperative networks is sparsely investigated [95], and is reported to achieve near optimal solution. This chapter investigates another evolutionary algorithm, i.e. EDA, for selecting the subset of relays that results in the error performance close to the error performance of the optimal relay subset in the cooperative network.

EDA creates a new population from the probability distribution estimated from previous generations. No significant parameter tuning is required for EDA as compared to other Evolutionary Algorithms (EAs). Our simulations with EDA show that SER performance achieved is significantly improved as compared to the scenario where random selections are performed. The EDA scheme is used to approach the optimal solution much faster and within a smaller number of iterations as compared with the heuristic evolutionary algorithms, which leads to a good system capacity with reduced hardware complexity and undistributed data rate in the cooperative network.

2.4.1 A brief introduction to EDA

Evolutionary algorithms have been often used to solve difficult optimization problems. Candidate solutions to an optimization problem are represented as individuals in the population. In EAs the cost function value of a candidate solution to the optimization problem indicates the fitness of the individual in the concept of natural selection [96]. Unlike other evolutionary algorithms, in EDA, a new population of individuals in each iteration is generated without crossover and mutation operators. Contrary to EAs, in EDA a new population is generated based on a probability distribution, which is estimated from the best selected individuals of previous iteration [97].

In general, conventional EDAs can be characterized by parameters and notations

$$(I_s, F, \Delta_l, \eta_l, \beta_l, p_s, \Gamma, I_{Ter}) \tag{2.43}$$

where

1) I_s is the space of all potential solutions (entire search space of individuals).

2) F denotes a fitness function.

3) Δ_l is the set of individuals (population) at the l^{th} iteration.

4) η_l is the set of best candidate solutions selected from set Δ_l at the l^{th} iteration.

5) Denote $\beta_l \equiv \Delta_l - \eta_l \equiv \Delta_l \cap \eta_l^C$, where η_l^C is the complement of η_l, and $\cap$ stands for the intersection operation.

6) p_s is the selection probability. The EDA algorithm selects $p_s\,|\Delta_l|$ individuals from set Δ_l to make up set η_l, where $|\Delta_l|$ represents the number of individuals in population Δ_l.

7) Γ represents the distribution estimated from Δ_l (the set of selected candidate solutions) at each iteration.

8) I_{Ter} is the number of iterations.

In conventional EDAs, each individual is designated by a binary string of length n (n-dimensional binary vector). The binary row vector $X = (x_1, x_2, \ldots, x_n)$ represents an individual. An EDA maintains a population of individuals in each iteration. Population Δ_l can be specified by the following matrix,

$$\mathbf{X} = \begin{pmatrix} X^1 \\ X^2 \\ \vdots \\ X^{|\Delta_l|} \end{pmatrix} = \begin{pmatrix} x_1^1 & x_2^1 & \vdots & x_n^1 \\ x_1^2 & x_2^2 & \vdots & x_n^2 \\ \ldots & \ldots & \ldots & \ldots \\ x_1^{|\Delta_l|} & x_2^{|\Delta_l|} & \vdots & x_n^{|\Delta_l|}, \end{pmatrix} \tag{2.44}$$

where superscript j in the row vector $X^j = \left(x_1^j, x_2^j, x_3^j, ..., x_n^j\right)$ indexes an individual in the population. A typical EDA is described in the following steps:

Step 0: Generate initial population Δ_0. The initial population ($|\Delta_0|$ individuals) is

typically obtained by sampling according to uniform distribution [97] [1]

$$\begin{aligned} p(\theta_1, \theta_2, \cdots, \theta_n) &= \prod_{i=1}^{n} p_i(\theta_i), \\ \forall i = 1, 2, ..., n, \quad &\text{and } p_i(\theta_i = 1) = p_i(\theta_i = 0) = 0.5 \end{aligned} \tag{2.45}$$

For iterations $l = 1, 2, \ldots$, follow steps 1 through 6.

Step 1: Evaluate the individuals in the current population Δ_{l-1} according to the fitness function F. Sort the candidate solutions (individuals in the current population) according to their fitness orders.

Step 2: If the best candidate solution satisfies the convergence criterion or the number of iterations exceeds its limit I_{Ter}, then terminate; else go to step 3.

Step 3: Select the best $p_s\Delta_{l-1}$ candidate solutions (individuals) from current population Δ_{l-1}. This selection is accomplished according to the sorted candidate solutions.

Step 4: Estimate the probability distribution $p(\theta_1, \theta_2, \cdots, \theta_n)$ on the basis of $|\eta_{l-1}|$ best candidate solutions. Denote this estimation by

$$\Gamma = P(\theta_1, \theta_2, \cdots, \theta_n | \, \eta_{l-1}). \tag{2.46}$$

Step 5: Generate new $|\Delta_l| - |\eta_{l-1}|$ individuals on the basis of this new estimated probability distribution Γ. Replace the bad $|\beta_{l-1}|$ individuals with newly generated $|\Delta_l| - |\eta_{l-1}|$ individuals.

Step 6: Go to step 1 and repeat the steps.

Fig. 2.2 represents the EDA block diagram. In the experimentation, to estimate (2.44), the marginal distributions are estimated separately and the following product form is used,

$$\begin{aligned} \Gamma = p(\theta_1, \theta_2, \cdots, \theta_n | \, \eta_{l-1}) &= \prod_{i=1}^{n} p_i(\theta_i | \, \eta_{l-1}) \\ &= \prod_{i=1}^{n} \left(\frac{\sum_{j=1}^{|\eta_{l-1}|} \delta(x_i^j = \theta_i | \, \eta_{l-1})}{|\eta_{l-1}|} \right) \end{aligned} \tag{2.47}$$

[1] in conventional EDAs, the joint probability distribution from which the initial population is sampled is a product of 'n' univariate marginal probability distributions, each following a Bernoulli distribution with parameter value equal to 0.5. This chapter finally discusses different methods of generating the initial population).

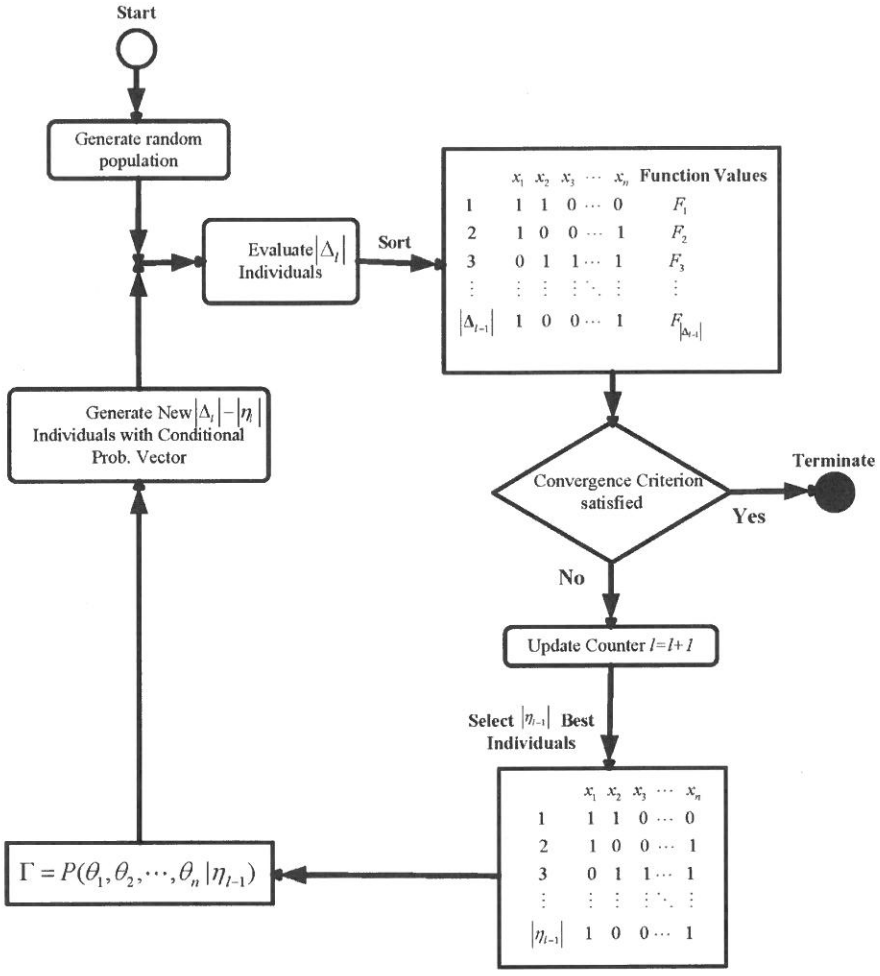

Figure 2.2: EDA block diagram.

where δ is an indicator function and can be expressed as

$$\delta\left(x_i^j = \theta | \eta_{l-1}\right) = \begin{cases} 1 & \text{if } x_i^j = \theta \\ 0 & \text{otherwise} \end{cases} \tag{2.48}$$

Even with this simple application of EDA, the simulation results show that performance of EDA is better than previously proposed algorithms.

Define the optimization problem and the optimization variables as follows:

I. The optimization problem can be the argument of any of the selection criteria previously described, i.e. SHARM, NBRS, CBRS, EQRS, and SFRS, subject to $K \leq \vartheta$, where ϑ stands

for the maximum number of the relays to be selected.[2]

II. Define the binary variables a_i, $i = 1, \ldots, N_R$, corresponding to each and every relay, such that

$$\begin{cases} a_i = 1 & i^{th} \textit{relay is selected} \\ a_i = 0 & \textit{Otherwise} \end{cases} \tag{2.49}$$

Components of the relay selection EDA problem:

A. Individual Representation

Each individual (a candidate solution) is represented by an $1 \times N_R$ vector containing all the binary variables a_i, $i = 1, \ldots, N_R$. For example, Fig. 2.3 illustrates the scenario where $N_R = 5$ and only relays R_1, R_3, and R_5 are selected. The individual is shown in Fig. 2.3.

B. Fitness Function and Constraint Check

It is natural to use the objective function in the optimization problem as the fitness function of the EDA. If a candidate solution (an individual in EDA) does not satisfy the constraint $K \leq \vartheta$, one should disregard that candidate as a valid solution and replace it with a feasible candidate.

Generating the Initial Population:

The initial population is typically constructed randomly such that each component of the individual is assigned 0 or 1 with equal probabilities. Note, however, that the size of the population in EDA is usually much smaller than the size of the entire search space, and thus it is quite likely that a randomly generated initial population may contain no feasible solution or a very small number of feasible solutions. This sub section proposes a novel method to deal with the initial population generation problem, specifically designated for the relay selection problem under consideration:

Subject to the the maximum number of relays to be selected, i.e. ϑ, the initial population includes individuals corresponding to the selection of the relays that would satisfy the argument of any of the selection criteria already discussed. As an example, assuming that SVRS is the selection criteria based on which the initial population individuals are generated, the relay index that maximizes (2.32) is assigned 1 in all individuals inside the initial population. The choice of number of relay indexes that are assigned 1 based on this approach is optional. Next, until the size of the initial population is reached, starting from

[2]The constraint may vary as per the problem formulation.

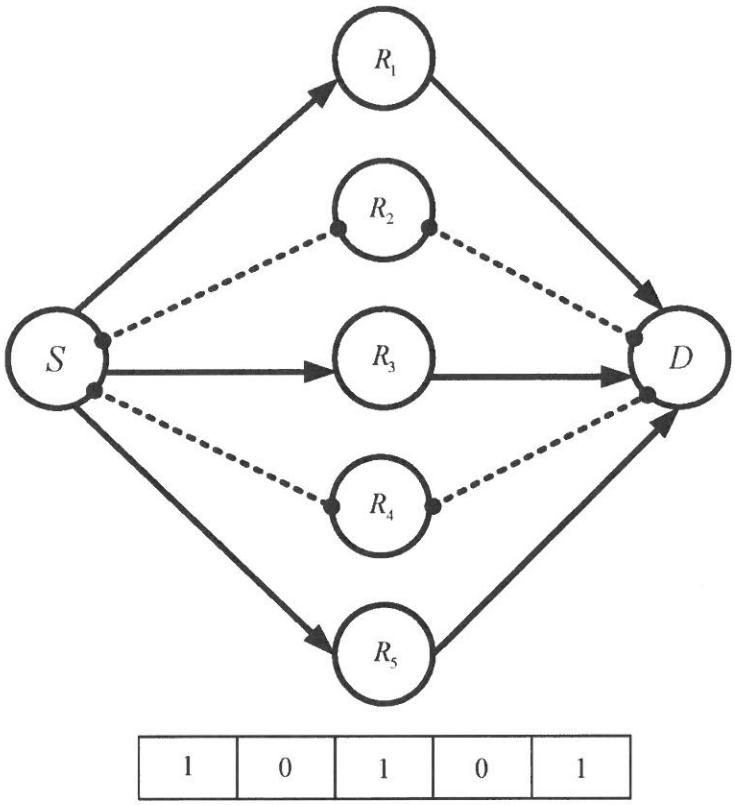

Figure 2.3: Represents the corresponding individual for the scenario where the first, third, and the fifth relays are selected.

two relays, i.e. 1 already assigned to the relay that is selected based on (2.32), 1 is assigned to the rest of the relays in a circular fashion.

2.5 Computational Complexity And Numerical Results

This section presents Monte-Carlo simulation results for different relay selection methods in the multi-relay system assuming a quasi-static Rayleigh fading channel for all the $S \rightarrow R_i$ and $R_i \rightarrow D$, $i = 1, \ldots, N_R$ links. Note that all simulations are performed using MATLAB software on a 3 GHz CPU.

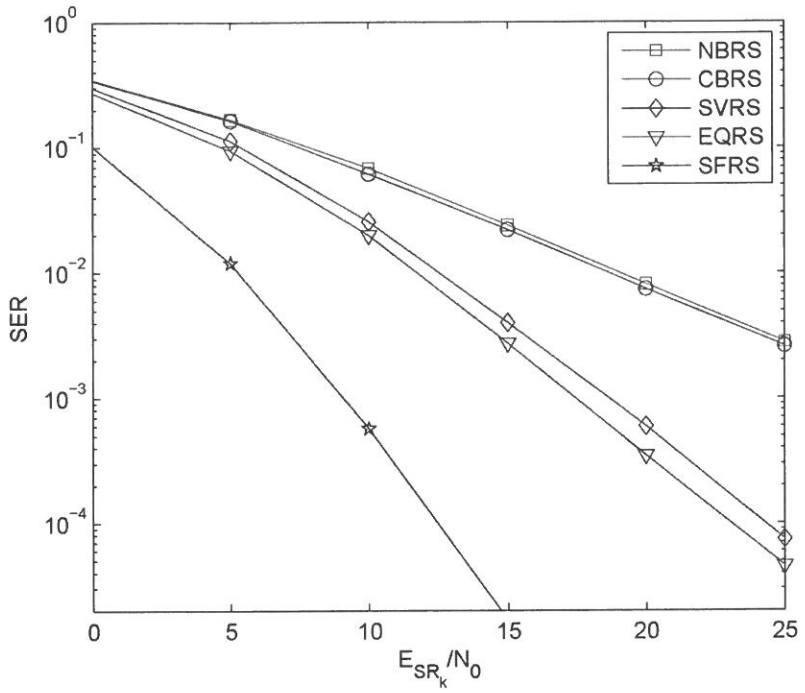

Figure 2.4: Single Relay Selection in a two relay network for SC-MMSE receiver with different selection strategies.

First, we assume that there are two relay nodes, where each node is equipped with one antenna, employing MMSE receiver. We set $E_{R_iD} = 5dB$ and the SER curve is plotted against $\frac{E_{SR}}{N_0} = \frac{E_{SR_1}}{N_0} = \frac{E_{SR_2}}{N_0}$. We further assume that $L_{SR_1} = L_{R_1D} = L_{SR_2} = L_{R_2D} = 1$, N=256 for the symbol block size, and 4-QAM modulation is used. The SER performance of different relay selection schemes for SC-FDE MMSE receiver is studied. As is illustrated in Fig. 2.4, the SER performance of the NBRS and CBRS schemes that is motivated by the receiver input power, is the worst. Moreover, The SVRS and EQRS schemes have almost similar SER performances, and both outperform the NBRS and CBRS methods by i.e. $\sim$ 10 dB at SER = 10^{-3}. The SFRS method provides the best SER performances, and also is the only scheme that extracts full diversity, similar to that of MRC. Note that SFRS outperforms SVRS and EQRS by $\sim$ 10 dB and outperforms CBRS and NBRS by $\sim$ 18 dB at SER = 10^{-3}, which is astonishing.

Fig. 2.5 illustrates the SER performance of different relay selection schemes assuming ML-SC-FDE receiver with $L_{SR_1} = L_{R_1D} = L_{SR_2} = L_{R_2D} = 1$. As can be seen from Fig. 2.5, the selection criteria based on minimization of the average error rate and the

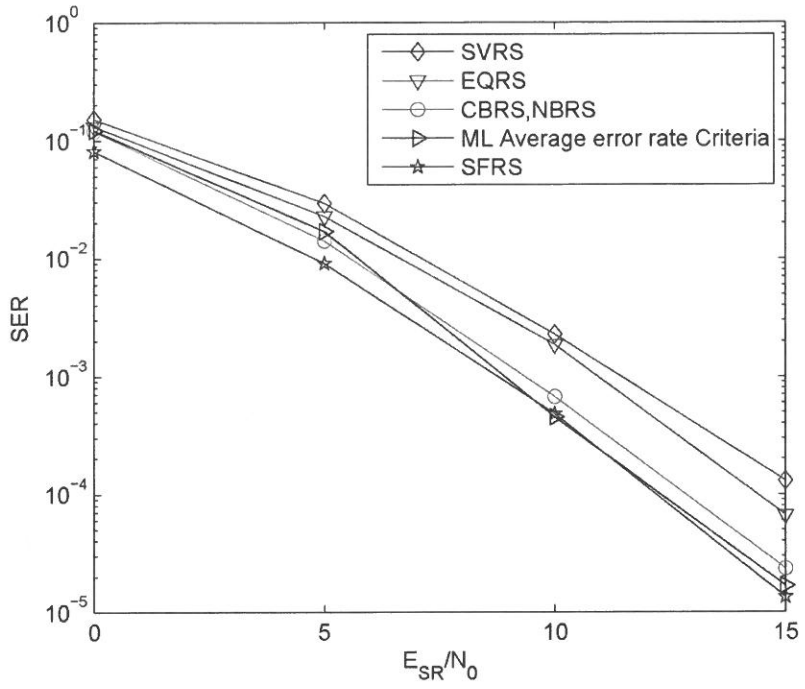

Figure 2.5: Single Relay Selection in a two relay network for ML-SC-FDE receiver with different selection strategies.

proposed method are the most powerful methods. Also, the CBRS and NBRS methods have acceptable performance, i.e. the proposed method outperforms them by only ~ 2 dB at SER $= 10^{-3}$. The SVRS and the EQRS have the worst SER performance, i.e. CBRS and NBRS outperform them by ~ 4 dB at SER $= 10^{-3}$. It can be concluded from the simulation results that regardless of the receiver type, the NBRS and CBRS methods have close SER performances, which are motivated by the receiver input signal power. Similarly, the SVRS and EQRS methods have close SER performances, which are motivated by minimizing the instantaneous SER.

Fig. 2.6 illustrates the SER performance of the SHARM selection scheme with an MMSE receiver implemented. We assume there are two relays and $SNR_{S_{R_i}} = 10$ dB, $i = 1, 2$. We further consider three scenarios:

Scenario I: $L_{SR_1} = L_{SR_2} = 6, L_{R_1D} = L_{R_2D} = 0$

Scenario II: $L_{SR_1} = L_{SR_2} = 5, L_{R_1D} = L_{R_2D} = 1$

Scenario III: $L_{SR_1} = L_{SR_2} = 6, L_{R_1D} = L_{R_2D} = 2$

According to (2.19), the diversity order (DO) for the scenarios I, II, and III should be 2, 4,

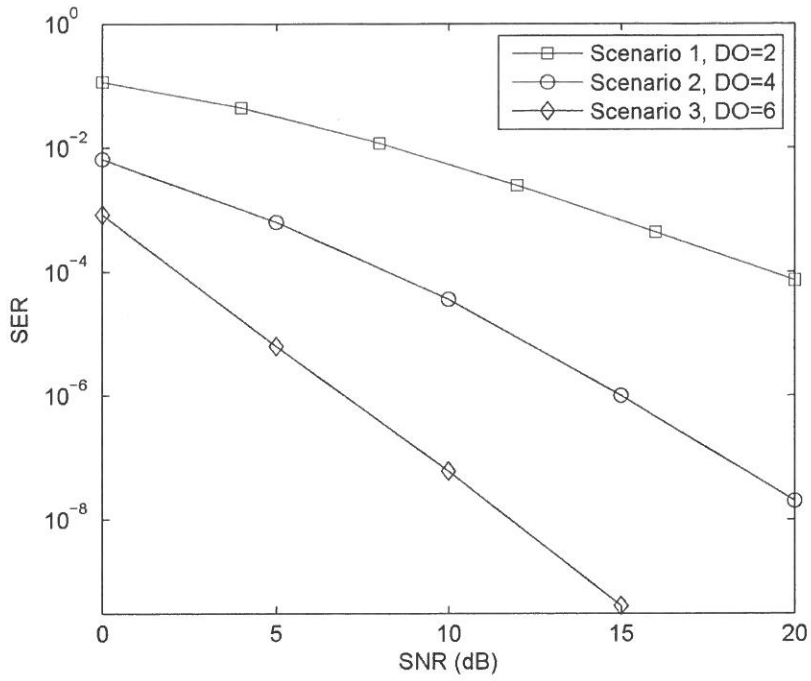

Figure 2.6: Single Relay Selection in a two relay network for SC-MMSE receiver with SHARM selection scheme.

and 6, correspondingly, which agrees with the simulation results. More importantly, even though an MMSE receiver is implemented, full diversity advantages are achieved.

In Fig. 2.7, we evaluate the performance of the proposed EDA method. The initial population is generated based on the SVRS scheme. The CBRS criterion is considered as the fitness function. We further assume 4-PSK modulation, 10 relays, $L_{S_{R_i}} = 5$, $L_{R_iD} = 1$, $i = 1, \ldots, 10$, and assume population size = 11 , i.e. 3% of the overall population, number of best population elements = 4, maximum number of relays to be selected = 4 for the EDA. Since the proposed EDA algorithm searches for the best subset of relays, i.e. maximum 4 number of relays to be selected, the size of the entire search space is equal to $|I_s| = \begin{pmatrix} 10 \\ 1 \end{pmatrix} + \begin{pmatrix} 10 \\ 2 \end{pmatrix} + \begin{pmatrix} 10 \\ 3 \end{pmatrix} + \begin{pmatrix} 10 \\ 4 \end{pmatrix} = 385$. Furthermore, we consider number of iterations $I_{Ter} = 20$. The EDA algorithm was paused at $I_{Ter} = 4, 8$, and the system SER performance was considered for three different scenarios at $I_{Ter} = 4, 8, 20$. SER performance of these three scenarios is compared with the performance of the optimal solution obtained through the exhaustive search algorithm which takes about 514 mili seconds to run. Note

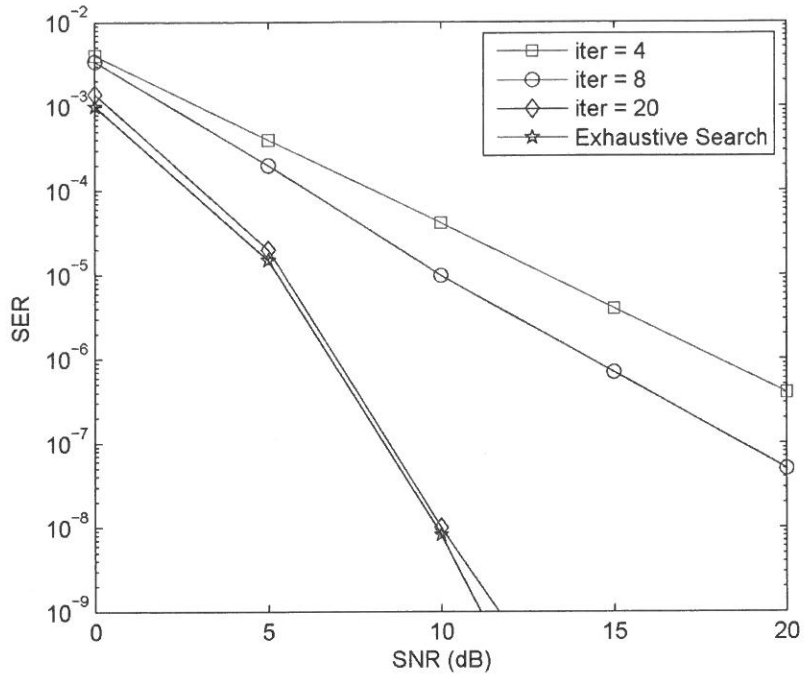

Figure 2.7: Relay Selection with EDA with 10 Relays.

that the average used time of these scenarios as compared with the exhaustive search is equal to 56.5, 113.1, and 293 mili seconds, respectively. As is illustrated in Fig. 2.7, by increasing the iterations, better SER performance is achieved, i.e. ~ 6 dB difference at SER $= 10^{-8}$ between scenarios 2, and 3. It can be seen that scenario 3 with $I_{Ter} = 20$ performs very close to the exhaustive search, while takes about only 0.57% time as compared with the exhaustive search.

Fig. 2.8 evaluates the performance of the proposed EDA scheme for 30 relays, $L_{S_{R_i}} = 2$, $L_{R_iD} = 1$, $i = 1, \ldots, 10$, 4-PSK modulation and assumes population size $= 50$, number of best population elements $= 15$, and maximum number of relays to be selected $= 3$ for the EDA. We consider number of iterations $I_{Ter} = 30$. The EDA algorithm was paused at $I_{Ter} = 1, 10, 20$, and the system SER performance was considered for four different scenarios at $I_{Ter} = 1, 10, 20, 30$. As is illustrated in Fig. 2.8, by increasing the iterations, better SER performance is achieved, i.e. ~ 4 dB difference at SER $= 10^{-7}$ between scenarios 2, and 3. Note that for large number of relays N_R, it is very inefficient to perform exhaustive search.

Fig. 2.9 compares the convergence rate of the proposed EDA scheme for different SNR values versus iteration number. We assume $N_R = 30$, $L_{S_{R_i}} = 2$, $L_{R_iD} = 1$, $i = 1, \ldots, 10$,

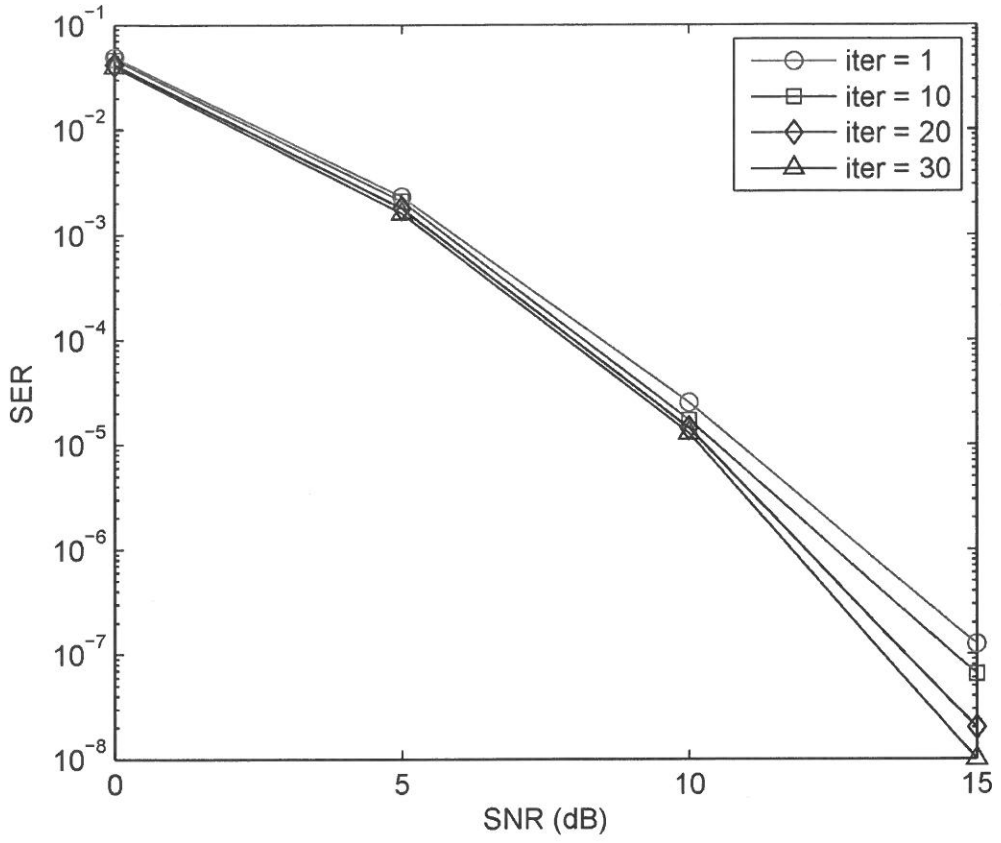

Figure 2.8: Relay Selection with EDA with 30 Relays.

4-PSK modulation and consider population size = 50 , number of best population elements = 15, and maximum number of relays to be selected = 3 for the EDA. As can be seen from Fig. 2.9, the proposed EDA method converges at 24 (1.6959 seconds), 27 (1.9079 s), 23 (1.6252 s), and 24 (1.6959 s) iterations for 0, 5, 10, and 15 dB, respectively.

To measure the computational complexity of the EDA algorithm as compared to the exhaustive search algorithm, we consider the number of complex multiplications and additions. The exhaustive search algorithm needs to compute $\sum_{r_k=1}^{N_{R,\max}} \begin{pmatrix} N_R \\ r_k \end{pmatrix}$ complex determinants in (2.28), with $N_{R,\max}$ being the maximum number of relays to be selected, and N_R being the physical relay terminals available. A matrix determinant can be computed with complexity $O(K^3)$ or better [98]. However, since in (2.28), only the diagonal matrices $\mathbf{\Lambda}(K)$ are involved, each determinant requires $2NK - 1$ complex multiplications only. The EDA

algorithm, on the other hand, needs to compute $|\Delta| I_{Ter}$ determinants. We consider two scenarios:

Scenario I:$[N_R, N_{R,\max}, |\Delta|, I_{Ter}] = [10, 4, 11, 20]$

Scenario II: $[N_R, N_{R,\max}, |\Delta|, I_{Ter}] = [30, 3, 50, 30]$

Note that since EDA selects a different relay subset at each iteration, the number of complex multiplications involved is subjective. Nevertheless, we can provide an upper bound for EDA's computational cost, by assuming that at each iteration, $N_{R,\max}$ number of relays are selected. Following this assumption, in scenario I, ESA requires 665212 complex multiplications, and the EDA algorithm requires maximum number of 450340 complex multiplications. Note that for EDA, we have assumed $I_{Ter} = 20$ which was illustrated in Fig. 2.7 to perform close to the optimal solution. In scenario II, ESA requires 6692435 complex multiplications, and the EDA algorithm requires maximum number of 2302500 complex multiplications. Note that for EDA, we have assumed $I_{Ter} = 30$ which was illustrated in Fig. 2.8 to perform close to the optimal solution. This complexity comparison shows that EDA requires less computational cost as compared to the exhaustive search algorithm. Note that similar complexity analysis can be performed for the rest of selection criteria discussed in Sec. III if chosen as the EDA fitness function.

2.6 Conclusion

This chapter investigates different relay selection methods for the multi-relay SC-FDE broadband cooperative networks with underlying frequency-selective Rayleigh fading channels, assuming both ML and MMSE receivers. Different relay selection criteria for the SC-FDE ML receivers motivated by minimizing the average symbol error rate, are discussed. Similarly, different relay selection schemes for SC-FDE MMSE receivers motivated by minimizing the instantaneous symbols error rate, are investigated. A novel PEP based scheme which is able to fully investigate the underlying multipath diversity, is proposed. Between the relay selection methods provided, the SFRS and the relay selection criteria minimizing the average symbol error rate, have the best SER performance for SC-FDE ML receiver. The proposed analysis is further extended to multiple relay selection scenarios by applying the EDA algorithm. By further defining the EDA parameters specifically for the relay selection problem under consideration, significant performance improvement was shown while maintaining comparable complexity.

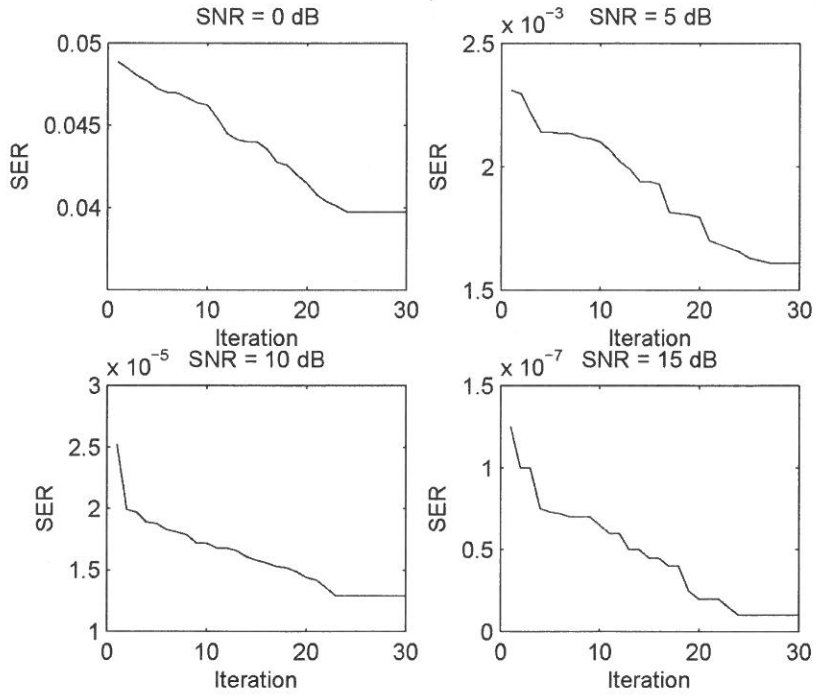

Figure 2.9: Convergence rate of the proposed EDA method

Chapter 3

Relay Selection for Two-Way Multiple Relay Networks

3.1 Introduction

As an alternative to multiple-antenna transmission schemes, recently, it has been demonstrated that "cooperative diversity", provides an effective means of improving power and spectral efficiency in wireless networks [79]. In traditional half-duplex dual-hop cooperative networks, the source and destination nodes require four time-slots to complete both the downlink and uplink transmissions. In TWR protocols, however, only two time slots are needed to complete the downlink and uplink signal transmissions, which improves system's spectral efficiency [99]. In TWR schemes, two sources transmit their corresponding information signals to the intermediate relay terminal, simultaneously. In the second time slot, the relay terminal broadcasts an amplified version of the overlapped messages to the two sources. Since two sources know their own transmitted messages, the back-propagating self-interference can be readily subtracted before decoding. TWR mechanism has proven to not only increase the spectral efficiency, but also to improve the system's overall capacity [100].

There has been recent research efforts on the performance of two-way relay networks employing OFDM over frequency selective channels [101]. However, performance of two-way relay networks for SC-FDE systems is not investigated in the literature to the best of our knowledge. In this chapter, we investigate cooperative SC-FDE for two-way multiple relay networks with selection. We present solid performance analysis for AF MMSE SC-FDE TWR system, by deriving the achievable diversity gain at each end user terminal

using the outage probability method. We prove that for ML SC-FDE TWR systems, the diversity gain at each source terminal is specifically dictated by the minimum of the channel multipath lengths associated with the links between the relay terminal and the two source terminals. We extend our analysis to the multiple relay AF SC-FDE TWR diversity systems with ML decoding and best relay node selection. Furthermore, asymptotic analysis on the average SER reveals that the diversity gain is determined by both the number of participating relay nodes and the minimum of the multipath diversity order experienced in the source to relay, and relay to destination links. We present a novel diversity gain analysis method based on the MGF approach [102], which characterizes the achievable diversity gain without having to evaluate the generally very complex MGF integral. Based on the results from the proposed diversity analysis technique, we introduce the bottleneck integral factor that dictates the diversity bottleneck in the TWR cooperative communication systems and cooperative communication systems, in general. Our diversity results exactly match with the results reported in the literature.

3.2 System Model

We consider a TWR channel, consisting of two source nodes S_1, and S_2 each equipped with a single antenna, and a relay node R. Figures 3.2 and 3.1 compare the schematics of a single-relay TWR system model with that of a typical single-relay cooperative communication system when the two cooperating user terminals attempt to exchange information via the relay terminal. We start our formulations for a TWR cooperative system with a single relay terminal, to get an insight on the achievable performance metrics, and later on extend our analysis to a multi-relay TWR communication system with selection. The channel impulse responses (CIRs) for $S_i \rightarrow R$ and $R \rightarrow S_i$ links for the i^{th} source terminal in the j^{th} transmission block are given by $\mathbf{h}_{S_iR}(j) = \left[h^j_{S_iR}[0], ..., h^j_{S_iR}[L_{S_iR}]\right]^{\mathrm{T}}$ and $\mathbf{h}_{RS_i}(j) = \left[h^j_{RS_i}[0], ..., h^j_{RS_i}[L_{RS_i}]\right]^{\mathrm{T}}$, respectively, where L_{S_iR} and L_{RS_i} denote the corresponding channel memory lengths. The random vectors $\mathbf{h}_{S_iR}$ and $\mathbf{h}_{RS_i}$ are assumed to be independent zero-mean complex Gaussian with uniform power delay profile vectors. The received signal at relay R during the first signaling phase, also known as the multiple access phase, can be expressed as below,

$$\mathbf{r}_R(2n) = \sqrt{E_{S_1R}}\mathbf{H}_{S_1R}(2n)\,\mathbf{x}_1(2n) + \sqrt{E_{S_2R}}\mathbf{H}_{S_2R}(2n)\,\mathbf{x}_2(2n) + \mathbf{n}_R(2n), \tag{3.1}$$

where $\sqrt{E_{S_iR}}$ denotes the average signal power transmitted by the source node S_i, $\mathbf{H}_{S_iR}$ is $N \times N$ circulant matrix with entries $[\mathbf{H}_{S_iR}]_{k,l} = \mathbf{h}_{S_iR}((k-l) \bmod N)$, and $\mathbf{n}_R(2n)$ is the

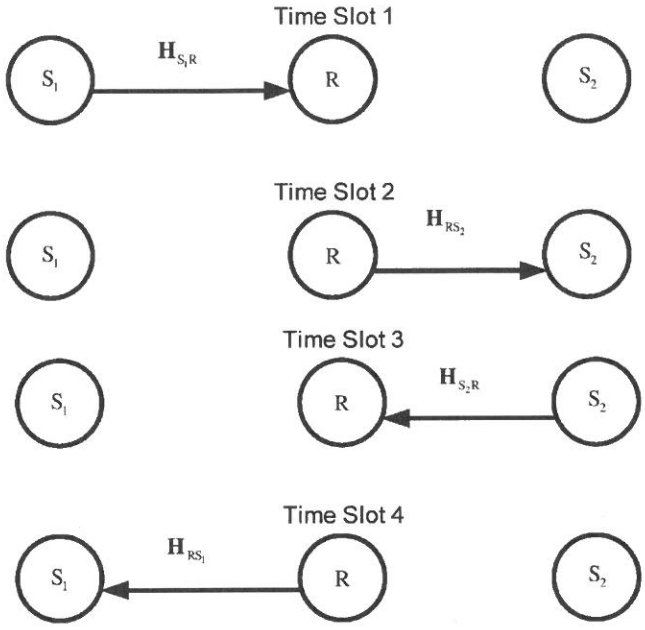

Figure 3.1: Conventional Cooperative SC-FDE System Model.

additive white Gaussian noise vector with each entry having zero-mean and variance of $\sigma^2_{n_R}$. Upon receiving the mixed signal from S_1 and S_2 , R processes it with AF relay operation, also known as linear analogue relaying, and then broadcasts the processed signal to S_1 and S_2 during the second signaling interval. The amplify-and-forwrd factor is given by

$$\alpha = \sqrt{\frac{E_R}{E_{S_1R} \sum_{k=0}^{L_{S_1R}-1} |h_{S_1R,k}|^2 + E_{S_2R} \sum_{k=0}^{L_{S_2R}-1} |h_{S_2R,k}|^2 + \sigma_n^2}}. \tag{3.2}$$

We can assume without loss of generality that the channel reciprocity holds for TWRC during uplink and downlink transmissions, i.e. the channel links $S_i \rightarrow R$ and $R \rightarrow S_i$ during the first and the second signaling intervals are symmetrical. The received signals at S_1 can

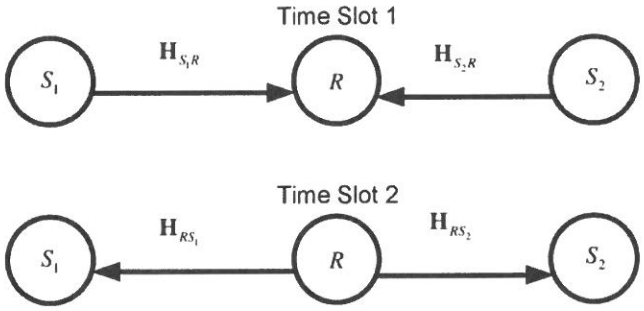

Figure 3.2: TWR-SC-FDE System Model.

be written as,

$$\begin{aligned}\mathbf{y}_R(2n+1) &= \alpha\sqrt{E_{S_1R}}\mathbf{H}_{S_1R}(2n+1)\,\mathbf{H}_{S_1R}(2n)\,\mathbf{x}_1(2n) + \\ &\alpha\sqrt{E_{S_2R}}\mathbf{H}_{S_1R}(2n+1)\,\mathbf{H}_{S_2R}(2n)\,\mathbf{x}_2(2n) + \alpha\mathbf{H}_{S_1R}(2n+1)\,\mathbf{n}_R(2n) + \mathbf{n}_{S_1}(2n+1),\end{aligned} \tag{3.3}$$

where $\mathbf{n}_{S_1}(2n)$ is the additive white Gaussian noise vector with each entry having zero-mean and variance of $\sigma^2_{n_{S_1}}$. Without loss of generality, we will henceforth suppress the subscripts $2n$ and $2n+1$. Note that on the right hand side of (3.2), the first term is the self interference of S_1, while the second term contains the desired message from S_2. Assuming that both $\mathbf{H}_{S_1R}\mathbf{H}_{S_1R}$ and $\mathbf{H}_{S_1R}\mathbf{H}_{S_2R}$ are perfectly known at S_1 via training-based channel estimation prior to data transmission, S_1 can first subtract its self-interference from $\mathbf{y}_{R_1}(2n+1)$ and then coherently demodulate $\mathbf{x}_2(2n)$. The above practice is known as analogue network coding (ANC). Following similar analysis for the received signal at S_2, $\mathbf{y}_{R_2}(2n+1)$, and further subtracting the back-propagating self-interference from $\mathbf{y}_{R_1}(2n+1)$ and $\mathbf{y}_{R_2}(2n+1)$, yields,

$$\mathbf{y}_1 = \alpha\sqrt{E_{S_2R}}\mathbf{H}_{S_1R}\mathbf{H}_{S_2R}\mathbf{x}_2 + \alpha\mathbf{H}_{S_1R}\mathbf{n}_R + \mathbf{n}_{S_1}, \tag{3.4}$$

and similarly,

$$\mathbf{y}_2 = \alpha\sqrt{E_{S_1R}}\mathbf{H}_{S_2R}\mathbf{H}_{S_1R}\mathbf{x}_1 + \alpha\mathbf{H}_{S_2R}\mathbf{n}_R + \mathbf{n}_{S_2}. \tag{3.5}$$

From this point on, we consider the processing performed at the first destination S_1 . Similar analysis is valid for S_2. At S_1, the received signal is transformed to the frequency domain by applying the DFT, i.e. multiplying by the $\mathbf{Q}$ matrix as follows,

$$\mathbf{Q}\mathbf{y}_1 = \alpha\sqrt{E_{S_2R}}\mathbf{Q}\mathbf{H}_{S_1R}\mathbf{H}_{S_2R}\mathbf{x}_2 + \alpha\mathbf{Q}\mathbf{H}_{S_1R}\mathbf{n}_R + \mathbf{Q}\mathbf{n}_{S_1}. \tag{3.6}$$

In here, $\mathbf{Q}$ is the discrete Fourier transform, as written below,

$$\mathbf{Q}(m,n) = \frac{1}{\sqrt{N}} \exp\left[-j\frac{2\pi}{N}(m-1)(n-1)\right], \quad for\ m,n = 1,\ldots,N \tag{3.7}$$

Such that $\mathbf{Q}^H\mathbf{Q} = \mathbf{I}$. Exploiting the circulant structure of the underlying channel matrices we get,

$$\mathbf{Q}\mathbf{y}_1 = \alpha\sqrt{E_{S_2R}}\mathbf{\Lambda}_{S_1R}\mathbf{\Lambda}_{S_2R}\mathbf{Q}\mathbf{x}_2 + \alpha\mathbf{\Lambda}_{S_1R}\mathbf{Q}\mathbf{n}_R + \mathbf{Q}\mathbf{n}_{S_1}, \tag{3.8}$$

Where $\mathbf{H}_{S_1R} = \mathbf{Q}^H\mathbf{\Lambda}_{S_1R}\mathbf{Q}$, and $\mathbf{H}_{S_2R} = \mathbf{Q}^H\mathbf{\Lambda}_{S_2R}\mathbf{Q}$. Note that the diagonal matrix $\mathbf{\Lambda}_i$ contains the N-point DFT of the channel matrix $\mathbf{H}_i$, with the following eigen decomposition, $\mathbf{H}_i = \mathbf{Q}^H\mathbf{\Lambda_i}\mathbf{Q}$. Having said this, the diagonal elements of $\mathbf{\Lambda}_i$ are the channelï£ · s eigen values as explained below,

$$\lambda_n \triangleq \mathbf{\Lambda}(n,n) = \sum_{i=0}^{N-1} \mathbf{h}_i e^{-j\frac{2\pi in}{N}}, \quad for\ \ n = 1,\ldots,N. \tag{3.9}$$

In sections III and IV, we investigate system performance metrics when the FFT-modulated received signal in (3.8) is processed by an MMSE equalizer and an ML equalizer, correspondingly.

3.3 MMSE SC-FDE in TWR Channels

We assume that the received signal in (3.8) is processed by an MMSE equalizer, represented by $\mathbf{W}$, where its output is,

$$\tilde{\mathbf{x}}_2 = \mathbf{W}\mathbf{Q}\mathbf{y}_1 = \alpha\sqrt{E_{S_2R}}\mathbf{W}\mathbf{\Lambda}_{S_1R}\mathbf{\Lambda}_{S_2R}\mathbf{Q}\mathbf{x}_2 + \alpha\mathbf{W}\mathbf{\Lambda}_{S_1R}\mathbf{Q}\mathbf{n}_R + \mathbf{W}\mathbf{Q}\mathbf{n}_{S_1}. \tag{3.10}$$

We start by finding the MMSE linear equalizer for (3.6). Note that the error vector between the filtered received signal $\mathbf{W}\mathbf{y}_1$ and the desired signal is

$$\mathbf{e} = \mathbf{W}\mathbf{Q}\mathbf{y}_1 - x_2. \tag{3.11}$$

We first examine the MSE of the considered system as follows,

$$\begin{aligned} &E\left[\mathbf{e}^H\mathbf{e}\right] = E\left[(\mathbf{W}\mathbf{Q}\mathbf{y}_1 - \mathbf{x}_2)^H(\mathbf{W}\mathbf{Q}\mathbf{y}_1 - \mathbf{x}_2)\right] = E\left[\alpha^2\mathbf{n}_R^H\mathbf{Q}^H\mathbf{\Lambda}_{S_1R}^H\mathbf{W}^H\mathbf{W}\mathbf{\Lambda}_{S_1R}\mathbf{Q}\mathbf{n}_R\right] + \\ &E\left[\alpha^2 E_{S_2R}\mathbf{x}_2^H\mathbf{Q}^H\mathbf{\Lambda}_{S_2R}^H\mathbf{\Lambda}_{S_1R}^H\mathbf{W}^H\mathbf{W}\mathbf{\Lambda}_{S_1R}\mathbf{\Lambda}_{S_2R}\mathbf{Q}\mathbf{x}_2\right] - E\left[\alpha\sqrt{E_{S_2R}}\mathbf{x}_2^H\mathbf{Q}^H\mathbf{\Lambda}_{S_2R}^H\mathbf{\Lambda}_{S_1R}^H\mathbf{W}^H\mathbf{x}_2\right] + \\ &+E\left[\mathbf{n}_{S_1}^H\mathbf{Q}^H\mathbf{W}^H\mathbf{W}\mathbf{Q}\mathbf{n}_{S_1}\right] - E\left[\alpha\sqrt{E_{S_2R}}\mathbf{x}_2^H\mathbf{W}\mathbf{\Lambda}_{S_1R}\mathbf{\Lambda}_{S_2R}\mathbf{Q}\mathbf{x}_2\right] + E\left[\mathbf{x}_2^H\mathbf{x}_2\right]. \end{aligned} \tag{3.12}$$

To simplify (3.12), we use the remarks given in the following lemma.

Lemma 1: Consider the quadratic structure of the form $\mathbf{Q} = \mathbf{s}^H\mathbf{A}\mathbf{s}$, $\mathbf{A} \in \mathcal{C}_{N\times N}, \mathbf{s} = [s_1, \ldots, s_N]^T \in \mathcal{C}_{N\times 1},$, which can be expanded as follows,

$$\begin{aligned}\mathbf{Q} = &\bar{s}_1 A_{11} s_1 + \bar{s}_2 A_{21} s_1 + \cdots + \bar{s}_N A_{N1} s_1 + \\ &\bar{s}_1 A_{12} s_2 + \bar{s}_2 A_{22} s_2 + \cdots + \bar{s}_N A_{N2} s_2 + \\ &\bar{s}_1 A_{13} s_3 + \bar{s}_2 A_{23} s_3 + \cdots + \bar{s}_N A_{N3} s_3 + \\ &\vdots \qquad\qquad \vdots \qquad\qquad \vdots \\ &\bar{s}_1 A_{1N} s_N + \bar{s}_2 A_{2N} s_N + \cdots + \bar{s}_N A_{NN} s_N.\end{aligned} \tag{3.13}$$

With the assumption that the transmitted symbols as well as the noise samples are uncorrelated to each other within a block, the average power of one symbol is σ_s^2 , the average noise power is σ_n^2 , the matrix $\mathbf{A}$ is statistically deterministic, i.e. we can express the expectation values as follows,

$$E\left[\bar{x}_k \mathbf{A}_{kl} x_l\right] = \begin{cases} 0 & k \neq l \\ \sigma_s^2 \mathbf{A}_{kl} & k = l \end{cases}, E\left[\bar{n}_{R,k} \mathbf{A}_{kl} n_{R,k}\right] = E\left[\bar{n}_{S_1,k} \mathbf{A}_{kl} n_{S_1,k}\right] = \begin{cases} 0 & k \neq l \\ \sigma_n^2 \mathbf{A}_{kl} & k = l \end{cases},$$
$$E\left[\bar{x}_k \mathbf{A}_{kl} n_{R,l}\right] = E\left[\bar{x}_k \mathbf{A}_{kl} n_{S_1,l}\right] = 0. \tag{3.14}$$

Using (3.14), we can simplify (3.12) as follows,

$$\begin{aligned}E\left[\mathbf{e}^H\mathbf{e}\right] = &\alpha^2 E_{S_2R}\sigma_s^2 Trace\left\{\mathbf{Q}^H\mathbf{\Lambda}_{S_2R}^H\mathbf{\Lambda}_{S_1R}^H\mathbf{W}^H\mathbf{W}\mathbf{\Lambda}_{S_1R}\mathbf{\Lambda}_{S_2R}\mathbf{Q}\right\} + \sigma_n^2 Trace\left\{\mathbf{Q}^H\mathbf{W}^H\mathbf{W}\mathbf{Q}\right\} \\ &-\alpha\sqrt{E_{S_2R}}\sigma_s^2 Trace\left\{\mathbf{Q}^H\mathbf{\Lambda}_{S_2R}^H\mathbf{\Lambda}_{S_1R}^H\mathbf{W}^H\right\} + \alpha^2\sigma_n^2 Trace\left\{\mathbf{Q}^H\mathbf{\Lambda}_{S_1R}^H\mathbf{W}^H\mathbf{W}\mathbf{\Lambda}_{S_1R}\mathbf{Q}\right\} \\ &-\alpha\sqrt{E_{S_2R}}\sigma_s^2 Trace\left\{\mathbf{W}\mathbf{\Lambda}_{S_1R}\mathbf{\Lambda}_{S_2R}\mathbf{Q}\right\} + \sigma_s^2 N.\end{aligned} \tag{3.15}$$

Note that the trace operator is similarity invariant, i.e. $Tr\left(\mathbf{A}^{-1}\mathbf{X}\mathbf{A}\right) = Tr\left(\mathbf{A}\mathbf{X}\mathbf{A}^{-1}\right) = Tr\left(\mathbf{X}\right)$ [103]. Therefore, (3.14) can be formulated as follows,

$$\begin{aligned}E\left[\mathbf{e}^H\mathbf{e}\right] = &\alpha^2 E_{S_2R}\sigma_s^2 Trace\left\{\mathbf{\Lambda}_{S_2R}^H\mathbf{\Lambda}_{S_1R}^H\mathbf{W}^H\mathbf{W}\mathbf{\Lambda}_{S_1R}\mathbf{\Lambda}_{S_2R}\right\} - \alpha\sqrt{E_{S_2R}}\sigma_s^2 Trace\left\{\mathbf{Q}^H\mathbf{\Lambda}_{S_2R}^H\mathbf{\Lambda}_{S_1R}^H\mathbf{W}^H\right\} \\ &+\sigma_n^2 Trace\left\{\mathbf{W}^H\mathbf{W}\right\} + \alpha^2\sigma_n^2 Trace\left\{\mathbf{\Lambda}_{S_1R}^H\mathbf{W}^H\mathbf{W}\mathbf{\Lambda}_{S_1R}\right\} - \alpha\sqrt{E_{S_2R}}\sigma_s^2 Trace\left\{\mathbf{W}\mathbf{\Lambda}_{S_1R}\mathbf{\Lambda}_{S_2R}\mathbf{Q}\right\} + \sigma_s^2 N.\end{aligned} \tag{3.16}$$

The expectation function can be minimized by taking partial differentiation with respect to $\mathbf{W}$ and setting this derivation to zero. For non-analytical complex function $f\left(\mathbf{X}\right)$, containing $\mathbf{X}^H$ or $\bar{\mathbf{X}}$, the following differentiation rule must be regarded [104],

$$\partial f\left(\mathbf{X}\right) = \frac{\partial f\left(\mathbf{X}\right)}{\partial \mathbf{X}}\partial\mathbf{X} + \frac{\partial f\left(\mathbf{X}\right)}{\partial \bar{\mathbf{X}}}\partial\bar{\mathbf{X}}, \tag{3.17}$$

where f is differentiated with respect to both $\mathbf{X}$ and $\bar{\mathbf{X}}$, i.e. conjugate of vector $\mathbf{X}$. Furthermore, following rules for derivation must be applied [103],

$$\frac{\partial Trace\left(\mathbf{A}\mathbf{X}^H\mathbf{B}\right)}{\partial\bar{\mathbf{X}}} = (\mathbf{B}\mathbf{A})^T \,, \frac{\partial Trace\left(\mathbf{A}\mathbf{X}\mathbf{B}\right)}{\partial\mathbf{X}} = (\mathbf{B}\mathbf{A})^T. \tag{3.18}$$

Therefore, the partial differentiation yields,

$$\frac{\partial}{\partial\mathbf{W}}\left\{E\left[\mathbf{e}^H\mathbf{e}\right]\right\} = \left[\begin{array}{l}\left(\alpha^2 E_{S_2R}\sigma_s^2\mathbf{W}\mathbf{\Lambda}_{S_1R}\mathbf{\Lambda}_{S_2R}\mathbf{\Lambda}_{S_2R}^H\mathbf{\Lambda}_{S_1R}^H + \alpha^2\sigma_n^2\mathbf{W}\mathbf{\Lambda}_{S_1R}\mathbf{\Lambda}_{S_1R}^H + \sigma_n^2\mathbf{W} - \alpha\sqrt{E_{S_2R}}\sigma_s^2\mathbf{Q}^H\mathbf{\Lambda}_{S_2R}^H\mathbf{\Lambda}_{S_1R}^H\right) + \\ \left(\alpha^2 E_{S_2R}\sigma_s^2\mathbf{W}\mathbf{\Lambda}_{S_1R}\mathbf{\Lambda}_{S_2R}\mathbf{\Lambda}_{S_2R}^H\mathbf{\Lambda}_{S_1R}^H + \alpha^2\sigma_n^2\mathbf{W}\mathbf{\Lambda}_{S_1R}\mathbf{\Lambda}_{S_1R}^H + \sigma_n^2\mathbf{W} - \alpha\sqrt{E_{S_2R}}\sigma_s^2\mathbf{Q}^H\mathbf{\Lambda}_{S_2R}^H\mathbf{\Lambda}_{S_1R}^H\right)^H\end{array}\right]^T. \tag{3.19}$$

By setting (3.19) equal to zero, we obtain the optimal MMSE feed forward filter as given below,

$$\mathbf{W} = \alpha\sqrt{E_{S_2R}}\sigma_s^2\mathbf{Q}^H\mathbf{\Lambda}_{S_2R}^H\mathbf{\Lambda}_{S_1R}^H\left(\alpha^2 E_{S_2R}\sigma_s^2\mathbf{\Lambda}_{S_1R}\mathbf{\Lambda}_{S_2R}\mathbf{\Lambda}_{S_2R}^H\mathbf{\Lambda}_{S_1R}^H + \alpha^2\sigma_n^2\mathbf{\Lambda}_{S_1R}\mathbf{\Lambda}_{S_1R}^H + \sigma_n^2\mathbf{I}\right)^{-1}. \tag{3.20}$$

Note that the expression given for $\mathbf{W}$ in (3.19) is equal to,

$$\mathbf{W} = \alpha^{-1}(E_{S_2R})^{-\frac{1}{2}}\mathbf{Q}^H\left(\mathbf{\Lambda}_{S_1R}\mathbf{\Lambda}_{S_2R}\right)^H\left[\mathbf{R}_{\mathbf{x}_2}^{-1} + \mathbf{R}_\nu^{-1}\mathbf{\Lambda}_{S_1R}\mathbf{\Lambda}_{S_2R}\left(\mathbf{\Lambda}_{S_1R}\mathbf{\Lambda}_{S_2R}\right)^H\right]^{-1}\mathbf{R}_\nu^{-1}, \tag{3.21}$$

where, $\nu = \alpha\mathbf{\Lambda}_{S_1R}\mathbf{Q}\mathbf{n}_R + \mathbf{Q}\mathbf{n}_{S_1}$, and $\mathbf{R}_\upsilon = E\left[\upsilon\upsilon^H\right] = \sigma_n^2\left(\alpha^2\mathbf{\Lambda}_{S_1R}\mathbf{\Lambda}_{S_1R}^H + \mathbf{I}\right)$. Next, in order to characterize the effective noise covariance matrix, combining (3.10) and (3.12), we revisit the effective noise term as formulated below,

$$\mathbf{e} = \left(\sqrt{E_{S_2R}}\mathbf{W}\mathbf{\Lambda}_{S_1R}\mathbf{\Lambda}_{S_2R}\mathbf{Q} - \mathbf{I}\right)\mathbf{x}_2 + \mathbf{W}\mathbf{\Lambda}_{S_1R}\mathbf{Q}\mathbf{n}_R + \mathbf{W}\mathbf{Q}\mathbf{n}_{S_1}, \tag{3.22}$$

Which accounts for the combined effect of the channel noise and the ISI residual due to MMSE interference suppression. Due to the MMSE orthogonality principal, we have

$$\mathbf{R}_\mathbf{e} = E\left[\left(\mathbf{x}_2 - \tilde{\mathbf{x}}_2\right)\left(\mathbf{x}_2 - \tilde{\mathbf{x}}_2\right)^H\right] = E\left[\left(\mathbf{x}_2 - \tilde{\mathbf{x}}_2\right)\mathbf{x}_2^H\right] - E\left[\left(\mathbf{x}_2 - \tilde{\mathbf{x}}_2\right)\tilde{\mathbf{x}}_2^H\right] = E\left[\left(\mathbf{x}_2 - \tilde{\mathbf{x}}_2\right)\mathbf{x}_2^H\right], \tag{3.23}$$

which reduces the MSE to the following form,

$$\begin{aligned}
\mathbf{R_e} &= E\left[\left(\mathbf{x}_2 - \left(\alpha\sqrt{E_{S_2R}}\mathbf{W}\mathbf{\Lambda}_{S_1R}\mathbf{\Lambda}_{S_2R}\mathbf{Q}\mathbf{x}_2 + \alpha\mathbf{W}\mathbf{\Lambda}_{S_1R}\mathbf{Q}\mathbf{n}_R + \mathbf{W}\mathbf{Q}\mathbf{n}_{S_1}\right)\right)\mathbf{x}_2^H\right] \\
&= \frac{1}{\alpha^2 E_{S_2R}}\mathbf{R}_{\mathbf{x}_2} - \underbrace{\alpha^{-1}(E_{S_2R})^{-\frac{1}{2}}\mathbf{Q}^H(\mathbf{\Lambda}_{S_1R}\mathbf{\Lambda}_{S_2R})^H\left[\mathbf{R}_{\mathbf{x}_2}^{-1} + \mathbf{R}_\nu^{-1}\mathbf{\Lambda}_{S_1R}\mathbf{\Lambda}_{S_2R}(\mathbf{\Lambda}_{S_1R}\mathbf{\Lambda}_{S_2R})^H\right]^{-1}\mathbf{R}_\nu^{-1}}_{\mathbf{W}} \\
&E\left[\left(\alpha\sqrt{E_{S_2R}}\mathbf{\Lambda}_{S_1R}\mathbf{\Lambda}_{S_2R}\mathbf{Q}\mathbf{x}_2 + \alpha\mathbf{\Lambda}_{S_1R}\mathbf{Q}\mathbf{n}_R + \mathbf{Q}\mathbf{n}_{S_1}\right)\mathbf{x}_2^H\right] = \\
&\frac{1}{\alpha^2 E_{S_2R}}\mathbf{Q}^H\left[\mathbf{R}_{\mathbf{x}_2} - (\mathbf{\Lambda}_{S_1R}\mathbf{\Lambda}_{S_2R})^H\left[\mathbf{R}_{\mathbf{x}_2}^{-1} + \mathbf{R}_\nu^{-1}\mathbf{\Lambda}_{S_1R}\mathbf{\Lambda}_{S_2R}(\mathbf{\Lambda}_{S_1R}\mathbf{\Lambda}_{S_2R})^H\right]^{-1}\mathbf{R}_\nu^{-1}\mathbf{\Lambda}_{S_1R}\mathbf{\Lambda}_{S_2R}\mathbf{R}_{\mathbf{x}_2}\right]\mathbf{Q}
\end{aligned} \tag{3.24}$$

From matrix theory we have,

$$(\mathbf{E} + \mathbf{BCD})^{-1} = \mathbf{E}^{-1} - \mathbf{E}^{-1}\mathbf{B}\left(\mathbf{DE}^{-1}\mathbf{B} + \mathbf{C}^{-1}\right)^{-1}\mathbf{DE}^{-1}. \tag{3.25}$$

Applying (3.25) on $\left[\mathbf{R}_{\mathbf{x}_2}^{-1} + \mathbf{R}_{\mathbf{x}_2}^{-1}\mathbf{R}_{\mathbf{x}_2}\mathbf{R}_\nu^{-1}\mathbf{\Lambda}_{S_1R}\mathbf{\Lambda}_{S_2R}\left(\mathbf{\Lambda}_{S_1R}\mathbf{\Lambda}_{S_2R}\right)^H\right]^{-1}$, using $\mathbf{R}_{\mathbf{x}_2}^{-1} = \mathbf{E}, \mathbf{C} = \mathbf{R}_{\mathbf{x}_2}, \mathbf{B} = \mathbf{R}_{\mathbf{x}_2}^{-1}, \mathbf{D} = \mathbf{R}_\nu^{-1}\mathbf{\Lambda}_{S_1R}\mathbf{\Lambda}_{S_2R}\left(\mathbf{\Lambda}_{S_1R}\mathbf{\Lambda}_{S_2R}\right)^H$ we get,

$$\begin{aligned}
&\mathbf{R_e} = \\
&\frac{1}{\alpha^2 E_{S_2R}}\mathbf{Q}^H\left[\frac{\left(\alpha^2\mathbf{\Lambda}_{S_1R}\mathbf{\Lambda}_{S_1R}^H + \mathbf{I}\right)}{\alpha^2 E_{S_2R}\sigma_s^2} + \frac{1}{\sigma_n^2}\mathbf{\Lambda}_{S_1R}\mathbf{\Lambda}_{S_2R}(\mathbf{\Lambda}_{S_1R}\mathbf{\Lambda}_{S_2R})^H\right]^{-1}\mathbf{Q}\mathbf{Q}^H\left(\alpha^2\mathbf{\Lambda}_{S_1R}\mathbf{\Lambda}_{S_1R}^H + \mathbf{I}\right)\mathbf{Q}.
\end{aligned} \tag{3.26}$$

3.4 received SINR and diversity analysis

Note that due to the underlying symmetry, the diagonal elements of $\mathbf{R}(\mathbf{e})$ are identical. Following (3.10), we have

$$\tilde{\mathbf{x}}_2 = \alpha\sqrt{E_{S_2R}}\mathcal{D}\left\{\mathbf{W}\mathbf{\Lambda}_{S_1R}\mathbf{\Lambda}_{S_2R}\mathbf{Q}\mathbf{x}_2\right\} + \underbrace{\alpha\sqrt{E_{S_2R}}\bar{\mathcal{D}}\left\{\mathbf{W}\mathbf{\Lambda}_{S_1R}\mathbf{\Lambda}_{S_2R}\mathbf{Q}\mathbf{x}_2\right\}}_{\text{Interference}} + \underbrace{\alpha\mathbf{W}\mathbf{\Lambda}_{S_1R}\mathbf{Q}\mathbf{n}_R + \mathbf{W}\mathbf{Q}\mathbf{n}_{S_1}}_{\text{Noise}}, \tag{3.27}$$

where the functions $\mathcal{D}\{\cdot\}$ and $\bar{\mathcal{D}}\{\cdot\}$, operating on an arbitrary square matrix $\mathbf{S}$ with $(m,n)^{th}$ entry s_{mn}, are defined as follows,

$$\mathcal{D}\{\mathbf{S}\} = \begin{bmatrix} s_{11} & 0 & \cdots & 0 \\ 0 & s_{22} & \ldots & \vdots \\ \vdots & \vdots & \ddots & 0 \\ 0 & \ldots & 0 & s_{nn} \end{bmatrix}, \tag{3.28a}$$

$$\bar{\mathcal{D}}\{\mathbf{S}\} = \begin{bmatrix} 0 & s_{12} & \cdots & s_{1n} \\ s_{21} & 0 & \cdots & \vdots \\ \vdots & \vdots & \ddots & s_{(n-1)n} \\ s_{n1} & \cdots & s_{n(n-1)} & 0 \end{bmatrix}. \tag{3.28b}$$

It can be seen from (3.27) that the n^{th} decision value consists of the desired signal, interference from other symbols, and noise components. The unbiased decision-point SINR of MMSE SC-FDE for detecting symbol $n, 1 \leqslant n \leqslant N$ is

$$SINR_n^{MMSE} = \frac{\sigma_s^2}{\mathbf{R}_e(n,n)} - 1, \tag{3.29}$$

where the -1 term is to account for the bias [105]. Due to the underlying symmetry, the diagonal elements of $\mathbf{R}_e$ are identical. Therefore, the conditional instantaneous output SINR for detecting $\mathbf{x}_2(n)$, $1 \leqslant n \leqslant N$, can be expressed as follows,

$$\begin{aligned} SINR^{MMSE}_{\mathbf{h}_{S_1R},\mathbf{h}_{S_2R}} &= \frac{1}{\frac{1}{N}Trace\left\{\frac{\alpha^2\mathbf{\Lambda}_{S_1R}\mathbf{\Lambda}_{S_1R}^H+\mathbf{I}}{\left(\alpha^2\mathbf{\Lambda}_{S_1R}\mathbf{\Lambda}_{S_1R}^H+\mathbf{I}\right)+\frac{\alpha^2E_{S_2R}\sigma_s^2}{\sigma_n^2}\mathbf{\Lambda}_{S_1R}\mathbf{\Lambda}_{S_2R}\left(\mathbf{\Lambda}_{S_1R}\mathbf{\Lambda}_{S_2R}\right)^H}\right\}} - 1 \\ &= \frac{1}{\underbrace{\frac{1}{N}\sum_{n=1}^{N}\frac{\left(\alpha^2|\lambda_{S_1R,n}|^2+1\right)}{\left(\alpha^2|\lambda_{S_1R,n}|^2+1\right)+\frac{\alpha^2E_{S_2R}\sigma_s^2}{\sigma_n^2}|\lambda_{S_1R,n}|^2|\lambda_{S_2R,n}|^2}}_{\omega}} - 1 = \frac{1}{\frac{1}{N}\sum_{n=1}^{N}Y_n} - 1. \end{aligned} \tag{3.30}$$

Note that $SINR^{MMSE}_{\mathbf{h}_{S_1R},\mathbf{h}_{S_2R}}$ doesn't depend on n and therefore is the same for all information streams. Moreover, the numerator and denominator in ω are not statistically independent. Otherwise, deriving the underlying distribution for $SINR^{MMSE}_{\mathbf{h}_{S_1R},\mathbf{h}_{S_2R}}$ would have been much simpler, and in fact, the average received $SINR^{MMSE}_{\mathbf{h}_{S_1R},\mathbf{h}_{S_2R}}$ with MMSE equalizer would have been exactly equal to the received average SNR with ML detector, as we will see in the next section.

Note that in the practical SINR region, Y_n can be approximated as follows,

$$Y_n \approx \frac{|\lambda_{S_1R,n}|^2}{|\lambda_{S_1R,n}|^2+\frac{E_{S_2R}\sigma_s^2}{\sigma_n^2}|\lambda_{S_1R,n}|^2|\lambda_{S_2R,n}|^2} = \frac{1}{1+\Upsilon|\lambda_{S_2R,n}|^2}, \tag{3.31}$$

where $\Upsilon = \frac{E_{S_2R}\sigma_s^2}{\sigma_n^2}$. Note that when $N = L_{S_2R}$, the eigenvalues of $\mathbf{\Lambda}_{S_2R}\mathbf{\Lambda}_{S_2R}^H$, i.e. $|\lambda_{S_2R,n}|^2$, are distributed according to exponential distribution. For $N > L_{S_2R}$, however, the Gaussian variables $\{\lambda_{S_2R,n}\}$ are no longer independent, and distribution of $|\lambda_{S_2R,n}|^2$ is unknown. To

derive the achievable diversity order by the MMSE SC-FDE TWR system, we can follow the outage probability method proposed in [102].

Due to the equalizer structure, the effective mutual information between $\mathbf{x}_2$ and $\tilde{\mathbf{x}}_2$ is equal to the sum of mutual information of their sub-streams,

$$I\left(\mathbf{x}_2;\tilde{\mathbf{x}}_2\right)=\frac{1}{N}\sum_{l=1}^{N}I\left(\mathbf{x}_{2,l};\tilde{\mathbf{x}}_{2,l}\right). \tag{3.32}$$

The outage probability of the MMSE receiver is given by

$$\begin{aligned}P_{out}&=P\left(I\left(\mathbf{x}_2;\tilde{\mathbf{x}}_2\right)<R\right)=P\left(\frac{1}{N}\sum_{n=1}^{N}\log\left(1+SINR^{MMSE}_{\mathbf{h}_{S_1R},\mathbf{h}_{S_2R}}\right)<R\right)\\&=P\left(-\log\left(\frac{1}{N}\sum_{n=1}^{N}Y_n\right)<R\right)=P\left(-\log\left(\frac{1}{N}\sum_{n=1}^{N}\frac{1}{1+\Upsilon\left|\lambda_{S_2R,n}\right|^2}\right)<R\right)\\&=P\left(\frac{1}{N}\sum_{n=1}^{N}\frac{1}{1+\Upsilon\left|\lambda_{S_2R,n}\right|^2}>2^{-R}\right).\end{aligned} \tag{3.33}$$

Define

$$\alpha_n\triangleq-\frac{\log\lambda_{S_2R,n}}{\log\Upsilon},\text{for}n=1,\ldots,N. \tag{3.34}$$

Based on (3.34), we can write the exponential equality

$$\frac{1}{1+\Upsilon\lambda_{S_2R,n}}\doteq\begin{cases}\Upsilon^{\alpha_n-1} & \alpha_n<1\\ 1 & \alpha_n>1.\end{cases} \tag{3.35}$$

Define $\alpha=\begin{bmatrix}\alpha_1 & \ldots & \alpha_N\end{bmatrix}$ and a new random variable

$$M\left(\alpha\right)\triangleq\sum_{\alpha_n>1}1. \tag{3.36}$$

(3.36) is mainly due to the fact that at high SNR regime, $\frac{1}{1+\Upsilon\lambda_{S_2R,n}}$ is either 0 or 1. Hence, to characterize $\sum_{n=1}^{N}\frac{1}{1+\Upsilon\left|\lambda_{S_2R,n}\right|^2}$ at high SNR regime, we only need to count the ones. Hence, the outage probability can be written as

$$P_{out}=P\left(\sum_{n=1}^{N}\frac{1}{1+\Upsilon\left|\lambda_{S_2R,n}\right|^2}>N2^{-R}\right)\doteq P\left(M\left(\alpha\right)>N2^{-R}\right). \tag{3.37}$$

For $N=L_{S_2R}$, we can evaluate $P\left(\alpha_n>1\right)$. The probability density function of $\left|\lambda_{S_2R,n}\right|^2$ is

$$f_{\left|\lambda_{S_2R,n}\right|^2}\left(x\right)=e^{-x}. \tag{3.38}$$

The probability density function and cumulative distribution function of α_n are therefore, given by

$$f_{\alpha_n}\left(x\right)=\Upsilon^{-x}e^{\Upsilon^{-x}}\ln\frac{1}{\Upsilon}, \tag{3.39a}$$

$$F_{\alpha_n}(x) = \int_{-\infty}^{x} f_{\alpha_n}(y)\,dy = \int_{\Upsilon^{-x}}^{\infty} e^{-r}dr = \int_{0}^{\infty} e^{-r}dr - \int_{0}^{\Upsilon^{-x}} e^{-r}dr = e^{-\Upsilon^{-x}}. \quad (3.39b)$$

Hence, $P(\alpha_n > 1) \doteq 1 - e^{-\Upsilon^{-1}} \doteq \Upsilon^{-1}$. Note that both $\{\lambda_{S_2R,n}\}$ and $\{\alpha_n\}$ are statistically independent, and as a result, $M(\alpha)$ is binomially distributed, and its binomial parameter is asymptotically equal to Υ^{-1}. As a result,

$$\begin{aligned} &P\left(\sum_{n=1}^{N} \frac{1}{1+\Upsilon|\lambda_{S_2R,n}|^2} > N2^{-R}\right) \doteq P\left(M(\alpha) > N2^{-R}\right) \\ &= \sum_{i=\lfloor N2^{-R}\rfloor+1}^{N} P(M(\alpha) = i) \doteq \sum_{i=\lfloor N2^{-R}\rfloor+1}^{N} \binom{N}{i} \Upsilon^{-i}(1-\Upsilon^{-1})^{N-i} \\ &\doteq \Upsilon^{-(\lfloor N2^{-R}\rfloor+1)}. \end{aligned} \quad (3.40)$$

Following (3.40), we can conclude that with $N = L_{S_2R}$, the achievable diversity order at user 1 is $(\lfloor N2^{-R} \rfloor + 1)$. Following similar steps as in [102], we can prove that for a system with block length $N_1 > L_{S_2R}$ and the other with $N_2 > N_1$, we have

$$P\left(\sum_{n=1}^{N_1} \frac{1}{1+\Upsilon|\lambda_{S_2R,n}|^2} > m\right) \doteq P\left(\sum_{n=1}^{N_2} \frac{1}{1+\Upsilon|\lambda_{S_2R,n}|^2} > m\right). \quad (3.41)$$

Following (3.40) and (3.41), the MMSE SC-FDE TWR diversity at user 1 is $\min\left(L_{S_2R}, \lfloor N2^{-R} \rfloor + 1\right)$. Similarly, the achievable diversity order at user 2 with MMSE detection is $\min\left(L_{S_1R}, \lfloor N2^{-R} \rfloor + 1\right)$.

3.5 ML SC-FDE in TWR Channels

In this section, we derive the received end-to-end SNR between the two source nodes via the relay node for the ML SC-FDE TWR systems, followed by detailed diversity analysis. Following (3.8), we have

$$\mathbf{y}_1 = \mathbf{Q}^H\mathbf{Q}\mathbf{y}_1 = \underbrace{\alpha\sqrt{E_{S_2R}}\mathbf{Q}^H\mathbf{\Lambda}_{S_1R}\mathbf{\Lambda}_{S_2R}\mathbf{Q}\mathbf{x}_2}_{\breve{\mathbf{x}}_2} + \underbrace{\alpha\mathbf{Q}^H\mathbf{\Lambda}_{S_1R}\mathbf{Q}\mathbf{n}_R + \mathbf{n}_{S_1}}_{\breve{\mathbf{n}}}. \quad (3.42)$$

Note that,

$$E_{\breve{\mathbf{x}}_2|\mathbf{h}_{S_1R},\mathbf{h}_{S_2R}}\left[\breve{\mathbf{x}}_2\breve{\mathbf{x}}_2^H\right] = E_{S_2R}\sigma_s^2 Trace\left\{\left(\mathbf{\Lambda}_{S_1R}\mathbf{\Lambda}_{S_2R}\right)^H\mathbf{\Lambda}_{S_1R}\mathbf{\Lambda}_{S_2R}\right\}, \quad (3.43a)$$

$$E_{\breve{\mathbf{n}}|\mathbf{h}_{S_1R},\mathbf{h}_{S_2R}}\left[\breve{\mathbf{n}}\breve{\mathbf{n}}^H\right] = \alpha^2\sigma_n^2 Trace\left\{\left(\mathbf{\Lambda}_{S_1R}\right)^H\mathbf{\Lambda}_{S_1R}\right\} + N\sigma_n^2. \quad (3.43b)$$

Therefore, the instantaneous output SNR expression, conditional on channel vectors, can be formulated as follows,

$$SNR^{ML}_{\mathbf{h}_{S_1R},\mathbf{h}_{S_2R}} = \frac{E_{S_2R}\sigma_s^2}{\sigma_n^2}\frac{\alpha^2 Trace\left\{\mathbf{\Lambda}^H_{S_2R}\mathbf{\Lambda}^H_{S_1R}\mathbf{\Lambda}_{S_1R}\mathbf{\Lambda}_{S_2R}\right\}}{Trace\left\{\alpha^2\mathbf{\Lambda}^H_{S_1R}\mathbf{\Lambda}_{S_1R}+\mathbf{I}\right\}}. \tag{3.44}$$

In this work, we assume perfect interference cancellation at end user terminals. As a result, for ML SC-FDE receivers, instead of the SINR notation used widely in TWR systems, we have used SNR notation.

When the channel elements $\mathbf{h}_{S_1R}$ and $\mathbf{h}_{S_2R}$ are i.i.d, we have,

$$E_{\mathbf{h}_{S_2R}}\left[Tr\left(\mathbf{\Lambda}_{S_2R}\mathbf{\Lambda}^H_{S_2R}\right)\right] = \sum_{m=0}^{N-1} E_{\mathbf{h}_{S_2R}}\left[\sum_{k=0}^{L_{S_2R}-1}\sum_{k'=0}^{L_{S_2R}-1} h_{S_2R,k}\bar{h}_{S_2R,k'}e^{-j2\pi m(k-k')}\right] = N\sum_{k=0}^{L_{S_2R}-1}|h_{S_2R,k}|^2, \tag{3.45a}$$

$$E_{\mathbf{h}_{S_1R}}\left[Tr\left(\mathbf{\Lambda}_{S_1R}\mathbf{\Lambda}^H_{S_1R}\right)\right] = \sum_{m=0}^{N-1} E_{\mathbf{h}_{S_1R}}\left[\sum_{k=0}^{L_{S_1R}-1}\sum_{k'=0}^{L_{S_1R}-1} h_{S_1R,k}\bar{h}_{S_2R,k'}e^{-j2\pi m(k-k')}\right] = N\sum_{k=0}^{L_{S_1R}-1}|h_{S_1R,k}|^2, \tag{3.45b}$$

$$E_{\mathbf{h}_{S_1R},\mathbf{h}_{S_2R}}\left[Tr\left(\mathbf{\Lambda}^H_{S_2R}\mathbf{\Lambda}^H_{S_1R}\mathbf{\Lambda}_{S_1R}\mathbf{\Lambda}_{S_2R}\right)\right] = \sum_{m=0}^{N-1} E_{\mathbf{h}_{S_1R}}\left[\sum_{k_2=0}^{L_{S_1R}-1}\sum_{k_1=0}^{L_{S_1R}-1}\bar{h}_{S_1R,k_2}h_{S_1R,k_1}e^{-j2\pi m(k_1-k_2)}\right]\times$$
$$E_{\mathbf{h}_{S_2R}}\left[\sum_{k_4=0}^{L_{S_2R}-1}\sum_{k_3=0}^{L_{S_2R}-1}\bar{h}_{S_2R,k_4}h_{S_2R,k_3}e^{-j2\pi m(k_3-k_4)}\right] = N\sum_{k=0}^{L_{S_2R}-1}|h_{S_2R,k}|^2\sum_{k=0}^{L_{S_1R}-1}|h_{S_1R,k}|^2. \tag{3.45c}$$

Following (3.44) and (3.45), the conditional, i.e. conditioned on channel realizations, SNR expression at each source node for the ML SC-FDE TWR system is found to be,

$$SNR^{ML} = \frac{\frac{E_{S_2R}\sigma_s^2}{\sigma_n^2}\frac{E_R}{\sigma_n^2}\left(\sum_{k=0}^{L_{S_1R}-1}|h_{S_1R,k}|^2\right)\left(\sum_{k=0}^{L_{S_2R}-1}|h_{S_2R,k}|^2\right)}{\frac{E_R+E_{S_1R}}{\sigma_n^2}\left(\sum_{k=0}^{L_{S_1R}-1}|h_{S_1R,k}|^2\right)+\frac{E_{S_2R}}{\sigma_n^2}\left(\sum_{k=0}^{L_{S_2R}-1}|h_{S_2R,k}|^2\right)+1}. \tag{3.46}$$

Assuming that the total transmission power E_T is equally distributed between the two source terminals and the relay terminal, i.e. $E_{S_1R} = E_{S_2R} = E_R = E_T/3$, we have

$$SNR = \frac{a\left(\sum_{k=0}^{L_{S_1R}-1}|h_{S_1R,k}|^2\right)\left(\sum_{k=0}^{L_{S_2R}-1}|h_{S_2R,k}|^2\right)}{2\left(\sum_{k=0}^{L_{S_1R}-1}|h_{S_1R,k}|^2\right)+\left(\sum_{k=0}^{L_{S_2R}-1}|h_{S_2R,k}|^2\right)+1/a}, \tag{3.47}$$

Where $a = \frac{E_T}{3\sigma_n^2}$, and we have further assumed that $\sigma_s^2 = 1$. At practical SNR regions, (37) can be approximated as follows,

$$SNR \approx \frac{a\left(\sum_{k=0}^{L_{S_1R}-1}|h_{S_1R,k}|^2\right)\left(\sum_{k=0}^{L_{S_2R}-1}|h_{S_2R,k}|^2\right)}{2\left(\sum_{k=0}^{L_{S_1R}-1}|h_{S_1R,k}|^2\right)+\left(\sum_{k=0}^{L_{S_2R}-1}|h_{S_2R,k}|^2\right)} = \frac{a\gamma_{S_1R}\gamma_{S_2R}}{2\gamma_{S_1R}+\gamma_{S_2R}}, \tag{3.48}$$

Where $\gamma_{S_1R} = \left(\sum_{k=0}^{L_{S_1R}-1}|h_{S_1R,k}|^2\right)$, and $\gamma_{S_2R} = \left(\sum_{k=0}^{L_{S_2R}-1}|h_{S_2R,k}|^2\right)$. Note that when the channel impulse responses are i.i.d. complex Guassian random variables with zero means and unit variances, that is $h_{S_1R,k} \sim \mathcal{CN}(0,1), k = 0,\ldots,L_{S_1R}-1$ and $h_{S_2R,k} \sim \mathcal{CN}(0,1), k = 0,\ldots,L_{S_2R}-1$, γ_{S_1R} and γ_{S_2R} have Chi-squared distributions with $2L_{S_1R}$ and $2L_{S_2R}$ degrees of freedom respectively. Note that SNR in (3.48) can be expressed in an alternative form as follows,

$$SNR \approx \frac{a}{2}\frac{2\left(\sum_{k=0}^{L_{S_1R}-1}|h_{S_1R,k}|^2\right)\left(\sum_{k=0}^{L_{S_2R}-1}|h_{S_2R,k}|^2\right)}{2\left(\sum_{k=0}^{L_{S_1R}-1}|h_{S_1R,k}|^2\right)+\left(\sum_{k=0}^{L_{S_2R}-1}|h_{S_2R,k}|^2\right)} = \frac{a}{2}\frac{XY}{X+Y} = \frac{a}{2}.Z, \tag{3.49}$$

where $X \sim Gamma(L_{S_1R},2)$, and $Y \sim Gamma(L_{S_2R},1)$, and $G \sim Gamma(a,b)$ has the following pdf,

$$f_G(x) = \frac{x^{a-1}e^{-\frac{x}{b}}}{b^a\Gamma(a)}u(x). \tag{3.50}$$

Note that (3.48) can be interpreted as the Harmonic mean of two independent Gamma random variables that are not identically distributed. Following [106], to find the pdf and MGF of (3.48), we define the two random variables $U = \frac{1}{X}$, and $V = \frac{1}{Y}$. The PDF of sum $W = U + V$ is obtained as follows,

$$f_W(w) = \int_0^w f_X\left(\frac{1}{\tau}\right)f_Y\left(\frac{1}{w-\tau}\right)\frac{d\tau}{\tau^2(w-\tau)^2}. \tag{3.51}$$

Following (3.48), the PDF of harmonic mean of X and Y is given by,

$$\begin{aligned} f_Z(z) &= \left(\frac{1}{z^2}\right)f_W\left(\frac{1}{z}\right) = z\int_0^1 f_X\left(\frac{z}{t}\right)f_Y\left(\frac{z}{1-t}\right)\frac{dt}{t^2(1-t)^2} \\ &= \frac{z^{L_{S_1R}+L_{S_2R}-1}}{2^{L_{S_1R}}\Gamma(L_{S_1R})\Gamma(L_{S_2R})}\int_0^1 \exp\left\{-z\left[\frac{1}{2t}+\frac{1}{1-t}\right]\right\}\frac{dt}{t^{L_{S_1R}+1}(1-t)^{L_{S_2R}+1}}, \end{aligned} \tag{3.52}$$

where we have used the change of variable $t = z\tau$.

To find the MGF of Z, we take the Laplace transform of the Harmonic mean as follows,

$$\Phi_Z(s) = \int_0^\infty e^{-sz} f_Z(z) dz = \frac{1}{2^{L_{S_1R}} \Gamma(L_{S_1R}) \Gamma(L_{S_2R})} \int_0^\infty \int_0^1 \exp\left\{-z\left[s + \frac{1}{2t} + \frac{1}{1-t}\right]\right\} \frac{z^{L_{S_1R}+L_{S_2R}-1} dt dz}{t^{L_{S_1R}+1}(1-t)^{L_{S_2R}+1}}$$

$$= \frac{1}{2^{L_{S_1R}} \Gamma(L_{S_1R}) \Gamma(L_{S_2R})} \int_0^1 \left[\int_0^\infty \exp\left\{-z\left[s + \frac{1}{2t} + \frac{1}{1-t}\right]\right\} z^{L_{S_1R}+L_{S_2R}-1} dz\right] \frac{dt}{t^{L_{S_1R}+1}(1-t)^{L_{S_2R}+1}}$$

$$= \frac{2^{L_{S_2R}} \Gamma(L_{S_1R} + L_{S_2R})}{\Gamma(L_{S_1R}) \Gamma(L_{S_2R})} \int_0^1 \frac{t^{L_{S_2R}-1}(1-t)^{L_{S_1R}-1}}{[-2st^2 + (2s+1)t + 1]^{L_{S_1R}+L_{S_2R}}} dt, \tag{3.53}$$

where we have used eq. (3.326.2) from [107].

3.5.1 SER Performance of ML SC-FDE TWR system

To find the error performance of the ML SC-FDE TWER system, we follow the MGF approach as provided in [108] for the optimal maximum likelihood receiver structure. Following (3.53), the SER for QPSK constellation can be obtained as follows,

$$P(e) = \frac{1}{\pi} \int_0^{\frac{3\pi}{4}} \Phi_{\gamma_s}\left(\frac{\sin^2\left(\frac{\pi}{4}\right)}{\sin^2(\theta)}\right) d\theta \leqslant \frac{3}{4} \Phi_{\gamma_s}\left(\sin^2\left(\frac{\pi}{4}\right)\right)$$

$$= 3 \cdot \frac{2^{L_{S_2R}-2} \Gamma(L_{S_1R} + L_{S_2R})}{\Gamma(L_{S_1R}) \Gamma(L_{S_2R})} \int_0^1 \frac{t^{L_{S_2R}-1}(1-t)^{L_{S_1R}-1}}{\left[-2\left(\frac{a}{2}\sin^2\left(\frac{\pi}{4}\right)\right)t^2 + \left(2\left(\frac{a}{2}\sin^2\left(\frac{\pi}{4}\right)\right) + 1\right)t + 1\right]^{L_{S_1R}+L_{S_2R}}} dt. \tag{3.54}$$

To find a finite sum representation for the system's error probability in (3.54), following similar steps provided in [109], we can rewrite (3.54) as follows,

$$\Phi_Z(s) = \frac{2^{L_{S_2R}}\Gamma(L_{S_1R}+L_{S_2R})}{\Gamma(L_{S_1R})\Gamma(L_{S_2R})}\times$$
$$\left[\begin{array}{l} A(s)^{L_{S_1R}+L_{S_2R}} \sum_{i=0}^{L_{S_1R}-1} \sum_{j=0}^{L_{S_1R}+L_{S_2R}-1} (-1)^i \binom{L_{S_1R}-1}{i} \\ \binom{j+L_{S_1R}+L_{S_2R}-1}{L_{S_1R}+L_{S_2R}-1} B(s)^j \mathcal{K}(i+L_{S_2R}-1, L_{S_1R}+L_{S_2R}-j-1, z_2(s)) \\ +B(s)^{L_{S_1R}+L_{S_2R}} \sum_{i=0}^{L_{S_1R}-1} \sum_{k=0}^{L_{S_1R}+L_{S_2R}-1} (-1)^i \binom{L_{S_1R}-1}{i} \binom{k+L_{S_1R}+L_{S_2R}-1}{L_{S_1R}+L_{S_2R}-1} A(s)^k \\ \times \mathcal{K}(i+L_{S_2R}-1, L_{S_1R}+L_{S_2R}-k-1, z_1(s)) \end{array}\right], \tag{3.55}$$

where

$$\mathcal{K}(p,q,x) = x^{-p-1}\left[\sum_{l=0, l\neq q}^{p} \binom{p}{l}(-1)^l \frac{1-(1-x)^{l-q}}{l-q} - \binom{p}{q}(-1)^q \ln(1-x)\right], \tag{3.56}$$

and $z_{1,2}(s) = \frac{4s}{1+2s\pm\sqrt{1+4s^2+12s}}$, $A(s) = \frac{z_2(s)}{z_2(s)-z_1(s)}$, and $B(s) = \frac{z_1(s)}{z_1(s)-z_2(s)}$. When a is sufficiently high, we have

$$z_1\left(\frac{as}{2}\right) \to 1, z_2\left(\frac{as}{2}\right) \to -2as, A\left(\frac{as}{2}\right) \to 1, B\left(\frac{as}{2}\right) \to (2as)^{-1}. \tag{3.57}$$

Using the following property of $\mathcal{K}(p,q,x)$,

$$\mathcal{K}(p,q,x) \triangleq \int_0^1 t^p(1-xt)^{q-1}dt, \tag{3.58}$$

and further Noting that when $x \to 1$, $\mathcal{K}(p,q,x) \to B(p+1,q)$, with the definition of beta function as provided below,

$$B(x,y) \triangleq \int_0^1 t^{x-1}(1-t)^{y-1}dt, \tag{3.59}$$

(3.55) can be expressed as follows,

$$\Phi_{SINR}(s) = 2^{L_{S_2R}} \frac{\Gamma(L_{S_1R}+L_{S_2R})}{\Gamma(L_{S_1R})\Gamma(L_{S_2R})} \left[\sum_{i=0}^{L_{S_1R}-1} \sum_{j=0}^{L_{S_1R}+L_{S_2R}-1} \binom{L_{S_1R}-1}{i} \binom{j+L_{S_1R}+L_{S_2R}-1}{L_{S_1R}+L_{S_2R}-1} \right.$$
$$\left(\sum_{\substack{l=0 \\ l \neq L_{S_1R}+L_{S_2R}-j-1}}^{i+L_{S_2R}-1} \binom{i+L_{S_2R}-1}{l} (-1)^{l-L_{S_2R}+1} \frac{(2as)^{l-L_{S_1R}-2L_{S_2R}+1-i}}{l-L_{S_1R}-L_{S_2R}+j+1} \right.$$
$$\left. + \binom{i+L_{S_2R}-1}{L_{S_1R}+L_{S_2R}-j-1} (-1)^{L_{S_1R}-j-1} (2as)^{-j-i-L_{S_2R}} \ln(1+as) \right)$$
$$+(2as)^{-(L_{S_1R}+L_{S_2R})} \sum_{i=0}^{L_{S_1R}-1} \sum_{k=0}^{L_{S_1R}+L_{S_2R}-1} (-1)^i \binom{L_{S_1R}-1}{i} \binom{k+L_{S_1R}+L_{S_2R}-1}{L_{S_1R}+L_{S_2R}-1}$$
$$\left. \times B(i+L_{S_2R}, L_{S_1R}+L_{S_2R}-k-1) \right]. \tag{3.60}$$

(3.60) provides a finite sum representation of the system's SER. Nevertheless, driving the system's maximum achievable diversity order from (3.60) is not straight forward. This is mainly due to the fact that in the finite sum representation associated with $\mathcal{K}(p,q,x)$, different powers of as are added and subtracted which makes it difficult to understand the rate of changes in $\mathcal{K}(p,q,x)$ with respect to as. In the following section, we provide novel technique that gives insight on the system's achievable diversity order by analyzing the SER integral expression given in (3.54).

3.6 Novel Diversity Gain Analysis

Note that the integral in (3.53) can be asymptotically represented as follows,

$$\begin{aligned} P(e) &= \frac{3\cdot 2^{L_{S_2R}-2}\Gamma\left(L_{S_1R}+L_{S_2R}\right)}{\Gamma\left(L_{S_1R}\right)\Gamma\left(L_{S_2R}\right)} \int_0^1 \frac{t^{L_{S_2R}-1}(1-t)^{L_{S_1R}-1}}{\left[-2\left(\frac{a}{2}\sin^2\left(\frac{\pi}{4}\right)\right)t^2+\left(2\left(\frac{a}{2}\sin^2\left(\frac{\pi}{4}\right)\right)+1\right)t+1\right]^{L_{S_1R}+L_{S_2R}}} dt \\ &\doteq \frac{3\cdot 2^{L_{S_2R}-2}\Gamma\left(L_{S_1R}+L_{S_2R}\right)}{\Gamma\left(L_{S_1R}\right)\Gamma\left(L_{S_2R}\right)\left(a\sin^2\left(\frac{\pi}{4}\right)\right)^{L_{S_1R}+L_{S_2R}}} \int_0^1 \frac{t^{L_{S_2R}-1}(1-t)^{L_{S_1R}-1}}{\left[t-t^2\right]^{L_{S_1R}+L_{S_2R}}} dt \\ &= \frac{3\cdot 2^{L_{S_2R}-2}\Gamma\left(L_{S_1R}+L_{S_2R}\right)}{\Gamma\left(L_{S_1R}\right)\Gamma\left(L_{S_2R}\right)\left(a\sin^2\left(\frac{\pi}{4}\right)\right)^{L_{S_1R}+L_{S_2R}}} \int_0^1 \frac{1}{t^{L_{S_1R}+1}(1-t)^{L_{S_2R}+1}} dt. \end{aligned} \tag{3.61}$$

(3.61) should be evaluated within the interval $\left[\begin{array}{cc} 0 & 1 \end{array}\right]$. In here, to derive the maximum achievable diversity order associated with the SC-FDE TWR system, we divide the interval $\left[\begin{array}{cc} 0 & 1 \end{array}\right]$ within which the SER integral has to be evaluated, into multiple sub-intervals, and analyze the MGF integral asymptotically i.e. $a \to \infty$. More specifically, from (3.61), we obtain

$$\begin{aligned} P(e) &= \underbrace{\frac{3 \cdot 2^{L_{S_2R}-2}\Gamma(L_{S_1R}+L_{S_2R})}{\Gamma(L_{S_1R})\Gamma(L_{S_2R})\left(a\sin^2\left(\frac{\pi}{4}\right)\right)^{L_{S_1R}+L_{S_2R}}}}_{\kappa} \int_0^1 \underbrace{\frac{1}{t^{L_{S_1R}+1}(1-t)^{L_{S_2R}+1}}}_{\Theta(t)} dt \\ &= \kappa \int_0^{0^+} \Theta(t)\, dt + \kappa \int_{0^+}^{1^-} \Theta(t)\, dt + \kappa \int_{1^-}^{1} \Theta(t)\, dt, \end{aligned} \tag{3.62}$$

where $0^+ < c < 1^-$. The proposed diversity technique analyzes the error sub-integrals in (3.62) instead. More specifically, to evaluate the limiting integrals $\kappa \int_0^{0^+} \Theta(t)\, dt$ and $\kappa \int_{1^-}^{1} \Theta(t)\, dt$, we had to relate a to t. More specifically, when $t \to 0^+$, when $a \to \infty$, one can substitute $1/a$ for t, and when $t \to 1^-$, in high SNR regions, one can substitute $1/a$ for $1-t$. Eventually, the overall system's diversity order is the minimum of the diversity orders achieved in different sub-intervals:

Case I: $t \to 0^+$

In this case, integral in (3.61) within the interval $\left[\begin{array}{cc} 0 & 0^+ \end{array}\right]$ can be expressed as follows,

$$\begin{aligned} &\frac{3 \cdot 2^{L_{S_2R}-2}\Gamma(L_{S_1R}+L_{S_2R})}{\Gamma(L_{S_1R})\Gamma(L_{S_2R})\left(a\sin^2\left(\frac{\pi}{4}\right)\right)^{L_{S_1R}+L_{S_2R}}} \underbrace{\int_0^{0^+} \frac{1}{t^{L_{S_1R}+1}} dt}_{t^{-L_{S_1R}}} \doteq \\ &\frac{3 \cdot 2^{L_{S_2R}-2}\Gamma(L_{S_1R}+L_{S_2R})}{\Gamma(L_{S_1R})\Gamma(L_{S_2R})\left(a\sin^2\left(\frac{\pi}{4}\right)\right)^{L_{S_1R}+L_{S_2R}}} a^{L_{S_1R}} \doteq \\ &\frac{3 \cdot 2^{L_{S_2R}-2}\Gamma(L_{S_1R}+L_{S_2R})}{\Gamma(L_{S_1R})\Gamma(L_{S_2R})\left(\sin^2\left(\frac{\pi}{4}\right)\right)^{L_{S_1R}+L_{S_2R}}} a^{-L_{S_2R}} \end{aligned} \tag{3.63}$$

where we have assumed $1/a \to t$. Noting that the scale parameter for Gamma distribution is greater than 0, i.e. exponent of a starts from 1, the achievable system diversity order within this sub-interval is L_{S_2R}.

Case II: $t \to 1^-$

Following similar steps as in Case I, the integral in (3.61) within the interval $\left[\begin{array}{cc} 1^- & 1 \end{array}\right]$ can be expressed as follows,

$$P(e) \doteq \frac{3 \cdot 2^{L_{S_2R}-2}\Gamma(L_{S_1R}+L_{S_2R})}{\Gamma(L_{S_1R})\Gamma(L_{S_2R})\left(\sin^2\left(\frac{\pi}{4}\right)\right)^{L_{S_1R}+L_{S_2R}}} a^{-L_{S_1R}} \tag{3.64}$$

where we have assumed $a \to 1/(1-t)$. Hence, the achievable system diversity order within this sub-interval is L_{S_1R} .

Case III: $t \to c$

In this case, the integral in (3.61) in a subinterval arbitrarily small within the interval $\left[\ 0^{+} \quad 1^{-}\ \right]$ can be expressed as follows,

$$P(e) \doteq \frac{3 \cdot 2^{L_{S_2R}-2}\Gamma\left(L_{S_1R}+L_{S_2R}\right)}{\Gamma\left(L_{S_1R}\right)\Gamma\left(L_{S_2R}\right)\left(\sin^2\left(\frac{\pi}{4}\right)\right)^{L_{S_1R}+L_{S_2R}} a^{L_{S_1R}+L_{S_2R}}} \int_{c^-}^{c^+} \frac{1}{t^{L_{S_1R}+1}(1-t)^{L_{S_2R}+1}} dt, \tag{3.65}$$

Hence, the achievable system diversity order within this sub-interval is $L_{S_1R} + L_{S_2R}$. Note that the overall system's achievable diversity order is equal to the minimum of the diversity gains obtained at different intervals discussed in Cases I, II, and III, i.e. $\min\{L_{S_1R}, L_{S_2R}, L_{S_1R} + L_{S_2R}\}$. From (3.63), (3.64), and (3.65), it can be concluded that SC-FDE TWR system's maximum achievable diversity order is determined by the minimum of the multipath channel lengths associated with the channel links between the relay terminal and the two source terminals., i.e. $\min\{L_{S_1R}, L_{S_2R}\}$.

3.7 SC-FDE with Relay Selection for TWR system

In this section we consider a TWR system comprising of two source terminals and multiple relay terminals, in which the two source nodes communicate with the aid of the best relay node. The best relay selection (BRS) scheme employs an approach similar to that of [100], i.e. in the second-phase transmission, only one best relay is selected out of the M available relays to forward the received superimposed signals . We assume that, at the beginning of each transmission, some pilot symbols are transmitted by two source nodes to assist in the relay selection. One source node (either source S_1 or S_2) will determine the best relay terminal with the best end-to-end SNR and broadcast the index of the selected relay to all relays. Then, only the selected relay, which is known by both source nodes, is active in the second phase of transmission, and the rest of the relays will keep idle.

To analyze the performance of the SC-FDE TWR system with BRS, it is required to know the exact distribution of $\gamma_{\max} = \max\{\gamma_1, \ldots, \gamma_M\}$, which is the maximum achievable SNR implementing the BRS scheme. Following the properties of the order statistics, the PDF of $\gamma_{\max}$ can be obtained as follows,

$$f_{\gamma_{\max}}(x) = M\left(F_{Z_i}\left(\frac{x}{b}\right)\right)^{M-1}\left(\frac{1}{b} f_{Z_i}\left(\frac{x}{b}\right)\right), \tag{3.66}$$

where $b = \frac{a}{2}$, and $\gamma_i = \frac{a}{2}\frac{X_i Y_i}{X_i + Y_i} = b.Z_i$ as per (3.49). We initially derive the expression for

cumulative density function (CDF) of the received SNR as follows,

$$F_{Z_i}(z) = \frac{1}{2^{L_{S_1R}}\Gamma(L_{S_1R})\Gamma(L_{S_2R})}\left(\int_0^1\left(\int_0^z \exp\left\{-z\left[\frac{1}{2t}+\frac{1}{1-t}\right]\right\} z^{L_{S_1R}+L_{S_2R}-1}dz\right)\frac{dt}{t^{L_{S_1R}+1}(1-t)^{L_{S_2R}+1}}\right) = \frac{2^{L_{S_2R}}}{\Gamma(L_{S_1R})\Gamma(L_{S_2R})}\left(\int_0^1 \frac{\gamma\left(L_{S_1R}+L_{S_2R},\left(\frac{1}{2t}+\frac{1}{1-t}\right)z\right)}{(1+t)^{L_{S_1R}+L_{S_2R}}}t^{L_{S_2R}-1}(1-t)^{L_{S_1R}-1}dt\right), \tag{3.67}$$

where we have used eq. (3.381.8) from [107]. Note that when $z/b \to 0$, we have

$$F_{Z_i}\left(\frac{z}{b}\right) = \frac{2^{L_{S_2R}}}{\Gamma(L_{S_1R})\Gamma(L_{S_2R})}\left(\int_0^1 \frac{\gamma\left(L_{S_1R}+L_{S_2R},\left(\frac{1}{2t}+\frac{1}{1-t}\right)\frac{z}{b}\right)}{(1+t)^{L_{S_1R}+L_{S_2R}}}t^{L_{S_2R}-1}(1-t)^{L_{S_1R}-1}dt\right), \tag{3.68a}$$

$$f_{Z_i}\left(\frac{z}{b}\right) = \frac{z^{L_{S_1R}+L_{S_2R}-1}}{2^{L_{S_1R}}b^{L_{S_1R}+L_{S_2R}-1}\Gamma(L_{S_1R})\Gamma(L_{S_2R})}\int_0^1 \exp\left\{-\frac{z}{b}\left[\frac{1}{2t}+\frac{1}{1-t}\right]\right\}\frac{dt}{t^{L_{S_1R}+1}(1-t)^{L_{S_2R}+1}}. \tag{3.68b}$$

Following (3.68) and (3.66), $f_{\gamma_{\max}}(z)$ can be formulated as follows,

$$f_{\gamma_{\max}}(z) = M\frac{2^{L_{S_2R}(M-1)-L_{S_1R}}z^{L_{S_1R}+L_{S_2R}-1}}{b^{L_{S_1R}+L_{S_2R}}\left(\Gamma(L_{S_1R})\Gamma(L_{S_2R})\right)^M}\left(\int_0^1 \frac{\gamma\left(L_{S_1R}+L_{S_2R},\left(\frac{1}{2t}+\frac{1}{1-t}\right)\frac{z}{b}\right)}{(1+t)^{L_{S_1R}+L_{S_2R}}}t^{L_{S_2R}-1}(1-t)^{L_{S_1R}-1}dt\right)^{M-1}\times$$
$$\int_0^1 \exp\left\{-\frac{z}{b}\left[\frac{1}{2t}+\frac{1}{1-t}\right]\right\}\frac{dt}{t^{L_{S_1R}+1}(1-t)^{L_{S_2R}+1}}$$
$$\approx M\frac{2^{-L_{S_1R}M}z^{L_{S_1R}+L_{S_2R}-1}}{b^{M\left(L_{S_1R}+L_{S_2R}\right)}\left(L_{S_1R}+L_{S_2R}\right)\left(\Gamma(L_{S_1R})\Gamma(L_{S_2R})\right)^M}\left(\int_0^1 \frac{z^{L_{S_1R}+L_{S_2R}}}{t^{L_{S_1R}+1}(1-t)^{L_{S_2R}+1}}dt\right)^{M-1}\int_0^1 \frac{dt}{t^{L_{S_1R}+1}(1-t)^{L_{S_2R}+1}}, \tag{3.69}$$

where we have used the approximation $\gamma(s,z) \doteq \frac{z^s}{s}$, when $z \to 0$. Accordingly, MGF $\phi_{\gamma_{\max}}(s)$ can be derived as follows,

$$\phi_{\gamma_{\max}}(s) = M\frac{2^{-L_{S_1R}M}\Gamma\left(M\left(L_{S_1R}+L_{S_2R}\right)\right)}{b^{M\left(L_{S_1R}+L_{S_2R}\right)}\left(L_{S_1R}+L_{S_2R}\right)\left(\Gamma(L_{S_1R})\Gamma(L_{S_2R})\right)^M}\frac{\left(\int_0^1 \frac{dt}{t^{L_{S_1R}+1}(1-t)^{L_{S_2R}+1}}\right)^M}{s^{M\left(L_{S_1R}+L_{S_2R}\right)}}. \tag{3.70}$$

Following similar steps provided in (3.54), we can find the error performance of the ML receiver associated with the SC-FDE TWR system with BRS as follows,

$$P(e) \leq \frac{3\cdot 2^{-L_{S_1R}M}\Gamma\left(M\left(L_{S_1R}+L_{S_2R}\right)\right)}{\left(\frac{a}{2}\right)^{M\left(L_{S_1R}+L_{S_2R}\right)}\left(L_{S_1R}+L_{S_2R}\right)\left(\Gamma(L_{S_1R})\Gamma(L_{S_2R})\right)^M}\cdot\frac{\left(\int_0^1 \frac{dt}{t^{L_{S_1R}+1}(1-t)^{L_{S_2R}+1}}\right)^M}{\left(\sin^2\left(\frac{\pi}{4}\right)\right)^{M\left(L_{S_1R}+L_{S_2R}\right)}}. \tag{3.71}$$

Following similar analysis provided in Sec. 3.6., we realize that the maximum achievable diversity order associated with the TWR SC-FDE system with BRS is $M\min\left(L_{S_1R}, L_{S_2R}\right)$. Details are provided in Appendix. B.

Note that the TWR system under consideration performs perfect interference cancelation and is analogous to one-directional cooperative communication. As a result, the proposed diversity analysis technique can be generalized to conventional one-directional cooperative communication systems. More specifically, the integral factor $H = \frac{1}{a^{L_{SR}+L_{RD}}} \int_0^1 \frac{1}{t^{L_{SR}+1}(1-t)^{L_{RD}+1}} dt$ imposes a bottleneck on the maximum achievable diversity gain by the cooperative communication systems in general. The detailed diversity analysis for the generic cooperative communication system with frequency selective underlying channels [79] is omitted for brevity. It can be shown that the integral $H = \frac{1}{a^{L_{SR}+L_{RD}}} \int_0^1 \frac{1}{t^{L_{SR}+1}(1-t)^{L_{RD}+1}} dt$ is indeed present in the error expression for the generic cooperative transmission, and it is the very heart of exitance of a bottleneck in system's achievable diversity order.

Results in this section prove the following,

- In cooperative communication systems where the relay terminal performs amplify-and-forward operation, the bottleneck integral appears in the system's average SER expression and imposes a bottleneck on the system's achievable diversity gain.
- One way to bypass this limitation, is to change the relaying operation performed at the relay terminal. More importantly, it is worth noting that the Harmonic mean format only appears in the system's end-to-end SNR expression due to the normalization operation performed at the relay terminal, following which the H integral appears in the MGF expressions.

As an example, if the relay terminal only amplifies the received signal without performing power normalization, the conditional and average SNR expressions can be formulated as follows,

$$SNR_{\mathbf{h}_{SR},\mathbf{h}_{RD}} = \frac{E_{SR}\sigma_s^2}{\sigma_n^2} \frac{\alpha^2 Trace\left\{\mathbf{\Lambda}_{SR}^H \mathbf{\Lambda}_{RD}^H \mathbf{\Lambda}_{RD} \mathbf{\Lambda}_{SR}\right\}}{Trace\left\{\alpha^2 \mathbf{\Lambda}_{RD}^H \mathbf{\Lambda}_{RD} + \mathbf{I}\right\}}, \tag{3.72a}$$

$$SNR = \frac{E_{SR}\sigma_s^2}{\sigma_n^2} \frac{cE_{RD}\left(\sum_{k=0}^{L_{SR}-1} \left|\mathbf{h}_{SR,k}\right|^2\right)\left(\sum_{k=0}^{L_{RD}-1} \left|\mathbf{h}_{RD,k}\right|^2\right)}{cE_{RD}\left(\sum_{k=0}^{L_{RD}-1} \left|\mathbf{h}_{RD,k}\right|^2\right) + 1}, \tag{3.72b}$$

where $\alpha = \sqrt{cE_{RD}}$ and c is chosen to follow the power control limits enforced on the system. As an example, assuming that $E_{SR} = E_{RD} = E_T/2 = a$, when a is sufficiently high, the SNR expression can be expressed as follows,

$$SNR \approx \frac{E_{SR}\sigma_s^2}{\sigma_n^2}\left(\sum_{k=0}^{L_{RD}-1} \left|\mathbf{h}_{RD,k}\right|^2\right), \tag{3.73}$$

following which the maximum achievable diversity order of the system is determined by the $R \rightarrow D$ link's channel length only, and the minimum bottleneck rule no more exists.

3.8 SC-FDE TWR with power control

In (3.48) we derived SNR expression for the ML SC-FDE TWR system assuming equal power distribution between the relay terminal and the two communicating source terminals, i.e. $E_{S_2R} = E_{S_1R} = E_R = E_T/3 = a$. We further performed diversity analysis and concluded that the maximum achievable diversity order by the system is $\min(L_{S_1R}, L_{S_2R})$. In this section we consider few other power allocation scenarios, and further investigate how the system's maximum achievable diversity order is affected following these power allocation schemes.

Case I: $E_{S_1R} = \alpha E_R \gg E_{S_2R}$

In this case, the SINR expression can be expressed as follows,

$$\begin{aligned} SNR &= \frac{\alpha ab \left(\sum_{k=0}^{L_{S_1R}-1} |h_{S_1R,k}|^2 \right) \left(\sum_{k=0}^{L_{S_2R}-1} |h_{S_2R,k}|^2 \right)}{(\alpha+1)\, a \left(\sum_{k=0}^{L_{S_1R}-1} |h_{S_1R,k}|^2 \right) + b \left(\sum_{k=0}^{L_{S_2R}-1} |h_{S_2R,k}|^2 \right) + 1} \\ &= \frac{\alpha b \gamma_{S_1R} \gamma_{S_2R}}{(\alpha+1)\, \gamma_{S_1R} + \underbrace{\frac{b}{a}\gamma_{S_2R} + \frac{1}{a}}_{\rightarrow 0}} \approx \frac{\alpha b \gamma_{S_2R}}{(\alpha+1)} \approx b\gamma_{S_2R}, \end{aligned} \tag{3.74}$$

where $a = \frac{E_R}{\sigma_n^2}$, $b = \frac{E_{S_2R}}{\sigma_n^2}$, and we have further assumed that a is sufficiently large. Note that γ_{S_2R} has Gamma distribution $Gamma(L_{S_2R}, 1)$ with the following moment generating function,

$$\Phi_{\gamma_{S_2R}}(s) = (1-s)^{-L_{S_2R}}, s < 1. \tag{3.75}$$

The SER for SC-FDE TWR SER with QPSK can be upper bounded as follows,

$$P(e) \leqslant \frac{3}{4}\Phi_{SINR}\left(\sin^2\left(\frac{\pi}{4}\right)\right) = \frac{3}{4}\left(1 - b\sin^2\left(\frac{\pi}{4}\right)\right)^{-L_{S_2R}}. \tag{3.76}$$

Following (3.76), we can see that the error probability is not dependent on a, nor any diversity gain is achievable. (3.76) can be alternatively explained by noting that the second source terminal is transmitting information symbols to the first source terminal with negligible power, which indeed results in very low error performance.

Case II: $E_{S_2R} = \beta E_R \gg E_{S_1R}$

In this case, the SNR expression can be expressed as follows,

$$\begin{aligned} SNR &= \frac{\beta a^2 \left(\sum_{k=0}^{L_{S_1R}-1} |h_{S_1R,k}|^2\right)\left(\sum_{k=0}^{L_{S_2R}-1} |h_{S_2R,k}|^2\right)}{(a+b)\left(\sum_{k=0}^{L_{S_1R}-1} |h_{S_1R,k}|^2\right) + \beta a \left(\sum_{k=0}^{L_{S_2R}-1} |h_{S_2R,k}|^2\right) + 1} \\ &= \frac{\beta a \gamma_{S_1R}\gamma_{S_2R}}{\left(1 + \underbrace{\frac{b}{a}}_{\to 0}\right)\gamma_{S_1R} + \beta\gamma_{S_2R} + \underbrace{\frac{1}{a}}_{\to 0}} \approx a\frac{\beta\gamma_{S_1R}\gamma_{S_2R}}{\gamma_{S_1R} + \beta\gamma_{S_2R}} = a\frac{XY}{X+Y}, \end{aligned} \tag{3.77}$$

where $a = \frac{E_R}{\sigma_n^2}$, $b = \frac{E_{S_1R}}{\sigma_n^2}$, $X \sim Gamma(L_{S_1R}, 1)$, $Y \sim Gamma(L_{S_2R}, \beta)$, and we have further assumed that a is sufficiently large. Following similar analysis provided in Sec. 3.6, we can conclude that the maximum achievable diversity order is determined by the minimum of the channel memory lengths between the relay terminal and the two source terminals.

Case III: $E_{S_1R} = \eta E_{S_2R} \gg E_R$

In this case, the SNR expression can be expressed as follows,

$$\begin{aligned} SNR &= \frac{ab \left(\sum_{k=0}^{L_{S_1R}-1} |h_{S_1R,k}|^2\right)\left(\sum_{k=0}^{L_{S_2R}-1} |h_{S_2R,k}|^2\right)}{(\eta a+b)\left(\sum_{k=0}^{L_{S_1R}-1} |h_{S_1R,k}|^2\right) + a \left(\sum_{k=0}^{L_{S_2R}-1} |h_{S_2R,k}|^2\right) + 1} \\ &= \frac{b\gamma_{S_1R}\gamma_{S_2R}}{\left(\eta + \underbrace{\frac{b}{a}}_{\to 0}\right)\gamma_{S_1R} + \gamma_{S_2R} + \underbrace{\frac{1}{a}}_{\to 0}} \approx b\frac{\gamma_{S_1R}\gamma_{S_2R}}{\eta\gamma_{S_1R} + \gamma_{S_2R}} = \frac{b}{\eta}\frac{XY}{X+Y}, \end{aligned} \tag{3.78}$$

where $a = \frac{E_{S_2R}}{\sigma_n^2}$, $b = \frac{E_R}{\sigma_n^2}$, $X \sim Gamma(L_{S_1R}, \eta)$,$Y \sim Gamma(L_{S_2R}, 1)$, and we have further assumed that a is sufficiently large. Following similar analysis provided in Sec. VI, we can conclude that firstly, the system's error rate is independent of a and is instead dependent on the relay terminal's SNR b. More over, with respect to the relay terminal's SNR within the low SNR regime, the achievable diversity order is still equal to the minimum of the channel link's memory lengths between the relay terminal and the two source terminals.

3.9 Numerical Results

In this section, we present Monte-Carlo simulations to verify the analytical results. We have used $N = 512$ for the symbol block size and the QPSK modulation for data symbols.

Fig. 3.3 shows MMSE SC-FDE TWR system's average SER performance at $E_{S_2R} = 10$ dB for different channel lengths $L_{S_2R} = 2, 4, 5, 9$. As can be verified from Fig. 3.3, the diversity order of the MMSE SC-FDE system at each of the end user terminals is determined specifically by the the multipath channel length experienced in the link between the relay terminal and the other source terminal.

Fig. 3.4 illustrates the SER performance of the suboptimal ML SC-FDE TWR system for various channel length scenarios. As a suboptimal ML receiver, we used the sphere decoder at each of the source nodes. According to Fig. 3.4, in the ML SC-FDE TWR system, overall system diversity order is determined by the minimum of the channel lengths experienced by the links between the relay node and the two source terminals. As can be seen from Fig. 3.4, there is a 1 dB difference between the numerical and the upper bound SER curves.

Fig. 3.5 illustrates the MMSE SC-FDE TWR system's performance with power control when implementing Case I. More specifically, we assume $E_{S_1R} = E_R \gg E_{S_2R}$, where $E_{S_2R} \in$ [0 dB, 5 dB, 10 dB], and $E_{S_1R} = E_R = 100E_{S_2R}$. Based on the analytical results from previous section, we expect the error performance to be dominated by L_{S_2R}. Following results provided in Fig. 3.5, we can see that system's achievable diversity order is dictated by L_{S_2R}, and the channel length between the first source terminal and the relay terminal doesn't affect the ensuring system diversity order.

Fig. 3.6 illustrates the MMSE SC-FDE TWR system's performance with power control when implementing Case II. More specifically, we assume $E_{S_2R} = E_R \gg E_{S_1R}$, where $E_{S_1R} \in$ [0 dB, 5 dB, 10 dB], and $E_{S_2R} = E_R = 100E_{S_2R}$. Based on the analytical results from previous section, we expect the error performance to be dominated by $\min(L_{S_1R}, L_{S_2R})$. Following results provided in Fig. 3.6, we can see that system's achievable diversity order is dictated by $\min(L_{S_1R}, L_{S_2R})$.

Fig. 3.7 illustrates the MMSE SC-FDE TWR system's performance with power control when implementing Case III. More specifically, we assume $E_{S_2R} = E_{S_1R} \gg E_R$, where $E_R \in$ [0 dB, 5 dB, 10 dB], and $E_{S_1R} = E_{S_1R} = 100E_R$. Based on the analytical results from previous section, we expect the error performance to be dominated by $\min(L_{S_1R}, L_{S_2R})$. Following results provided in Fig. 3.7, we can see that system's achievable diversity order is dictated by the minimum of the channel link's memory lengths between the relay terminal and the two source terminals.

Fig. 3.8 illustrates the SER performance of the ML SC-FDE TWR system with relay selection. We have three participating relays in the system, where only the relay with

maximum end-to-end received SNR is globally selected for transmission. The SER performance results provided in Fig. 3.8 corroborate the numerical results provided in Sec. 3.7. Specifically, the maximum achievable diversity order is dominated by the number of available relays, as well as the minimum of the channel link's memory lengths between the relay terminal and the two source terminals.

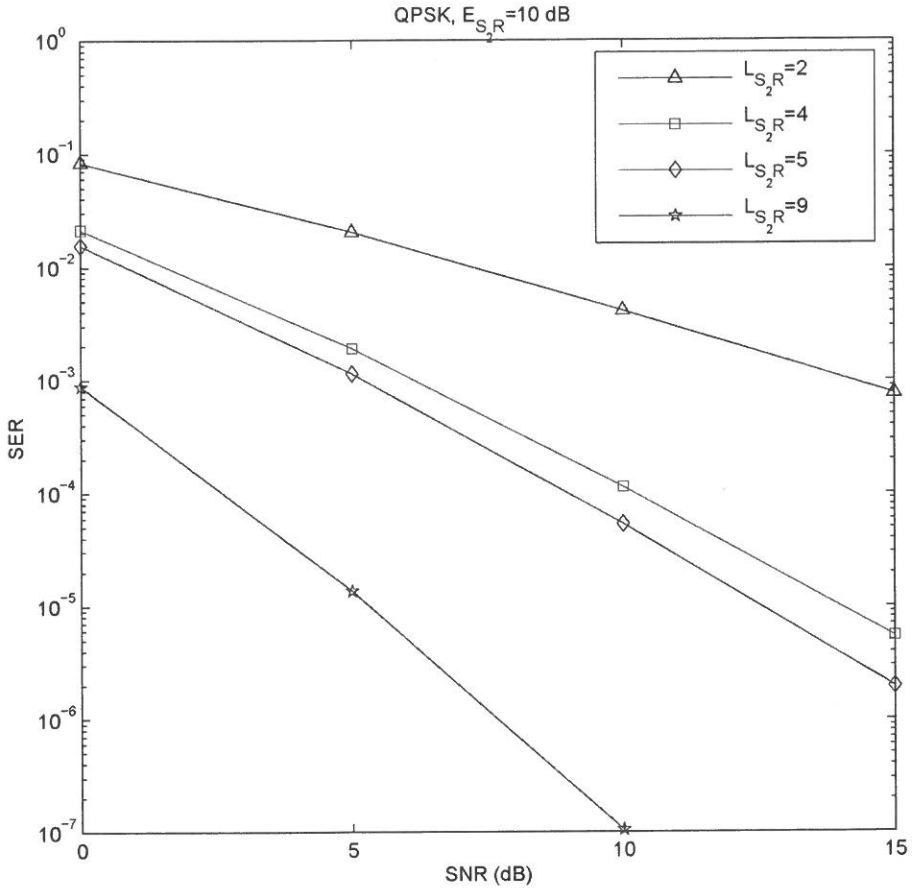

Figure 3.3: SER performance of the MMSE SC-FDE TWR system.

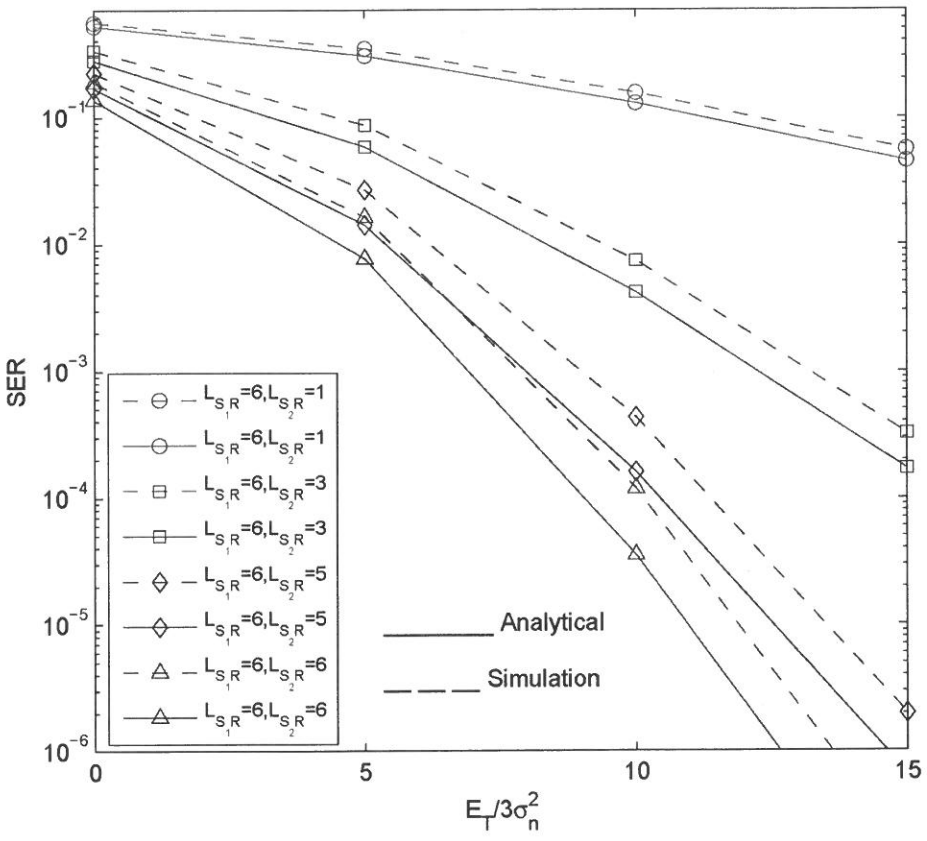

Figure 3.4: SER performance of the ML SC-FDE TWR system.

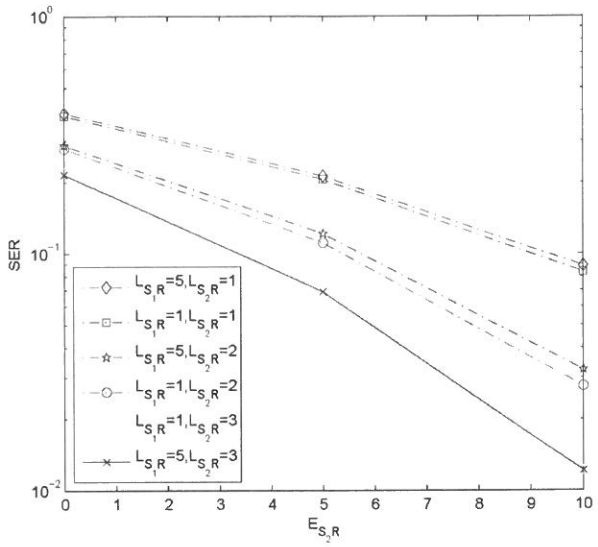

Figure 3.5: SER performance of the MMSE SC-FDE TWR system with power control where $E_{S_1R} = E_R \gg E_{S_2R}$

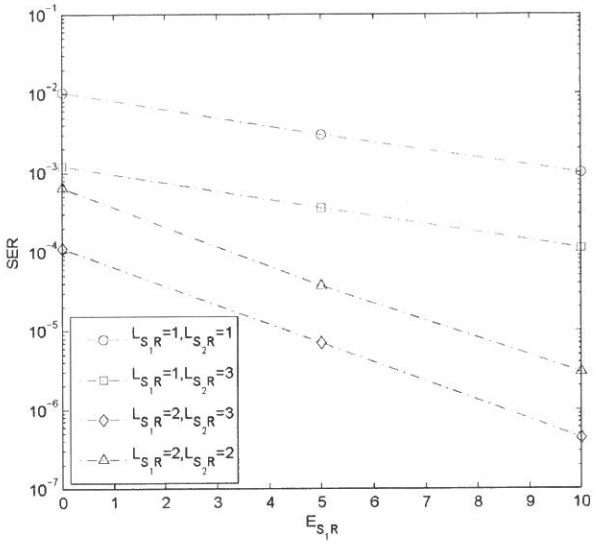

Figure 3.6: SER performance of the MMSE SC-FDE TWR system with power control where $E_{S_2R} = E_R \gg E_{S_1R}$.

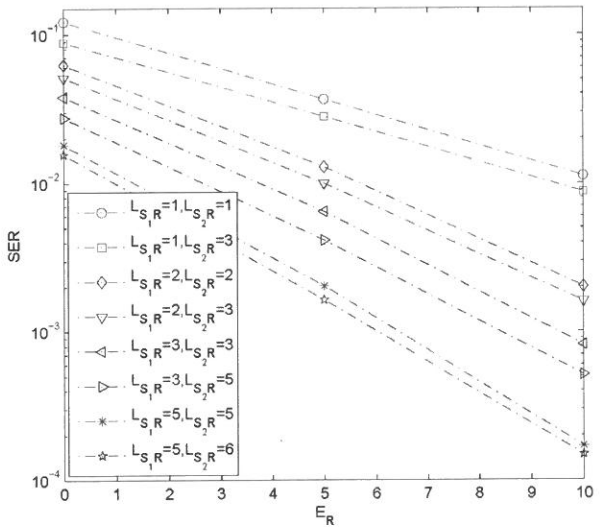

Figure 3.7: SER performance of the MMSE SC-FDE TWR system with power control where $E_{S_2R} = E_{S_1R} \gg E_R$.

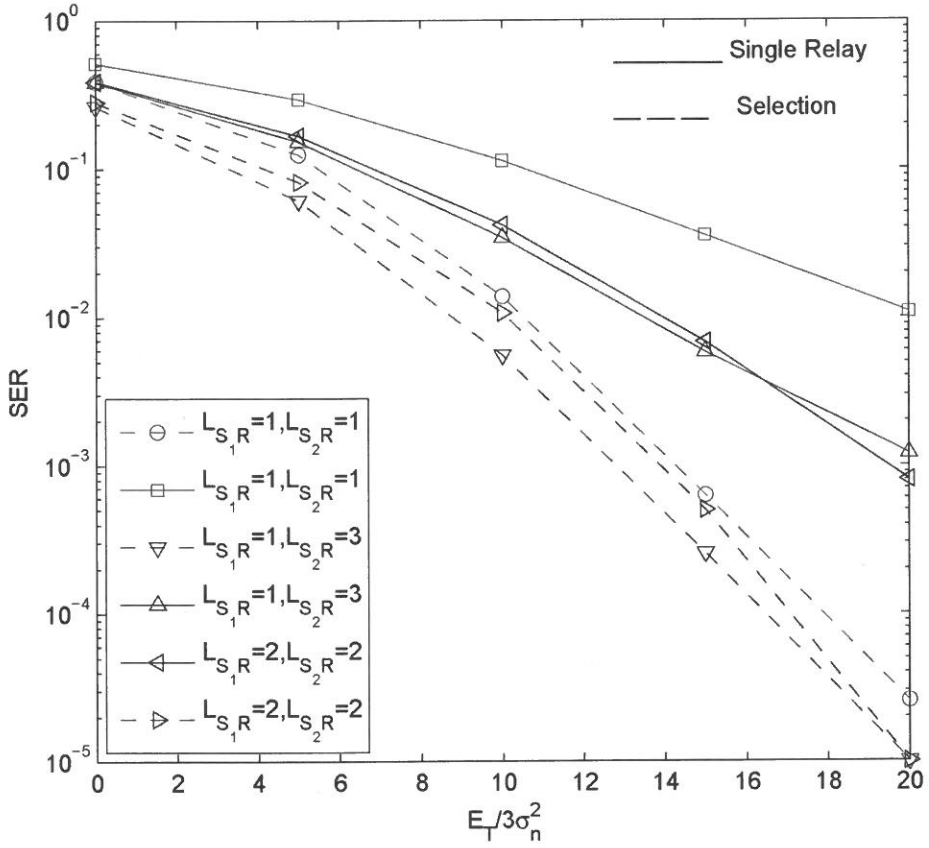

Figure 3.8: SER performance of the ML SC-FDE TWR system with relay selection.

Chapter 4

Multiuser Two-Way Relaying with Power Control for SC-FDE Systems

4.1 Introduction

In this chapter, we investigate cooperative SC-FDE for two-way relay networks, where multiple users each equipped with multiple antennas exchange their information through a multi-antenna relay node in a bi-directional manner. Under network total power constraint, we present optimal relay beamforming for the multiuser two-way relay system, where the relay transceiver processor is designed based on the MMSE criterion. We drive a closed-form expression for the SINR at each of the user terminals, and further present a joint user-relay antenna selection algorithm by applying the EDA. The proposed EDA has a low computational complexity, and its effectiveness is verified through simulation results.

4.2 System Model

We consider a TWR channel, consisting of $2K$ user terminals, $U_1, \ldots, U_{2K}$, each equipped with $N_i, i \in \{1, \ldots, 2K\}$ antennas, and a relay node R equipped with M antennas, as illustrated in Fig. 4.1. It is assumed that the TWR protocol uses two consecutive equal-duration time-slots for one round of information exchange between the user terminals via R , which linearly processes the received signal during the first time slot and then broadcasts the resulting signal to the users nodes during the second time slot. The $2K$ user nodes form

K pairs, where each pair is communicating in a bid-directional manner. Without loss of generality, we assume that the $(2k)^{th}$ and $(2k-1)^{th}$ users communicate with each other, for $k \in \{1, \ldots, K\}$. The CIRs for the link between the the m^{th} antenna at the relay node and n^{th} antenna at the k^{th} user node are given by $\mathbf{h}_k^{m,n} = [h_k^{m,n}[0], ..., h_k^{m,n}[L_k^{m,n}]]^{\mathrm{T}}$, where $L_k^{m,n}$ denotes the corresponding channel memory length. All channel links are assumed to experience frequency selective Rayleigh fading. The random vectors $\mathbf{h}_k^{m,n}$ are assumed to be independent zero-mean complex Gaussian with uniform power delay profile vectors. The corresponding $N \times N$ circulant channel matrices $\mathbf{H}_k^{m,n}$ are built upon the CIRs with entries $[\mathbf{H}_k^{m,n}]_{i,j} = \mathbf{h}_k^{m,n}((i-j) \bmod N)$. The overall channel matrix $\mathbf{H}_k$ between the k^{th} user and the relay terminal can be expressed as $\mathbf{H}_k \in \mathcal{C}_{NM \times NN_k}$, $\mathbf{H}_k = \begin{bmatrix} \mathbf{H}_k^{1,1} & \ldots & \mathbf{H}_k^{1,N_k} \\ \vdots & \ddots & \vdots \\ \mathbf{H}_k^{M,1} & \ldots & \mathbf{H}_k^{M,N_k} \end{bmatrix}$.

Let $\mathbf{x}_k \in \mathcal{C}_{N \times 1}$ denote the data stream parsed by user k. The k^{th} user performs transmit

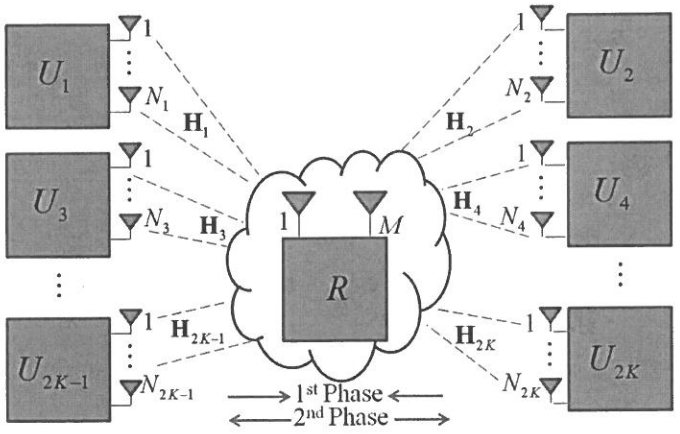

Figure 4.1: Multiuser TWR-SC-FDE system model.

beamforming with $\mathbf{A}_k \in \mathcal{C}_{NN_k \times N}$ and transmits the vector $\mathbf{d}_k$ to the relay terminal, as given below,

$$\mathbf{d}_k = \mathbf{A}_k \mathbf{x}_k. \tag{4.1}$$

Note that $\mathbf{A}_k = \begin{bmatrix} \mathbf{A}_k^1 & \ldots & \mathbf{A}_k^{N_k} \end{bmatrix}^T \in \mathcal{C}_{NN_k \times N}$, where $\mathbf{A}_k^i \in \mathcal{C}_{N \times N}, i \in \{1, \ldots, N_k\}$, are circulant matrices. The received signal at the relay terminal is given by,

$$\mathbf{r}_R = \sum_{k=1}^{2K} \mathbf{H}_k \mathbf{d}_k + \mathbf{n}_R, \tag{4.2}$$

where $\mathbf{n}_R \in \mathcal{C}_{NM\times 1}$ is a zero-mean additive white Guassian noise vector and $E\left\{\mathbf{n}_R\mathbf{n}_R^H\right\} = \sigma_n^2\mathbf{I}_{NM}$. The relay terminal processes the received signals before forwarding them to the destination. Specifically, each antenna at the relay terminal first converts $\mathbf{r}_R$ into the frequency domain using M parallel FFTs. Subsequently, the frequency domain vector $(\mathbf{Q}\otimes\mathbf{I}_M)\,\mathbf{r}_R$ is multiplied by a block diagonal frequency domain processing matrix $\mathbf{F}_f \in \mathcal{C}_{NM\times NM} = blkdiag\{\mathbf{F}_{f,i} \in \mathcal{C}_{N\times N}, i = 1,\ldots,M\}$. The resulting frequency domain matrices are transformed back to the time domain using M parallel IFFTs, leading to the time domain vector $\mathbf{s}_R \in \mathcal{C}_{NM\times 1}$ as follows,

$$\mathbf{s}_R = \mathbf{F}\mathbf{r}_R. \tag{4.3}$$

Note that $\mathbf{F} = \begin{bmatrix} \mathbf{F}_1 & \ldots & 0_{N\times N} \\ \vdots & \ddots & \vdots \\ 0_{N\times N} & \ldots & \mathbf{F}_M \end{bmatrix}$, $\mathbf{F}_i \in \mathcal{C}_{N\times N}, i \in \{1,\ldots,M\}$ are circulant matrices, and further $\mathbf{F} = (\mathbf{Q}\otimes\mathbf{I}_M)^H\mathbf{F}_f\,(\mathbf{Q}\otimes\mathbf{I}_M)$. Assuming that the first and second-phase channels are symmetric and static, the received signal vector $\mathbf{y}_k \in \mathcal{C}_{NN_k\times 1}$, at the k^{th} user can be written as

$$\mathbf{y}_k = \mathbf{H}_k^T\mathbf{s}_R + \mathbf{n}_k = \sum_{i=1}^{2K} \underbrace{\mathbf{H}_k^T\mathbf{F}\mathbf{H}_i}_{\bar{\mathbf{H}}_i}\mathbf{d}_i + \underbrace{\mathbf{H}_k^T\mathbf{F}\mathbf{n}_R + \mathbf{n}_k}_{\bar{\mathbf{n}}_k}. \tag{4.4}$$

where $\mathbf{n}_k \in \mathcal{C}_{NN_k\times 1}$ is the additive white Gaussian noise vector with each entry having zero-mean and variance of σ_n^2, $\bar{\mathbf{H}}_i = \mathbf{H}_k^T\mathbf{F}\mathbf{H}_i \in \mathcal{C}_{NN_k\times NN_k}$ represents the effective channel matrix between the k^{th} user and the relay terminal, and $\bar{\mathbf{n}}_k = \mathbf{H}_k^T\mathbf{F}\mathbf{n}_R + \mathbf{n}_k \in \mathcal{C}_{NN_k\times 1}$ represents the effective noise vector. The k^{th} user converts its own received signal from (4) into the frequency domain and then filters them using a frequency domain beamforming matrix $\mathbf{B}_{f,k} \in \mathcal{C}_{N\times NN_k}$, and transforms it back into the time domain to get

$$\hat{\mathbf{x}}_{k'} = \mathbf{B}_k\mathbf{y}_k, \tag{4.5}$$

where $(2k)' = 2k-1$, $(2k-1)' = 2k$, and $\mathbf{B}_k = \begin{bmatrix} \mathbf{B}_k^1 & \cdots & \mathbf{B}_k^{N_k} \end{bmatrix} \in \mathcal{C}_{N\times NN_k}$, with $\mathbf{B}_k^i \in \mathcal{C}_{N\times N}, i \in \{1,\ldots,N_k\}$ being circulant matrices. Note that, in order to control the transmit power of $\mathbf{x}_k$, $\mathbf{A}_k$ can be expressed as $\mathbf{A}_k = \lambda_k\bar{\mathbf{A}}_k$, where $\bar{\mathbf{A}}_k$ is normalized such that $Trace\left(\bar{\mathbf{A}}_k\bar{\mathbf{A}}_k^H\right) = 1$. Similarly, users' beamforming matrices can be represented as $\mathbf{B}_k = q^{-1}\bar{\mathbf{B}}_k$, where $Trace\left(\bar{\mathbf{B}}_k\bar{\mathbf{B}}_k^H\right) = 1$. In the following section, we design the relay beamforming matrix $\mathbf{F}$ for predetermined user beamforming matrices $\mathbf{A}_k$ and $\mathbf{B}_k$.

4.3 Design of the relay transceiver processing matrix

Denoting the multiuser transmitted data stream by $\mathbf{x} = \begin{bmatrix} \mathbf{x}_1 & \dots & \mathbf{x}_{2K} \end{bmatrix}^T \in 2NK \times 1$, the transmit beam-formed stream by $\mathbf{d} = \begin{bmatrix} \mathbf{d}_1 & \dots & \mathbf{d}_{2K} \end{bmatrix}^T \in 2NKN_k \times 1$, and the multiuser channel matrix by $\mathbf{H} = \begin{bmatrix} \mathbf{H}_1 & \dots & \mathbf{H}_{2K} \end{bmatrix} \in \mathcal{C}_{NM \times N\sum N_k}$, the received signal at the relay terminal can be written as follows,

$$\mathbf{r}_R = \underbrace{\mathbf{HAx}}_{\mathbf{x}_U} + \mathbf{n}_R = \mathbf{Hd} + \mathbf{n}_R, \tag{4.6}$$

where $\mathbf{x}_U$ represents the collective signal transmitted by the user terminals, and the transmit beamforming matrix $\mathbf{A} \in \mathcal{C}_{N\sum N_k \times 2NK}$, can be expressed as follows,

$$\mathbf{A} = \begin{bmatrix} \mathbf{A}_1 & 0_{NN_1 \times N} & \dots & 0_{NN_1 \times N} \\ 0_{NN_2 \times N} & \mathbf{A}_2 & \dots & 0_{NN_2 \times N} \\ \vdots & \ddots & \ddots & \vdots \\ 0_{NN_{2K} \times N} & 0_{NN_{2K} \times N} & \dots & \mathbf{A}_{2K} \end{bmatrix}. \tag{4.7}$$

Therefore, the multiuser received signal after beamforming can be represented as follows,

$$\hat{\mathbf{x}} = \mathbf{BH}^T\mathbf{FHAx} + \mathbf{BH}^T\mathbf{Fn}_R + \mathbf{Bn}, \tag{4.8}$$

where $\mathbf{B} = \begin{bmatrix} \mathbf{B}_1 & 0_{N \times NN_2} & \dots & 0_{N \times NN_{2K}} \\ 0_{N \times NN_1} & \mathbf{B}_2 & \dots & 0_{N \times NN_{2K}} \\ \vdots & \ddots & \ddots & \vdots \\ 0_{N \times NN_1} & 0_{N \times NN_2} & \dots & \mathbf{B}_{2K} \end{bmatrix} \in \mathcal{C}_{2NK \times N\sum N_k}$.

4.3.1 MMSE-based Design

The MMSE optimization can be formulated as follows,

$$\begin{aligned} &\arg\min_{\mathbf{F}} E\left[(\mathbf{x} - \mathbf{P}\hat{\mathbf{x}})^H (\mathbf{x} - \mathbf{P}\hat{\mathbf{x}})\right] \\ &s.t. \ \underbrace{E\left[\mathbf{x}_U^H \mathbf{x}_U\right]}_{P_U} + \underbrace{E\left[\mathbf{s}_R^H \mathbf{s}_R\right]}_{P_R} \leqslant P_T, \end{aligned} \tag{4.9}$$

where in (4.9) the overall system power is constrained to be not greater than P_T, and $\mathbf{P}$ is a $2NK$-dimensional block diagonal matrix with k^{th} block diagonal matrix being

$$\begin{bmatrix} 0 & 0 & \dots & 1 \\ 0 & \cdots & 1 & 0 \\ \vdots & \iddots & \vdots & \vdots \\ 1 & \cdots & 0 & 0 \end{bmatrix}$$ which exchanges the $(2k-1)^{th}$ and the $(2k)^{th}$ users' data. Note that the objective function in (4.9) can be expressed as follows,

$$\begin{aligned} &E\left[(\mathbf{x}-\mathbf{P}\hat{\mathbf{x}})^H(\mathbf{x}-\mathbf{P}\hat{\mathbf{x}})\right] = \\ &E\begin{bmatrix} \mathbf{x}^H\mathbf{x}-\mathbf{x}^H\mathbf{P}\mathbf{B}\mathbf{H}^T\mathbf{F}\mathbf{H}\mathbf{A}\mathbf{x}-\mathbf{x}^H\mathbf{A}^H\mathbf{H}^H\mathbf{F}^H\mathbf{H}^*\mathbf{B}^H\mathbf{P}^H\mathbf{x}+ \\ \mathbf{x}^H\mathbf{A}^H\mathbf{H}^H\mathbf{F}^H\mathbf{H}^*\mathbf{B}^H\mathbf{B}\mathbf{H}^T\mathbf{F}\mathbf{H}\mathbf{A}\mathbf{x}+\mathbf{n}_R^H\mathbf{F}^H\mathbf{H}^*\mathbf{B}^H\mathbf{P}\mathbf{B}\mathbf{H}^T\mathbf{F}\mathbf{n}_R+\mathbf{n}^H\mathbf{B}^H\mathbf{B}\mathbf{n} \end{bmatrix}. \end{aligned} \tag{4.10}$$

To simplify this term, we do some general considerations. Consider the quadratic structure of the form $\mathbf{Q}=\mathbf{s}^H\mathbf{A}\mathbf{s}$, which can be expanded as follows,

$$\begin{aligned} \mathbf{Q} = {} & \bar{s}_1A_{11}s_1+\bar{s}_2A_{21}s_1+\cdots+\bar{s}_NA_{N1}s_1+ \\ & \bar{s}_1A_{12}s_2+\bar{s}_2A_{22}s_2+\cdots+\bar{s}_NA_{N2}s_2+ \\ & \bar{s}_1A_{13}s_3+\bar{s}_2A_{23}s_3+\cdots+\bar{s}_NA_{N3}s_3+ \\ & \vdots \qquad\qquad \vdots \qquad\qquad \vdots \\ & \bar{s}_1A_{1N}s_N+\bar{s}_2A_{2N}s_N+\cdots+\bar{s}_NA_{NN}s_N \end{aligned} \tag{4.11}$$

With the assumption that the transmitted symbols as well as the noise samples are uncorrelated to each other within a block, the average power of one symbol is σ_s^2, the average noise power is σ_n^2, the matrix $\mathbf{A}$ is perfectly known, and therefore deterministic, i.e. we can express the expectation values as follows,

$$\begin{aligned} &E\left[\bar{x}_k\mathbf{A}_{kl}x_l\right] = \begin{cases} 0 & k\neq l \\ \sigma_s^2\mathbf{A}_{kl} & k=l \end{cases}, \\ &E\left[\bar{x}_k\mathbf{A}_{kl}n_{R,l}\right] = E\left[\bar{x}_k\mathbf{A}_{kl}n_{S_1,l}\right] = 0, \\ &E\left[\bar{n}_{R,k}\mathbf{A}_{kl}n_{R,k}\right] = E\left[\bar{n}_{S_1,k}\mathbf{A}_{kl}n_{S_1,k}\right] = \begin{cases} 0 & k\neq l \\ \sigma_n^2\mathbf{A}_{kl} & k=l \end{cases}. \end{aligned} \tag{4.12}$$

Using (4.12), we can simplify (4.10) as formulated in (4.13).

$$\begin{aligned} &E\left[(\mathbf{x}-\mathbf{P}\hat{\mathbf{x}})^H(\mathbf{x}-\mathbf{P}\hat{\mathbf{x}})\right] = 2NK\sigma_x^2-\sigma_x^2Tr\left(\mathbf{P}\mathbf{B}\mathbf{H}^T\mathbf{F}\mathbf{H}\mathbf{A}\right)-\sigma_x^2Tr\left(\mathbf{A}^H\mathbf{H}^H\mathbf{F}^H\mathbf{H}^*\mathbf{B}^H\mathbf{P}^H\right)+ \\ &\sigma_n^2Tr\left(\mathbf{F}^H\mathbf{H}^*\mathbf{B}^H\mathbf{B}\mathbf{H}^T\mathbf{F}\right)+\sigma_x^2Tr\left(\mathbf{A}^H\mathbf{H}^H\mathbf{F}^H\mathbf{H}^*\mathbf{B}^H\mathbf{B}\mathbf{H}^T\mathbf{F}\mathbf{H}\mathbf{A}\right)+\sigma_n^2Tr\left(\mathbf{B}^H\mathbf{B}\right) \end{aligned} \tag{4.13}$$

Similarly, for the constraint in (4.9) we have,

$$\begin{aligned} E\left[\mathbf{s}_R^H \mathbf{s}_R\right] &= \sigma_x^2 Tr\left(\mathbf{A}^H \mathbf{H}^H \mathbf{F}^H \mathbf{F} \mathbf{H} \mathbf{A}\right) + \sigma_n^2 Tr\left(\mathbf{F}^H \mathbf{F}\right), \\ E\left[\mathbf{x}_U^H \mathbf{x}_U\right] &= \sigma_x^2 Tr\left(\mathbf{A}^H \mathbf{H}^H \mathbf{H} \mathbf{A}\right). \end{aligned} \tag{4.14}$$

To tackle the optimization problem in (4.9), we apply the Lagranigian method, as explained below,

$$\arg\min_{\{\mathbf{F},\lambda\}} \underbrace{\left[E\left[(\mathbf{x}-\mathbf{P}\hat{\mathbf{x}})^H (\mathbf{x}-\mathbf{P}\hat{\mathbf{x}})\right] + \lambda\left[E\left[\mathbf{x}_U^H \mathbf{x}_U\right] + E\left[\mathbf{s}_R^H \mathbf{s}_R\right] - P_T\right]\right]}_{J}. \tag{4.15}$$

Following (4.13) and (4.14), the cost function J in (4.15) can be expanded as formulated in (4.16).

$$\begin{aligned} J &= 2NK\sigma_x^2 - \sigma_x^2 Tr\left(\mathbf{P}\mathbf{B}\mathbf{H}^T \mathbf{F}\mathbf{H}\mathbf{A}\right) - \sigma_x^2 Tr\left(\mathbf{A}^H \mathbf{H}^H \mathbf{F}^H \mathbf{H}^* \mathbf{B}^H \mathbf{P}^H\right) \\ &+\sigma_x^2 Tr\left(\mathbf{A}^H \mathbf{H}^H \mathbf{F}^H \mathbf{H}^* \mathbf{B}^H \mathbf{B}\mathbf{H}^T \mathbf{F}\mathbf{H}\mathbf{A}\right) + \sigma_n^2 Tr\left(\mathbf{F}^H \mathbf{H}^* \mathbf{B}^H \mathbf{B}\mathbf{H}^T \mathbf{F}\right) + \sigma_n^2 Tr\left(\mathbf{B}^H \mathbf{B}\right) + \\ &\lambda\left(\sigma_x^2 Tr\left(\mathbf{A}^H \mathbf{H}^H \mathbf{F}^H \mathbf{F}\mathbf{H}\mathbf{A}\right) + \sigma_n^2 Tr\left(\mathbf{F}^H \mathbf{F}\right) + \sigma_x^2 Tr\left(\mathbf{A}^H \mathbf{H}^H \mathbf{H}\mathbf{A}\right) - P_T\right). \end{aligned} \tag{4.16}$$

Finding a direct solution for J in its current format in (4.16) is difficult. Following [110], to circumvent this problem, we introduce

$$\mathbf{F} \triangleq q\bar{\mathbf{F}}, \tag{4.17}$$

and substitute it in (4.16). Note that for non-analytical complex function $f(\mathbf{X})$ that contains $\mathbf{X}^H$ or $\mathbf{X}^*$, the following differentiation rule must be regarded

$$\partial f(\mathbf{X}) = \frac{\partial f(\mathbf{X})}{\partial \mathbf{X}} \partial \mathbf{X} + \frac{\partial f(\mathbf{X})}{\partial \bar{\mathbf{X}}} \partial \bar{\mathbf{X}}. \tag{4.18}$$

Furthermore, the following rules for matrix derivation must be applied,

$$\begin{aligned} \frac{\partial Tr\left(\mathbf{A}\mathbf{X}^H \mathbf{B}\right)}{\partial \bar{\mathbf{X}}} &= (\mathbf{B}\mathbf{A})^T, \\ \frac{\partial Tr(\mathbf{A}\mathbf{X}\mathbf{B})}{\partial \mathbf{X}} &= (\mathbf{B}\mathbf{A})^T. \end{aligned} \tag{4.19}$$

By setting the partial derivatives of (4.16) with respect to $\bar{\mathbf{F}}$, λ, and q to zero we obtain,

$$\begin{aligned} &\frac{\partial J}{\partial q} = 0 \rightarrow q^4 = \sigma_n^2 \lambda^{-1} Tr\left(\bar{\mathbf{B}}^H \bar{\mathbf{B}}\right)\left(\sigma_x^2 Tr\left(\mathbf{A}^H \mathbf{H}^H \bar{\mathbf{F}}^H \bar{\mathbf{F}} \mathbf{H}\mathbf{A}\right) + \sigma_n^2 Tr\left(\bar{\mathbf{F}}^H \bar{\mathbf{F}}\right)\right)^{-1}, \\ &\frac{\partial J}{\partial \lambda} = 0 \rightarrow q^2 Tr\left(\bar{\mathbf{F}} \chi \bar{\mathbf{F}}^H\right) = P_T - \sigma_x^2 Tr\left(\mathbf{A}^H \mathbf{H}^H \mathbf{H}\mathbf{A}\right), \chi = \sigma_x^2 \mathbf{H}\mathbf{A}\mathbf{A}^H \mathbf{H}^H + \sigma_n^2 \mathbf{I}, \\ &\frac{\partial J}{\partial \bar{\mathbf{F}}} = 0 \rightarrow \bar{\mathbf{F}} = \sigma_x^2 \left(\mathbf{H}^* \bar{\mathbf{B}}^H \bar{\mathbf{B}} \mathbf{H}^T + \lambda q^2 \mathbf{I}_{NM}\right)^{-1} \times \\ &\left(\mathbf{H}\mathbf{A}\mathbf{P}\bar{\mathbf{B}}\mathbf{H}^T\right)\left(\sigma_x^2 \mathbf{H}\mathbf{A}\mathbf{A}^H \mathbf{H}^H + \sigma_n^2 \mathbf{I}_{NM}\right)^{-1}. \end{aligned} \tag{4.20}$$

To avoid the exhaustive search on λ, we apply the techniques presented in [110]. Introducing $\xi \triangleq \lambda q^2$, note that

$$\bar{\mathbf{F}} \triangleq \bar{\mathbf{F}}(\xi), \tag{4.21}$$

where $\bar{\mathbf{F}}(\xi) = \sigma_x^2 \mathbf{\Phi}^{-1}(\xi) \mathbf{\Psi} \chi^{-1}$, $\mathbf{\Phi}(\xi) = \mathbf{H}^* \bar{\mathbf{B}}^H \bar{\mathbf{B}} \mathbf{H}^T + \lambda q^2 \mathbf{I}_{NM}$, $\mathbf{\Psi} = \mathbf{HAP}\bar{\mathbf{B}}\mathbf{H}^T$, and $\chi = \sigma_x^2 \mathbf{HAA}^H \mathbf{H}^H + \sigma_n^2 \mathbf{I}_{NM}$. Note that $\mathbf{\Phi}(\xi) = (\mathbf{\Phi}(\xi))^H$, and $\chi = \chi^H$ are Hermitian matrices. Substituting (4.21) into (4.20), we obtain

$$q = \sqrt{\frac{P_T - \sigma_x^2 Tr\left(\mathbf{A}^H \mathbf{H}^H \mathbf{HA}\right)}{Tr\left(\bar{\mathbf{F}} \chi \bar{\mathbf{F}}^H\right)}}. \tag{4.22}$$

Following (4.22) and (4.20), we can rewrite J in terms of ξ and find the optimal ξ_0 to minimize the MSE. Note that (4.22) satisfies the term multiplied by λ in (4.15), and therefore the MSE can be obtained as formulated in (4.23).

$$\arg\min_{\xi} \underbrace{E\left[\left(\mathbf{x} - \mathbf{P}\bar{\mathbf{B}}\left(\mathbf{H}^T \bar{\mathbf{F}}(\xi)\mathbf{HAx} + \mathbf{H}^T \bar{\mathbf{F}}(\xi)\mathbf{n}_R + \sigma_x^2 \sqrt{\frac{Tr\left(\Psi^H \Phi^{-2}(\xi)\Psi\chi^{-1}\right)}{P_T - \sigma_x^2 Tr\left(\mathbf{A}^H\mathbf{H}^H\mathbf{HA}\right)}}\mathbf{n}\right)\right)^H \left(\mathbf{x} - \mathbf{P}\bar{\mathbf{B}}\left(\mathbf{H}^T \bar{\mathbf{F}}(\xi)\mathbf{HAx} + \mathbf{H}^T \bar{\mathbf{F}}(\xi)\mathbf{n}_R + \sigma_x^2 \sqrt{\frac{Tr\left(\Psi^H \Phi^{-2}(\xi)\Psi\chi^{-1}\right)}{P_T - \sigma_x^2 Tr\left(\mathbf{A}^H\mathbf{H}^H\mathbf{HA}\right)}}\mathbf{n}\right)\right)\right]}_{J}. \tag{4.23}$$

Using the identity $(\mathbf{W}^*\mathbf{W} + w\mathbf{I})^{-1}\mathbf{W}^* = \mathbf{W}^*(\mathbf{WW}^* + w\mathbf{I})^{-1}$ [111] and further forcing the derivative of (4.23) $\frac{\partial J}{\partial \xi}$ to zero, we obtain (4.24).

$$2\sigma_x^4 Tr\left(\left(\xi \mathbf{I}_{NM} - \frac{\sigma_n^2 Tr\left(\bar{\mathbf{B}}^H \bar{\mathbf{B}}\right)}{P_T - \sigma_x^2 Tr\left(\mathbf{A}^H \mathbf{H}^H \mathbf{HA}\right)} \mathbf{I}_{NM}\right) \Phi^{-3}(\xi) \Psi \chi^{-1} \Psi^H\right) = 0. \tag{4.24}$$

Following (4.24), we find the optimal ε_0 to be

$$\xi_0 = \frac{\sigma_n^2 Tr\left(\bar{\mathbf{B}}^H \bar{\mathbf{B}}\right)}{P_T - \sigma_x^2 Tr\left(\mathbf{A}^H \mathbf{H}^H \mathbf{HA}\right)}. \tag{4.25}$$

Following (4.21) and (4.25) we find the closed form MMSE solution to be

$$\mathbf{F}_{MMSE} = \sqrt{\frac{P_T - \sigma_x^2 Tr\left(\mathbf{A}^H \mathbf{H}^H \mathbf{HA}\right)}{Tr\left(\bar{\mathbf{F}}(\varepsilon_0) \chi \bar{\mathbf{F}}^H(\varepsilon_0)\right)}} \bar{\mathbf{F}}(\varepsilon_0). \tag{4.26}$$

4.4 Conditional Average End-to-End SINR

Remember that the received signal at user terminal k, after the self interference cancellation, can be expressed as below,

$$\hat{\mathbf{x}}_k = \mathbf{B}_k\left(\mathbf{H}_k^T\mathbf{s}_R + \mathbf{n}_k\right) = \overbrace{\underbrace{\mathbf{B}_k\mathbf{H}_k^T\mathbf{F}_{MMSE}\mathbf{H}_{k'}\mathbf{A}_{k'}}_{\breve{\mathbf{H}}_{k'}}\mathbf{x}_{k'} + \underbrace{\sum_{\substack{j=1\\ j\neq k,k'}}^{2K}\mathbf{B}_k\mathbf{H}_k^T\mathbf{F}_{MMSE}\mathbf{H}_j\mathbf{A}_j\mathbf{x}_j + \mathbf{B}_k\mathbf{H}_k^T\mathbf{F}_{MMSE}\mathbf{n}_R + \mathbf{B}_k\mathbf{n}_k}}^{\tilde{\mathbf{n}}_k}}^{\tilde{\mathbf{x}}_k}. \tag{4.27}$$

Notice that in $\tilde{\mathbf{x}}_k$, the effective channel coefficient $\breve{\mathbf{H}}_{k'}$ can be expressed as follows,

$$\breve{\mathbf{H}}_{k'} \in \mathcal{C}_{N\times N} = \sum_{t=1}^{N_{k'}}\sum_{l=1}^{M}\sum_{i=1}^{N_k}\mathbf{B}_k^i\mathbf{H}_k^{l,i}\mathbf{F}_{MMSE}^l\mathbf{H}_{k'}^{l,t}\mathbf{A}_{k'}^t. \tag{4.28}$$

Note that all the underlying matrices in (4.28) are circulant matrices, and therefore, $\breve{\mathbf{H}}_{k'}$ is circulant. Similarly, $\widehat{\mathbf{H}}^j \in \mathcal{C}_{N\times N} = \mathbf{B}_k\mathbf{H}_k^T\mathbf{F}_{MMSE}\mathbf{H}_j\mathbf{A}_j$, $j = 1,\ldots,2K, j\neq k,k'$ are circulant matrices and can be diagonalized. We define the diagonal matrices $\breve{\mathbf{\Lambda}}_{k'}$ and $\widehat{\mathbf{\Lambda}}^j$ which contain the N-point DFT of the channel matrices $\breve{\mathbf{H}}_{k'}$ and $\widehat{\mathbf{H}}^j$ with the following eigen decompositions, $\breve{\mathbf{H}}_{k'} = \mathbf{Q}^H\breve{\mathbf{\Lambda}}_{k'}\mathbf{Q}$, and $\widehat{\mathbf{H}}^j = \mathbf{Q}^H\widehat{\mathbf{\Lambda}}^j\mathbf{Q}$. In here,$\mathbf{Q}$ is the discrete Fourier transform, as written below,

$$\mathbf{Q}(m,n) = \frac{1}{\sqrt{N}}\exp\left[-j\frac{2\pi}{N}(m-1)(n-1)\right], \quad , \tag{4.29}$$

Such that $\mathbf{Q}^H\mathbf{Q} = \mathbf{I}$. For i.i.d channel processes we have

$$\begin{aligned}
&E\left[\hat{\mathbf{x}}_k\hat{\mathbf{x}}_k^H\right] = \sigma_x^2 Tr\left(\mathbf{Q}^H\breve{\mathbf{\Lambda}}_{k'}\breve{\mathbf{\Lambda}}_{k'}^H\mathbf{Q}\right) = \sigma_x^2\sum_{n=0}^{N-1}\left|\breve{h}_{k'}^n\right|^2,\\
&E\left[\tilde{\mathbf{n}}_k\tilde{\mathbf{n}}_k^H\right] = \sigma_x^2 Tr\left(\mathbf{Q}^H\sum_{j=1}^{2K}\widehat{\mathbf{\Lambda}}^j\left(\widehat{\mathbf{\Lambda}}^j\right)^H\mathbf{Q}\right) \quad ,\\
&+\sigma_n^2 Tr\left(\mathbf{Q}^H\left(\mathbf{\Lambda}_{n_R}\mathbf{\Lambda}_{n_R}^H + \mathbf{\Lambda}_B\right)\mathbf{Q}\right) = \sigma_x^2\sum_{j=1}^{2K}\sum_{n=0}^{N-1}\left|\widehat{h}^{j,n}\right|^2 + \sigma_n^2\sum_{n=0}^{N-1}\left|h_{n_R}^n\right|^2 + \sigma_n^2\sum_{n=0}^{N-1}\lambda_B^n,
\end{aligned} \tag{4.30}$$

where $\mathbf{H}_{n_R} = \mathbf{B}_k \mathbf{H}_k^T \mathbf{F}_{MMSE}$, $\mathbf{H}_{n_R} = \mathbf{Q}^H \mathbf{\Lambda}_{n_R} \mathbf{Q}$, $\mathbf{B}_k \mathbf{B}_k^H = \mathbf{Q}^H \mathbf{\Lambda}_B \mathbf{Q}$. Having $\breve{\lambda}_{k'}^n$, $\widetilde{\lambda}^{j,n}$, $\lambda_{n_R}^n$, λ_B^n to be the $(n,n)^{th}$ diagonal elements of $\breve{\mathbf{\Lambda}}_{k'}$, $\widetilde{\mathbf{\Lambda}}^j$, $\mathbf{\Lambda}_{n_R}$, $\mathbf{\Lambda}_B$, we explicitly find the $SINR_k^n$ expression for the k^{th} user as formulated in (4.31).

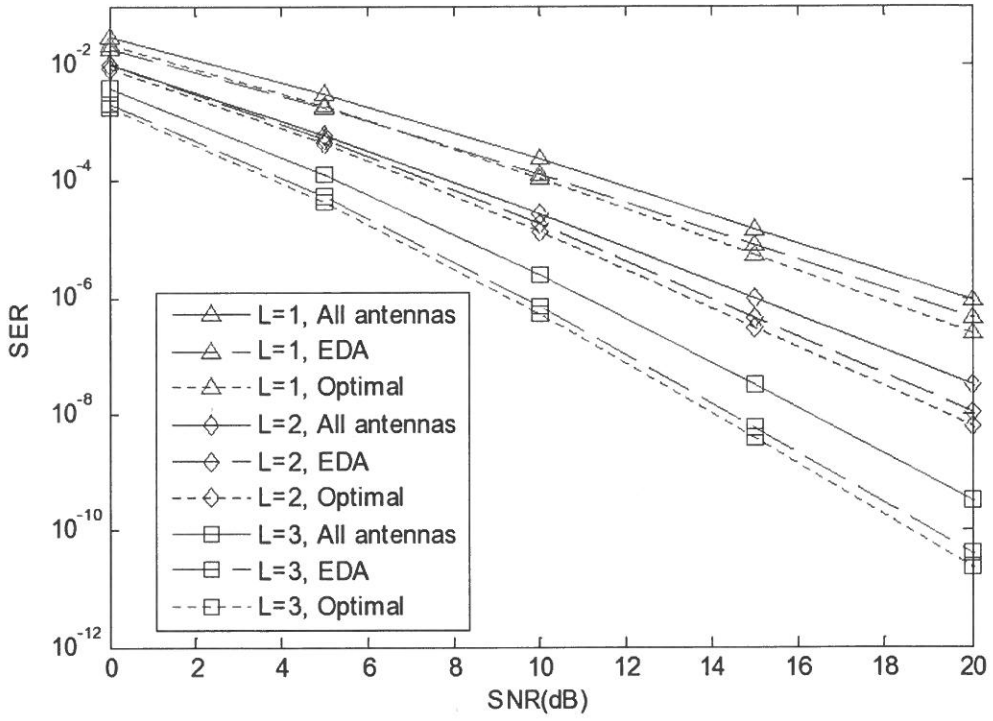

Figure 4.2: SER performance of the multiuser TWR system and the impact of joint user-relay antenna selection with EDA

$$SINR_k^n = \frac{\sigma_x^2 \frac{1}{N} \sum_{n=0}^{N-1} \left| \breve{h}_{k'}^n \right|^2}{\frac{\sigma_x^2}{N} \sum_{j=1}^{2K} \sum_{n=0}^{N-1} \left| \widetilde{h}^{j,n} \right|^2 + \frac{\sigma_n^2}{N} \sum_{n=0}^{N-1} \left| h_{n_R}^n \right|^2 + \frac{\sigma_n^2}{N} \sum_{n=0}^{N-1} \lambda_B^n}. \tag{4.31}$$

4.5 Relay antenna selection based on EDA

The signal processing in the multiuser TWR system presented is carried out with the aid of large number of antennas which results in a high hardware costs due to large number of RF chains, and consequently increases the overall system cost. In [112], Molisch et al. showed that selection of a subset of antennas from the set of physically available antennas, while

taking advantage of the multiantenna diversity by using the signals from the selected antennas only, can significantly reduce the hardware cost. Exhaustive Search Algorithm (ESA) evaluates all possible selections of the available antennas and selects the antenna combination that gives the best performance. Nevertheless, it's complexity increases exponentially with the number of available antennas, and is computationally inefficient. Moreover, in a real-time environment, the channel conditions and their corresponding antenna selections change quickly, which requires a computationally efficient search algorithm. In our multiuser TWR system, when deploying the antenna selection algorithm, we perform a search focused on the number of antennas to be selected at each terminal (user/relay). Following (4.28) and (4.31), for moderate $N_k, N_{k'}$, and M, it is the number of antennas selected at each terminal that significantly affects $SINR_k^n$, rather than the specific combination of antennas selected from that terminal. More importantly, this consideration significantly reduces problem's search space, and consequently, the search algorithm's complexity cost as compared to the ESA.

Evolutionary algorithms have been often used to solve difficult optimization problems. Unlike other evolutionary algorithms, in EDA, a new population of individuals in each iteration is generated without crossover and mutation operators. In this section, we revisit the EDA algorithm and define its parameters specifically for our joint user-relay antenna selection problem. More specifically, by selecting a subset of antennas at each terminal, the system's complexity is reduced.

We denote by I_s the collection of all possible joint user-relay antenna selections. Note that the number of possible ways of selecting antennas is $|I_s| = M \prod_{k=1}^{2K} N_k$. We denote by X in I_s, a selection of user-relay antennas. Each X can be represented by a discrete vector $[n_1, \ldots, n_{2K}, m], n_k \in \{1, \ldots, N_k\}, m \in \{1, \ldots, M\}$, where n_k is a discrete indicator of how many antennas from the k^{th} user terminal is selected, and m_k is a discrete indicator of how many antennas from the relay terminal is selected. As an example, $X = [2, 3, 2, 1, 4]$ represents a scenario where 2 antennas from user 1, 3 antennas from user 2, 2 antennas from user 3, 1 antenna from the fourth user, and 4 antennas from the relay terminal are selected. Each element of the discrete vector X is associated with a user and the number of antennas selected at that user, so the dimension of the vector X is $2K+1$. Following (4.31), we model the joint user-relay antenna selection problem by a combinatorial optimization problem as follows,

$$\max_{X \in I_s} \min SINR_{k,X}^n \tag{4.32}$$

where

$SINR^n_{k,X} = \dfrac{\sigma_x^2 \frac{1}{N} \sum_{n=0}^{N-1} \left| \breve{h}^{\,n}_{k',X} \right|^2}{\frac{\sigma_x^2}{N} \sum_{i=1}^{2K} \sum_{n=0}^{N-1} \left| \widehat{h}^{\,i,n}_{k,X} \right|^2 + \frac{\sigma_n^2}{N} \sum_{n=0}^{N-1} \left| h^n_{n_R,X} \right|^2 + \frac{\sigma_n^2}{N} \sum_{n=0}^{N-1} \lambda_B^n}$, and the superscript X denotes the channels formed between the selected user and relay antenna subset. In general, conventional EDAs can be characterized by parameters and notations

$$(I_s, F, \Delta_l, \eta_l, \beta_l, p_s, \Gamma, I_{Ter}) \tag{4.33}$$

where I_s is the space of all potential solutions (entire search space of individuals), F denotes the EDA fitness function which is $\min SINR^n_{k,X}$, Δ_l is the set of individuals (population) at the l^{th} iteration, η_l is the set of best candidate solutions selected from set Δ_l at the l^{th} iteration, We denote $\beta_l \equiv \Delta_l - \eta_l \equiv \Delta_l \cap \eta_l^C$, where η_l^C is the complement of η_l, $\cap$ stands for the intersection operation, and p_s is the selection probability. The EDA algorithm selects $p_s |\Delta_l|$ individuals from set Δ_l to make up set η_l, where $|\Delta_l|$ represents the number of individuals in population Δ_l, Γ represents the distribution estimated from Δ_l (the set of selected candidate solutions) at each iteration, and I_{Ter} is the number of iterations. To present EDA performance, each individual is designated by a discrete string of length *2K+1* (2K+1-dimensional discrete vector). The discrete variable vector X which was detailed before, represents an individual. An EDA maintains a population of individuals in each iteration. To implement EDA, we follow the steps below:

Step 0: Generate initial population Δ_0. The initial population ($|\Delta_0|$ individuals) is typically obtained by sampling according to uniform distribution

$$\begin{aligned} & p(\theta_1, \theta_2, \cdots, \theta_{2K}, \theta_M) = \prod_{i=1}^{2K+1} p_i(\theta_i), \\ & p_i(\theta_i = 1) = \cdots = p_i(\theta_i = N_i) = \frac{1}{N_i}, i = 1, \ldots, 2K \\ & p_M(\theta_M = M) = \frac{1}{M} \end{aligned} \tag{4.34}$$

For iterations $l = 1, 2, \ldots$, follow steps 1 through 6.

Step 1: Evaluate the individuals in the current population Δ_{l-1} according to the fitness function F. Sort the candidate solutions (individuals in the current population) according to their fitness orders.

Step 2: If the best candidate solution satisfies the convergence criterion or the number of iterations exceeds its limit I_{Ter}, then terminate; else go to step 3.

Step 3: Select the best $p_s \Delta_{l-1}$ candidate solutions (individuals) from current population Δ_{l-1}. This selection is accomplished according to the sorted candidate solutions.

Step 4: Estimate the probability distribution $p(\theta_1, \theta_2, \cdots, \theta_n)$ on the basis of $|\eta_{l-1}|$ best candidate solutions. We denote this estimation by

$$\Gamma = P(\theta_1, \theta_2, \cdots, \theta_n | \, \eta_{l-1}). \tag{4.35}$$

Step 5: Generate new $|\Delta_l| - |\eta_{l-1}|$ individuals on the basis of this new estimated probability distribution Γ. Replace the bad $|\beta_{l-1}|$ individuals with newly generated $|\Delta_l| - |\eta_{l-1}|$ individuals.

Step 6: Go to step 1 and repeat the steps. In our experimentation, for estimation (4.35), we used a simple scheme of estimating the marginal distributions separately and using product form

$$\begin{aligned} \Gamma = p(\theta_1, \cdots, \theta_{2K}, \theta_M | \eta_{l-1}) &= p_M(\theta_M | \eta_{l-1}) \prod_{i=1}^{2K} p_i(\theta_i | \eta_{l-1}) \\ &= \left(\frac{\sum_{j=1}^{|\eta_{l-1}|} \delta(x_i^j = \theta_M | \eta_{l-1})}{|\eta_{l-1}|} \right) \prod_{i=1}^{2K} \left(\frac{\sum_{j=1}^{|\eta_{l-1}|} \delta(x_i^j = \theta_i | \eta_{l-1})}{|\eta_{l-1}|} \right) \end{aligned} . \tag{4.36}$$

4.6 Numerical Results

In this section, we present Monte-Carlo simulations to verify the multiuser TWR system's performance. We have used $N = 512$ for the symbol block size and the QPSK modulation. We assume $2K = 6, N_k = 4$ for $k = 1, \ldots, 2K$, $M = 5$, and further define the system SER as the SER averaged over the users.

Fig. 4.2 shows system's SER performance for different channel lengths $L_k^{m,n} = 1, 2, 3$. We assume that all the underlying channel links have same channel lengths. Random beamforming [113] is employed at the user terminals. We further assume that $P_T = 30$ dB. It can be seen that for larger $L_k^{m,n}$, better SER performance is achieved. We also evaluate the performance of the EDA method with user-relay antenna selection, assuming population size $|\Delta_l| = 615$, i.e. 3% of the overall population $|I_s| = 4^6 \times 5 = 2048$, number of best population elements = 205. Note that by choosing $p_s = 0.30$, number of best population elements $= p_s \cdot |\Delta_l| = 205$. SER performance of the EDA algorithm is evaluated for $L_k^{m,n} = 1, 2, 3$ after $I_{Ter} = 15$. Note that the EDA algorithm with joint user-relay antenna subset selection shows better SER performance as compared to the case employing all available physical antennas . This is mainly because by increasing the number of users and their associated antennas, the corresponding CCI increases, which lowers the system SER performance. Note that EDA's SER performance is comparable with the optimal solution obtained by the exhaustive search, as is illustrated in Fig. 4.2.

Fig. 4.3 shows EDA fitness function-vs-iterations graph for different channel lengths $L_k^{m,n} = 1, 2, 3$. As can be seen from Fig. 4.3, by increasing the iterations, larger $\min SINR_{k,p}^n$ is achieved which results in better SER performance. Also note that, for larger $L_k^{m,n}$, the fitness function level is larger, which justifies the results illustrated in Fig. 4.2.

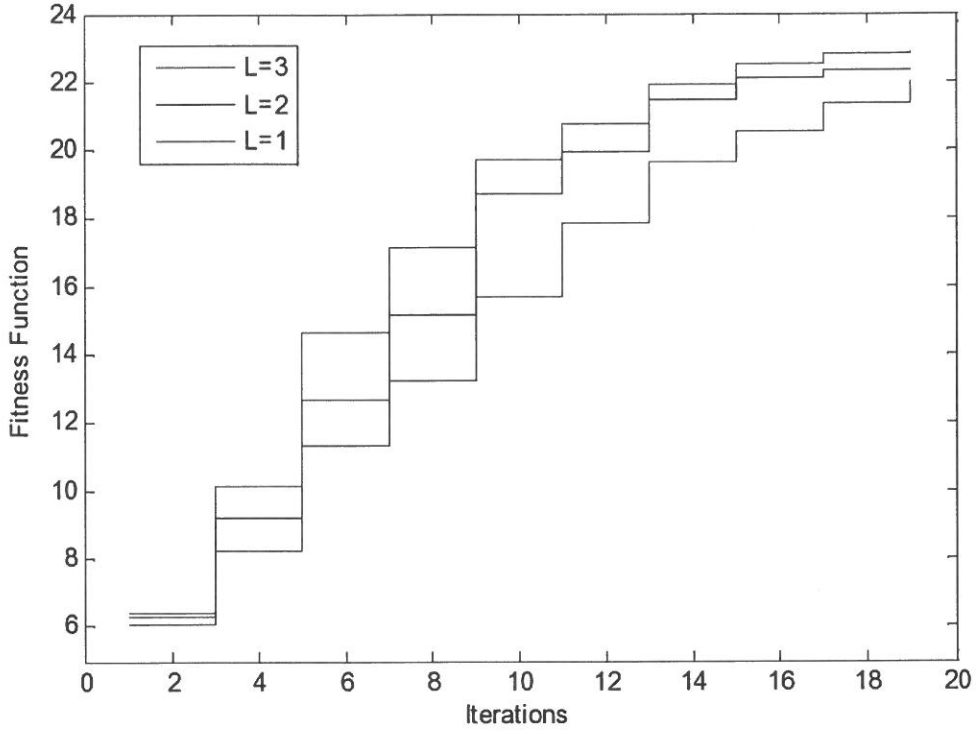

Figure 4.3: EDA fitness function versus number of iterations.

4.7 Conclusion

We have considered a multiuser TWR system and have designed the optimal relay processing matrix under system's overall power constraint. To further reduce system's hardware cost, we have employed the EDA algorithm which performs the joint user-relay antenna selection. Simulation results are provided to verify system's performance.

Chapter 5

Exploiting Sparsity for Beamforming with Power Control in Large AF Two-Way Relay Networks

5.1 Introduction

TWR mechanism has proven to not only increase the spectral efficiency, but also to improve the overall system's capacity [100,114]. The main bottleneck on the multipair TWR systems' performance is the interference imposed from other users. Many interference alignment methods have been proposed to null out the inter-pair interference and enable multi-pair transmission [115,116]. The method of signal space alignment (SSA) aligns the interferences and maximizes the overlap between the signal spaces of the interference signals at the receiving terminals such that the size of the interference-free space for the desired signal is maximized [117].

Exploiting the underlying spatial diversity through the employment of MIMO techniques at the transmitter or receiver side, can significantly improve the transmission reliability and channel capacity. Recently, few studies have focused on MIMO techniques for two-way relaying channels. Beamforming design for multiple user TWR systems under the DF strategy, is similar to the conventional MIMO beamforming schemes and hence the existing MIMO techniques can be applied [118–120]. The beamforming design for multiple user AF

TWR networks, however, is more challenging. In [121], authors develop an algorithm to compute the globally optimal relay beamforming matrix in a TWR system, where only the relay antenna is equipped with multiple antennas. Design of optimal relay beamforming matrix based on minimization of MSE at user terminals with single and multiple multi-antenna relay terminals is discussed in [122]. The optimal design of relay beamforming matrix in a multiple user TWR network is studied in [123]. sum-rate maximization and mean-square minimization for MIMO AF TWR with two multi-antenna users and a multi-antenna relay terminal is studied in [124–127]. low-complexity sub-optimal algorithms based on diagonalizaition of the MIMO channel and singular value decomposition (SVD) or the generalized SVD (GSVD) through which the beamforming problem is transformed into a power allocation problem, are studied in [125, 127]. Nevertheless, the optimal solution usually requires iterative algorithms with high complexity costs [126, 127].

In this chapter, we incorporate the MIMO techniques into two-way relaying while considering the joint design of user and relay beamforming matrices, where the participating nodes are equipped with multiple antennas. Large relay networks which consist of large number of cooperating nodes, are excessively practiced in device-to-device (D2D) communication networks and wireless sensor networks. Our focus in this work is specifically, on **large** AF MIMO TWR networks for three main reasons: (i) the prohibitive computational complexity of the exhaustive joint transceiver/relay beamforming matrix design in large networks. (ii) The significant reduction in implementation complexity achieved by the sparse beamforming performed at the participating terminals. (iii) The sparse structure of the relay and the user beamforming matrices which can be exploited to improve performance at practical complexity. We optimize the user/relay beamforming matrices to minimize the MSE under the sparsity constraint. We build on recent advances in sparse signal recovery to theory to solve the user/relay beamforming matrix design problem efficiently, using the OMP algorithm [128]. We present comprehensive Monte-Carlo simulations to give insight on system's error performance and convergence.

5.2 System Model

We consider a TWR channel, consisting of $2K$ user terminals, $U_1, \ldots, U_{2K}$, each equipped with $N_i, i \in \{1, \ldots, 2K\}$ antennas, and a relay node R equipped with M antennas, as illustrated in Fig. 5.1. It is assumed that the TWR protocol uses two consecutive equal-duration time-slots for one round of information exchange between the user terminals via R,

which linearly processes the received signal during the first time slot, and then broadcasts the resulting signal to the users nodes during the second time slot. The $2K$ user nodes form K pairs, where each pair is communicating in a bid-directional manner. Without loss of generality, we assume that the $(2k)^{th}$ and $(2k-1)^{th}$ users communicate with each other, for $k \in \{1, \ldots, K\}$. The channel impulse responses (CIRs) for the link between the the m^{th} antenna at the relay node and n^{th} antenna at the k^{th} user node are given by $h_k^{m,n}$. The random channel gains $h_k^{m,n}$ are assumed to be flat fading independent zero-mean complex Gaussian variables. The overall channel matrix $\mathbf{H}_k$ between the k^{th} user and the relay terminal can be expressed as $\mathbf{H}_k \in \mathcal{C}_{M \times N_k}$, $\mathbf{H}_k = \begin{bmatrix} h_k^{1,1} & \ldots & h_k^{1,N_k} \\ \vdots & \ddots & \vdots \\ h_k^{M,1} & \ldots & h_k^{M,N_k} \end{bmatrix}$. Let x_k denote

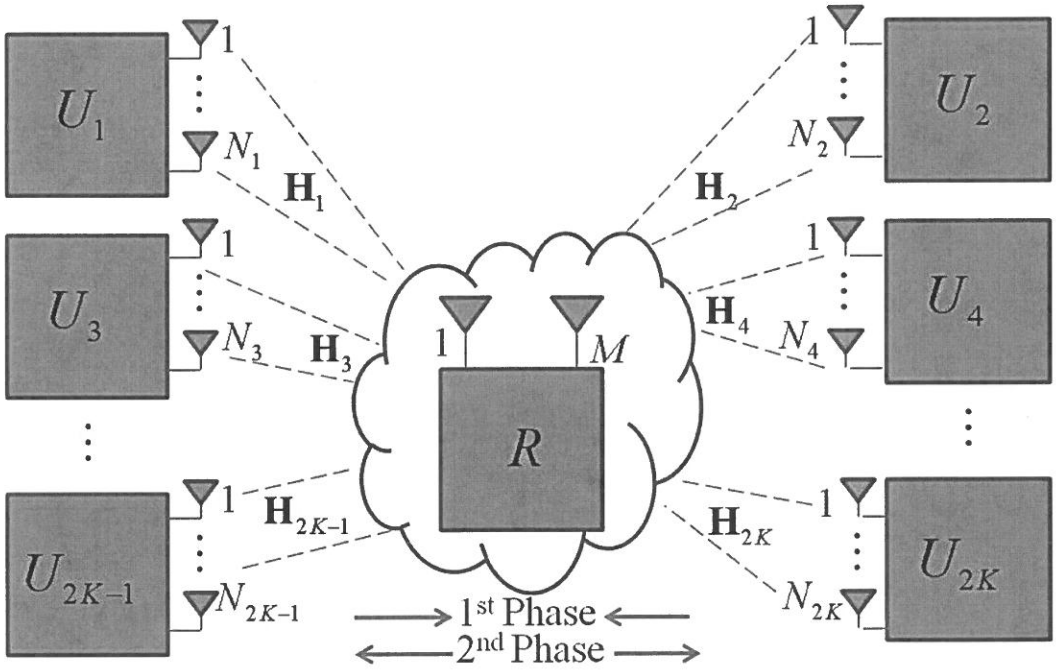

Figure 5.1: Multiuser TWR-SC-FDE system model.

the transmit signal parsed by user k to the relay terminal. The k^{th} user performs transmit beamforming with the unitary beamforming vector $\mathbf{a}_k \in \mathcal{C}_{N_k \times 1}$ and transmits the vector $\mathbf{d}_k$ to the relay terminal, as given below,

$$\mathbf{d}_k = \mathbf{a}_k x_k, \tag{5.1}$$

which satisfies the power constraint $E\left\{Trace\left[\mathbf{d}_k\mathbf{d}_k^H\right]\right\} \leq P_{U_k}$. Note that $\mathbf{a}_k = \begin{bmatrix} a_k^1 & \dots & a_k^{N_k} \end{bmatrix}^T \in \mathcal{C}_{N_k \times 1}$. The received signal at the relay terminal is given by,

$$\mathbf{r}_R = \sum_{k=1}^{2K} \mathbf{H}_k \mathbf{d}_k + \mathbf{n}_R, \tag{5.2}$$

where $\mathbf{n}_R \in \mathcal{C}_{M \times 1}$ is a zero-mean additive white Guassian noise vector and $E\left\{\mathbf{n}_R\mathbf{n}_R^H\right\} = \sigma_n^2\mathbf{I}_M$.

The relay terminal processes the received signals by the beamforming matrix $\mathbf{F}$ before forwarding them to the destination user terminals. Specifically, vector $\mathbf{s}_R \in \mathcal{C}_{M \times 1}$ is given as follows,

$$\mathbf{s}_R = \mathbf{F}\mathbf{r}_R, \tag{5.3}$$

where $\mathbf{F} \in \mathcal{C}_{M \times M}$, and further, due to the relay power constraint at the relay terminal, we have $E\left\{tr\left[\mathbf{S}_R\mathbf{S}_R^H\right]\right\} \leq P_R$. Assuming that the first and second-phase channels are symmetric and static, the received signal vector $\mathbf{y}_k \in \mathcal{C}_{N_k \times 1}$, at the k^{th} user can be written as

$$\mathbf{y}_k = \mathbf{H}_k^T\mathbf{s}_R + \mathbf{n}_k = \sum_{i=1}^{2K} \underbrace{\mathbf{H}_k^T\mathbf{F}\mathbf{H}_i}_{\bar{\mathbf{H}}_i}\mathbf{d}_i + \underbrace{\mathbf{H}_k^T\mathbf{F}\mathbf{n}_R + \mathbf{n}_k}_{\bar{\mathbf{n}}_k}. \tag{5.4}$$

where $\mathbf{n}_k \in \mathcal{C}_{N_k \times 1}$ is the additive white Gaussian noise vector with each entry having zero-mean and variance of σ_n^2, $\bar{\mathbf{H}}_i = \mathbf{H}_k^T\mathbf{F}\mathbf{H}_i \in \mathcal{C}_{N_k \times N_k}$ represents the effective channel matrix between the k^{th} user and the relay terminal, and $\bar{\mathbf{n}}_k = \mathbf{H}_k^T\mathbf{F}\mathbf{n}_R + \mathbf{n}_k \in \mathcal{C}_{N_k \times 1}$ represents the effective noise vector. The k^{th} user processes the received signal by a receive beamforming vector $\mathbf{b}_k \in \mathcal{C}_{1 \times N_k}$ to generate an estimate of the symbol transmitted by user k', as formulated below

$$\hat{\mathbf{x}}_{k'} = \mathbf{b}_k\mathbf{y}_k, \tag{5.5}$$

where $(2k)' = 2k-1$, $(2k-1)' = 2k$, and $\mathbf{b}_k = \begin{bmatrix} \mathbf{b}_k^1 & \cdots & \mathbf{b}_k^{N_k} \end{bmatrix} \in \mathcal{C}_{1 \times N_k}$.

5.3 Multiple user TWR system design

Denoting the multiuser transmitted data stream by $\mathbf{x} = \begin{bmatrix} \mathbf{x}_1 & \dots & \mathbf{x}_{2K} \end{bmatrix}^T \in 2K \times 1$, the transmit beam-formed stream by $\mathbf{d} = \begin{bmatrix} \mathbf{d}_1 & \dots & \mathbf{d}_{2K} \end{bmatrix}^T \in 2KN_k \times 1$, and the multiuser channel matrix by $\mathbf{H} = \begin{bmatrix} \mathbf{H}_1 & \dots & \mathbf{H}_{2K} \end{bmatrix} \in \mathcal{C}_{M \times \sum N_k}$, the received signal at the relay

terminal can be written as follows,

$$\mathbf{r}_R = \underbrace{\mathbf{HAx}}_{\mathbf{x}_U} + \mathbf{n}_R = \mathbf{Hd} + \mathbf{n}_R, \tag{5.6}$$

where $\mathbf{x}_U$ represents the collective signal transmitted by the user terminals, and the transmit beamforming matrix $\mathbf{A} \in \mathcal{C}_{\sum N_k \times 2K}$, can be expressed as follows,

$$\mathbf{A} = \begin{bmatrix} \mathbf{a}_1 & \mathbf{0}_{N_1\times 1} & \cdots & \mathbf{0}_{N_1\times 1} \\ \mathbf{0}_{N_2\times 1} & \mathbf{a}_2 & \cdots & \mathbf{0}_{N_2\times 1} \\ \vdots & \vdots & \ddots & \vdots \\ \mathbf{0}_{N_{2K}\times 1} & \mathbf{0}_{N_{2K}\times 1} & \cdots & \mathbf{a}_{2K} \end{bmatrix}. \tag{5.7}$$

Assuming that transmit power of the multiuser signal and the relayed signal is limited by P_{MU} and P_R, respectively, we have

$$E\|\mathbf{Ax}\|^2 = \sigma_{\mathbf{x}}^2 Trace\left\{\mathbf{A}^H\mathbf{A}\right\} = P_{MU}, \tag{5.8a}$$

$$E\|\mathbf{FHAx} + \mathbf{Fn}_R\|^2 = \sigma_{\mathbf{x}}^2 Trace\left\{(\mathbf{FHA})^H(\mathbf{FHA})\right\} + \sigma_{n_R}^2 Trace\left\{\mathbf{F}^H\mathbf{F}\right\} = P_R. \tag{5.8b}$$

The multiuser received signal after beamforming can be represented as follows,

$$\hat{\mathbf{x}} = \mathbf{BH}^T\mathbf{Fr}_R + \mathbf{Bn} = \mathbf{BH}^T\mathbf{FHAx} + \mathbf{BH}^T\mathbf{Fn}_R + \mathbf{Bn}, \tag{5.9}$$

where $\mathbf{B} = \begin{bmatrix} \mathbf{b}_1 & \mathbf{0}_{1\times N_2} & \cdots & \mathbf{0}_{1\times N_{2K}} \\ \mathbf{0}_{1\times N_1} & \mathbf{b}_2 & \cdots & \mathbf{0}_{1\times N_{2K}} \\ \vdots & \ddots & \ddots & \vdots \\ \mathbf{0}_{1\times N_1} & \mathbf{0}_{1\times N_2} & \cdots & \mathbf{b}_{2K} \end{bmatrix} \in \mathcal{C}_{2K\times\sum N_k}$.

5.4 Necessary Conditions on the number of user and relay antennas

Following (5.9), for a multi-antenna multiuser TWR system with $2K$ users, M number of antennas at the relay terminal, and $N_i, i \in \{1,\ldots,2K\}$ antennas at i^{th} user terminal, the number of relay antennas M and the total number of active antennas at user terminals must be greater than or equal to $2K$.

Proof: Following (5.9) and from the rank property we have,

$$rank\left(\underbrace{\mathbf{BH}^T\mathbf{FHA}}_{\in\mathcal{C}_{2K\times 2K}}\right) \leqslant rank\left(\mathbf{BH}^T\mathbf{F} \text{ or } \mathbf{HA}\right) = \min(2K, M) = M \Rightarrow 2K \leqslant M, \tag{5.10a}$$

$$rank\left(\underbrace{\mathbf{B}\mathbf{H}^T\mathbf{F}\mathbf{H}\mathbf{A}}_{\in \mathbb{C}_{2K\times 2K}}\right) = 2K \leqslant rank\left(\mathbf{B} \text{ or } \mathbf{H}^T\mathbf{F}\mathbf{H}\mathbf{A}\right) = \min\left(2K, \sum_{i=1}^{2K} N_i\right) \Rightarrow 2K \leqslant \sum_{i=1}^{2K} N_i. \tag{5.10b}$$

5.5 Iterative Sparse MMSE-based User/Relay Beamforming Design

In this section, we formulate the problem of iterative user/relay gain beamforming design algorithm with power allocation while minimizing the sum MSE associated with the participating user terminals. The MMSE optimization can be formulated as follows,

$$\arg\min_{\mathbf{F}} E\left[(\mathbf{x} - \mathbf{P}\hat{\mathbf{x}})^H (\mathbf{x} - \mathbf{P}\hat{\mathbf{x}})\right], \tag{5.11}$$

where $\mathbf{e} = \mathbf{x} - \mathbf{P}\hat{\mathbf{x}}$ denotes the error signal vector, and $\mathbf{P}$ is a $2K$-dimensional block diagonal matrix as given below,

$$\mathbf{P} = \begin{bmatrix} 0 & 0 & \dots & 1 \\ 0 & \cdots & 1 & 0 \\ \vdots & \iddots & \vdots & \vdots \\ 1 & \cdots & 0 & 0 \end{bmatrix}, \tag{5.12}$$

which exchanges the $(2k-1)^{th}$ and the $(2k)^{th}$ users' transmitted symbols. Consider the quadratic structure of the form $\mathbf{Q} = \mathbf{s}^H\mathbf{A}\mathbf{s}$, which can be expanded as follows,

$$\begin{aligned} \mathbf{Q} = {} & \bar{s}_1 A_{11} s_1 + \bar{s}_2 A_{21} s_1 + \cdots + \bar{s}_N A_{N1} s_1 + \\ & \bar{s}_1 A_{12} s_2 + \bar{s}_2 A_{22} s_2 + \cdots + \bar{s}_N A_{N2} s_2 + \\ & \bar{s}_1 A_{13} s_3 + \bar{s}_2 A_{23} s_3 + \cdots + \bar{s}_N A_{N3} s_3 + \quad . \\ & \vdots \qquad\qquad \vdots \qquad\qquad \vdots \\ & \bar{s}_1 A_{1N} s_N + \bar{s}_2 A_{2N} s_N + \cdots + \bar{s}_N A_{NN} s_N \end{aligned} \tag{5.13}$$

With the assumption that the transmitted symbols as well as the noise samples are uncorrelated to each other within a block, the average power of one symbol is σ_s^2, the average noise power is σ_n^2, the matrix $\mathbf{A}$ is perfectly known, and therefore deterministic, i.e. we can

express the expectation values as follows,

$$
\begin{aligned}
&E\left[\bar{x}_k \mathbf{A}_{kl} x_l\right] = \begin{cases} 0 & k \neq l \\ \sigma_s^2 \mathbf{A}_{kl} & k = l \end{cases}, \\
&E\left[\bar{x}_k \mathbf{A}_{kl} n_{R,l}\right] = E\left[\bar{x}_k \mathbf{A}_{kl} n_{S_1,l}\right] = 0, \\
&E\left[\bar{n}_{R,k} \mathbf{A}_{kl} n_{R,k}\right] = E\left[\bar{n}_{S_1,k} \mathbf{A}_{kl} n_{S_1,k}\right] = \begin{cases} 0 & k \neq l \\ \sigma_n^2 \mathbf{A}_{kl} & k = l \end{cases}.
\end{aligned} \tag{5.14}
$$

Using (5.14), we can express (5.11) as follows,

$$
\begin{aligned}
&MSE = E\left[\begin{array}{c} \left(\mathbf{BH}^T\mathbf{FHAx} + \mathbf{BH}^T\mathbf{Fn}_R + \mathbf{Bn} - \mathbf{Px}\right) \\ \left(\mathbf{BH}^T\mathbf{FHAx} + \mathbf{BH}^T\mathbf{Fn}_R + \mathbf{Bn} - \mathbf{Px}\right)^H \end{array}\right] = \\
&Trace\left\{\mathbf{BR}_{\mathbf{nn}}\mathbf{B}^H\right\} + Trace\left\{\mathbf{BH}^T\mathbf{FR}_{\mathbf{n}_R\mathbf{n}_R}\left(\mathbf{BH}^T\mathbf{F}\right)^H\right\} + \\
&Trace\left\{\left(\mathbf{BH}^T\mathbf{FHA} - \mathbf{P}\right)\mathbf{R}_{\mathbf{xx}}\left(\mathbf{BH}^T\mathbf{FHA} - \mathbf{P}\right)^H\right\}.
\end{aligned} \tag{5.15}
$$

Note that the joint design of the users and relay beamforming matrices for total MSE minimization in the considered MIMO TWR relay system in (5.15), is non-linear and non-convex and therefore, the optimal solution is not easily tractable. To approach the global optimal solution, we propose an iterative algorithm based on alternating optimization that updates one beamforming matrix at a time while fixing the others, as follows,

$$
\begin{aligned}
&\min_{\mathbf{F},\mathbf{A},\mathbf{B}} MSE, \\
&\text{s.t. (5.8a) (5.8b).}
\end{aligned} \tag{5.16}
$$

For each subproblem, we firstly prove that it is convex, and then we provide the sparse optimization method that solves for the sparse beamforming matrix under consideration.

5.5.1 Relay Antenna Selection and Design of the Sparse Relay Beamforming Matrix F :

First, given the user transmit and receive beamforming matrices **A** and **B**, we try to find the optimal sparse relay beamforming matrix **F**, formulated as follows,

$$
\begin{aligned}
&\min_{\mathbf{F}} MSE_{\mathbf{F}} \\
&\text{s.t. (5.8b),}
\end{aligned} \tag{5.17}
$$

where

$$MSE_{\mathbf{F}} = Trace\left\{\mathbf{BH}^T\mathbf{FR}_{\mathbf{n}_R\mathbf{n}_R}\left(\mathbf{BH}^T\mathbf{F}\right)^H\right\} + Trace\left\{\mathbf{BH}^T\mathbf{FHAR}_{\mathbf{xx}}\left(\mathbf{BH}^T\mathbf{FHA}\right)^H\right\}$$
$$-Trace\left\{\mathbf{PR}_{\mathbf{xx}}\left(\mathbf{BH}^T\mathbf{FHA}\right)^H\right\} - Trace\left\{\left(\mathbf{BH}^T\mathbf{FHA}\right)\mathbf{R}_{\mathbf{xx}}(\mathbf{P})^H\right\}. \tag{5.18}$$

In this work, we are interested in performing relay antenna selection at the relay terminal. More specifically, the resultant relay beamforming $\mathbf{F}$ matrix must comprise of all zero rows corresponding to the relay antennas that will not be utilized for relaying operation. As a result, to perform sparse optimization with selection in this subproblem, we implement the BOMP sparse algorithm, which provides sparsity on the block level. In the following, we firstly prove that (5.17) is convex, to corroborate the convergence of the ensuing subproblem, followed by detailed formulation of the sparse subproblem algorithm.

Convexity of (5.17)

Following the matrix manipulations in [129] [Eq.1.10.62, Eq.1.10.64], (5.18) can be reformulated as follows,

$$\begin{aligned} MSE_{\mathbf{F}} &= \mathrm{vec}(\mathbf{F})^H\left((\mathbf{R}_{\mathbf{n}_R\mathbf{n}_R})^T \otimes \left(\mathbf{BH}^T\right)^H\mathbf{BH}^T\right)\mathrm{vec}\left(\mathbf{F}\right) + \\ &\mathrm{vec}(\mathbf{F})^H\left(\left(\mathbf{HAR}_{\mathbf{xx}}(\mathbf{HA})^H\right)^T \otimes \left(\mathbf{BH}^T\right)^H\mathbf{BH}^T\right)\mathrm{vec}\left(\mathbf{F}\right) + \\ &\mathrm{vec}\left(\left(\mathbf{HAR}_{\mathbf{xx}}(\mathbf{P})^H\mathbf{BH}^T\right)^T\right)^T\mathrm{vec}\left(\mathbf{F}\right) + \mathrm{vec}(\mathbf{F})^H\mathrm{vec}\left(\mathbf{HAR}_{\mathbf{xx}}(\mathbf{P})^H\mathbf{BH}^T\right)^H \end{aligned} \tag{5.19}$$

Based on the vector differential rule in [130], the four Hessian matrices are derived as follows,

$$\begin{aligned} &\underset{\mathrm{vec}(\mathbf{F})^*,\mathrm{vec}(\mathbf{F})}{\mathcal{H}}(MSE_{\mathbf{F}}) = \left[\left((\mathbf{R}_{\mathbf{n}_R\mathbf{n}_R})^T + \mathbf{HAR}_{\mathbf{xx}}(\mathbf{HA})^H\right)^T \otimes \left(\mathbf{BH}^T\right)^H\mathbf{BH}^T\right]^T, \\ &\underset{\mathrm{vec}(\mathbf{F}),\mathrm{vec}(\mathbf{F})^*}{\mathcal{H}}(MSE_{\mathbf{F}}) = \left[\left((\mathbf{R}_{\mathbf{n}_R\mathbf{n}_R})^T + \mathbf{HAR}_{\mathbf{xx}}(\mathbf{HA})^H\right)^T \otimes \left(\mathbf{BH}^T\right)^H\mathbf{BH}^T\right], \\ &\underset{\mathrm{vec}(\mathbf{F}),\mathrm{vec}(\mathbf{F})}{\mathcal{H}}(MSE_{\mathbf{F}}) = \mathbf{0}, \\ &\underset{\mathrm{vec}(\mathbf{F})^*,\mathrm{vec}(\mathbf{F})^*}{\mathcal{H}}(MSE_{\mathbf{F}}) = \mathbf{0}. \end{aligned} \tag{5.20}$$

In order to show the convexity of $MSE_{\mathbf{F}}$, the following Hessian block matrix should be positive semidefinite.

$$\mathcal{H}\left(MSE_{\mathbf{F}}\right) = \begin{bmatrix} \mathbf{K}^T & \mathbf{0} \\ \mathbf{0} & \mathbf{K} \end{bmatrix}, \tag{5.21}$$

where $\mathbf{K} = \left[\underbrace{\left((\mathbf{R}_{\mathbf{n}_R\mathbf{n}_R})^T + \mathbf{HAR_{xx}(HA)}^H\right)^T}_{\mathbf{K}_1} \otimes \underbrace{\left(\mathbf{BH}^T\right)^H \mathbf{BH}^T}_{\mathbf{K}_2}\right]$. Noting that the Kronecker product of any two positive semidefinite matrices is also positive semidefinite [127], we derive that with $\mathbf{K}_1$ and $\mathbf{K}_2$ being positive semidefinite,$\mathbf{K}$ should be positive semidefinite. Hence, the convexity of $MSE_{\mathbf{F}}$ is proven. Therefore, the objective function in (5.17) is convex.

Next, we prove that the feasible set provided by (8.b) is convex. We can prove this by showing that $f = \frac{\sigma_{\mathbf{x}}^2 Trace\left\{(\mathbf{FHA})^H(\mathbf{FHA})\right\} + \sigma_{n_R}^2 Trace\left\{\mathbf{F}^H\mathbf{F}\right\}}{\sigma_n^2}$ is convex. Similar to the previous manipulation, f can be expressed as $f = \mathrm{vec}(\mathbf{F})^H \left(\left(\mathbf{HAA}^H\mathbf{H}^H\right)^T \otimes \mathbf{I}_M\right) \mathrm{vec}(\mathbf{F}) + \mathrm{vec}(\mathbf{F})^H \mathrm{vec}(\mathbf{F})$, with the following four Hessian matrices,

$$\begin{aligned}
&\underset{\mathrm{vec}(\mathbf{F})^*,\mathrm{vec}(\mathbf{F})}{\mathcal{H}}(f) = \left[\left(\mathbf{HAA}^H\mathbf{H}^H\right)^T \otimes \mathbf{I}_M\right]^T, \\
&\underset{\mathrm{vec}(\mathbf{F}),\mathrm{vec}(\mathbf{F})^*}{\mathcal{H}}(f) = \left[\left(\mathbf{HAA}^H\mathbf{H}^H\right)^T \otimes \mathbf{I}_M\right], \\
&\underset{\mathrm{vec}(\mathbf{F}),\mathrm{vec}(\mathbf{F})}{\mathcal{H}}(f) = 0, \\
&\underset{\mathrm{vec}(\mathbf{F})^*,\mathrm{vec}(\mathbf{F})^*}{\mathcal{H}}(f) = 0.
\end{aligned} \tag{5.22}$$

Therefore, the block matrix $\mathcal{H}(f)$ is positive semidefinite. Since both the objective function and the feasible set in (5.17) are convex, the optimization problem (5.17) is convex.

Design of F

Now, we proceed with the sparse approximation of $\mathbf{F}$. Note that (5.18) can be reformulated as follows,

$$\begin{aligned}
MSE_{\mathbf{F}} = &Trace\left\{\mathbf{Z}\underbrace{\left(\sigma_{\mathbf{n}_R}^2\mathbf{I}_M + \sigma_{\mathbf{x}}^2\mathbf{HA(HA)}^H\right)}_{\mathbf{D}\in\mathcal{C}_{M\times M}}\mathbf{Z}^H\right\} - \\
&Trace\left\{\underbrace{\sigma_{\mathbf{x}}^2\mathbf{P(HA)}^H}_{\mathbf{E}\in\mathcal{C}_{2K\times M}}\mathbf{Z}^H\right\} - Trace\left\{\mathbf{Z}\underbrace{\sigma_{\mathbf{x}}^2\mathbf{HA(P)}^H}_{\mathbf{E}^H}\right\},
\end{aligned} \tag{5.23}$$

where $\mathbf{Z} = \underbrace{\mathbf{BH}^T\mathbf{F}}_{\mathbf{Z}\in\mathcal{C}_{2K\times M}}$. Therefore, the $MSE_{\mathbf{F}}$ minimization problem can be transformed into the following problem,

$$\begin{aligned}
&\min MSE_{\mathbf{F}} \\
&\text{s.t. (5.8b)},
\end{aligned} \tag{5.24}$$

with

$$\begin{aligned} MSE_{\mathbf{F}} &= Trace\left\{\left(\mathbf{B}\mathbf{H}^T\mathbf{F}\mathbf{D}^{\frac{1}{2}} - \mathbf{E}\mathbf{D}^{-\frac{1}{2}}\right)\left(\mathbf{B}\mathbf{H}^T\mathbf{F}\mathbf{D}^{\frac{1}{2}} - \mathbf{E}\mathbf{D}^{-\frac{1}{2}}\right)^H\right\} = \\ &\left\|\mathbf{B}\mathbf{H}^T\mathbf{F}\mathbf{D}^{\frac{1}{2}} - \mathbf{E}\mathbf{D}^{-\frac{1}{2}}\right\|_F^2 = \left\|\left(\mathbf{B}\mathbf{H}^T \otimes \left(\mathbf{D}^{\frac{1}{2}}\right)^T\right) vec\left(\mathbf{F}^T\right) - vec\left(\mathbf{E}\mathbf{D}^{-\frac{1}{2}}\right)^T\right\|_2^2. \end{aligned} \tag{5.25}$$

where $vec\left(\mathbf{F}^T\right)$ is the block sparse vector with length M^2, $\otimes$ denotes the Kronecker product of matrices. The optimization (5.25) is called the multiple measurement vectors (MMV) problem in compressed sensing (CS) literature. To minimize the MMV problem in (5.25), there are several classes of algorithms, including the mixed norm approach (convex relaxation) [131], block sparsity approach [132], and Bayesian framework [133]. To minimize $MSE_{\mathbf{F}}$ with sparse structure and power constraints, in this work, we use the BOMP sparse algorithm [132], which is developed based on OMP. The sparse approximation of $\mathbf{F}$ can be obtained as follows,

$$vec\left(\mathbf{F}^T\right) = BOMP\left(\mathbf{B}\mathbf{H}^T \otimes \left(\mathbf{D}^{\frac{1}{2}}\right), vec\left(\mathbf{E}\mathbf{D}^{-\frac{1}{2}}\right)^T, G, S, P_R\right), \tag{5.26}$$

where G includes different block labels corresponding to different row indices in $\mathbf{F}$, S suggests the level of sparsity, and P_R follows the relay power constraint. As an example, when $M = 4$, $G = [1,1,1,1,2,2,2,2,3,3,3,3,4,4,4,4]$, and $S = 2$, the resultant sparse $\mathbf{F}$ beamforming matrix comprises of two non-zero rows corresponding to the selected relay antennas and two all zero rows corresponding to the relay antennas that will not participate in the relaying.

5.5.2 Design of the Sparse Transmit Beamforming Matrix A:

Secondly, we consider the optimization of the transmit beamforming matrix $\mathbf{A}$, for fixed relay and receive beamforming matrices $\mathbf{F}$ and $\mathbf{B}$, formulated as follows,

$$\begin{aligned} &\min_{\mathbf{A}} MSE_{\mathbf{A}} \\ &\text{s.t. (5.8a)}, \end{aligned} \tag{5.27}$$

where

$$\begin{aligned} MSE_{\mathbf{A}} &= Trace\left\{\left(\mathbf{B}\mathbf{H}^T\mathbf{F}\mathbf{H}\mathbf{A} - \mathbf{P}\right)\mathbf{R}_{\mathbf{xx}}\left(\mathbf{B}\mathbf{H}^T\mathbf{F}\mathbf{H}\mathbf{A} - \mathbf{P}\right)^H\right\} = \\ &Trace\left\{\mathbf{A}^H\mathbf{H}^H\mathbf{F}^H(\mathbf{B}\mathbf{H})^*\mathbf{B}\mathbf{H}^T\mathbf{F}\mathbf{H}\mathbf{A}\mathbf{R}_{\mathbf{xx}}\right\} - Trace\left\{\mathbf{A}\mathbf{R}_{\mathbf{xx}}\mathbf{P}^H\mathbf{B}\mathbf{H}^T\mathbf{F}\mathbf{H}\right\} \\ &-Trace\left\{\mathbf{A}^H\left(\mathbf{B}\mathbf{H}^T\mathbf{F}\mathbf{H}\right)^H\mathbf{P}\mathbf{R}_{\mathbf{xx}}\right\} + Trace\left\{\mathbf{P}\mathbf{P}^H\right\}. \end{aligned} \tag{5.28}$$

In the following, we firstly prove that (5.27) is convex, to corroborate the convergence of the ensuing subproblem, followed by detailed formulation of the sparse subproblem algorithm.

convexity of (27)

Following the matrix manipulations in [129] [*Eq*.1.10.62, *Eq*.1.10.64], (5.28) can be reformulated as follows,

$$\begin{aligned} MSE_{\mathbf{A}} = & \operatorname{vec}(\mathbf{A})^H \left((\mathbf{R_{xx}})^T \otimes \mathbf{H}^H \mathbf{F}^H (\mathbf{BH})^* \mathbf{B}\mathbf{H}^T \mathbf{F}\mathbf{H} \right) \operatorname{vec}(\mathbf{A}) + \\ & \operatorname{vec}\left(\left(\mathbf{R_{xx}} \mathbf{P}^H \mathbf{B}\mathbf{H}^T \mathbf{F}\mathbf{H} \right)^T \right)^T \operatorname{vec}(\mathbf{A}) + \operatorname{vec}(\mathbf{A})^H \operatorname{vec}\left(\mathbf{R_{xx}} \mathbf{P}^H \mathbf{B}\mathbf{H}^T \mathbf{F}\mathbf{H} \right)^H. \end{aligned} \tag{5.29}$$

Based on the vector differential rule in [130], the four Hessian matrices are derived as follows,

$$\begin{aligned} & \underset{\operatorname{vec}(\mathbf{A})^*, \operatorname{vec}(\mathbf{A})}{\mathcal{H}} (MSE_{\mathbf{A}}) = \left[(\mathbf{R_{xx}})^T \otimes \mathbf{H}^H \mathbf{F}^H (\mathbf{BH})^* \mathbf{B}\mathbf{H}^T \mathbf{F}\mathbf{H} \right]^T, \\ & \underset{\operatorname{vec}(\mathbf{A}), \operatorname{vec}(\mathbf{A})^*}{\mathcal{H}} (MSE_{\mathbf{A}}) = \left[(\mathbf{R_{xx}})^T \otimes \mathbf{H}^H \mathbf{F}^H (\mathbf{BH})^* \mathbf{B}\mathbf{H}^T \mathbf{F}\mathbf{H} \right], \\ & \underset{\operatorname{vec}(\mathbf{A}), \operatorname{vec}(\mathbf{A})}{\mathcal{H}} (MSE_{\mathbf{A}}) = \mathbf{0}, \\ & \underset{\operatorname{vec}(\mathbf{A})^*, \operatorname{vec}(\mathbf{A})^*}{\mathcal{H}} (MSE_{\mathbf{A}}) = \mathbf{0}. \end{aligned} \tag{5.30}$$

In order to show the convexity of $MSE_{\mathbf{A}}$, the following block matrix should be positive semidefinite.

$$\mathcal{H}(MSE_{\mathbf{A}}) = \begin{bmatrix} \hat{\mathbf{K}}^T & \mathbf{0} \\ \mathbf{0} & \hat{\mathbf{K}} \end{bmatrix}, \tag{5.31}$$

where $\hat{\mathbf{K}} = \left[(\mathbf{R_{xx}})^T \otimes \mathbf{H}^H \mathbf{F}^H (\mathbf{BH})^* \mathbf{B}\mathbf{H}^T \mathbf{F}\mathbf{H} \right]$. Noting that the Kronecker product of any two positive semidefinite matrices is also positive semidefinite [127], we derive that $\hat{\mathbf{K}}$ should be positive semidefinite. Hence, the convexity of $MSE_{\mathbf{A}}$ is proven. Therefore, the objective function in (5.27) is convex.

Next, we prove that the feasible set provided by (5.8a) is convex. We can prove this by showing that $f = \sigma_{\mathbf{x}}^2 Trace\left\{ \mathbf{A}^H \mathbf{A} \right\}$ is convex. Similar to the mathematical manipulations in subsection A part 1, we can readily prove that the block matrix $\mathcal{H}(f)$ is positive semidefinite. Since both the objective function and the feasible set in (5.27) are convex, the optimization problem (5.27) is convex.

Design of A

We proceed with the sparse approximation of $\mathbf{A}$. Note that in (5.27), the sparse approximation of $\mathbf{A}$ can be performed separately, per column, as follows,

$$\mathbf{a}_1 = OMP\left(\mathbf{\Lambda}_{1:N_1}, \mathbf{p}_1, \left\|\mathbf{BH}^T\mathbf{FH}\mathbf{a}_1 - \mathbf{p}_1\right\|_2^2 \leqslant \varepsilon, Trace\left\{\mathbf{a}_1^H\mathbf{a}_1\right\} = P_{u_1}\right),$$

$$\vdots$$

$$\mathbf{a}_{2K} = OMP\left(\mathbf{\Lambda}_{\sum_{i=1}^{2K-1} N_i+1:\sum_{i=1}^{2K} N_i}, \mathbf{p}_{2K}, \left\|\mathbf{BH}^T\mathbf{FH}\mathbf{a}_{2K} - \mathbf{p}_{2K}\right\|_2^2 \leqslant \varepsilon, Trace\left\{\mathbf{a}_{2K}^H\mathbf{a}_{2K}\right\} = P_{u_{2K}}\right), \tag{5.32}$$

where $\mathbf{a}_i, i = 1, \ldots, 2K$ represents the i^{th} column of $\mathbf{A}$, $\mathbf{\Lambda}_{a:b}$ represents the row elements in $\mathbf{\Lambda}$ that belong to columns a to b with $\mathbf{\Lambda} = \mathbf{BH}^T\mathbf{FH}$, $\mathbf{p}_j, j = 1, \ldots, 2K$, represents the j^{th} column of $\mathbf{P}$, and $\sigma_{\mathbf{x}}^2 \sum_{i=1}^{2K} P_{u_i} = P_{MU}$. Note that following (5.32), we can keep a tight control over each user's transmit power, while the overall user transmit power is limited by (5.8b).

5.5.3 Design of the Sparse Receive Beamforming Matrix B:

The third subproblem is to optimize $\mathbf{B}$, for fixed transmit and relay beamforming matrices $\mathbf{A}$ and $\mathbf{F}$, formulated as follows,

$$\min_{\mathbf{B}} MSE_{\mathbf{B}}\ , \tag{5.33}$$

where

$$\begin{aligned} MSE_{\mathbf{B}} = {} & Trace\left\{\mathbf{BR_{nn}B}^H\right\} + Trace\left\{\mathbf{BH}^T\mathbf{FR}_{\mathbf{n}_R\mathbf{n}_R}\left(\mathbf{BH}^T\mathbf{F}\right)^H\right\} + \\ & Trace\left\{\mathbf{BH}^T\mathbf{FHAR_{xx}}\left(\mathbf{BH}^T\mathbf{FHA}\right)^H\right\} - Trace\left\{\mathbf{PR_{xx}}\left(\mathbf{BH}^T\mathbf{FHA}\right)^H\right\} \\ & -Trace\left\{\left(\mathbf{BH}^T\mathbf{FHA}\right)\mathbf{R_{xx}}(\mathbf{P})^H\right\}. \end{aligned} \tag{5.34}$$

In the following, we firstly prove that (5.33) is convex, to corroborate the convergence of the ensuing subproblem, followed by detailed formulation of the sparse subproblem algorithm.

Convexity of (5.33)

Following the matrix manipulations in [129] [Eq.1.10.62, Eq.1.10.64], (5.34) can be reformulated as follows,

$$MSE_{\mathbf{B}} = \mathrm{vec}(\mathbf{B})^H \left(\sigma_{\mathbf{n}}^2 \mathbf{I}_{\sum N_k} + \sigma_{\mathbf{n}_R}^2 \mathbf{H}^T\mathbf{F}\left(\mathbf{H}^T\mathbf{F}\right)^H + \sigma_{\mathbf{x}}^2 \mathbf{H}^T\mathbf{F}\mathbf{H}\mathbf{A}\left(\mathbf{H}^T\mathbf{F}\mathbf{H}\mathbf{A}\right)^H\right)\mathrm{vec}\,(\mathbf{B}) + \mathrm{vec}\left(\left(\left(\mathbf{H}^T\mathbf{F}\mathbf{H}\mathbf{A}\right)\mathbf{R}_{\mathbf{xx}}(\mathbf{P})^H\right)^T\right)^T \mathrm{vec}\,(\mathbf{B}) + \mathrm{vec}(\mathbf{B})^H \mathrm{vec}\left(\left(\mathbf{H}^T\mathbf{F}\mathbf{H}\mathbf{A}\right)\mathbf{R}_{\mathbf{xx}}(\mathbf{P})^H\right)^H. \tag{5.35}$$

The four Hessian matrices as defined in [130] are derived as follows,

$$\begin{aligned}
&\underset{\mathrm{vec}(\mathbf{B})^*,\mathrm{vec}(\mathbf{B})}{\mathcal{H}}(MSE_{\mathbf{B}}) = \left[\sigma_{\mathbf{n}}^2 \mathbf{I}_{\sum N_k} + \sigma_{\mathbf{n}_R}^2 \mathbf{H}^T\mathbf{F}\left(\mathbf{H}^T\mathbf{F}\right)^H + \sigma_{\mathbf{x}}^2 \mathbf{H}^T\mathbf{F}\mathbf{H}\mathbf{A}\left(\mathbf{H}^T\mathbf{F}\mathbf{H}\mathbf{A}\right)^H\right]^T,\\
&\underset{\mathrm{vec}(\mathbf{B}),\mathrm{vec}(\mathbf{B})^*}{\mathcal{H}}(MSE_{\mathbf{B}}) = \left[\sigma_{\mathbf{n}}^2 \mathbf{I}_{\sum N_k} + \sigma_{\mathbf{n}_R}^2 \mathbf{H}^T\mathbf{F}\left(\mathbf{H}^T\mathbf{F}\right)^H + \sigma_{\mathbf{x}}^2 \mathbf{H}^T\mathbf{F}\mathbf{H}\mathbf{A}\left(\mathbf{H}^T\mathbf{F}\mathbf{H}\mathbf{A}\right)^H\right],\\
&\underset{\mathrm{vec}(\mathbf{B}),\mathrm{vec}(\mathbf{B})}{\mathcal{H}}(MSE_{\mathbf{B}}) = \mathbf{0},\\
&\underset{\mathrm{vec}(\mathbf{B})^*,\mathrm{vec}(\mathbf{B})^*}{\mathcal{H}}(MSE_{\mathbf{B}}) = \mathbf{0}.
\end{aligned} \tag{5.36}$$

In order to show the convexity of $MSE_{\mathbf{B}}$, the following block matrix should be positive semidefinite.

$$\mathcal{H}(MSE_{\mathbf{B}}) = \begin{bmatrix} \tilde{\mathbf{K}}^T & 0 \\ 0 & \tilde{\mathbf{K}} \end{bmatrix}, \tag{5.37}$$

where $\tilde{\mathbf{K}} = \left[\sigma_{\mathbf{n}}^2 \mathbf{I}_{\sum N_k} + \sigma_{\mathbf{n}_R}^2 \mathbf{H}^T\mathbf{F}\left(\mathbf{H}^T\mathbf{F}\right)^H + \sigma_{\mathbf{x}}^2 \mathbf{H}^T\mathbf{F}\mathbf{H}\mathbf{A}\left(\mathbf{H}^T\mathbf{F}\mathbf{H}\mathbf{A}\right)^H\right]$. Following similar steps as in the previous subsections, we can derive that $\tilde{\mathbf{K}}$ is positive semidefinite. Hence, the convexity of $MSE_{\mathbf{B}}$ is proven.

Desing of B

The optimization problem can be reformulated as follows,

$$MSE_{\mathbf{B}} = Trace\left\{\mathbf{B}\underbrace{\left(\sigma_{\mathbf{n}}^2\mathbf{I}_{\sum N_k} + \sigma_{\mathbf{n}_R}^2\mathbf{H}^T\mathbf{F}\left(\mathbf{H}^T\mathbf{F}\right)^H + \sigma_{\mathbf{x}}^2\mathbf{H}^T\mathbf{FHA}\left(\mathbf{H}^T\mathbf{FHA}\right)^H\right)}_{\hat{\mathbf{D}}\in\mathcal{C}_{\sum N_k\times\sum N_k}}\mathbf{B}^H\right\} -$$
$$Trace\left\{\underbrace{\sigma_{\mathbf{x}}^2\mathbf{P}\left(\mathbf{H}^T\mathbf{FHA}\right)^H}_{\mathbf{E}\in\mathcal{C}_{2K\times M}}\mathbf{B}^H\right\} - Trace\left\{\mathbf{B}\underbrace{\sigma_{\mathbf{x}}^2\mathbf{H}^T\mathbf{FHA}(\mathbf{P})^H}_{\mathbf{E}^H}\right\}. \tag{5.38}$$

Therefore, the $MSE_{\mathbf{B}}$ minimization problem can be transformed into the following problem,

$$\min MSE(\text{Transformed})_{\mathbf{B}}, \tag{5.39}$$

with

$$MSE(\text{Transformed})_{\mathbf{B}} = Trace\left\{\left(\mathbf{B}\hat{\mathbf{D}}^{\frac{1}{2}} - \mathbf{E}\hat{\mathbf{D}}^{-\frac{1}{2}}\right)\left(\mathbf{B}\hat{\mathbf{D}}^{\frac{1}{2}} - \mathbf{E}\hat{\mathbf{D}}^{-\frac{1}{2}}\right)^H\right\}. \tag{5.40}$$

The sparse estimation of $\mathbf{B}$ can be performed per column, as follows,

$$\begin{aligned}
\hat{\mathbf{z}}_1 &= OMP\left(\left(\hat{\mathbf{D}}^{\frac{1}{2}}\right)^T, \hat{\mathbf{I}}_1, \left\|\left(\hat{\mathbf{D}}^{\frac{1}{2}}\right)^T\hat{\mathbf{z}}_1 - \hat{\mathbf{I}}_1\right\|_2^2 \leqslant \varepsilon, Trace\left\{\hat{\mathbf{z}}_1^H\hat{\mathbf{z}}_1\right\} = \rho_1\right),\\
&\vdots\\
\hat{\mathbf{z}}_{2K} &= OMP\left(\left(\hat{\mathbf{D}}^{\frac{1}{2}}\right)^T, \hat{\mathbf{I}}_{2K}, \left\|\left(\hat{\mathbf{D}}^{\frac{1}{2}}\right)^T\hat{\mathbf{z}}_{2K} - \hat{\mathbf{I}}_{2K}\right\|_2^2 \leqslant \varepsilon, Trace\left\{\hat{\mathbf{z}}_1^H\hat{\mathbf{z}}_2K\right\} = \rho_{2K},\right),
\end{aligned} \tag{5.41}$$

where $\hat{\mathbf{z}}_i, i = 1,\ldots,2K$ represents the i^{th} column of $\hat{\mathbf{Z}}$, with $\hat{\mathbf{Z}} = \mathbf{B}^T$, $\hat{\mathbf{I}}_j, j = 1,\ldots,2K$, represents the j^{th} column of $\hat{\mathbf{I}} = \left(\mathbf{E}\hat{\mathbf{D}}^{-\frac{1}{2}}\right)^T$, and aiming to minimize the first term in (5.15) to minimize the total system MSE, $\rho_j, j = 1,\ldots,2K$ is chosen to be sufficiently small. Note that the optimal beamforming matrix $\mathbf{B}$ is thus obtained as follows,

$$\mathbf{B} = \hat{\mathbf{Z}}^T. \tag{5.42}$$

In summary, we outline the iterative beamforming design algorithm as provided in Algorithm 1, where MSE_i denotes the total MSE at i^{th} iteration based on (5.15).

Note that the proposed sparse iterative method in Algorithm 1 is convergent. More specifically, even though the primal problem in (5.16) is non-linear and non-convex, yet, each

Algorithm 1: Iterative sparse beamforming design algorithm

Initialize $\mathbf{A}$ to meet (5.8a);
Initialize $\mathbf{B}$ to get small $Trace\left\{\mathbf{B}\mathbf{R}_{\mathbf{nn}}\mathbf{B}^H\right\}$;
repeat
- Design $\mathbf{F}$ using (5.24) and (5.26);
- Following (5.15), compute MSE_i;
- Compute $\delta = |MSE_i - MSE_{i-1}|^2$;

if δ not sufficiently small **then**
- Design $\mathbf{A}$ using (5.27) and (5.32);
- Design $\mathbf{B}$ using (5.33) and (5.41);

end if
until δ is sufficiently small.

of the three subproblems under consideration is convex, and therefore, can be optimized. At each iteration, not only the MSE associated with that step ($MSE_{\mathbf{A}}$, $MSE_{\mathbf{B}}$, or $MSE_{\mathbf{F}}$) is minimized, but also the total system MSE in (5.15) is minimized, and therefore, the algorithm converges.

5.6 Numerical Results

In this section, we present Monte-Carlo simulations to verify the sparse beamforming algorithm's error performance and convergence. We have used quadrature phase shift keying (QPSK) modulation. We consider multiuser TWR systems with different number of users, and different number of antennas at the participating user and relay terminals, and further define the system SER as the SER averaged over the users.

In Fig. 5.2, the SER performance of the proposed iterative sparse beamforming algorithm is analyzed for different number of relay antennas. We have 10 number of available antennas at each user terminal and $2K = 2$. We further fix P_R at 20 dB. The iterative algorithm selects 2 number of antennas at user and relay terminals. As the number of available antennas at the relay terminal increases, the SER performance is improved.

In Fig. 5.3, it can be seen that as the number of selected antennas at each user terminal increases, better SER performance is achieved. In particular, for multiuser SNR levels at SNR_{MU}=6 dB and 8 dB, the acheivable SER performance with 6 selected user antennas is comparable with the case when all antennas at each user is active. This proves the diminishing returns in the average SER versus the number of selected antennas.

Fig. 5.4 shows the convergence behavior of the proposed sparse iterative algorithm for

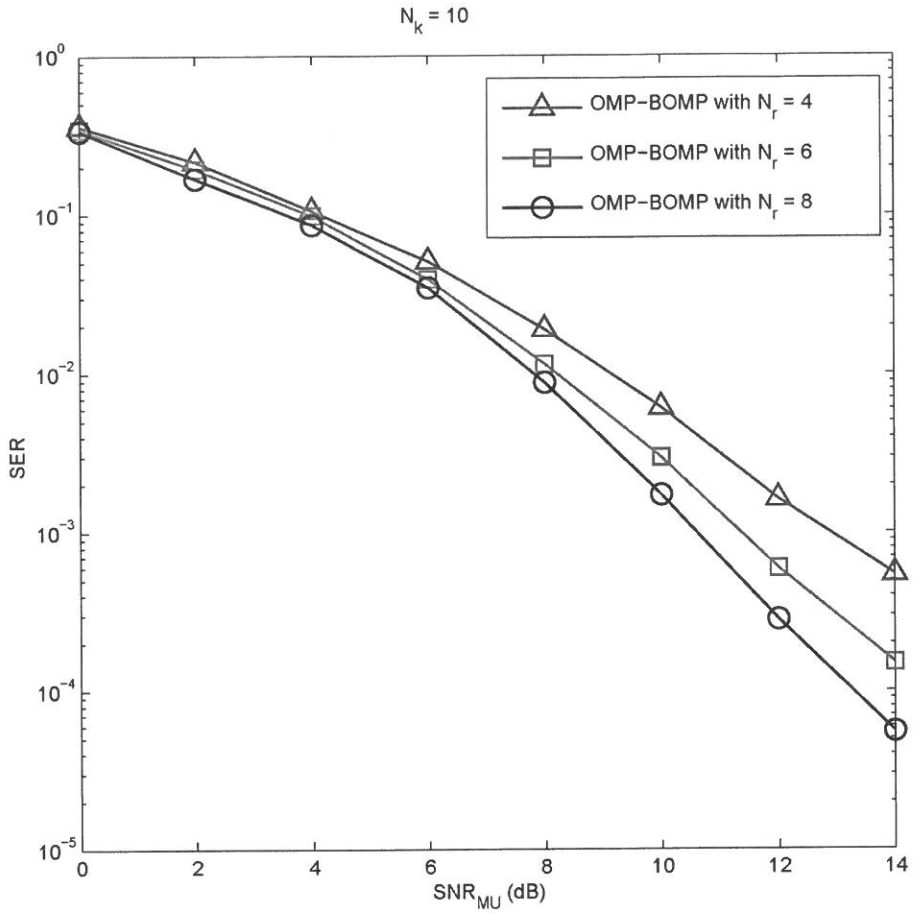

Figure 5.2: SER performance of the proposed sparse iterative beamforming method.

different network scenarios with different number of user antennas and $M = 4$, when received SNR at the relay terminal is fixed at 25 dB. For $N_k = 2$, all transmit and receive antennas are active, where as for $N_k = 6$ and $N_k = 10$, only 2 transmit and receive antennas are active. As is illustrated in Fig. 5.4, by increasing the number of available antennas at user terminals, more number of iterations are required to achieve convergence. Nevertheless, the extra number of iterations required in large networks to reach convergence is negligible.

In Fig. 5.5 and Fig. 5.6, the total system MSE of the proposed sparse iterative algorithm provided in (5.15) is studied for a network with $M = 4$ and $N_k = 2$, when the received SNR at the relay terminal is fixed at 25 dB. The total system MSE in (5.15) is broken into three

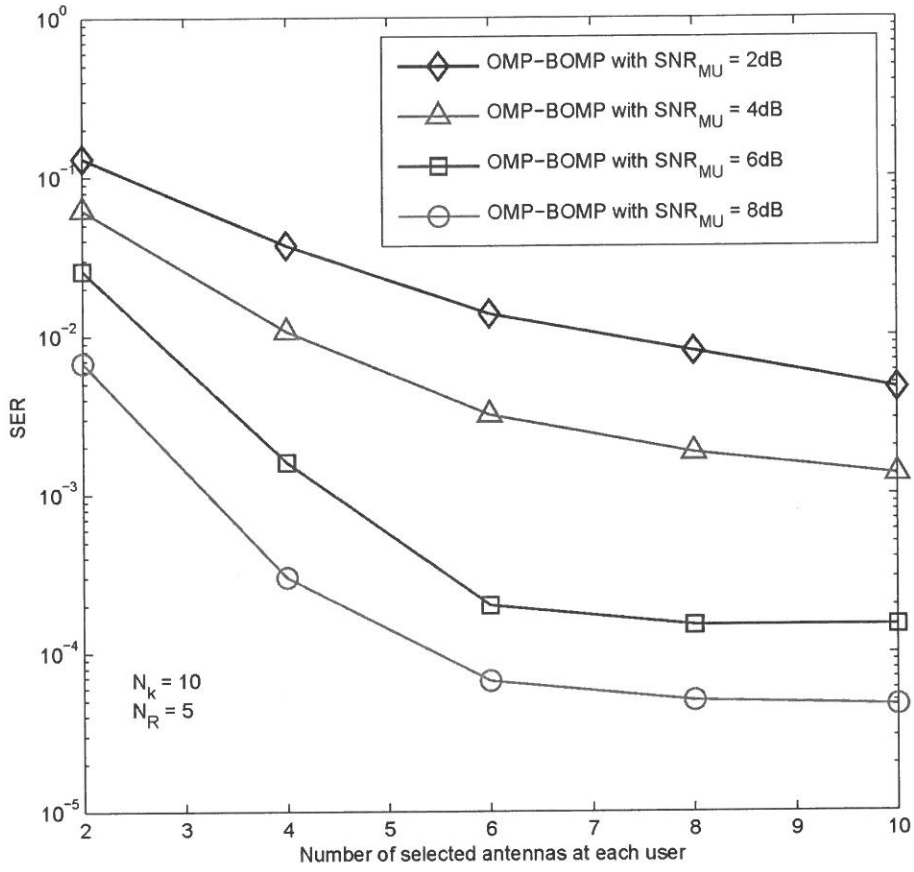

Figure 5.3: SER performance of the proposed sparse iterative beamforming method with varying number of selected antennas at user terminals.

parts, i.e. MSE_1, MSE_2, and MSE_3, where

$$MSE_1 = Trace\left\{\mathbf{B}\mathbf{R}_{\mathbf{nn}}\mathbf{B}^H\right\}, \tag{5.43a}$$

$$MSE_2 = Trace\left\{\mathbf{B}\mathbf{H}^T\mathbf{F}\mathbf{R}_{\mathbf{n}_R\mathbf{n}_R}\left(\mathbf{B}\mathbf{H}^T\mathbf{F}\right)^H\right\}, \tag{5.43b}$$

$$MSE_3 = Trace\left\{\left(\mathbf{B}\mathbf{H}^T\mathbf{F}\mathbf{H}\mathbf{A} - \mathbf{P}\right)\mathbf{R}_{\mathbf{xx}}\left(\mathbf{B}\mathbf{H}^T\mathbf{F}\mathbf{H}\mathbf{A} - \mathbf{P}\right)^H\right\}. \tag{5.43c}$$

It can be seen from Fig. 5.5 and Fig. 5.6 that MSE_1 is fixed at a constant level. This is mainly due to (5.43), where trace of $\mathbf{B}$ is maintained in an arbitrarily low level. MSE_3 is much less than MSE_1 and MSE_2, and therefore is the least dominant term. Following

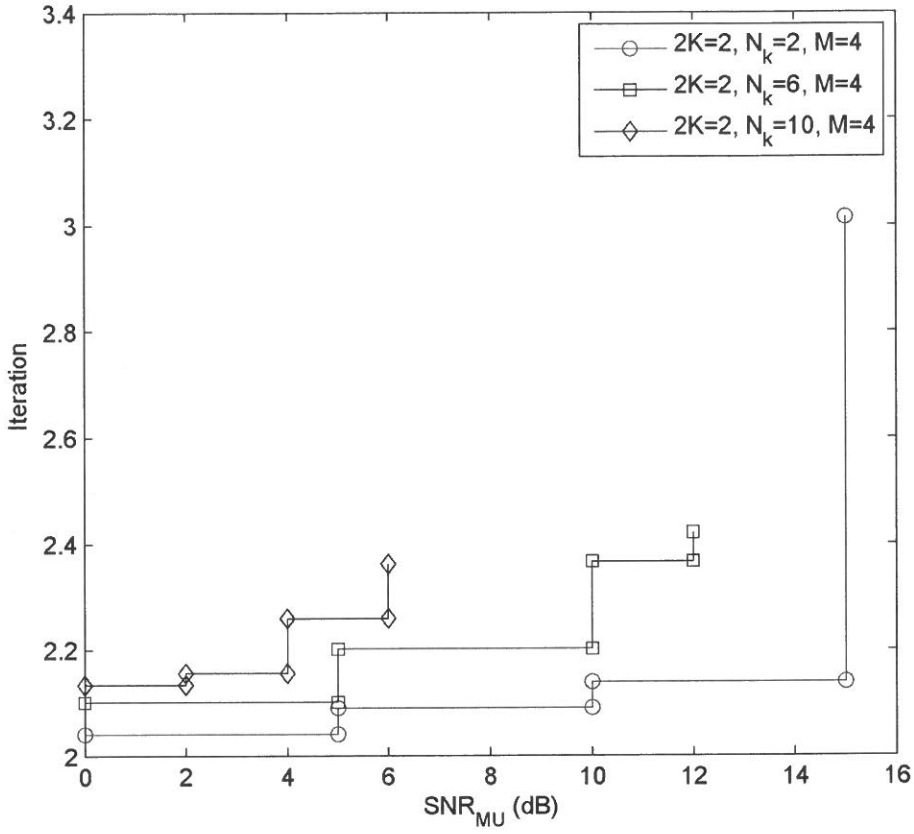

Figure 5.4: Convergence behavior of the proposed sparse iterative beamforming method.

Fig. 5.6, it can be realized that MSE_3 is the most dominant term out of the three in (5.15), whose value is continuously decreasing as SNR_{MU} increases. This, in fact ensures the convergence of the proposed iterative MMSE-based beamforming algorithm.

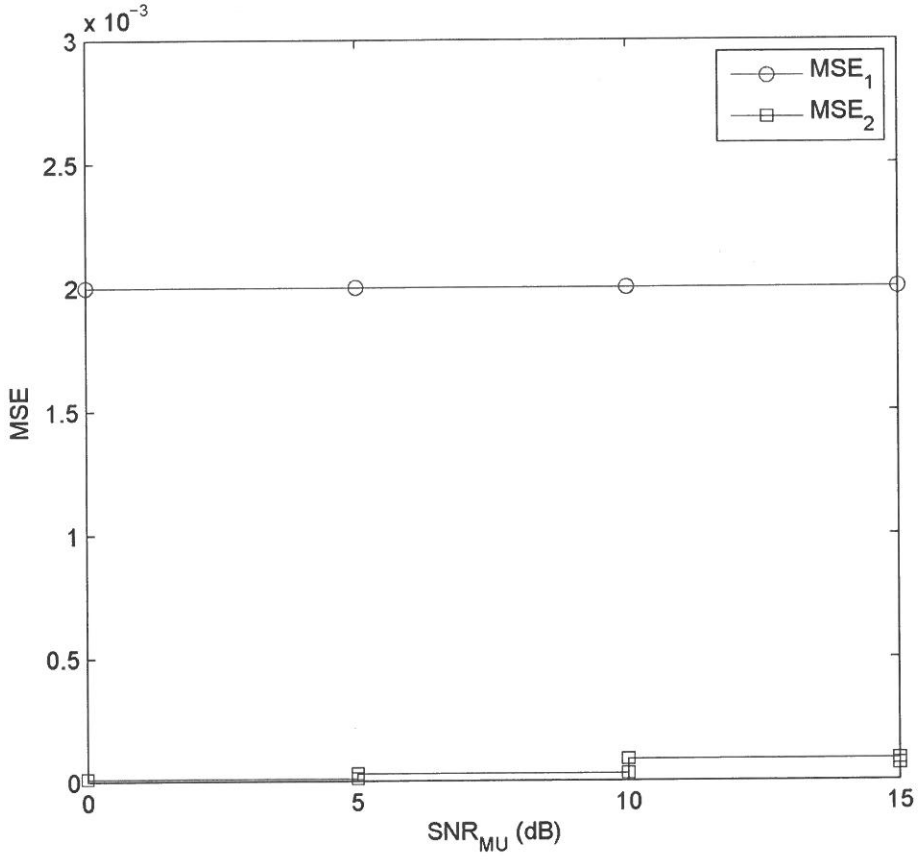

Figure 5.5: MSE behavior of the proposed sparse iterative beamforming method.

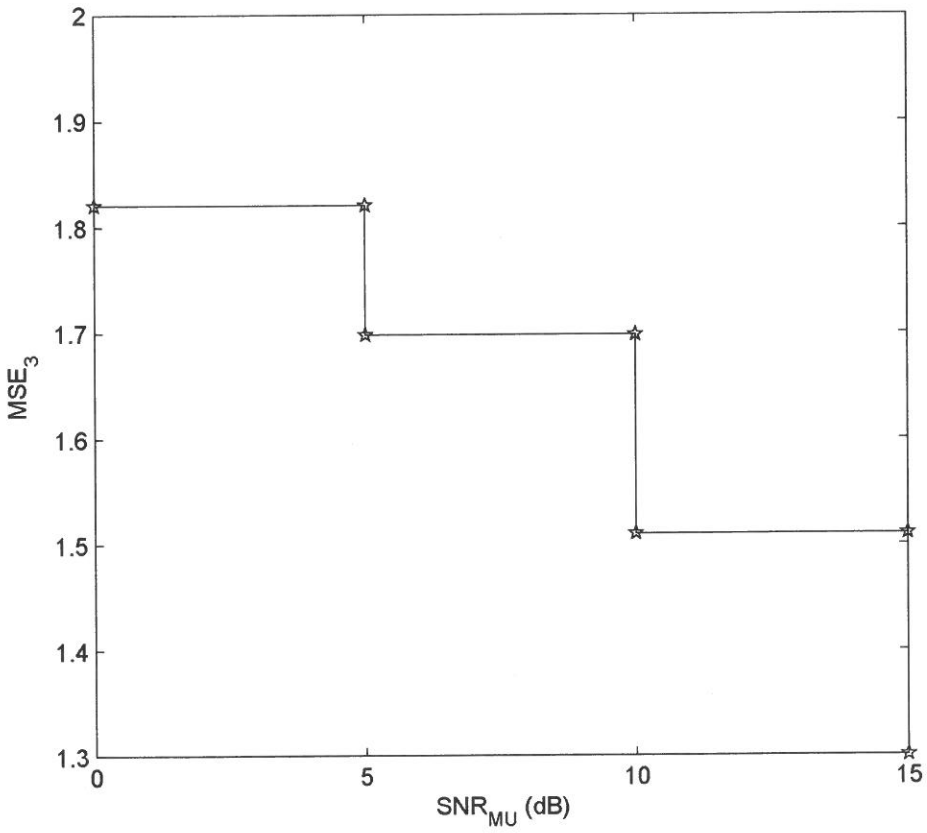

Figure 5.6: MSE behavior of the proposed sparse iterative beamforming method.

Chapter 6

Differential Space-Time Block Coding with Linear constellation Precoding for OFDM Cooperative Networks

6.1 Introduction

For multi-antenna systems operating over frequency-selective fading channels, as either the number of antennas or the fade rate increases, it is desirable to develop techniques that do not require CSI at the receiver side. Differential modulation was proposed as an encoding scheme that doesn't require CSI at the receiver side. Hughes [134] and Hochwald and Sweldens [49] independently proposed a differential unitary space-time modulation scheme for frequency flat fading channels, where the constellation groups were formed based on matrix multiplication. [135] proposed another differential space-time (DST) coding scheme based on orthogonal designs. Full spatial diversity group constellations of finite order and infinite group codes with full spatial diversity were proposed in [136] and [137], respectively. Treating each subchannel as a transmit antenna, Liu and Giannakis [138] proposed a differential encoding scheme for single-antenna OFDM transmissions over frequency-selective fading channels with maximum multipath diversity.

In [139], Diggavi et al. proposed a simple extension of DST coding in a multiantenna OFDM system in which the DST codes for frequency flat fading channels were applied

to each subcarrier across the transmit antennas. However, such an extension does not exploit the underlying multipath diversity in frequency-selective fading channels. Recently, maximum-diversity differential modulation schemes over frequency-selective fading channels have been proposed in [140], [141], and [142]. In [140], unitary diagonal codes are utilized to achieve the maximum underlying diversity gain. The approach in [142], uses the orthogonal designs and obtains maximum spatial and multipath diversity. In [143], It is proven that with differential coding, full spatial and multipath diversity can be achieved, where simultaneous coding over space and frequency is implemented.

Most the current works on cooperative diversity consider coherent detection and assume the availability of perfect CSI at the receiver. In fading channels where the coherence time is large enough, the channel estimation can be carried out through the use of pilot symbols [144]. For fast fading channels where the phase carrier recovery is more difficult, differential detection provides a more practical solution. In [144–148], differential detection has been investigated for cooperative transmission scenarios. The works in [144–148] assume an idealized transmission environment with an underlying frequency-flat fading channel. This assumption can be justified for narrowband cooperative scenarios with fixed infrastructure; however, it is impractical if wideband cooperative networks are considered. In [149], the applicability of differential STBC to broadband cooperative transmission over frequency-selective channels was investigated for OFDM systems. However, the proposed system could not fully exploit the underlying multipath diversity. Motivated by this practical concern, we extend the work in [149] to linearly coded and grouped precoded OFDM systems for cooperative communications.

LCP-OFDM was developed in [150] for multicarrier wireless transmissions over frequency selective fading channels. Not only LCP improves the uncoded OFDM performance, but also doesn't reduce the transmission rates of uncoded OFDM, and guarantees symbol detectability [151]. LCP-OFDM was extended to GLCP-OFDM to exploit the correlation structure of subchannels, such that, the set of correlated sunchannels are split into subsets of less correlated subchannels. Within each subset of subcarriers, a LCP is designed to maximize diversity and coding gains. The LCPs are in general complex and could possibly be nonunitary. While greatly reducing the system complexity, subcarrier grouping maintains the maximum possible diversity and coding gains [150]. GLCP-OFDM is a considerably flexible system that offers maximum multipath diversity, as well as large coding gains, and guaranteed symbol detectability with low decoding complexity.

Although there have been considerable research efforts on differential STBC (conventional and distributed) for frequency flat fading channels (see for example [144–148, 152–154]), only a few isolated results have been reported on conventional differential STBC for frequency-selective channels [139, 155, 156]. Distributed differential STBC multi-carrier transmission for broadband cooperative networks was investigated in [149], yet was sub-optimal. In this chapter, We study the performance of differential space-time codes with LCP for OFDM cooperative networks over frequency selective channels. Through exploiting the unitary structure of the orthogonal STBCs, we design a low complexity differential STBC-LCP-OFDM receiver for cooperative networks. We assume the amplify-and-forward protocol and consider both single relay and multi-relay scenarios. Under the assumption of perfect power control for the relay terminal and high signal-to-noise ratio for the underlying links, our performance analysis demonstrates that the considered scheme is able to exploit fully the spatial diversity.

6.2 System Model

A single-relay assisted cooperative communication scenario is considered. All terminals are equipped with single transmit and receive antennas. We assume AF relaying and adopt the user cooperation protocol proposed by Nabar *et. al.* [68]. Specifically, the source terminal communicates with the relay terminal during the first signaling interval. There is no transmission from source-to-destination within this period. In the second signaling interval, both the relay and source terminals communicate with the destination terminal.

The CIRs for $S \rightarrow R$, $S \rightarrow D$ and $R \rightarrow D$ links for the j^{th} transmission block are given by $\mathbf{h}_{SR}^{j} = \left[h_{SR}^{j}[0], ..., h_{SR}^{j}[L_{SR}]\right]^{\mathrm{T}}$, $\mathbf{h}_{SD}^{j} = \left[h_{SD}^{j}[0], ..., h_{SD}^{j}[L_{SD}]\right]^{\mathrm{T}}$ and $\mathbf{h}_{RD}^{j} = \left[h_{RD}^{j}[0], ..., h_{RD}^{j}[L_{RD}]\right]^{\mathrm{T}}$, respectively, where L_{SR}, L_{SD} and L_{RD} denote the corresponding channel memory lengths. All $S \rightarrow R$, $S \rightarrow D$, and $R \rightarrow D$ links are assumed to experience frequency selective Rayleigh fading. The random vectors $\mathbf{h}_{SR}^{j}$, $\mathbf{h}_{RD}^{j}$ and $\mathbf{h}_{SD}^{j}$ are assumed to be independent zero-mean complex Gaussian with power delay profile vectors denoted by $\mathbf{v}_{SR} = [\sigma_{SR}^{2}(0), ..., \sigma_{SR}^{2}(L_{SR})]$, $\mathbf{v}_{RD} = [\sigma_{RD}^{2}(0), ..., \sigma_{RD}^{2}(L_{RD})]$, and $\mathbf{v}_{SD} = [\sigma_{SD}^{2}(0), ..., \sigma_{SD}^{2}(L_{SD})]$ that are normalized such that $\sum_{l_{SR}=0}^{L_{SR}} \sigma_{SR}^{2}(l_{SR}) = 1$, $\sum_{l_{RD}=0}^{L_{RD}} \sigma_{RD}^{2}(l_{RD}) = 1$, and $\sum_{l_{SD}=0}^{L_{SD}} \sigma_{SD}^{2}(l_{SD}) = 1$. The CIRs are assumed to be constant over four consecutive blocks and vary independently every four blocks.

We consider LCP-OFDM transformation [150] where the LCP is defined by the $N \times N$ matrix $\mathbf{\Phi}$ that has entries over the *complex* field. $\mathbf{\Phi}$ should satisfy the transmit-power

constraint $tr\left(\mathbf{\Phi}\mathbf{\Phi}^H\right) = N$. Information symbols are parsed into frames, where each frame consists of two information blocks. Let the $N \times 1$ vector $\mathbf{y}_{SRD}$ represent the data vector that is transmitted to the relay terminal during the first block of each frame, whose entries are complex MPSK symbols that are generated through differential space-time encoding.

After linear constellation precoding, the $N \times 1$ precoded block $\tilde{\mathbf{y}}_{SRD} = \mathbf{\Phi}\mathbf{y}_{SRD}$ is IFFT processed by the inverse FFT matrix $\mathbf{Q}^H$ to yield the discrete time signal $\mathbf{Q}^H\mathbf{\Phi}\mathbf{y}_{SRD}$. To further remove the IBI, a cyclic prefix of length $l \geq \max(L_{SR}, L_{RD}, L_{SD})$ is inserted per transmitted OFDM block and is removed from the corresponding received block.

The signal received at the relay terminal during the first signalling interval (broadcasting phase) of each frame after the CP removal is

$$\mathbf{r}_R = \sqrt{E_{SR}}\mathbf{H}_{SR}\mathbf{Q}^H\mathbf{\Phi}\mathbf{y}_{SRD} + \mathbf{n}_R, \tag{6.1}$$

where E_{SR} is the average signal energy over one symbol period received at relay terminal, $\mathbf{H}_{SR}$ is the $N \times N$ circulant matrix with entries $[\mathbf{H}_{SR}]_{m,n} = \mathbf{h}_{SR}((m-n) \bmod N)$, and $\mathbf{n}_R$ is the additive white Gaussian noise vector with each entry having zero-mean and variance of $N_0/2$ per dimension. To ensure that the power budget is not violated, the relay terminals normalizes each entry of the respective received signal $[\mathbf{r}_R]_n$, $n = 1, 2, ..., N$, by a factor of $\mathrm{E}\left(|[\mathbf{r}_R]_n|^2\right) = E_{SR} + N_0$ to ensure unit average energy and retransmits the signal during the second signalling interval (relaying phase) of each frame. After some mathematical manipulations, the received signal at the destination terminal during the relaying phase is given by

$$\mathbf{r}_D = \sqrt{\frac{E_{RD}E_{SR}}{E_{SR}+N_0}}\mathbf{H}_{RD}\mathbf{H}_{SR}\mathbf{Q}^H\mathbf{\Phi}\mathbf{y}_{SRD} + \sqrt{E_{SD}}\mathbf{H}_{SD}\mathbf{Q}^H\mathbf{\Phi}\mathbf{y}_{SD} + \mathbf{n}_D, \tag{6.2}$$

where E_{RD} and E_{SD} are the average signal energies over one symbol period received at destination terminal, $\mathbf{H}_{RD}$ and $\mathbf{H}_{SD}$ are the $N \times N$ circulant matrices with entries $[\mathbf{H}_{RD}]_{m,n} = \mathbf{h}_{RD}((m-n) \bmod N)$ and $[\mathbf{H}_{SD}]_{m,n} = \mathbf{h}_{SD}((m-n) \bmod N)$, respectively, and $\mathbf{n}_D$ is conditionally (conditioned on $\mathbf{h}_{RD}$) complex Gaussian with zero mean and variance $\sigma^2_{\mathbf{n}_D} = N_0\left(1 + \frac{E_{RD}}{E_{SR}+N_0}\sum_{m=0}^{L_{RD}}|\mathbf{h}_{RD}(m)|^2\right)$. The destination terminal further normalizes the received signal by a factor of $\sqrt{\rho}$, where $\rho = 1 + \frac{E_{RD}}{E_{SR}+N_0}\sum_{m=0}^{L_3}|\mathbf{h}_{RD}(m)|^2$. Note that this does not affect the SNR, but simplifies the ensuing presentation [68]. After normalization, we obtain

$$\mathbf{r} = \sqrt{\gamma_1}\mathbf{H}_{RD}\mathbf{H}_{SR}\mathbf{Q}^H\mathbf{\Phi}\mathbf{y}_{SRD} + \sqrt{\gamma_2}\mathbf{H}_{SD}\mathbf{Q}^H\mathbf{\Phi}\mathbf{y}_{SD} + \mathbf{n}, \tag{6.3}$$

where $\mathbf{n}$ is $\mathcal{CN}(0, N_0)$ and the scaling coefficients γ_1, γ_2 are defined as $\gamma_1 = \frac{a}{b}$, and $\gamma_2 = \frac{c}{b}$

respectively, where $a = (E_{SR}/N_0)E_{RD}$, $b = 1 + E_{SR}/N_0 + \sum_{m=0}^{L_3} |\mathbf{h}_{RD}(m)|^2 E_{RD}/N_0$, and $c = (1 + E_{SR}/N_0)E_{SD}$. Note that at the end of each frame, the receiver is provided with the time-domain observation $\mathbf{r}$ in (6.3).

Inspired by Alamouti code [10], we can further extend (6.3) to a distributed (D)STBC-LCP-OFDM scenario, by using the transmit diversity scheme $\mathbf{y}_{SRD}(t+1) = -\mathbf{y}_{SD}^*(t)$ and $\mathbf{y}_{SD}(t+1) = \mathbf{y}_{SRD}^*(t)$, leading to

$$\begin{aligned} \mathbf{r}(t) &= \sqrt{\gamma_1}\mathbf{H}_{RD}\mathbf{H}_{SR}\mathbf{Q}^H\mathbf{y}_{SRD}(t) + \sqrt{\gamma_2}\mathbf{H}_{SD}\mathbf{Q}^H\mathbf{\Phi}\mathbf{y}_{SD}(t) + \mathbf{n}(t), \\ \mathbf{r}(t+1) &= -\sqrt{\gamma_1}\mathbf{H}_{RD}\mathbf{H}_{SR}\mathbf{Q}^H\mathbf{\Phi}\mathbf{y}_{SD}^*(t) + \sqrt{\gamma_2}\mathbf{H}_{SD}\mathbf{Q}^H\mathbf{\Phi}\mathbf{y}_{SRD}^*(t) + \mathbf{n}(t+1), \end{aligned} \tag{6.4}$$

Exploiting the circulant structure of the channel matrices $\mathbf{H}_{RD}$, $\mathbf{H}_{SR}$, and $\mathbf{H}_{SD}$, we have $\mathbf{H}_i = \mathbf{Q}^H\mathbf{\Lambda}_i\mathbf{Q}$, where $\mathbf{\Lambda}_i$, i denotes SR, RD, SD, is a diagonal matrix whose $(n,n)^{th}$ element is equal to the n^{th} DFT coefficient of $\mathbf{h}_i$. Thus, transforming the received signal $\mathbf{r}(2t)$ to the frequency domain by multiplying it with $\mathbf{Q}$ matrix and further writing the result in matrix form we have

$$\overbrace{\begin{bmatrix} \mathbf{Q}\mathbf{r}(t) \\ \mathbf{Q}\mathbf{r}^*(t+1) \end{bmatrix}}^{\mathbf{R}} = \begin{bmatrix} \mathbf{Q}\mathbf{n}(t) \\ \mathbf{Q}\mathbf{n}^*(t+1) \end{bmatrix} + \begin{bmatrix} \sqrt{\gamma_1}\Lambda_{RD}\Lambda_{SR}\Phi & \sqrt{\gamma_2}\Lambda_{SD}\Phi \\ \sqrt{\gamma_2}\Lambda_{SD}^*\Phi & -\sqrt{\gamma_1}\Lambda_{RD}^*\Lambda_{SR}^*\Phi \end{bmatrix} \begin{bmatrix} \mathbf{y}_{SRD}(t) \\ \mathbf{y}_{SD}(t) \end{bmatrix}. \tag{6.5}$$

Assuming without loss of generality the symbols to have variance $\sigma^2_{\mathbf{y}_{SRD}} = \sigma^2_{\mathbf{y}_{SD}} = 1$, applying the MMSE equalization we have

$$\begin{bmatrix} \hat{\mathbf{y}}_{SRD}(t) \\ \hat{\mathbf{y}}_{SD}(t) \end{bmatrix} = \begin{bmatrix} \sqrt{\gamma_1}\Lambda_{RD}^*\Lambda_{SR}^*\mathbf{A} & \sqrt{\gamma_2}\Lambda_{SD}\mathbf{A} \\ \sqrt{\gamma_2}\Lambda_{SD}^*\mathbf{A} & -\sqrt{\gamma_1}\Lambda_{RD}\Lambda_{SR}\mathbf{A} \end{bmatrix} \mathbf{R}, \tag{6.6}$$

where $\mathbf{A} = \left(\Lambda_{RD}\Lambda_{SR}\Phi\Phi^H\Lambda_{SR}^*\Lambda_{RD}^* + \Lambda_{SD}\Phi\Phi^H\Lambda_{SD}^*\right)^{-1}$. In the following, we will discuss the distributed differential (DD)-LCP-OFDM system and the ST encoding and decoding procedures employed by it.

6.3 DD-LCP-OFDM

The data vectors $\mathbf{d}_i(t) = \left[d_i^0(t), \ldots, d_i^{N-1}(t)\right]^T$ $i = 1, 2$, represent the OFDM-STBC symbols, where t is the time index and complex symbols $d_i^n(t)$ $n = 1, \ldots, N$, are drawn from an unit-energy MPSK constellation. We are encoding the LCP-OFDM-STBC data vectors

$\mathbf{d}_1(t) = \mathbf{\Phi}\mathbf{d}_1(t)$ and $\mathbf{d}_2(t) = \mathbf{\Phi}\mathbf{d}_2(t)$ into their linear constellation precoded differentially encoded frequency domain counterparts $\mathbf{y}_{SRD}(m) = \left[y^0_{SRD}(m), \ldots, y^{N-1}_{SRD}(m)\right]^T$ and $\mathbf{y}_{SD}(m) = \left[y^0_{SD}(m), \ldots, y^{N-1}_{SD}(m)\right]^T$ $m = 2t, 2t+1$ as following

$$\mathbf{Y}^n(t) = \mathbf{D}^n(t)\,\mathbf{Y}^n(t-1) \tag{6.7}$$

where

$$\mathbf{D}^n(t) = \frac{1}{\sqrt{2}}\begin{bmatrix} d^n_1(t) & d^n_2(t) \\ -(d^n_2(t))^* & (d^n_1(t))^* \end{bmatrix}, \tag{6.8}$$

and

$$\mathbf{Y}^n(t) = \begin{bmatrix} y^n_{SRD}(2t) & y^n_{SD}(2t) \\ y^n_{SRD}(2t+1) & y^n_{SD}(2t+1) \end{bmatrix}, \tag{6.9}$$

having

$$\begin{aligned} y^n_{SRD}(2t+1) &= -(y^n_{SD}(2t))^*, \\ y^n_{SD}(2t+1) &= (y^n_{SRD}(2t))^*. \end{aligned} \tag{6.10}$$

Note that (6.7) is relating 4 frames of information in a differential manner. Applying (6.10) at the sequence level to the OFDM blocks $(2t)$ and $(2t+1)$ in (6.9) and substituting them into (6.4), we obtain

$$\mathbf{r}(2t) = \sqrt{\gamma_1}\mathbf{H}_{RD}\mathbf{H}_{SR}\mathbf{Q}^H\mathbf{y}^n_{SRD}(2t) + \sqrt{\gamma_2}\mathbf{H}_{SD}\mathbf{Q}^H\mathbf{y}^n_{SD}(2t) + \mathbf{n}(2t),$$

$$\mathbf{r}(2t+1) = -\sqrt{\gamma_1}\mathbf{H}_{RD}\mathbf{H}_{SR}\mathbf{Q}^H(\mathbf{y}^n_{SD}(2t))^* + \sqrt{\gamma_2}\mathbf{H}_{SD}\mathbf{Q}^H(\mathbf{y}^n_{SRD}(2t))^* + \mathbf{n}(2t+1), \tag{6.11}$$

which represents the two consecutive received OFDM frames $(2t)$ and $(2t+1)$ at the destination terminal.

To recover the OFDM data vectors $\mathbf{d}_1(t)$ and $\mathbf{d}_2(t)$ from the differentially encoded received signals in (6.12), we exploit the circulant structure of the channel matrices $\mathbf{H}_{RD}$, $\mathbf{H}_{SR}$, and $\mathbf{H}_{SD}$, similar to (6.7) as following

$$\mathbf{Q}\mathbf{r}(2t) = \tilde{\mathbf{r}}(2t) = \sqrt{\gamma_1}\Lambda_{RD}\Lambda_{SR}\mathbf{y}^n_{SRD}(2t) + \sqrt{\gamma_2}\Lambda_{SD}\mathbf{y}^n_{SD}(2t) + \underbrace{\mathbf{Q}\mathbf{n}(2t)}_{\tilde{\mathbf{n}}(2t)},$$

$$\mathbf{Q}\mathbf{r}(2t+1) = \tilde{\mathbf{r}}(2t+1) = -\sqrt{\gamma_1}\Lambda_{RD}\Lambda_{SR}(\mathbf{y}^n_{SD}(2t))^* + \sqrt{\gamma_2}\Lambda_{SD}(\mathbf{y}^n_{SRD}(2t))^* + \underbrace{\mathbf{Q}\mathbf{n}(2t+1)}_{\tilde{\mathbf{n}}(2t+1)}, \tag{6.12}$$

Note that in here, we are performing the differential decoding upon the n^{th} subchannel and n^{th} subcarrier to recover $d_1^n(t)$ and $d_2^n(t)$. Considering the n^{th} subchannel, writing (12) in the matrix form we have

$$\overbrace{\begin{bmatrix} \tilde{\mathbf{r}}^n(2t) \\ \tilde{\mathbf{r}}^n(2t+1) \end{bmatrix}}^{\mathbf{R}^n(t)} = \overbrace{\begin{bmatrix} \tilde{\mathbf{n}}^n(2t) \\ \tilde{\mathbf{n}}^n(2t+1) \end{bmatrix}}^{\tilde{\mathbf{n}}^n(t)} + \overbrace{\begin{bmatrix} y_{SRD}^n(2t) & y_{SD}^n(2t) \\ -(y_{SD}^n(2t))^* & (y_{SRD}^n(2t))^* \end{bmatrix}}^{\mathbf{Y}^n(t)} \overbrace{\begin{bmatrix} \sqrt{\gamma_1}\mathbf{\Lambda}_{RD}^n\mathbf{\Lambda}_{SR}^n \\ \sqrt{\gamma_2}\mathbf{\Lambda}_{SD}^n \end{bmatrix}}^{\mathbf{\Lambda}^n}, \tag{6.13}$$

where $\mathbf{\Lambda}_{SR}^n$, $\mathbf{\Lambda}_{RD}^n$, and $\mathbf{\Lambda}_{SD}^n$, stand for the n^{th} diagonal elements of matrices $\mathbf{\Lambda}_{SR}$, $\mathbf{\Lambda}_{RD}$, and $\mathbf{\Lambda}_{SD}$. Thus, substituting (6.7) into (6.13), the current input to the distributed STBC differential detector, $\mathbf{R}^n(t)$, for each sub-channel is related to the previous input, $\mathbf{R}^n(t-1)$, according to

$$\mathbf{R}^n(t) = \mathbf{D}^n(t) \overbrace{\mathbf{Y}^n(t-1)\mathbf{\Lambda}^n}^{\mathbf{R}^n(t-1)-\tilde{\mathbf{n}}^n(t-1)} + \tilde{\mathbf{n}}^n(t) = \mathbf{D}^n(t)\mathbf{R}^n(t-1) + \underbrace{\tilde{\mathbf{n}}^n(t) - \mathbf{D}^n(t)\tilde{\mathbf{n}}^n(t-1)}_{\mathbf{U}^n(t)}. \tag{6.14}$$

We set $\mathbf{Y}^n(0)$; $n = 0, \ldots, N-1$ to $\mathbf{I}_2$ and linearly detect $\mathbf{D}^n(t)$ from $\mathbf{Y}^n(t)$ using the orthogonal structure in (6.13). this can be done by rewriting (6.14) as follows

$$\begin{bmatrix} \tilde{r}^n(2t) \\ (\tilde{r}^n(2t+1))^* \end{bmatrix} = \begin{bmatrix} U_1^n(t) \\ (U_2^n(t))^* \end{bmatrix} + \frac{1}{\sqrt{2}} \begin{bmatrix} \tilde{r}^n(2t-2) & \tilde{r}^n(2t-1) \\ (\tilde{r}^n(2t-1))^* & -(\tilde{r}^n(2t-2))^* \end{bmatrix} \begin{bmatrix} d_1^n(t) \\ d_2^n(t) \end{bmatrix}. \tag{6.15}$$

To perform MMSE equalization, we can further cascade every n^{th} elements to use the vector forms in (6.15) as follows

$$\begin{bmatrix} \tilde{\mathbf{r}}(2t) \\ \tilde{\mathbf{r}}^*(2t+1) \end{bmatrix} = \begin{bmatrix} \mathbf{U}_1(t) \\ \mathbf{U}_2^*(t) \end{bmatrix} + \frac{1}{\sqrt{2}} \begin{bmatrix} \tilde{\mathbf{r}}(2t-2) & \tilde{\mathbf{r}}(2t-1) \\ \tilde{\mathbf{r}}^*(2t-1) & -\tilde{\mathbf{r}}^*(2t-2) \end{bmatrix} \begin{bmatrix} \mathbf{d}_1(t) \\ \mathbf{d}_2(t) \end{bmatrix}. \tag{6.16}$$

Thus, performing blind MMSE equalization with no access to CSI, we have

$$\begin{bmatrix} \mathbf{d}_1(t) \\ \mathbf{d}_2(t) \end{bmatrix} = \begin{bmatrix} \sqrt{\gamma_1}\mathbf{\Phi}^H\tilde{\mathbf{r}}^H(2t-2)\mathbf{B} & \sqrt{\gamma_2}\mathbf{\Phi}^H\tilde{\mathbf{r}}(2t-1)\mathbf{B} \\ \sqrt{\gamma_2}\mathbf{\Phi}^H\tilde{\mathbf{r}}^H(2t-1)\mathbf{B} & -\sqrt{\gamma_1}\mathbf{\Phi}^H\tilde{\mathbf{r}}(2t-2)\mathbf{B} \end{bmatrix} \tilde{\mathbf{R}}, \tag{6.17}$$

where $\tilde{\mathbf{R}} = \begin{bmatrix} \tilde{\mathbf{r}}(2t) & \tilde{\mathbf{r}}^*(2t+1) \end{bmatrix}^T$ and $\mathbf{B} = \left(\tilde{\mathbf{r}}(2t-2)\mathbf{\Phi}\mathbf{\Phi}^H\tilde{\mathbf{r}}^H(2t-2) + \tilde{\mathbf{r}}(2t-1)\mathbf{\Phi}\mathbf{\Phi}^H\tilde{\mathbf{r}}^H(2t-1)\right)^{-1}$.

6.4 DD-GLCP-OFDM

Due to high decoding complexity of LCP-OFDM, an optimal subcarrier grouping technique was proposed in [150] in which the decoder's complexity is reduced by dividing the set

of all subcarriers into nonintersecting subsets of subcarriers, called subcarrier groups. In this approach, every information symbol is transmitted over subcarriers within only one of these subsets. Note that if the subcarrier grouping is properly done, not only the decoding complexity is reduced, but also systems performance is preserved [150].

The GLCP matrix, θ, is designed such that the decoding complexity is reduced, while preserving the maximum diversity and coding gains. Assuming that $N = KM$, in DD-GLCP-OFDM STBC system, the information symbols $\mathbf{d}_i(t), i = 1, 2$, are divided into M blocks, $\mathbf{d}_i^m(t) = \psi_m \mathbf{d}_i(t)$, where ψ_m is a $K \times N$ permutation matrix built from the rows $(m-1)K + 1 \rightarrow mK$ of $\mathbf{I}_N$; and then precoded by the GLCP matrix θ. Thus, as an example, (6.12) can be rewritten as

$$\begin{aligned} \tilde{\mathbf{r}}(2t) &= \sqrt{\gamma_1}\Lambda_{RD}^m \Lambda_{SR}^m \mathbf{g}_{SRD}^m(2t) + \sqrt{\gamma_2}\Lambda_{SD}^m \mathbf{g}_{SD}^m(2t) + \tilde{\mathbf{n}}(2t), \\ \tilde{\mathbf{r}}(2t+1) &= -\sqrt{\gamma_1}\Lambda_{RD}^m \Lambda_{SR}^m (\mathbf{g}_{SD}^m(2t))^* + \sqrt{\gamma_2}\Lambda_{SD}^m (\mathbf{g}_{SRD}^m(2t))^* + \tilde{\mathbf{n}}(2t+1), \end{aligned} \tag{6.18}$$

where $\Lambda_i^m = \psi_m \Lambda_i \psi_m^T$, $i = SR, RD, SD$, and $\mathbf{g}_i^m(2t)$, $i = SRD, SD$, are differentially encoded from the GLCP-OFDM symbols $\mathbf{g}_i^m(t) = \theta \mathbf{d}_i^m(t)$ following similar steps as in (6.7).

Following [150,151], for any K, QAM, PAM, BPSK, and QPSK constellation, the optimal can be constructed through LCP-A , which can be generally written as a Vandermonde matrix as following

$$\theta = \frac{1}{\beta} \begin{bmatrix} 1 & \alpha_1 & \cdots & \alpha_1^{K-1} \\ 1 & \alpha_2 & \cdots & \alpha_2^{K-1} \\ \vdots & \vdots & \vdots & \vdots \\ 1 & \alpha_K & \cdots & \alpha_K^{K-1} \end{bmatrix}, \tag{6.19}$$

where β is a constant such that $tr\left(\theta\theta^H\right) = K$, and the parameters $\{\alpha_k\}_{k=1}^K$ are selected depending on K [150].

6.5 Numerical Results

In this section, we present Monte-Carlo simulation results for the proposed receiver.

Fig. 6.1. depicts the SER performance of the DD-LCP-OFDM STBC scheme assuming for the following three different scenarios:

1) $L_{SR} = L_{RD} = L_{SD} = 0$,

2) $L_{SR} = L_{RD} = L_{SD} = 1$,

3) $L_{SR} = 5, L_{RD} = 2, L_{SD} = 1$.

For LCP-OFDM to achieve maximum diversity order, maximum diversity encoders should be used. Two classes of maximum achievable diversity order (MADO) enabling LCP encoders are introduced in [151], namely: Vandermonde encoders and cosine encoders. In here, we are using Vandermonde encoders and we assume 4-PSK modulation. To further minimize the receiver complexity, we are applying the low-cost MMSE equalizer. Our simulation results indicate that with the optimal design of LCP encoder matrix, the DD-LCP-OFDM STBC system is able to achieve full spatial and multipath diversity, $\min(L_{SR}, L_{RD})+L_{SD}+1$ and it has been confirmed.

Following [150], we suggest an alternative low complexity implementation of the DD-LCP-OFDM STBC system, namely, DD grouped linear constellation precoded GLCP-OFDM STBC subsystems. The aim is to reduce system complexity while preserving maximum possible diversity and coding gains. The proposed system's optimal performance relies on the design of the GLCP matrix [150].

Fig. 6.2 depicts the SER performance of the DD-GLCP-OFDM STBC scheme for the following combinations of the underlying channel memory lengths:

1) $L_{SR} = L_{RD} = L_{SD} = 0$,

2) $L_{SR} = L_{RD} = L_{SD} = 1$,

3) $L_{SR} = 5, L_{RD} = 2, L_{SD} = 1$.

The MADO GLCP encoders used for scenarios 1, 2, and 3 are θ_2, θ_4, and θ_8, respectively [150]. We analyze system's performance for $\alpha = 1, 10$. To minimize the receiver complexity, MMSE equalizer is implemented at the receiver side. In the case of $\alpha = 1$, for all three scenarios where the $S \to R$ and $S \to D$ links are balanced, the SER performance degrades compared to the corresponding scenario when $\alpha = 10$, while preserving the achieved diversity order.

In Fig. 6.3 the SER performance of DD-OFDM-STBC is compared with that of DD-LCP-OFDM-STBC and DD-GLCP-OFDM-STBC, for $L_{SR} = L_{RD} = L_{SD} = 1$, $\alpha = 10$, and θ_4 [150]. As can be observed from Fig. 6.3, DD-LCP-OFDM-STBC outperforms both DD-GLCP-OFDM-STBC and DD-OFDM-STBC. However, both DD-LCP-OFDM-STBC and DD-GLCP-OFDM-STBC achieve the same diversity gain. As an example, at BER=10^{-4}, the DD-LCP-OFDM-STBC system outperforms DD-GLCP-OFDM-STBC and DD-OFDM-STBC systems by 2 dB and 4 dB, respectively.

In Fig. 6.4 the SER performance of DD-GLCP-OFDM is provided with optimal and sub-optimal subcarrier grouping, assuming $L_{SR} = L_{RD} = L_{SD} = 1$ and QPSK modulation. The optimal and suboptimal grouping are specified with $\mathfrak{I}_{m,opt} = \{m-1, M+m-1, \ldots, (K-1)M+m-1\}$ and $\mathfrak{I}_{m,opt} = \{(m-1)K+1, (m-1)K+2, \ldots, mK\}$ $m \in [1, M]$ subsets, respectively, where $N = MK$. As is illustrated in Fig. 6.4, the optimal subcarrier grouping improves performance, i.e. by 2 dB at BER=10^{-3}.

Next, we extend our analysis to a multiple relay scenario, where we adopt the transmission protocol in [157] and consider non-regenrative relays. Note that unlike [157], we assume that there is no direct transmission between the source and destination terminals due to the presence of shadowing. we assume that there are three relay nodes, where each node is equipped with one antenna. We set $\mathrm{SNR}_{SR_1} = \mathrm{SNR}_{SR_3} = 25$dB and $\mathrm{E}_{R_1D} = \mathrm{E}_{R_2D} = \mathrm{E}_{R_3D} = 5$ dB , and the SER curve is plotted against $\frac{E_{SR_2}}{N_0}$. QPSK modulation and $\mathcal{G}_3$ code [28] are used. The scenarios with different combinations of channel memory lengths are considered for DD-LCP-OFDM-STBC system:

1) $L_{SR_1} = L_{R_1D} = L_{SR_2} = L_{R_2D} = L_{SR_3} = L_{R_3D} = 0$,

2) $L_{SR_1} = L_{SR_2} = L_{SR_3} = 1, L_{R_1D} = L_{R_2D} = L_{R_3D} = 1$,

3) $L_{SR_1} = L_{SR_2} = L_{SR_3} = 1, L_{R_1D} = L_{R_2D} = L_{R_3D} = 2$,

As is illustrated in Fig. 6.5, for high $\frac{E_{SR_2}}{N_0}$ values, we are achieving the full diversity order of $\sum_{i=1}^{3} \min(L_{SR_i}, L_{R_iD}) + 3$.

6.6 Conclusion

We have investigated distributed differential LCP-OFDM STBC and GLCP-OFDM for cooperative communications over frequency-selective fading channels. We have carefully exploited the unitary structure of STBCs to design a low complexity distributed differential STBC receiver for broadband cooperative networks. We have presented the comprehensive Monte-Carlo simulations to corroborate the theoretical presentation.

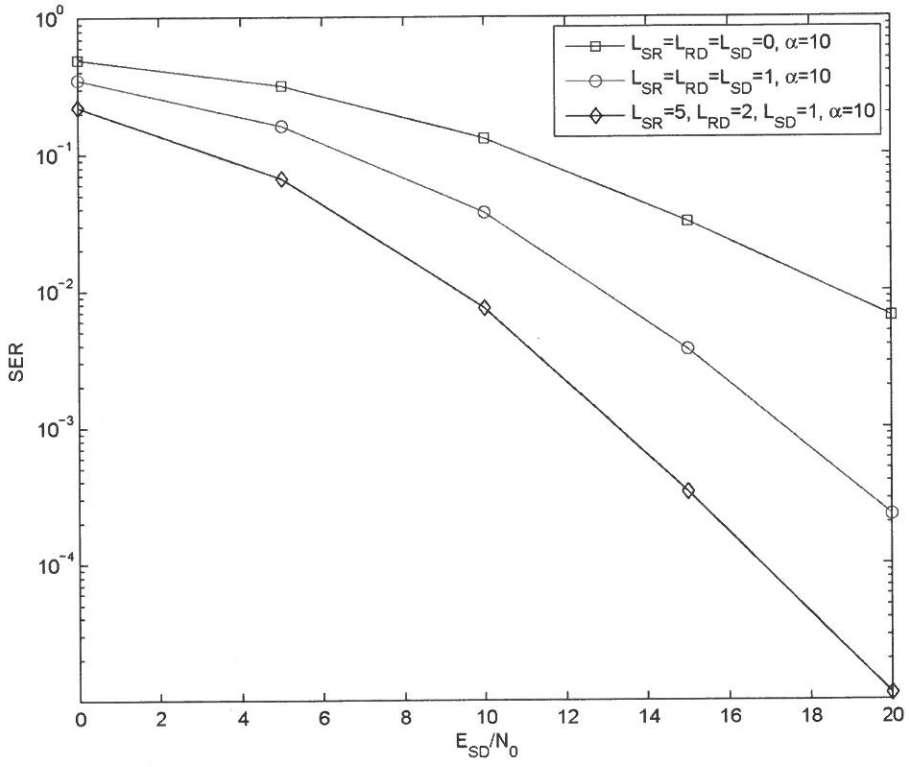

Figure 6.1: SER performances of DD-LCP-OFDM STBC over frequency- selective $S \rightarrow R$, $R \rightarrow D$and $S \rightarrow D$ links ($E_{SR}/N_0 = \alpha E_{SD}/N_0, \alpha = 10$)

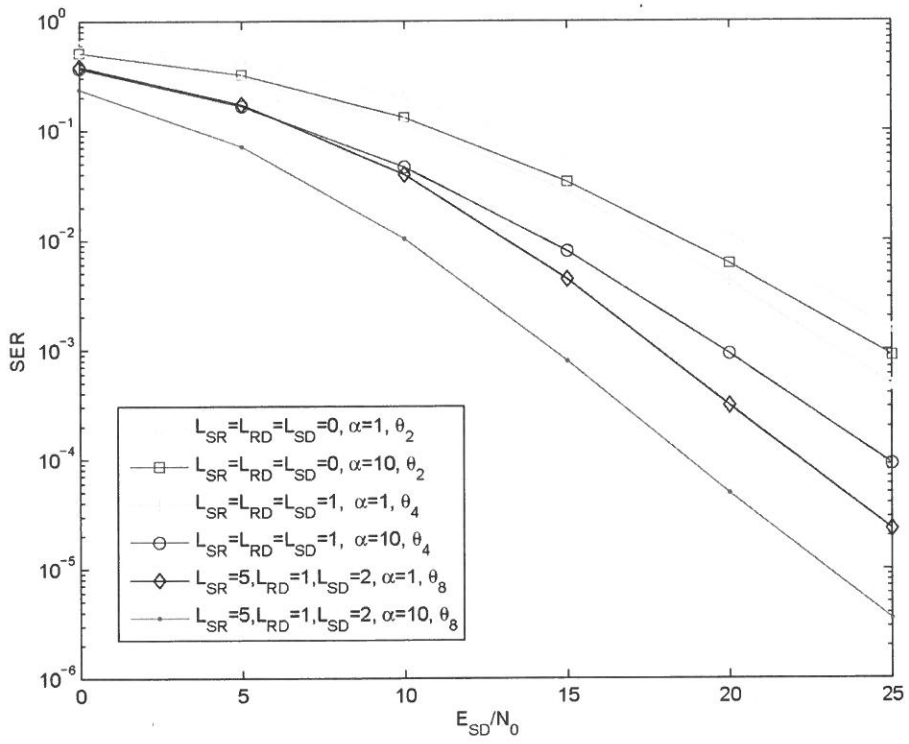

Figure 6.2: SER performances of DD-GLCP-OFDM STBC over frequency- selective $S \rightarrow R$, $R \rightarrow D$and $S \rightarrow D$ links ($E_{SR}/N_0 = \alpha E_{SD}/N_0, \alpha = 1, 10$)

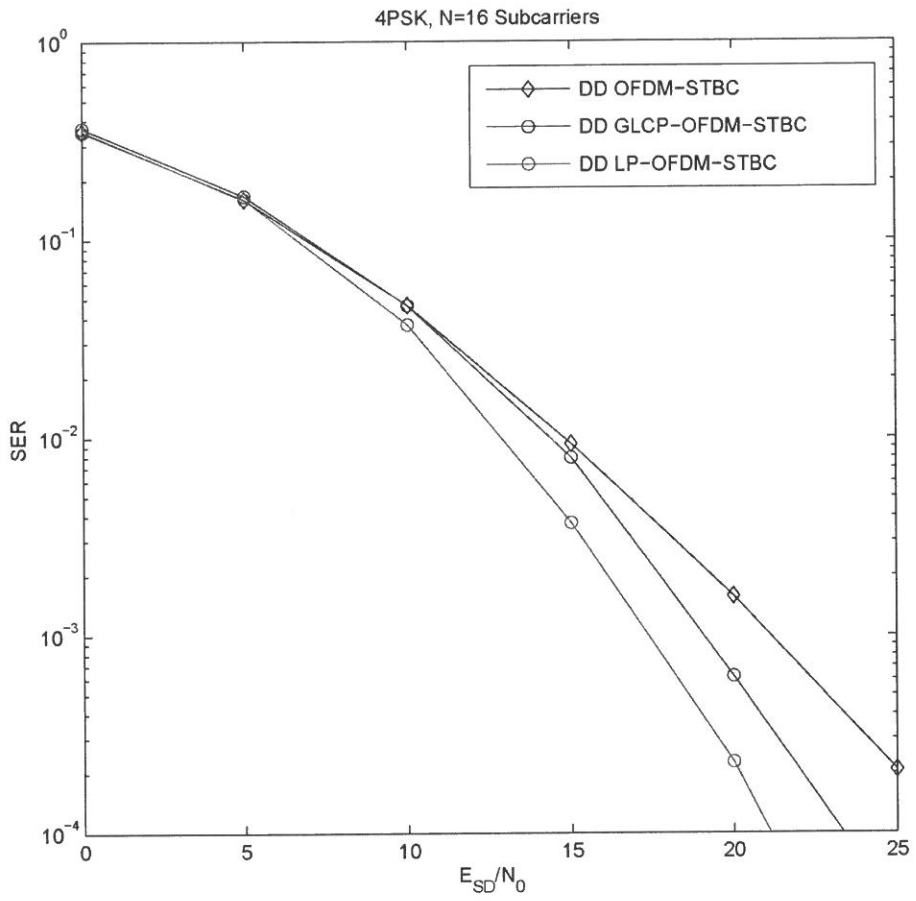

Figure 6.3: SER performance comparison between DD-OFDM-STBC, DD-LCP- OFDM STBC, and DD-GLCP-OFDM-STBC systems

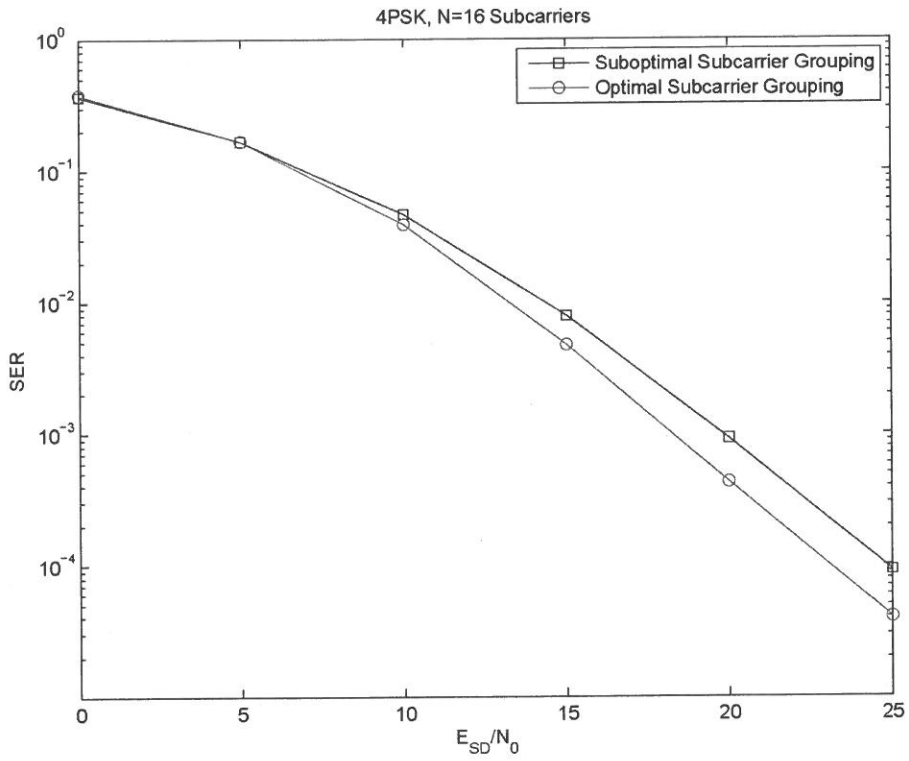

Figure 6.4: Optimal versus suboptimal subcarrier grouping for the DD-LCP-OFDM STBC system

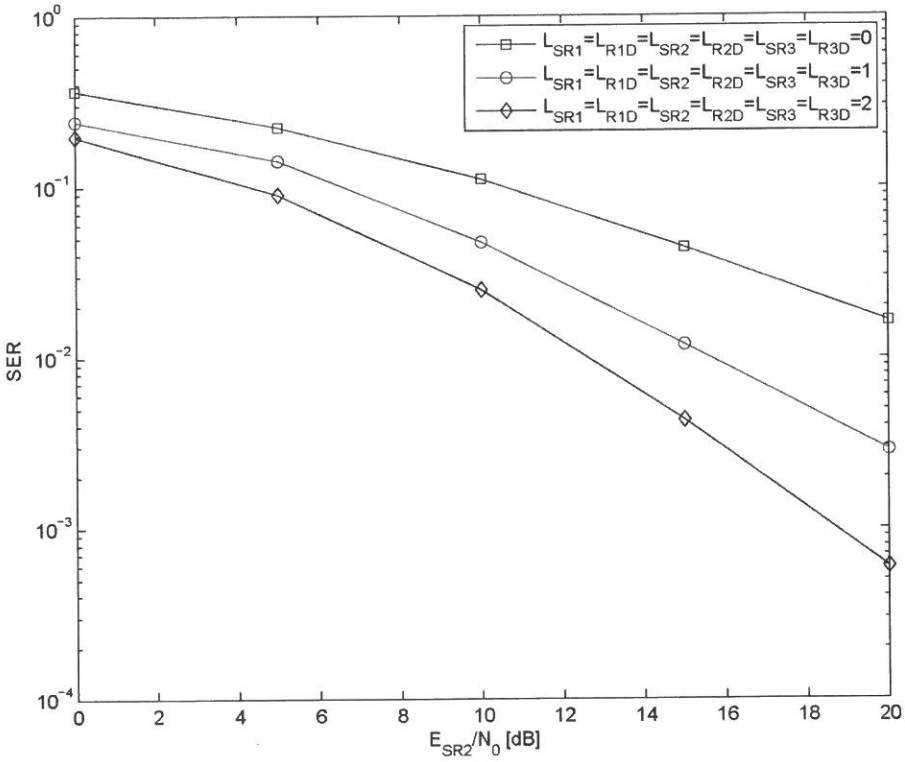

Figure 6.5: SER performance of DD-LCP-OFDM STBC system with three relays

Chapter 7

Differential Decoding for SFBC OFDM systems in Underwater MIMO Channels

7.1 Introduction

Due to the increasing interest for high speed communication over underwater acoustic (UWA) channels , multicarrier modulation in the form of OFDM has prevailed in recent UWA research studies. OFDM enables low complexity equalization of highly dispersive UWA channels via the low-complexity fast Fourier transform (FFT) signal processing techniques. OFDM entails narrowband signaling on each subbcarrier and is therefore, conducive to various MIMO configurations. Moreover, unlike the traditional single carrier modulation techniques, multicarrier modulation techniques, including OFDM, allow the use of differentially coherent detection schemes [158, 159].

The feasibility of UWA OFDM transmission in multiple transmit-receive configuration has been proven in recent experimental studies [160, 161]. MIMO OFDM systems have been considered for UWA channels to exploit spatial multiplexing [160, 161], as well as spatial diversity through Alamouti coding [162, 163], while [162] considers Alamouti STBC, and [163] considers SFBC. SFBC involves coding across OFDM carriers, whereas STBC involves coding across OFDM blocks in time. Due to the rapidly changing nature of the UWA channels, SFBCs are better suited for use in these channels than STBCs. It should be noted that for fast-varying, also referred to as time-selective channels, the key assumption for STBC that the channel is fixed over two time intervals does not hold. In this case, space-time coding

can be implemented as a SFBC, where adjacent subcarriers, rather than time slots, are coded over. This assumes that the adjacent subcarriers have the same frequency response, which is approximately true as long as the channel coherence bandwidth is much larger than the subcarrier width. More specifically, SFBC data symbols are applied over groups of adjacent subcarriers within a single OFDM block [164]. Since in SFBC-OFDM systems, space-frequency block encoded data symbols are transmitted within a single OFDM block, SFBC-OFDM systems outperform STBC-OFDM systems under fast-fading channels [164]. Moreover, compared to STBC-OFDM, SFBC-OFDM comes with distinct advantages with regards to receiver implementation. As an example, in [164], it is shown that compared to the simple two-transmit antenna STBC system proposed in [10], SFBC-OFDM reduces the decoder memory and latency to half. The SFBC-OFDM system proposed in [165] requires the channel frequency response to be invariant over the number of adjacent subcarriers spanning one SFBC group. This quasi-static assumption, however, is not easily met in most frequency-selective channels with large delay spreads. Therefore, applying conventional linear processing decoders renders poor performance due to inter-carrier interference caused by CFR variations over adjacent sub-carriers. One solution to alleviate this problem is to increase the number of subcarriers per OFDM block. Increasing the number of subcarriers per OFDM block in SFBC-OFDM system, however, narrows down the bandwidth of each sub-channel which in turn results in more sensitivity to impairments such as carrier frequency offset and phase noise. SFBCs coincides with the basic OFDM design principle. OFDM design principle calls for closely spaced carriers such that the channel frequency response can be considered as flat fading over each subband. Since the STBC coherence assumption between adjacent OFDM blocks may be violated in UWA channels [163], SFBC using coherent detection was studied in [163]. In [159, 166], it was experimentally shown that by eliminating the need for channel estimation and thus reducing the error floor due to imperfect channel tracking, differentially coherent detection can outperform the traditional coherent detection schemes, on the highly time-varying UWA channels.

In this chapter, we consider differential SFBC as a means for obtaining transmit diversity over UWA channels without the need for explicit channel estimation. We apply the resulting algorithm to the experimental data obtained during 2011 Kauaii Acoustic Communications (KAM'11) experiment, where acoustic signals were transmitted over 3 km in the 20–32 kHz band. We present results on the performance of differential SFBC receiver in terms of the MSE, and SER, which show that this technique can indeed outperform the traditional coherent detection.

In this chapter, we investigate the performance of differential SFBCs for OFDM signals over underwater acoustic channels. By applying the unitary structure of the orthogonal SFBCs over the carriers of an OFDM system, the underlying transmit diversity in an underwater acoustic channel is exploited. Differential detection is further applied to eliminate the need for expensive signal processing required for channel tracking. We assume that there is sufficient spatial diversity between the channels of the transmitters, and that each channel changes slowly over the carriers, thus satisfying the basic Alamouti coherence requirement. System performance is demonstrated using real data transmitted in the 20-32 kHz acoustic band from a vehicle moving at 0.5–2 m/s and received over a shallow water channel, using 4-QAM and a varying number of carriers ranging from 128 to 2048. Performance results demonstrate the advantage of the differential coherent SFBC detector over the conventional coherent SFBC detector which suffers from imperfect channel estimation.

7.2 System Model

We consider a MIMO OFDM system with two transmitters and M_R receivers. The system employs differential SFBC over K carriers, whose frequencies $f_k = f_0 + k\Delta f$, $k = 0, \ldots K-1$ are separated by $\Delta f = B/K$, where f_0 is the lowest carrier frequency, and B is the system bandwidth. The information symbols belong to a QPSK alphabet.

Let X_l^i denote the complex data symbol, transmitted from the i^{th} source transceiver on the l^{th} subcarrier of frequency $f_l = f_0 + l \cdot \Delta f$. The symbols $\{X_l^i, l = 1, \ldots, N, i = 1, 2\}$ are transmitted in parallel, on N carriers by the participating source transceivers. After the IFFT processing and insertion of the zero guard intervals, the discrete-time sequence at the i^{th} transmit element is given by

$$x_n^i = \frac{1}{N} \sum_{l=0}^{N-1} X_{l+1}^i e^{\frac{j2\pi nl}{N}}. \tag{7.1}$$

In the DSFBC-OFDM system, however, OFDM data symbols are initially encoded using the Alamouti SFBC scheme, i.e. the data symbols on carriers $2l$ and $2l+1$ are respectively, X_{2l}^1 and X_{2l+1}^1 from the first transmitter, and X_{2l}^2 and X_{2l+1}^2, from the second transmitter, where $X_{2l+1}^1 = -(X_{2l}^2)^*$, and $X_{2l+1}^2 = (X_{2l}^1)^*$. We differentially encode the SFBC-OFDM symbols using the following technique:

$$\mathbf{Y}_l = \mathbf{X}_l \mathbf{Y}_{l-1}, \tag{7.2}$$

where $\mathbf{X}_l$ represents the l^{th} SFBC-OFDM codeword, as expressed below,

$$\mathbf{X}_l = \frac{1}{\sqrt{|X_{2l}^1|^2 + |X_{2l}^2|^2}} \begin{bmatrix} X_{2l}^1 & X_{2l}^2 \\ -(X_{2l}^2)^* & (X_{2l}^1)^* \end{bmatrix} \tag{7.3}$$

and $\mathbf{Y}_l$ and $\mathbf{Y}_{l-1}$ represent the l^{th} and $(l-1)^{th}$ differentially encoded SFBC-OFDM codewords. The matrix $\mathbf{Y}_l$ can be expressed as

$$\mathbf{Y}_l = \begin{bmatrix} Y_{2l}^1 & Y_{2l}^2 \\ -(Y_{2l}^2)^* & (Y_{2l}^1)^* \end{bmatrix}. \tag{7.4}$$

Note that (7.2) is relating four information symbols in a differential manner.

After performing FFT processing, the received signal at the j^{th} receiver on carriers $2l$ and $2l+1$ can be expressed as follows,

$$r_{2l}^j = Y_{2l}^1 \Lambda_{2l}^{S_1 R_j} + Y_{2l}^2 \Lambda_{2l}^{S_2 R_j} + n_{2l}, \tag{7.5a}$$

$$r_{2l+1}^j = -\left(Y_{2l}^2\right)^* \Lambda_{2l+1}^{S_1 R_j} + \left(Y_{2l}^1\right)^* \Lambda_{2l+1}^{S_2 R_j} + n_{2l+1}, \tag{7.5b}$$

where $\Lambda_l^{S_i R_j}$ is the channel transfer function observed on the l^{th} subcarrier between the i^{th} transmitter and thej^{th} receiver. Assuming $\Lambda_{2l}^{S_i R_j} \approx \Lambda_{2l+1}^{S_i R_j}$, (7.5) can be expressed as follows,

$$\underbrace{\begin{bmatrix} r_{2l}^j \\ r_{2l+1}^j \end{bmatrix}}_{\mathbf{R}_l^j} = \underbrace{\begin{bmatrix} Y_{2l}^1 & Y_{2l}^2 \\ -(Y_{2l}^2)^* & (Y_{2l}^1)^* \end{bmatrix}}_{\mathbf{Y}_l} \underbrace{\begin{bmatrix} \Lambda_{2l}^{S_1 R_j} \\ \Lambda_{2l}^{S_2 R_j} \end{bmatrix}}_{\Lambda_l^{S_i R_j}} + \underbrace{\begin{bmatrix} n_{2l} \\ n_{2l+1} \end{bmatrix}}_{\mathbf{n}_l}. \tag{7.6}$$

Substituting (7.2) into (7.6), the current input to the D-SFBC-OFDM detector, $\mathbf{R}_l^j$, for the l^{th} differentially decoded SFBC codeword and the associated $2l$ and $2l+1$ carriers, is related to the previous input, $\mathbf{R}_{l-1}^j$ as

$$\mathbf{R}_l^j = \mathbf{Y}_l \Lambda_l^{S_i R_j} + \mathbf{n}_l = \mathbf{D}_l \mathbf{Y}_{l-1_l} \Lambda_l^{S_i R_j} + \mathbf{n}_l = \mathbf{D}_l \left(\mathbf{R}_{l-1}^j - \mathbf{n}_{l-1}\right) + \mathbf{n}_l = \mathbf{D}_l \mathbf{R}_{l-1}^j \underbrace{-\mathbf{D}_l \mathbf{n}_{l-1} + \mathbf{n}_l}_{\mathbf{U}_l}. \tag{7.7}$$

Note that (7.7) can be further expressed in the following matrix form,

$$\begin{bmatrix} r_{2l}^j \\ \left(r_{2l+1}^j\right)^* \end{bmatrix} = \frac{1}{\sqrt{|X_{2l}^1|^2 + |X_{2l}^2|^2}} \begin{bmatrix} r_{2l-2}^j & r_{2l-1}^j \\ \left(r_{2l-1}^j\right)^* & -\left(r_{2l-2}^j\right)^* \end{bmatrix} \begin{bmatrix} X_{2l}^1 \\ X_{2l}^2 \end{bmatrix} + \begin{bmatrix} U_{2l}^j \\ \left(U_{2l+1}^j\right)^* \end{bmatrix}. \tag{7.8}$$

Multiplying both sides by

$$\frac{1}{\sqrt{\left|r_{2l-2}^{j}\right|^{2}+\left|r_{2l-1}^{j}\right|^{2}}}\begin{bmatrix} r_{2l-2}^{j} & r_{2l-1}^{j} \\ \left(r_{2l-1}^{j}\right)^{*} & -\left(r_{2l-2}^{j}\right)^{*} \end{bmatrix}^{H}, \tag{7.9}$$

yields the following decision statistics,

$$\rho_{2l}^{j}=\sqrt{\frac{\left|r_{2l-2}^{j}\right|^{2}+\left|r_{2l-1}^{j}\right|^{2}}{\left|X_{2l}^{1}\right|^{2}+\left|X_{2l}^{2}\right|^{2}}}X_{2l}^{1}+\tilde{U}_{2l}^{j}, \tag{7.10a}$$

$$\rho_{2l+1}^{j}=\sqrt{\frac{\left|r_{2l-2}^{j}\right|^{2}+\left|r_{2l-1}^{j}\right|^{2}}{\left|X_{2l}^{1}\right|^{2}+\left|X_{2l}^{2}\right|^{2}}}X_{2l}^{2}+\tilde{U}_{2l+1}^{j}, \tag{7.10b}$$

where

$$\begin{bmatrix} \tilde{U}_{2l}^{j} \\ \tilde{U}_{2l+1}^{j} \end{bmatrix}=\frac{1}{\sqrt{\left|r_{2l-2}^{j}\right|^{2}+\left|r_{2l-1}^{j}\right|^{2}}}\begin{bmatrix} r_{2l-2}^{j} & r_{2l-1}^{j} \\ \left(r_{2l-1}^{j}\right)^{*} & -\left(r_{2l-2}^{j}\right)^{*} \end{bmatrix}^{H}\begin{bmatrix} U_{2l}^{j} \\ \left(U_{2l+1}^{j}\right)^{*} \end{bmatrix}. \tag{7.11}$$

Following (7.11), the decision rule for detecting the OFDM symbols can be formulated as follows,

$$\hat{X}_{2l}^{i}=\arg\min_{m}\left\{\sum_{j=1}^{M_R}\left|\rho_{2l}^{j}-\sqrt{\frac{\left|r_{2l-2}^{j}\right|^{2}+\left|r_{2l-1}^{j}\right|^{2}}{\left|X_{2l}^{1}\right|^{2}+\left|X_{2l}^{2}\right|^{2}}}X\left(m\right)\right|^{2}\right\}, \tag{7.12}$$

where $X\left(m\right)$ belongs to the unitary constellation under consideration.

7.3 Performance Analysis Through Experiment

The KAM'11 experiment was a multi-university research initiative focused on studying the impact of environmental fluctuations on underwater acoustic communication systems. The KAM'11 experiment was conducted off of the west coast of Kauai in a roughly 100 m downward refracting environment. Data were collected during the experiment on a 16 element receiving array from two independent sources separated vertically by 15 m while transmitting over the acoustic frequency range between 20 kHz and 32 kHz, at a range of approximately 3 km. The experiment configuration is illustrated in Fig. 7.1.The bandwidth of the OFDM signal is $B = 12$ kHz, and the lowest carrier frequency is $f_0 = 20$ kHz. A zero-padded guard interval of $T_G = 60$ ms per OFDM block is used. The number of carriers used in the experiment varies from $N = 128$ to $N = 2048$. Each packet consists of

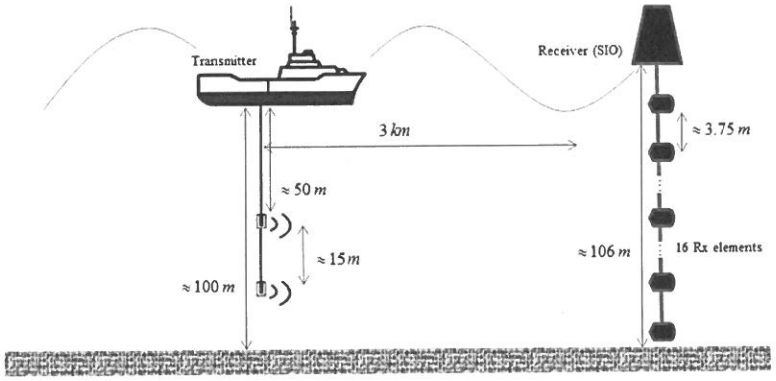

Figure 7.1: Geometry of the KAM'11 experiment.

$N_d = 16384$ information symbols. For $N = 128, 256, 512, 1024, 2048$, each frame consists of $N_b = 128, 64, 32, 16, 8$ blocks, respectively. Each packet consists of a preamble, N_b blocks of data, and a postamble, as illustrated in Fig. 7.2. Moreover, each data burst consists

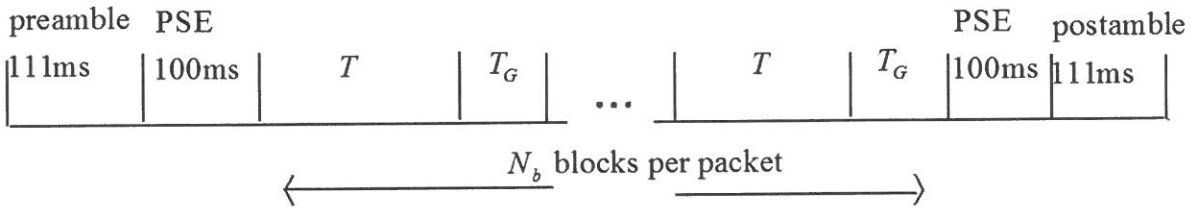

Figure 7.2: One frame consists of preamble, N_b blocks, and a postamble.

of 5 packets corresponding to $N = 128, 256, 512, 1024$, and 2048. To compensate for the frequency dependent Doppler drifts over fast-varying UWA channels, we have applied the two step approach proposed in [167]. Specifically, each packet is correlated by the known preamble and postamble signals, and the corresponding correlation peaks are used to identify time dilation/compensation, based on which the Doppler scaling factor is estimated. The received packet under consideration is then resampled accordingly, and partitioned into its OFDM blocks. Each block is down-converted, and the resulting signal is passed to FFT demodulation and further detection.

Fig. 7.3 illustrates the performance of differentially coherent detection for SFBC schemes in UWA channels based on KAM'11 experiment, with 12 and 16 receiving elements. In this figure, MSE performance of differentially coherent SFBC OFDM is illustrated versus the number of carriers. Similar results are provided for single-transmitter differential OFDM and SFBC OFDM with 12 receiving elements. Fig. 7.3 demonstrates that differential SFBC

OFDM outperforms the single-transmitter differential OFDM, thus offering a spatial diversity gain. More importantly, it shows that D-SFBC indeed outperforms its coherent counterpart, a SFBC scheme based on [167]. As the number of carriers in the given bandwidth is increased, adaptive channel estimation becomes more difficult across longer blocks, causing coherent detection to fail with $N > 512$. In contrast, narrower carrier spacing enhances frequency coherence between adjacent carriers, allowing superior performance of D-SFBC with up to 2048 carriers (a 78% increase in bit rate). Fig. 7.4 illustrates the MSE perfor-

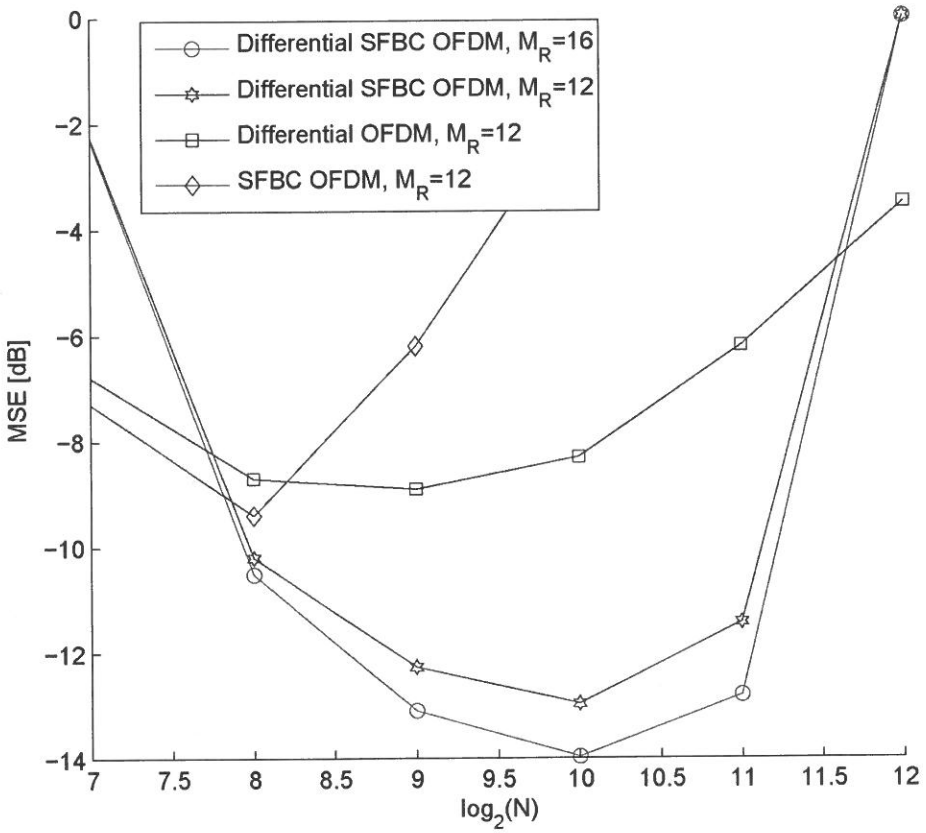

Figure 7.3: MSE performance of differential SFBC OFDM versus differential OFDM and coherent SFBC OFDM.

mance of the differential SFBC OFDM receiver for varying number of receiving elements. The performance is shown in terms of the MSE at the input to the decision device versus the number of carriers. The performance improves with the number of receiving elements, but we note an effect of diminishing returns. Fig. 7.5 illustrates the corresponding SER

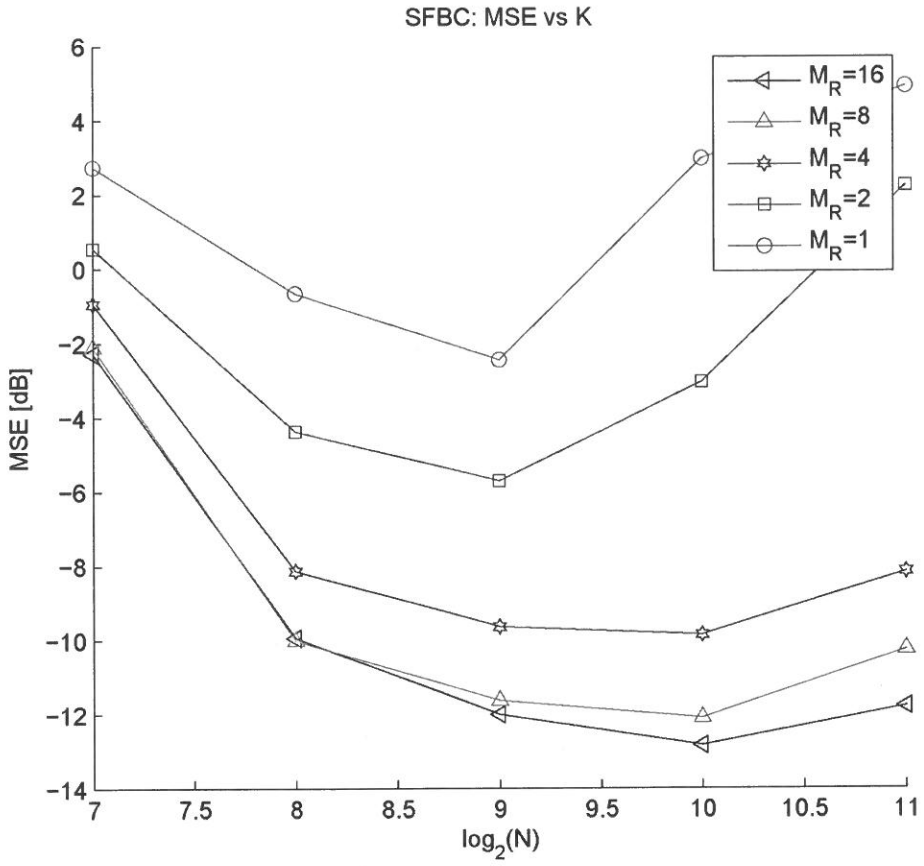

Figure 7.4: MSE performance of differential SFBC OFDM versus the number of carriers for varying number of receive elements.

performance. There is no additional error correction coding in this example. Nonetheless, multi-channel combining significantly improves the system performance, bringing the raw SER below 0.001 with 10 or more receiving elements.

7.4 Conclusion

The performance of differential SFBC OFDM was investigated for UWA channels. Our experimental results demonstrate that differential SFBC OFDM could successfully integrate the benefits from space frequency block coding and differential detection, i.e. by eliminating the need for explicit channel estimation algorithms, while exploiting the underlying spatial diversities. Our simulation results demonstrate that the D-SFBC scheme outperforms the

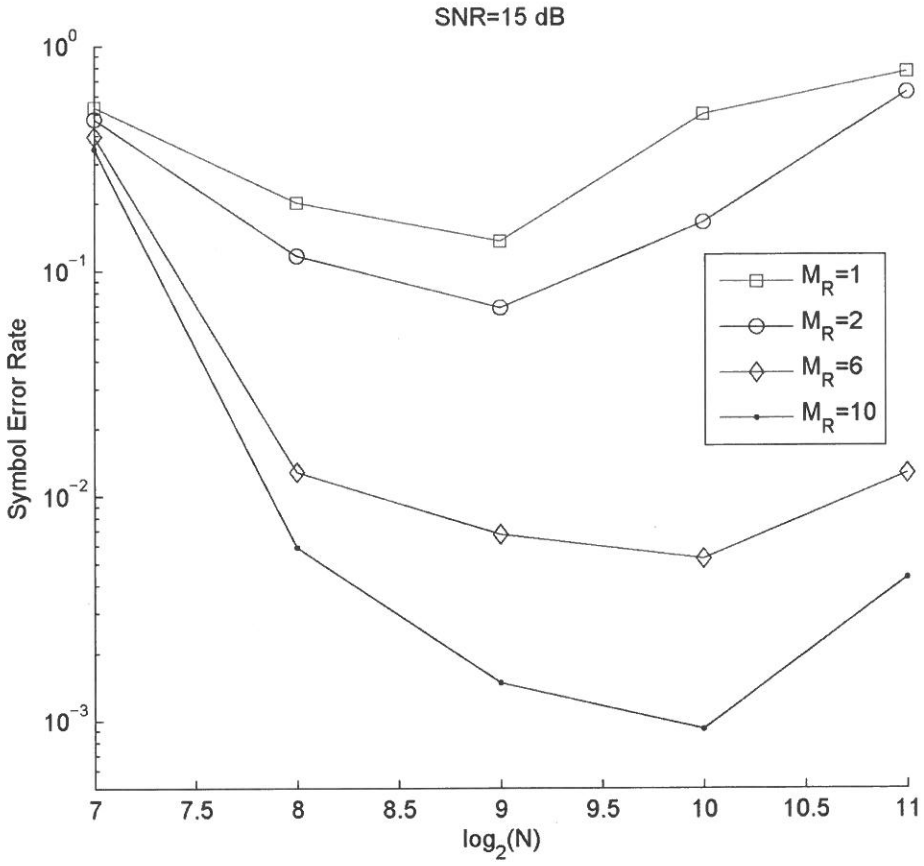

Figure 7.5: SER performance of differential SFBC OFDM versus the number of carriers for different number of receive elements.

single-transmitter differential OFDM and the coherent SFBC scheme in the MSE sense, i.e. outperforming the SFBC scheme by ≈6 dB and the single transmitter differential scheme by ≈10 dB for $N = 2048$. Moreover, it was demonstrated that 78% higher bit rate was achieved by D-SFBC compared to the coherent SFBC scheme. D-SFBC was also shown to outperform the coherent SFBC scheme at larger number of subcarriers, which results in better bandwidth efficiency.

Chapter 8

Conclusion

8.1 Conclusions

In this thesis, we investigate the analysis and design of diversity techniques for terrestrial and underwater acoustic communication channels.

We first investigate different relay selection methods for the multi-relay SC-FDE broadband cooperative networks with underlying frequency-selective Rayleigh fading channels, assuming both ML and MMSE receivers. We investigate the relay selection criteria for the SC-FDE ML receivers motivated by minimizing the average symbol error rate. Similarly, we investigate different relay selection schemes for SC-FDE MMSE receivers motivated by minimizing the instantaneous symbols error rate. We also propose novel relay selection schemes in which only the relay with the frequency selective source to destination link that acquires the highest norm flat fading tab is selected, along with a PEP based scheme which is able to fully investigate the underlying multipath diversity. Among the relay selection methods provided, the SFRS and the relay selection criteria based on minimizing the average symbol error rate, have the best SER performance for SC-FDE ML receiver. We finally extend our analysis to multiple relay selection scenarios by applying the EDA algorithm. By further defining the EDA parameters specifically for our relay selection problem, significant performance improvement was shown while maintaining comparable complexity.

We next investigate cooperative SC-FDE for two-way multiple relay networks with selection. We consider both ML-SC-FDE and MMSE-SC-FDE receivers. We derive closed-form expressions for the conditional and average end-to-end SNR and SER for the participating source terminals. The maximum achievable diversity gain by the single relay SC-FDE TWR

system is investigated under different power control policies, and the existence of the performance bottleneck is verified. We extend our analysis to multiple relay cooperative SC-FDE TWR systems with best relay selection. Further, asymptotic analysis on the average SER reveals that the diversity gain is determined by both the number of participating relay nodes and the minimum of the multipath diversity order experienced in the source to relay, and relay to destination links, which acts like a performance bottleneck for the relaying paths. We complete our analysis by introducing the bottleneck integral factor that dictates the performance bottleneck existing in the TWR cooperative communication systems and cooperative communication systems, in general. The existence of the bottleneck integral in the error performance expression associated with the generic single relay cooperative channels is analytically corroborated and verified.

To further incorporate the network total power constraints, we investigate optimal relay beamforming for the multiuser TWR systems, where the relay transceiver processor is designed based on the MMSE criterion. We drive a closed-form expression for the SINR at each of the user terminals, and further present a joint user-relay antenna selection algorithm by applying the EDA. The proposed EDA has a low computational complexity, and its effectiveness is verified through simulation results.

Next, aiming to find an efficient way to solve for the sparse beamforming matrices, we propose a novel iterative sparse algorithm to design the underlying transmit, relay, and receive matrices. More specifically, we first decouple the primal problem into three convex sub-problems, and then propose an iterative algorithm, which solves for the sparse suboptimal beamforming matrices, one at a time. The solution to each subproblem aims to minimize MSE, which also minimizes the total MSE, and hence the convergence of the iterative algorithm is guaranteed. Comprehensive simulation is conducted to evaluate the effectiveness of the sparse beamforming design algorithm in terms of the error performance and convergence.

Next, we study the performance of differential space-time codes with LCP for OFDM cooperative networks over frequency selective channels. Through exploiting the unitary structure of the orthogonal STBCs, we design a low complexity differential STBC-LCP-OFDM receiver for cooperative networks. We assume the amplify-and-forward protocol and consider both single relay and multi-relay scenarios. Under the assumption of perfect power control for the relay terminal and high signal-to-noise ratio for the underlying links, our performance analysis demonstrates that the considered scheme is able to exploit fully the spatial diversity.

Finally, we investigate the performance of differential SFBCs for OFDM signals over underwater acoustic channels. By applying the unitary structure of the orthogonal SFBCs over the carriers of an OFDM system, the underlying transmit diversity in an underwater acoustic channel is exploited. Differential detection is further applied to eliminate the need for expensive signal processing required for channel tracking. We assume that there is sufficient spatial diversity between the channels of the transmitters, and that each channel changes slowly over the carriers, thus satisfying the basic Alamouti coherence requirement. System performance is demonstrated using real data transmitted in the $12-26$ kHz acoustic band from a vehicle moving at $0.5-2$ m/s and received over a shallow water channel, using 4-QAM and a varying number of carriers ranging from 128 to 2048. Performance results demonstrate the advantage of the differential coherent SFBC detector over the conventional coherent SFBC detector which suffers from imperfect channel estimation.

8.2 Future works

The work in this thesis also reveals some interesting topics for future research. In the study of sparse beamforming algorithms for TWR communication networks in Chapter 5, one interesting future research topic is to address the effect of the channel estimation errors on the system's overall performance. It is also worth while to revise the proposed beamforming algorithm to study the sparse beamforming channel estimation idea for TWR systems with DF relaying protocols.

In the study of differential decoding for SFBC OFDM systems in underwater MIMO channels, after combining, the signal is subject to conventional OFDM detection. A particularly interesting future research topic is to incorporate partial FFT demodulation to suppress ICI. More specifically, FFT outputs can be weighted before combining to suppress the ICI. An interesting future work on this subject is to investigate the performance improvement that can be obtained by partial FFT demodulation for differential SFBC OFDM where aperiori channel information is not available. Driving an algorithm for computing the combiner weights without the a priori knowledge of the channel variation or the Doppler distortion is another interesting future research topic that can be investigated.

Bibliography

[1] T. S. Rappaport, *Wireless Communications: Principles and Practice*, 2nd ed. Upper Saddle River, NJ: Prentice-Hall, 2002.

[2] W. C. Jakes, *Microwave Mobile Communications*, 1st ed. New York: John Wiley and Sons, 1974.

[3] D. Tse and P. Viswanath, *Fundamentals of Wireless Communication.* Cambridge University Press, 2005.

[4] A. Paulraj, D. Gore, R. Nabar, and H. Bolcskel, "An overview of mimo communications- a key to gigabit wireless," *Proc. IEEE*, vol. 92, no. 2, pp. 198–218, February 2004.

[5] D. Tse, P. Viswanath, and L. Zheng, "Diversity-multiplexing tradeoff in multiple access channels," *IEEE Trans. Info. Theory*, vol. 50, no. 9, pp. 1859–1874, September 2004.

[6] Brennan, "Linear diversity combining techniques," *Proc. IRE*, pp. 1075–1102, February 1959.

[7] W. C. Jakes, *Microwave mobile communication.* New York: NY: John Wiley and Sons, 1974.

[8] J. G. Proakis, *Digital Communications*, 4th ed. New York: NY: McGraw-Hill, 2001.

[9] V. Tarokh, N. Seshadri, and A. R. Calderbank, "Space-time codes for high data rate wireless communication: Performance criterion and code construction," *IEEE Transactions on Information Theory*, vol. 44, no. 2, pp. 744–765, March 1998.

[10] S. M. Alamouti, "A simple transmit diversity technique for wireless communications," *IEEE JSAC*, vol. 16, pp. 1451–1458, 1998.

[11] H. Jafarkhani, "A quasi-orthogonal space-time block code," *IEEE Trans. Commun.*, vol. 49, no. 1, pp. 1–4, January 2001.

[12] V. Tarokh, H. J. Jafarkhani, and A. R. Calderbank, "Space-time block codes from orthogonal designs," *IEEE Transactions on Information Theory*, vol. 45, no. 5, pp. 1456–1467, July 1999.

[13] A. Wittneben, "Basestation modulation diversity for digital simulcast," in *Proc. IEEE Veh. Technol. Conf.*, St. Louis, Missouri, 1991, pp. 848–853.

[14] T. Lo, "Maximal ratio transmission," *IEEE Trans. Commun.*, vol. 47, no. 10, pp. 1458–1461, October 1999.

[15] J. G. Foschini, "Layered space-time architecture for wireless communication in a fading environment when using multi element antennas," *Bell Labs Tech. J.*, vol. 2, pp. 41–59, 1996.

[16] G. J. Foschini and M. J. Gans, "On limits of wireless communications in a fading environment when using multiple antennas," *Wireless Personal Commun.*, vol. 6, no. 3, pp. 311–335, March 1998.

[17] E. Telatar, "Capacity of multi-antenna gaussian channels," *European Trans. Telecommun.*, vol. 10, no. 6, pp. 585–595, December 1999.

[18] L. Zheng and D. Tse, "Diversity and multiplexing: a fundamental tradeoff in multiple antenna channels," *IEEE Trans. Info. Theory*, vol. 49, no. 5, pp. 1073–1096, May 2003.

[19] G. J. Foschini, G. D. Golden, R. A. Valenzuela, and P. W. Wolniansky, "Simplified processing for high spectral ef„ciency wireless communication employing multi-element arrays," *IEEE J. Select. Areas Commun.*, vol. 17, no. 11, pp. 1841–1852, November 1999.

[20] T. M. Cover and J. A. Thomas, *Elements of Information Theory*, ser. New York. NY: John Wiley and Sons, 1991.

[21] A. El Gamal and T. M. Cover, "Multiuser information theory," *Proc. IEEE*, vol. 68, no. 2, pp. 1466–1483, December 1980.

[22] A. Goldsmith, S. A. Jafar, N. Jindal, and S. Vishwanath, "Capacity limits of mimo channels," *IEEE J. Select. Areas Commun.*, vol. 21, no. 5, pp. 684–702, June 2003.

[23] V. Lau, Y. Liu, and T. A. Chen, "The role of transmit diversity on wireless communicationsÛreverse link analysis with partial feedback„" *IEEE Trans. Commun.*, vol. 50, no. 12, pp. 2082–2090, December 2002.

[24] C. G. and S. Shamai, "On the achievable throughput of a multiantenna gaussian broadcast channel," *IEEE Trans. Info. Theory*, vol. 49, no. 7, pp. 1691–1706, July 2003.

[25] S. Vishwanath, N. Jindal, and A. Goldsmith, "Duality, achievable rates, and sum-rate capacity of gaussian mimo broadcast channels," *IEEE Trans. Info. Theory*, vol. 49, no. 10, pp. 2658–2668, october 2003.

[26] C. Kose and R. D. Wesel, "Universal space-time trellis codes," *IEEE Trans. Inf. Theory*, vol. 49, pp. 2717–2727, October 2003.

[27] Z. Safar and K. J. R. Liu, "Systematic space-time trellis code construction for correlated rayleigh-fading channels," *IEEE Trans. Inf. Theory*, vol. 50, no. November, pp. 2855–2865, 2004.

[28] L. Yonghui, B. Vucetic, Y. Tang, and Q. Zhang, "Space-time trellis codes with li-near transformation for fast fading channels," *IEEE Signal Process. Lett.*, vol. 50, no. 11, pp. 895–898, November 2004.

[29] H. Wang and X. G. Xia, "Upper bounds of rates of complex orthogonal space-time block codes," *IEEE Trans. Inf. Theory*, vol. 49, no. 10, pp. 2788–2796, October 2003.

[30] J. Boyer, D. Falconer, and H. Yanikomeroglu, "Multihop diversity in wireless relaying channels," *IEEE Transactions on Communications*, vol. 52, no. 10, pp. 1820–1830, October 2004.

[31] A. Sendonaris, E. Erkip, and B. Aazhang, "User cooperation diversity part i: system description," *IEEE Trans. Comm.*, vol. 51, no. 11, 2003.

[32] ——, "User cooperation diversity part ii: implementation aspects and performance analysis," *IEEE Trans. Comm.*, vol. 51, no. 11, 2003.

[33] J. N. Laneman, G. W. Wornell, and D. N. C. Tse, "An efficient protocol for realizing cooperative diversity in wireless networks," Washington, DC, 2001, p. 294.

[34] J. N. Laneman, D. N. C. Tse, and G. W. Wornell, "Cooperative diversity in wireless networks: Efficient protocols and outage behavior," *IEEE Trans. Inf. Theory*, 2004.

[35] E. C. van der Meulen, "Three-terminal communication channels," *Advances in Applied Probability*, vol. 3, pp. 120–154, 1971.

[36] ——, "A survey of multi-way channels in information theory: 1961Ű1976," *IEEE Transactions on Information Theory*, vol. 23, no. 1, pp. 1–37, January 1977.

[37] G. Kramer, M. Gastpar, and G. P., "Cooperative strategies and capacity theorems for relay networks," *IEEE Transactions on Information Theory*, vol. 51, no. 9, pp. 3037–3306, September 2005.

[38] A. Reznik, S. R. Kulkarni, and V. S., "Degraded gaussian multi-relay channel: capacity and optimal power allocation," *IEEE Transactions on Information Theory*, vol. 50, no. 12, pp. 3037–3046, 2004.

[39] A. A. El Gamal and Z. S., "Capacity of a class of relay channels with orthogonal components," *IEEE Transactions on Information Theory*, vol. 51, no. 5, pp. 1815–1817, May 2005.

[40] J. N. Laneman and G. W. Wornell, "Distributed space-time-coded protocols for exploiting cooperative diversity in wireless networks," *IEEE Trans. on Information Theory*, vol. 49, no. 10, pp. 2415–2425, October 2003.

[41] Z. Xiong, A. D. Liveris, and C. S., "Distributed source coding for sensor networks," *IEEE Signal Processing Magazine*, vol. 21, pp. 80–94, September 2004.

[42] T. Cover and A. E. Gammel, "Capacity theorems for the relay channel," *IEEE Transactions on Information Theory*, vol. 22, no. 5, pp. 572–584, September 1979.

[43] B. Zhao and M. Valenti, "Practical relay networks: a generalization of hybrid arq," *IEEE Journal on Selected Areas in Communications*, vol. 23, no. 1, pp. 7–18, January 2005.

[44] M. Zorzi and R. R. Rao, "Geographic random forwarding (geraf) for ad hoc and sensor networks: multihop performance," *IEEE Transactions on Mobile Computing*, vol. 2, no. 4, pp. 337–348, December 2003.

[45] J. Luo, R. S. Blum, L. J. Greenstein, L. J. Cimini, and A. M. Haimovich, "New approaches for cooperative use of multiple antennas in ad hoc wireless networks," in *IEEE Vehicular Technology Conference (VTCŠ04)*, vol. 4, September 2004, pp. 2769–2773.

[46] A. Ibrahim, A. Sadek, W. Su, and K. J. R. Liu, "Cooperative communications with partial channel state information: when to cooperate?" in *The IEEE Global Telecommunications Conference (GLOBECOM)*, vol. 5, November 2005, pp. 3068–3072.

[47] H. Mheidat, M. Uysal, and N. Al-Dhahir, "Comparative analysis of equalization techniques for stbc with application to edge," in *IEEE Vehicular Technology Conference (VTCŠ04) Spring,*, Milan, Italy, May 2004.

[48] T. L. Marzetta and B. M. Hochwald, "Capacity of a mobile multiple-antenna communication link in rayleigh flat-fading," *IEEE Transactions on Information Theory*, vol. 45, pp. 139–157, January 1999.

[49] B. M. Hochwald and W. Sweldens, "Differential unitary spaceŰtime modulation," *IEEE Trans. Commun.*, vol. 48, no. 12, p. 2041Ű2052, December 2000.

[50] V. Tarokh and H. Jafarkhani, "A differential detection scheme for transmit diversity," *IEEE Journal on Selected Areas in Communications*, vol. 18, pp. 1169–1174, July 2000.

[51] *Amendment to Air Interface for Fixed and Mobile Broadband Wireless Access SysTems Ű Physical and Medium Access Control Layers for Combined Fixed and Mobile Operation in Licensed Bands*, IEEE Std. 802.16e-2005, 2005.

[52] *Air Interface for Fixed Broadband Broadband*, IEEE Std. 802.16-2004, 2004.

[53] O. Oyman, N. J. Laneman, and S. Sandhu, "Multihop relaying for broadband wireless mesh networks: From theory to practice," *IEEE Communications Magazine*, vol. 45, no. 11, pp. 116–122, 2007.

[54] *IEEE 802.16 Relay Task Group, 2008; http://www.ieee802.org/16/relay/.*

[55] C. B. Chae, T. Tang, R. W. Heath Jr., and S. Cho, "Mimo relaying with linear processing for multiuser transmission in fixed relay networks," *IEEE Transactions on Signal Processing*, vol. 56, no. 2, pp. 727–738, 2008.

[56] *3GPP TSG RAN TR 36.913 v8.0.0, Requirements for Further Advancements.*

[57] *IEEE802.16m-07/002r4, TGm System Requirements Document (SRD).*

[58] R. Pabst, B. H. Walke, and D. C. Schultz, "Relay-based deployment concepts for wireless and mobile broadband radio," *IEEE Communications Magazine*, vol. 42, no. 9, pp. 80–89, 2004.

[59] L. Le and E. Hossain, "Multihop cellular networks: Potential gains, research challenges, and a resource allocation framework," *IEEE Communications Magazine*, vol. 45, no. 9, pp. 66–73, 2007.

[60] H. Wu, C. Qiao, S. De, and O. Tonguz, "Integrated cellular and ad hoc relaying systems: icar," *IEEE Journal on Selected Areas in Communications*, vol. 19, no. 10, pp. 2105–2115, 2001.

[61] V. Sreng, H. Yanikomeroglu, and D. D. Falconer, "Coverage enhancement through two-hop rayleigh in cellular radio systems," in *IEEE Wireless Communications and Networking Conference*, vol. 5, March 2002, pp. 881–885.

[62] A. Bletsas, A. Khisti, D. P. Reed, and A. Lippman, "A simple cooperative diversity method based on network path selection," *IEEE Journal on Selected Areas in Communications*, vol. 24, no. 3, pp. 659–672, 2006.

[63] M. Qin and R. S. Blum, "Capacity of wireless ad hoc networks with cooperative diversity: A warning on the interaction of relaying and multi-hop routing," in *IEEE International Conference on Communications*, vol. 2, May 2005, pp. 1128–1131.

[64] G. Scutari, S. Barbarossa, and D. Ludovici, "Cooperation diversity in multihop wireless networks using opportunistic driven multiple-access," in *IEEE Workshop on Signal Processing Advances in Wireless Communications (SPAWC '03)*, June 2003, pp. 170–174.

[65] E. H. Drucker, "Development and application of a cellular repeater," in *IEEE Vehicular Technology Conference (VTC '88)*, June 1988, pp. 321–325.

[66] E. C. Van Der Meulen, "Transmission of information in a t-terminal discrete memoryless channel," Dept. of Statistics, Univ. of California, Berkeley, CA, Tech. Rep., 1968.

[67] M. Dohler and Y. Li, *Cooperative Communications: Hardware, Channel and Phy.* Wiley, Feb 2010.

[68] R. U. Nabar, H. Bolcskei, and F. Kneubuhler, "Fading relay channels: Performance limits and space-time signal design," *IEEE J. Sel. Areas Comm.*, vol. 22, no. 6.

[69] Z. Wang and G. B. Giannakis, "Linearly precoded or coded ofdm against wireless channel fades?" *Proc. of the IEEE Workshop on Signal Processing Advances for Wireless Communications*, 2001.

[70] W. W. Lu, "Compact multi-dimensional broadband wireless - convergence of wireless mobile and access," *IEEE Commun. Mag.*, pp. 119–123, November 2000.

[71] S. Govardhanagiri, T. Karp, P. Heller, and T. Nguyen, "Performance analysis of multicarrier modulation systems using cosine modulated filter banks," *Proc. ICASSP '99*, vol. 3, pp. 1405–1408, 1999.

[72] B. Muquet, Z. Wang, G. B. Giannakis, M. de Courville, and P. Duhamel, "Cyclic prefix or zero padding for wireless multicarrier transmission?" *IEEE Trans. Commun.*, vol. 50, pp. 2136–2148, December 2002.

[73] D. P. Palomar, J. M. Cioffi, and M. A. Lagunas, "oint tx-rx beamforming design for multicarrier mimo channels: A unified framework for convex optimization," *IEEE Trans. Signal Process*, vol. 51, no. 9, September 2003.

[74] H. Sari, G. Karam, and I. Jeanclaude, "Transmission techniques for digital terrestrial tv broadcasting," *IEEE Commun. Mag.*, vol. 33, no. 2, pp. 100–109, February 1995.

[75] H. Eghbali, S. Muhaidat, M. Dianati, and R. Tafazolli, *Single-Carrier Frequency Domain Equalization for Broadband Wireless Networks communications Ű A Review.* USA: Nova Science, 2013.

[76] Y. Jing and H. Jaffarkhani, "Single and multiple relay selection schemes an their achievable diversity orders," *IEEE Trans. Wireless Commun.*, no. 3, pp. 1414–1423, March 2009.

[77] V. Shah, N. B. Mehta, and R. Yim, "The relay selection and transmission tradeoff in cooperative communication systems," *IEEE Trans. Wireless Commun.*, vol. 9, pp. 2505–2515, Aug. 2010.

[78] M. Seyfi, S. Muhaidat, and J. Liang, "Performance analysis of relay selection with feedback delay and channel estimation errors," *IEEE Signal Process. Lett.*, vol. 18, pp. 67–70, Jan. 2011.

[79] H. Muheidat, M. Uysal, and N. Al-Dhahir, "Equalization techniques for distributed space-time block codes with amplify-and-forward relaying," *IEEE Trans. Signal Process*, vol. 55, no. 5, pp. 1839–1852, May 2007.

[80] H. Muhaidat, M. Uysal, and R. Adve, "Pilot-symbol-assisted detection scheme for distributed orthogonal space-time block coding," *IEEE Trans. Wireless Commun.*, vol. 8, no. 3, pp. 1057–1061, May 2009.

[81] *Time-reversal space-time equalization for amplify-and-forward relaying*, Istanbul, Turkey, June 2006.

[82] H. Eghbali, S. Muhaidat, and N. Al-Dhahir, "novel receiver design for single-carrier frequency domain equalization in broadband wireless networks with amplify-and-forward relaying," *IEEE Trans.Wireless Commun.*, vol. 10, no. 3, pp. 721–727, 2011.

[83] H. E. Eghbali and S. Muhaidat, "Single-carrier frequency-domain equalization for multi-relay cooperative systems with relay selection," 2011, pp. 1353–1358.

[84] O. Shin, A. Chan, H. T. Kung, and V. Tarokh, "Design of an ofdm co-operative diversity system," *IEEE Trans. Veh. Technol.*, vol. 56, no. 4, pp. 2203–2215, July 2007.

[85] Y. Ding and M. Uysal, "Amplify-and-forward cooperative ofdm with multiple-relays: Performance analysis and relay selection methods," *IEEE Trans. Wireless Commun.*, vol. 8, no. 10, pp. 4963–4968, Oct. 2009.

[86] W. P. Siriwongpairat, A. K. Sadek, and K. J. R. Liu, "Cooperative communications protocol for multiuser ofdm networks„" *IEEE Trans. Wireless Commun.*, vol. 7, no. 7, pp. 2430–2435, July 2008.

[87] W. Dang, M. Tao, H. Mu, and J. Huang, "Subcarrier-pair based resource allocation for cooperative multi-relay ofdm systems," *IEEE Trans. Wireless Commun.*, vol. 9, no. 5, pp. 1640–1649, May 2010.

[88] R. Kwan and C. Leung, "Gamma variate ratio distribution with application to cdma performance analysis," April 2005, pp. 188–191.

[89] M. Abramowitz and I. A. Stegun, *Handbook of Mathematical Functions With Formulas, Graphs, and Mathematical Tables*, 9th ed. New York: Dover, 1970.

[90] D. A. Gore and A. Paulraj, "Mimo antenna subset selection with space-time coding," *IEEE Trans. Signal Processing*, vol. 50, pp. 2580–2588, Oct. 2002.

[91] A. F. Molisch and M. Z. Win, "Mimo systems with antenna selection," *IEEE Microwave Magazine*, vol. 5, no. 1, pp. 45–56, 2004.

[92] S. Sanayei and A. Nosratinia, "Antenna selection in mimo systems," *IEEE Communications Magazine*, vol. 42, no. 10, pp. 68–73, 2004.

[93] X. Shao, J. Yuan, and P. Rapajic, "Antenna selection for mimo-ofdm spatial multiplexing system," *IEEE International Symposium on Information Theory*, July 2003.

[94] A. Wilzeck, P. Pan, and T. Kaiser, "Transmit and receive antenna subset selection for mimo sc-fde in frequency selective channels," in *Proceedings of the 14th European Signal Processing Conference*, Florence, Italy, Sep. 2006.

[95] J. Xu, H. Zhang, D. Yuan, and M. Jiang, "A new multiple relay selection scheme in dual-hop amplify-and-forward cooperative network based on genetic algorithm," in *Proc. of IEEE International Conference on Communication Technology (ICCT2011)*, Jinan, China, Sep. 2011.

[96] A. E. Eiben and J. E. Smith, *Introduction to Evolutionary Computing.* Springer Verlag, 2003.

[97] P. Larraaga and J. A. Lozano, *Estimation of Distribution Algorithms: A New Tool for Evolutionary Computation.* Kluwer Academic Publishers, 2001.

[98] G. H. Golub and C. F. VanLoan, *Matrix Computations.* The Johns Hopkins Univ. Press, 1983.

[99] J. Ping and S. Ting, "Rate performance of af two-way relaying in low snr region," *IEEE Commun.Letters*, vol. 13, pp. 1–3, April 2009.

[100] L. Song, "Relay selection for two-way relaying with amplify-and-forward protocols," *IEEE Trans.Vehic.Tech.*, vol. 60, pp. 1954–1959, May 2011.

[101] Y. Liu and M. Tao, "Optimal channel and relay assignment in ofdm based multi-relay multi-pair two-way communication networks," *IEEE Trans. Commun.*, vol. 1, no. 2, April 2012.

[102] A. Tajer and A. Nosratinia, "Diversity order in isi channels with singlecarrier," *IEEE Trans. Wireless Commun.*, vol. 9, no. 3, p. 1022Ű1032, March 2010.

[103] H. Lutkepoh, *Handbook of matrices.* Newyork: Wiley and Sons, 1996.

[104] A. Hjorungnes, "Complex-valued matrix differentiation: Techniques and key results," *IEEE Transactions on Signal Processing*, vol. 55, no. 6, pp. 2740 – 2746, June 2007.

[105] J. Cioffi, *Class Reader for EE379a - Digital Communication: Signal Processing.*, Stanford University, Stanford, CA.

[106] K. Peppas, "Moments generating function of the harmonic mean of two non-identical gamma random variables and its applications in wireless communications," *Journal of the Franklin Institute*, pp. 845–860, 2011.

[107] I. S. Gradshteyn and I. M. Ryzhik, *Table of Integrals, Series, and Products.* Academic Press, 2007.

[108] M. K. Simon and M. S. Alouini, *Digital Communication Over Fading Channels. A Unified Approach to Performance Analysis.* New York: Wiley, 2000.

[109] A. Cuyt, K. Driver, J. Tan, and B. Verdonk, "A finite sum representation of the appell series," *Journal of Computational and Applied Mathematics*, vol. 105, pp. 213–219, 1999.

[110] J. Joung and Y. H. Lee, "Regularized channel diagonalization for multiuser mimo downlink using a modiiňĄed mmse criterion," *IEEE Trans. Signal Process.*, vol. 55, no. 4, pp. 1573–1579, April 2007.

[111] A. H. Sayed, *Adaptive Filters.* New York: Wiley, 2008.

[112] A. Molisch, M. Win, Y. CHoi, and J. Winters, "Capacity of mimo systems with antenna selection," *IEEE Transactions on Wireless Communications*, vol. 4, pp. 1759–1772, July 2005.

[113] J. Chung, C. S. Hwang, K. Kim, and Y. K. Kim, "A random beamforming technique in mimo systems exploiting multiuser diversity," *IEEE J. Sel. Areas Commun.*, vol. 21, pp. 848–855, June 2003.

[114] J. Yang, P. Fan, T. Q. Duong, and X. Lei, "Exact performance of two-way af relaying in nakagami-m fading environment," *IEEE Trans.Wireless Commun.*, vol. 10, no. 3, pp. 1–7, March 2011.

[115] C. Leow, Z. Ding, K. Leung, and D. Geockel, "On the study of analogue network coding for multi-pair, bidirectional relay channels," *IEEE Trans. Wireless Commun.*, vol. 10, no. February, pp. 670–681, 2011.

[116] S. W. Peters and R. W. Heath, "Interference alignment via alternating minimization," in *Proc. 2009 IEEE Intern. Conf. Acoustics, Speech Signal Proc. (ICASSP 2009)*, Taipei, Taiwan, April 2009.

[117] V. R. Cadambe and S. Jafar, "Interference alignment and degrees of freedom of the k-user interference channel," vol. 54, no. 8, pp. 3425–344, August 2008.

[118] I. Hammerstrom, M. Kuhn, C. Esli, J. Zhao, A. Wittneben, and G. Bauch, "Mimo two-way relaying with transmit csi at the relay," *in Proc. IEEE SPAWC07*, 2007.

[119] T. J. Oechtering, R. F. Wyrembelski, and H. Boche, "Multiantenna bidirectional broadcast channels? optimal transmit strategies," *IEEE Trans. Signal Process.*, vol. 57, no. 5, pp. 1948–1958, May 2009.

[120] C. Esli and A. Wittneben, "One- and two-way decode-and-forward relaying for wireless multiuser mimo networks," *in Proc. IEEE GLOBECOM08*, 2008.

[121] Y. C. Zhang, C. C. Chai, and S. Cui, "Optimal beamforming for two-way multi-antenna relay channel with analogue network coding," *IEEE J. Sel. Areas Commun.*, vol. 29, no. 5, pp. 699–712, June 2009.

[122] G. Li, Y. Wang, and P. Zhang, "Optimal linear mmse beamforming for two way multi-antenna relay systems," *IEEE Commun. Lett*, vol. 15, no. 5, pp. 533–535, May 2011.

[123] J. Joung and A. H. Sayed, "Multiuser two-way amplify-and-forward relay processing and power control methods for beamforming systems," *IEEE Trans. Signal Process.*, vol. 58, no. 3, pp. 1833–1846, March 2010.

[124] A. Khabbazibasmenj, F. Roemer, S. A. Vorobyov, and M. Haardt, "Sum-rate maximization in two-way af mimo relaying: Polynomial time solutions to a class of dc

programming problems," *IEEE Trans. Signal Process.*, vol. 60, no. 10, pp. 5478–5493, October 2012.

[125] C. Y. Leow, Z. Ding, and K. K. Leung, "Joint beamforming and power management for nonregenerative mimo two-way relaying channels," *IEEE Trans. Veh. Technol.*, vol. 60, no. 9, pp. 4374–4383, November 2011.

[126] S. Xu and Y. Hua, "Optimal design of spatial source-and-relay matrices for a non-regenerative two-way mimo relay system," *IEEE Trans. Wireless Commun.*, vol. 10, no. 5, pp. 1645–1655, May 2011.

[127] R. Wang and M. Tao, "Joint source and relay precoding designs for mimo two-way relaying based on mse criterion," *IEEE. Trans. Signal Process.*, vol. 60, no. 3, pp. 1352–1365, March 2012.

[128] J. A. Tropp and A. C. Gilbert, "Signal recovery from random measurements via orthogonal matching pursuit," *IEEE Trans. Inf. Theory*, vol. 53, no. 12, pp. 4655–4666, December 2007.

[129] X. Zhang, *Matrix analysis and applications.* Tsinghua University Press, 2004.

[130] A. Hjorungnes and D. Gesbert, "Hessians of scalar functions of complex-valued matrices: A systematic computational approach," *in Proc. 9th Int. Symp. Signal Processing and Its Applications (ISSPA) 2007*, 2007.

[131] J. Chen and X. Huo, "Theoretical results on sparse representations of multiple measurement vectors," *IEEE Transactions on Signal Processing*, vol. 54, no. 12, pp. 4634–4643, 2006.

[132] P. Eldar, Y. C. Kuppinger and H. Bolcskei, "Compressed sensing of block-sparse signals: Uncertainty relations and efficient recovery," *Transactions on Signal Processing*, vol. 58, no. 6, pp. 3042–3054, 2010.

[133] Z. Zhang and B. D. Rao, "Sparse signal recovery with temporally correlated source vectors using sparse bayesian learning," *IEEE Journal of Selected Topics in Signal Processing, Special Issue on Adaptive Sparse Representation of Data and Applications in Signal and Image Processing*, vol. 5, no. 5, pp. 912–926, Sept. 2011.

[134] B. L. Hughes, "Differential spaceŰtime modulation," *IEEE Trans. Inf. Theory*, vol. 46, no. 7, p. 2567Ű2578, November 2000.

[135] H. Jafarkhani and V. Tarokh, "Multiple transmit antenna differential detection from generalized orthogonal designs," *IEEE Trans. Inf. Theory*, vol. 47, no. 6, p. 2626Ű2631, September 2001.

[136] A. Shokrollahi, B. Hassibi, B. M. Hochwald, and W. Sweldens, "Representation theory for high-rate multiple-antenna code design," *IEEE Trans. Inf. Theory*, vol. 47, no. 6, p. 2335Ű2367, September 2001.

[137] B. Hassibi and M. Khorrani, "Fully-diverse multiple-antenna signal constellations and „xed-point-free lie groups," Washington, DC, June 2001.

[138] Z. Liu and G. B. Giannakis, "Block differentially encoded ofdm with maximum multipath diversity," *IEEE Trans. Wireless Commun.*, vol. 2, no. 3, pp. 420–423, May 2003.

[139] S. N. Diggavi, N. Al-Dhahir, A. Stamoulis, and A. R. Calderbank, "Differential space-time coding for frequency-selective channels," *IEEE Commun. Lett.*, vol. 6, pp. 253–255, June 2002.

[140] J. Wang and K. Yao, "Differential unitary spaceŰtimeŰfrequency coding for mimo-ofdm systems," in *36th Asilomar Conf. Signals, Systems and Computers,*, Paci„c Grove, CA, November 2002, pp. 1867–1871.

[141] Q. Ma, C. Tepedelenlio, and Z. Liu, "Differential spaceŰtimeŰrequency coded ofdm with maximum diversity," in *37th Conf. Information Sciences and Systems*, Baltimore, MD, March 2003, pp. 12–13.

[142] H. Li, "Differential spaceŰtime modulation with full spatio-spectral diversity and arbitrary number of transmit antennas in isi channels," in *IEEE Int. Conf. Acoustic, Speech, and Signal Processing*, Hong Kong, China, April 2003, pp. IV–37ŰIV–40.

[143] H. Bölcskei and M. Borgmann, "Code design for non-coherent mimoŰofdm systems," in *Allerton Conf. Communication, Control, and Computing*, Monticello, IL, October 2002, p. 237Ű246.

[144] H. Muhaidat and M. Uysal, "Non-coherent and mismatched-coherent receivers for distributed stbcs with amplify-and-forward relaying," *IEEE Transactions on Wireless Communications*, vol. 6, no. 11, pp. 4060–4070, November 2007.

[145] D. Chen and J. N. Laneman, "Non-coherent demodulation for cooperative wireless systems," in *Proc. IEEE Global Communications Conference (GLOBECOM)*, November 2004.

[146] P. Tarasak, H. Minn, and V. K. Bhargava, "Differential modulation for two-user cooperative diversity systems," *IEEE J. Sel. Areas Commun.*, vol. 23, no. 9, pp. 1891–1900, September 2005.

[147] T. Wang, Y. Yao, and G. B. Giannakis, "Non-coherent distributed spacetime processing for multiuser cooperative transmissions," in *Proc. IEEE Global Communications Conference (GLOBECOM)*, December 2005.

[148] S. Yiu, R. Schober, and L. Lampe, "Non-coherent distributed spacetime block coding," in *IEEE Vehicular Technology Conference (VTC)*, September 2005.

[149] S. Muhaidat, P. Ho, and M. Uysal, "Distributed differential space-time coding for broadband cooperative networks," in *IEEE VTC'09-Spring*, Barcelona, Spain, April 2009.

[150] Z. Liu, Y. Xin, and G. B. Giannakis, "Linear constellation precoding for ofdm with maximum multipath diversity and coding gains," *IEEE Trans. Commun.*, vol. 51, pp. 416–427, March 2003.

[151] Z. Wang and G. B. Giannakis, "Complex-field coding for ofdm over fading wireless channels," *IEEE Trans. Inform. Theory*, vol. 49, pp. 707–720, March 2003.

[152] M. Riediger and P. Ho, "An eigen-assisted non-coherent receiver for alamouti-type space-time modulation," *IEEE J. Select. Areas Commun.*, vol. 23, no. 9, pp. 1811–1820, September 2005.

[153] M. Riediger, P. Ho, and J. H. Kim, "An iterative receiver for differential space-time pi/2-shifted bpsk modulation," *EURASIP Journal (special issue on Advanced Signal Processing Algorithms for Wireless Communications)*, vol. 5, no. 2, pp. 83–91, April 2005.

[154] M. Riediger and P. Ho, "A differential space-time code receiver using the em-algorithm," *Canadian Journal on Electrical and Computer Engineering*, vol. 29, no. 4, pp. 227–230, October 2004.

[155] H. Li, "Differential space-time-frequency modulation over frequency-selective fading channels," *IEEE Commun. Lett.*, vol. 7, no. 8, pp. 349–351, August 2003.

[156] Q. Ma, C. Tepedelenlioglu, and Z. Liu, "Differential space-time-frequency coded ofdm with maximum multipath diversity," *IEEE Transactions on Wireless Communications*, vol. 4, no. 5, September 2005.

[157] M. Uysal, C. Campolat, and M. M. Fareed, "Asymptotic performance analysis of distributed space-time codes," *IEEE Commun. Lett*, vol. 10, no. 11, pp. 757–777, November 2006.

[158] H. Eghbali and S. Muhaidat, "Precoded differential ofdm for relay networks," *Journal of Selected Areas in Telecommunications*, pp. 59–66, January 2011.

[159] S. Lu and N. Al-Dhahir, "Coherent and differential ici cancellation for mobile ofdm with application to dvb-h," *IEEE Trans. Wireless Commun*, vol. 11, no. 12, pp. 4110–4116, November 2008.

[160] B. Li, J. Huang, S. Zhou, K. Ball, M. Stojanovic, L. Freitag, and P. Willett, "Mimo-ofdm for high rate underwater acoustic communications," *IEEE J. Oceanic Eng.*, vol. 34, no. 4, pp. 634–644, October 2009.

[161] M. Stojanovic, "Mimo ofdm over underwater acoustic channels," in *Conference Record of the Forty Third Asilomar Conference on Signals, Systems and Computers*, November 2009, pp. 605–609.

[162] B. Li and M. Stojanovic, "A simple design for joint channel estimation and data detection in an alamouti ofdm system," in *2010*, September 2010, pp. 1–5.

[163] E. V. Zorita and M. Stojanovic, "Space-frequency coded ofdm for underwater acoustic communications," in *OCEANS 2012*, October 2012, pp. 14–19.

[164] K. F. Lee and D. B. Williams, "A space-frequency transmitter diversity technique for ofdm systems," in *Proc. IEEE Global Communications Conference (GLOBECOM)*, vol. 3, December 2000, pp. 1473–1477.

[165] K. Lee, K. W. Lee, H. Sung, and I. Lee, "Sum-rate maximization for two-way mimo amplify-and-forward relaying systems," in *IEEE 69th Vehic.Tech.Confer.*, April 2009, pp. 1–5.

[166] Y. Aval and M. Stojanovic, "A method for differentially coherent multichannel processing of acoustic ofdm signals," in *7th IEEE Sensor Array and Multichann. Sig. Proc. Workshop (SAM)*, June 2012.

[167] B. Li, S. Zhou, M. Stojanovic, L. Freitag, and P. Willett, "Multicarrier communication over underwater acoustic channels with nonuniform doppler shifts," *IEEE J. Oceanic Eng.*, vol. 33, no. 2, April 2008.

Appendices

Appendix A

On the summation of the largest K out of N_R available numbers

Assuming $\frac{\sum_{i=1}^{N} a_i}{N} = E$, with $a_1 \geq a_2 \geq \ldots \geq a_N$, we have

$$\begin{aligned} \sum_{i=1}^{K} a_i &= N \cdot E - \sum_{j=K+1}^{N} a_j = K \cdot E + (N-K)\, E - \sum_{j=K+1}^{N} a_j \\ &= K \cdot E + (N-K)\, \frac{\sum_{i=1}^{K} a_i + \sum_{j=K+1}^{N} a_j}{N} - \sum_{j=K+1}^{N} a_j \geqslant 0 \end{aligned} \tag{A.1}$$

where

$$(N-K) \sum_{i=1}^{K} a_i - K \sum_{j=K+1}^{N} a_j \geq 0. \tag{A.2}$$

Appendix B

Diversity gain analysis with BRS

To find the maximum achievable diversity order associated with the SC-FDE TWR system with BRS, we again consider three limiting scenarios where $t \to 0^+$, $t \to 1^-$, and $t \to c$, where c is sufficiently distant from 0^+, and 1^-, and further divide the interval $\left[\begin{array}{cc} 0 & 1 \end{array}\right]$ within which (3.71) is to be evaluated into many non-overlapping sub-intervals, as detailed below

$$P(e) \to \xi \left(c_1 a^{-\left(L_{S_1R}(M+1)\right)} + \cdots + c_m a^{-\left(L_{S_1R}+L_{S_2R}\right)(M+1)} + \ldots + c_n a^{-\left(L_{S_2R}(M+1)\right)} \right), \tag{B.1}$$

where

$$\xi = \frac{2^{(M+1)L_{S_2R}-1} 3\Gamma\left((M+1)\left(L_{S_1R}+L_{S_2R}\right)\right)}{\left(\Gamma\left(L_{S_1R}\right)\Gamma\left(L_{S_2R}\right)\right)^{M+1}\left(\sin\left(\frac{\pi}{4}\right)\right)^{(M+1)\left(L_{S_1R}+L_{S_2R}\right)-1}}, \tag{B.2}$$

and $c_i, i = 1, \ldots, n$ are constants, and n is the number of sub-intervals. (69) confirms that the maximum achievable diversity order by this system is $(M+1)\min\left(L_{S_1R}, L_{S_2R}\right)$.